The Dissertation Committee for Jason Michael Vaughn Certifies that this is the approved version of the following dissertation:

Improved Bioavailability and Site Specific Delivery of Poorly Water Soluble Drugs through the Production of Stabilized Drug Nanoparticles

Committee:

Robert O. Williams III, Supervisor

Keith P. Johnston

James W. McGinity

Robert L. Talbert

Nikolaos A Peppas

Improved Bioavailability and Site Specific Delivery of Poorly Water Soluble Drugs through the Production of Stabilized Drug Nanoparticles

by

Jason Michael Vaughn, B.S. (Pharm.)

Dissertation

Presented to the Faculty of the Graduate School of

The University of Texas at Austin

in Partial Fulfillment

of the Requirements

for the Degree of

Doctor of Philosophy

The University of Texas at Austin

August, 2005

Dedication

To my loving and inspirational wife and best friend, Kasey.

To my role models and loving parents, Mr. Terry R Vaughn and Mrs. Sharon K. Vaughn.

Acknowledgements

First and foremost, I acknowledge my creator for guiding me and providing me with the tools and capacity for knowledge such that I may design and provide medicinal products which are vital and beneficial to all human kind. I would like to thank my supervisor, Dr. Robert O. Williams III, for his invaluable guidance and teachings during my graduate program. He was an excellent role model, knowledgeable instructor and confidant who was there for me anytime I needed his scholarly guidance.   I would also like to thank Dr. Keith P. Johnston for his insight and instruction in chemical engineering and meticulous nature which have improved my ability to communicate and write in a manner which can bridge multiple disciplines.   I would like to thank Dr. James W. McGinity for his extensive knowledge base and his life lessons, which have helped me to become a better researcher and communicator which will be beneficial to my career and interpersonal relationships throughout my life. I would like to thank Dr. Robert L. Talbert for his invaluable clinical and pharmacokinetic knowledge which has helped me to construct a meaningful dissertation. In addition, I would like to thank Dr. Nikolaos A Peppas for his helpful tips and ideas to further my dissertation topic and for being a member of my dissertation committee.

I wish to extend my gratitude to all of the faculty and staff of the College of Pharmacy, Department of Chemical Engineering and Department of Biomedical

Improved Bioavailability and Site Specific Delivery of Poorly Water Soluble Drugs through the Production of Stabilized Drug Nanoparticles

Publication No._____

Jason Michael Vaughn, Ph.D.

The University of Texas at Austin, 2005

Supervisor: Robert O. Williams III

Bioavailability enhancement of poorly water soluble active pharmaceutical ingredients (API) is key for improving existing therapies and allowing for formulation of certain new chemical entities. The rate limiting step for absorption of these APIs is dependent on the dissolution rate and the APIs apparent solubility. Particle engineering processes such as evaporative precipitation into aqueous solution (EPAS) and spray freezing into liquid (SFL) were developed to enhance API dissolution and bioavailbality through the production of amorphous and nanoparticulate API.

The morphology, primary API domain size and miscibility of particles produced by EPAS and SFL were investigated by several complementary and novel techniques. It was found that the SFL composition displayed amorphous character, a primary danazol particle size of 30 nm and was consistent with a solid solution. The EPAS composition was mostly amorphous with slight crystallinity, a primary danazol particle size of 500 nm and was consistent with a solid dispersion.

The ability of the nanoparticulate and amorphous particles to supersaturate dispersions and how this impacts oral bioavailability was tested through *in vitro* and *in vivo* models. Through the use of a testing method for supersaturation, it was found that EPAS and SFL compositions achieve higher apparent solubilities when compared to the physical mixture and commercial Danocrine® capsules. This improvement in solubility allowed for more danazol to be available for absorption in vivo.

Pulmonary delivery of SFL nanoparticulate itraconazole was evaluated for pharmacokinetic parameters and steady state trough levels compared to oral delivery of an SFL oral composition and the commercial product. Inhalation of ITZ compositions is an effective method of antifungal therapy for the treatment and prophylaxis of invasive fungal infections. High and sustained lung tissue concentrations are achieved via inhalation of an amorphous ITZ pulmonary composition while maintaining serum levels which are above the minimum lethal concentration for *A. fumigatus*.

Histology, macrophage uptake and IL-12 induction was evaluated for aerosolized amorphous ITZ nanoparticles. Pulmonary administration of amorphous ITZ nanoparticles or excipient placebo does not cause inflammation or changes in alveolar and airway histology. Uptake of ITZ by alveolar and airway macrophages occurs following inhalation of an amorphous ITZ composition

Table of Contents

List of Tables

List of Figures

Chapter 1: Nanoparticle Engineering

1.1 INTRODUCTION

Technological advances in both biotechnology and molecular biology have yielded a surge in the number of new chemical entities which are produced to treat specific diseases or ailments. However, a growing portion of these new chemical entities display poor aqueous solubility, leading to poor oral bioavailability and an inability to form intravenous formulations.   Nanoparticle formation has been proposed and utilized as a method to improve oral bioavailability of poorly soluble drugs and as a method for delivery of particles via parenteral, pulmonary and topical administration. Nanotechnology, as it is described by the National Institutes of Health, comprises particles or structures which are in the size range of 1-100 nm in diameter.   Included in this designation are nanoparticles and nanospheres for the delivery of drug molecules. However, much of the pharmaceutical literature recognizes nanoparticles to include particles which are less than 1 μm in diameter. The utility of nanoparticles within the pharmaceutical industry has been studied extensively in recent years and has received increased focus from researchers and government funding agencies. Hydrophobic drugs which do not benefit from micronization or solubilization in cosolvents can be used effectively as nanoparticles. Also, controlled release and drug targeting has shown promise when administered as nanoparticles or nanocapsules, especially parenteral delivery of peptides and nucleotides. The delivery of biomolecules such as polypeptides and nucleotides has seen improved uptake and localization due to the production of specialized nanoparticle carriers. Controlled release of parenteral doses can be achieved through the production of biodegradable nanoparticles which are used to encapsulate

drug molecules, and these delivery systems can be delivered via intravenous, subcutaneous or depot intramuscular injection.

This chapter will cover properties inherent to nanoparticles as well as methods for their production and use. Also, current and novel methods for viewing and characterizing nanoparticles will be discussed through theoretical and practical considerations.

1.2 BENEFIT OF NANOPARTICLES

Nanoparticles have many desirable properties which have been exploited in research as well as commercialization of specific dosage forms. For example, Liversidge *et al* has reported enhanced bioavailability of danazol through the production and delivery of nanocrystalline drug particles. In their study, absolute bioavailability of the nanoparticle formulation was 77% higher than a similar formulation consisting of microparticles.[1] It is reported that nanoparticles possess improved dissolution and bioavailability when delivered orally. This aspect has yielded drug products for specific molecules that were previously thought to be undeliverable or displayed sub-optimum absorption. Elan's NanoCrystal™ technology has yielded two products which have been approved by the United States Food and Drug Administration (FDA). Rapimune (sirolimus), which was previously only available as a solution and required additional storage and delivery requirements, is now available as a solid dosage form due to the production of nanoparticulate drug particles. Also, nanoparticle dispersions may be delivered via parenteral routes, without the need for complete solubilization in the delivery vehicle or the addition of harmful solubilizers. The FDA recently approved Abraxane which is a protein-stabilized, nanoparticle formulation of paclitaxel that does not require Cremophor EL to improve solubilization. This formulation significantly reduces hypersensitivity reactions due to Cremophor administration which eliminates the need for premedication to prevent such reactions.[2] Localization of drug molecules is

possible through binding of specific ligands to the surface of nanoparticles which aid in cell recognition and internalization. Figure 1.1 illustrates the localization of paclitaxel micellar nanoparticles which selectively bind to the surface and are internalized by tumor cells.

1.3 PROPERTIES OF NANOPARTICLES

Particles and structures which are in the nanoscale size range display many favorable properties compared to their microparticle counterparts. Most importantly is the level of dissolution enhancement which can be achieved through nanoparticle production. Also, particle interactions can be tailored to facilitate production, while maintaining their functional characteristics. However, concern should be given to particle size stability, due to the metastable state achieved through nanoparticle formation. This section will focus on properties inherent in nanoparticles and how these properties can be exploited for drug delivery and aid in characterization.

1.3.1 Rate of Dissolution

Not withstanding the use of nanoparticles for intravenous and topical applications, improvement in oral bioavailability is one of the most important contributions attained through nanotechnology.[3] Molecules which are poorly water soluble may be poorly absorbed due to a lack of sufficient concentrations of solubilized drug. Formulations which are amorphous can overcome this by supersaturation of the dissolution medium allowing for greater absorption of the delivered dose.[4] However, stability problems are significant for amorphous pharmaceuticals, leading to recrystallization and particle

growth, while in the solid form.[4] Nanotechnology can achieve similar results, while bypassing these stability issues.

$$\frac{dC}{dt} = \frac{AD(Cs - C)}{h}$$
(1)

The dissolution rate of a particle can be described by the Noyes-Whitney equation (1) where dC/dt is the rate of dissolution, A is the surface area of the particle, D is the diffusion coefficient, Cs is the apparent solubility of the drug in the dissolution medium, C is the concentration of the drug in the dissolution medium at time t, and h is the thickness of the diffusion boundary layer. The diffusion coefficient is dependent on the drug in question and cannot be adjusted. Also, the thickness of the boundary layer can be manipulated in vitro through increased agitation; however, this proves to be difficult in vivo.   The rate of dissolution can be improved (increased) by creating particles which have a high surface area, improved wettability (higher surface area in contact with dissolution medium) or by increasing the apparent solubility of the drug. Through the production of nanoparticles, the surface area of the particle increases significantly, thereby increasing the rate of dissolution. It is also theorized that very small particles, such as nanoparticles, may be able to supersaturate within the dissolution medium due to a phenomenon related to Ostwald ripening. According to the Ostwald-Freundlich/Kelvin equations, small droplets of liquid dispersed in a gas-liquid medium evaporate more quickly and to a greater extent than do large droplets due to increased curvature at the droplet surface which raises the vapor pressure of the liquid.[5] This theory has been suggested to apply to solid-liquid interfaces as well. By decreasing the size of solid particles to the nanometer scale, the high energy state which is achieved will increase the extent to which it can dissolve due to an increase in dissolution pressure. In turn, this will increase the apparent solubility of the dissolving particles. However, as will be discussed later in this section, particle dispersions which are not of a uniform size distribution will see a shift in particle size due to this phenomenon over time.

4

Thermodynamically, larger particles (lower energy) which may be present in the dispersion during dissolution will attract molecules from the supersaturated solution (high energy) and grow over time; thereby limiting the time that supersaturation can be maintained. Particles which have a nearly monodisperse size distribution will show the greatest propensity for long term supersaturation.

1.3.2 Particle Interactions

The dynamics of nanoparticles dispersed in a liquid medium are determined by several forces. Gravitational forces act on particles of sufficient size (>1μm) and will cause settling based on Stoke's Law, assuming that the density of the particle is greater than that of the dispersing medium. Nanoparticle or colloidal dispersions typically display Brownian motion, which is random, irregular motion within the dispersing medium. Attractive and repulsive forces between nanoparticles will determine the level of aggregation of particles and is determined by the zeta potential.

1.3.2.1 Brownian motion

The motion or movement of colloidal particles in a dispersing medium was first observed by Robert Brown in 1827 and theorized by Albert Einstein in 1905 to describe Brownian motion. Interactions of colloidal particles with the dispersing medium, liquid or gas, causes a random, irregular movement of the particle away from its original position in space.[6] According to the Stokes-Einstein theory, the degree of motion or its velocity is dependent on the suspending medium's viscosity, temperature and molecular size. This theory is the basis for particle size measurements using dynamic light scattering which measures the velocity of suspended particles when the viscosity and

temperature of the dispersing medium are known. Brownian motion also prevents settling or creaming of nanoparticle dispersion which is advantageous for long term stability.

1.3.2.2 Zeta potential

Particles composed of hetero-atomic molecules typically display a surface charge which may be positive or negative, depending on the orientation and ionization of the particle components. Electrostatic interactions between particles will determine the propensity of aggregation and repulsion phenomena. The zeta potential is a measure of the surface charge of the dispersed particles in relation to the dispersing medium.[7] Ideally, the particles should have a high net charge or zeta potential compared to the dispersing medium to prevent aggregation. The repulsive forces brought on by similar ionic charges on particle surfaces will prevent the natural attractive forces determined by hydrogen bonding and van der Waals. Dispersions which are allowed to aggregate to form microparticles or larger will not be governed by Brownian motion and may settle to form irreversible cakes or cream at the liquid surface. However, by controlling the zeta potential, aggregation can be prevented.

1.3.2.3 Ostwald ripening

Stability of dispersed nanocrystals is determined not only by its propensity to aggregate, but also by the tendency for the particle size distribution to grow in magnitude over time. This phenomenon is described by the theory of Ostwald ripening.[8] Nanoparticles are thermodynamically unfavorable compared to their larger counterparts. Smaller particles have a larger surface area-to-volume ratio than large particles. This

leads to instability of the molecules at the surface of the particle, compared to molecules which are packed appropriately in the center of the particle. The high energy state is unfavorable and will cause migration of the molecules from the smaller particles to the larger ones over time, thus causing overall growth of the distribution of particles. Uniformly monodisperse particles would therefore not display Ostwald ripening due to a lack of larger particles in the dispersion; however, uniformly monodisperse suspensions are atypical in the pharmaceutical industry. Although, nanoparticle suspensions which are relatively monodisperse may display longer stability compared with heterodisperse systems. [3]

1.4 METHODS FOR MANUFACTURE

1.4.1 Spray Drying

Although this is not a new method, several researchers have used this method for removal of solvent from other micronization techniques (e.g. Nanocrystals[®]).[1] Initially, spray drying was used for the removal of solvent from solutions, which caused rapid evaporation of the feed solution and precipitation of the dissolved API/Stabilizers. This method, although well established, requires that the drug be stable at the working temperatures (upwards of 120 - 150°C). Also, for water insoluble drugs, organic solvents must be used which can be explosive at the elevated temperatures and expensive for recovery and disposal. Dollo et al has used spray drying to remove solvent from emulsions of drug and stabilizer.[9] In this case, the droplet size, which effects the particle size of the dried material, is predetermined during the homogenization step of the process. Figure 1.2 is an example of an emulsion which was spray-dried to form dry

particles.   As can be seen by the figure, following reconstitution of the particles, nanoparticles still remain, similar in size to that of the original emulsion.

1.4.2 Aerosol Flow Reactor

The Aerosol Flow Reactor method utilizes similar principles to that of spray drying.[10] Drug and stabilizers are dissolved in a biocompatible organic solvent which is atomized into a chamber using an inert gas as a propellant. The droplets are passed through the heated flow chamber where the solvent is rapidly evaporated yielding nanoparticulate particles.   Temperature, solvent type, atomizer type and solution concentration are key parameters for the process. Particles which are produced below 120°C are dense and are not significantly different than particles produced at 40°C. Temperatures above 160°C create particles that are small and porous, due to an increased evaporation rate of the solvent. The atomizer that is used must create nanodroplets, since the particle size is directly related to the size of the droplet from which it was precipitated.   This is a continuous method which produces narrow particle size distribution. Scanning electron microscopy (SEM) micrographs of particles formed by an aerosol flow reactor are shown in Figure 1.3. These particles are on the order of 200nm in diameter and display a hollow spherical morphology.

1.4.3 Mechanical Techniques

1.4.3.1 Milling

Conventional dry milling processes such as ball milling and hammer milling are limited to production of microparticles on the order of 1-10 mm in size.   These

limitations are due to difficulties in processing as well as handling. Dry milling generates heat during processing as well as a lack of stabilization excipients during processing to prevent particle growth and aggregation. Furthermore, nanoparticles in the dry state are very difficult to handle and process into drug products, due to the high electrostatic forces which make recovery difficult. However, Nanosystems, now a division of Elan, developed a technology which utilizes wet milling as a method to circumvent many of these problems.[1] A schematic representation of the NanoCrystal milling apparatus is shown in Figure 1.4. The milling apparatus consists of a milling chamber, milling shaft and recirculation feed. High energy shear forces mechanically break down microparticles which are suspended in a polymer solution. The milling media can consist of glass, zirconium oxide or highly cross-linked polystyrene resin. Temperature is controlled through coolant recirculation and when using the batch mode, the process can create particles <200nm in 30-60 min. This process creates narrow particle size distributions with good batch-to-batch reproducibility. However, residue from the milling media can be introduced into the final dispersion and may lead to toxicity.[11] This problem is reduced when polystyrene resin is used as the primary milling substrate.

1.4.3.2 High pressure homogenization

Similar to milling processes, high pressure homogenization uses high shear forces to break down particles in suspension. Typically, piston-gap homogenizers (Figure 1.5) are used at pressures up to 2000 bar.[12, 13] A suspension of milled microparticulate drug is forced through the narrow opening at high pressure, causing cavitation, high shear and particle collision at high velocity within the gap of the homogenizer. Within the gap, the aqueous carrier begins to boil, causing gas to form. Upon leaving the gap, rapid implosion of the carrier creates high shear and cavitation which disintegrates the suspended microparticles into nanoparticles. Particle-particle collision within the gap

9

occurs at high velocity, causing further mechanical breakdown of the particles. The homogenization pressure is an important parameter for the production of nanoparticles using this technique and should be investigated for each situation. Also, the number of cycles for recirculation of particles through the homogenization gap can be adjusted to achieve optimum results.

1.4.4 Precipitation Techniques

Other solution based particle engineering applications have been introduced in the past several years. Each process requires the dissolution of a drug into a solvent and then precipitation in an antisolvent or evaporation of the solvent. The processes differ by the type of solvent/antisolvent, and the temperature and pressure at which the technique is carried out. Surfactants and stabilizers typically are incorporated into either or both the antisolvent and solvent. Solvent and supercritical solution technologies have been extensively reviewed.[14, 15]

1.4.4.1 Antisolvent precipitation

1.4.4.1.1 Controlled precipitation (CP)

Developed by the The Dow Chemical Company, CP efficiently creates nanoparticle dispersions containing drug and stabilizers.[16] The process involves dissolution of drug and stabilizers within a water miscible solvent which is dispersed within an aqueous solution in a controlled manner. Upon introduction into the aqueous solution, solvent power of the organic solution is lost, leading to nucleation and precipitation of the dissolved drug. Stabilizers and crystal growth inhibitors can be

present in both the organic and aqueous phase. Adsorption of the stabilizers to the particle surface prevents particle growth. Removal of solvent can be conducted through is conducted using vacuum distillation followed by spray drying or lyophilization. Solvent type, temperature within the mixing chamber, stabilizer type and stabilizer location are important parameters for nanoparticle production. Increasing the temperature within the mixing zone tends to increase the particle size as well as lead to bimodal particle size distributions, due to increased particle growth within the mixing chamber. Median particle sizes have been produced at less than 200nm in diameter, with good recovery and low residual solvent levels. The decrease in particle size yields significantly higher surface areas compared with the bulk microparticulate drug particles and physical mixtures. Furthermore, the increased surface area significantly improved the rate of dissolution for model poorly water soluble drugs. Scale-up of this process was shown to be successful for producing large batches, on the kilogram scale, of nanoparticles.

1.4.4.1.2 *Evaporative precipitation into aqueous solution (EPAS)*

In the EPAS process, the poorly soluble drug precipitates due to evaporation of the organic solvent near or above the boiling point and contact with an aqueous solution.[17] The drug loaded organic solvent is pressurized, heated and atomized through an elliptical conical stainless steel nozzle into a heated water bath containing stabilizing excipients. The large pressure drop across the 125 micron diameter nozzle orifice creates intense atomization with rapid evaporation of the primary organic solvent due to the high temperature of the feed solution and aqueous receiving solution. The rapid evaporation of the feed solvent results in supersaturation, nucleation and precipitation of the drug into nanoparticles. The excipients within the organic feed solution and/or aqueous receiving vessel stabilize the particles by preventing particle

growth and recrystallization of the drug precipitates. In addition, the excipients also enhanced the drug particle dissolution rate and long term storage stability. Dissolution curves for particles produced by EPAS are shown in Figure 1.6. As can be seen in the figure, the formation of nanoparticles dispersed in solubilizing excipients significantly enhances the rate of dissolution compared to the bulk drug.

1.4.4.2 Supercritical fluid technologies

1.4.4.2.1 Precipitation into a compressed antisolvent (PCA)

PCA involves the atomization of a solvent feed solution into compressed liquid or supercritical CO_2. [15] Because of the high surface area produced by the atomization process, the loss in solvent strength and precipitation is more rapid creating much smaller particle sizes. This process requires that the organic solvent be miscible with the compressed gas and can produce particles in the size range of 500nm. This technique can also be accomplished within a coaxial nozzle, which improves mass transfer rates, thereby creating smaller, more stable particles. The addition of an ultrasonic tip to the nozzle creates much higher atomization and smaller droplet production by the nozzle which increases the interfacial area. Hydrocortisone, which was processed using the ultrasonic nozzle antisolvent precipitation, was formed into discrete, nearly spherical particles which were distributed around 500nm in diameter. A nozzle geometry which elicits a hollow swirling cone jet for use in PCA was introduced by Jarmer et al.[18] A photo of the mixing zone of a PCA process utilizing the swirl cone nozzle can be seen in Figure 1.7. This design yielded better mixing and was able to precipitate nanoparticles with very narrow distributions.

12

1.4.4.2.2 Rapid expansion from supercritical solutions (RESS)

In the case of RESS, the solvent is supercritical CO_2 and the loss in solvent power is due to atomization of the CO_2 into a chamber at atmospheric pressure.[19] A Schematic representation of the RESS process is shown in Figure 1.8. The rapid change in pressure causes evaporation of the supercritical CO_2 and precipitation of the dissolved solute. This process requires that the API be soluble in the supercritical CO_2 and the particle sizes achieved by this process are determined by the temperature, pressure, nozzle geometry and solution concentration. Initial studies using this technique yielded problems with recovery and stabilization. More recently, researchers have begun atomizing the supercritical CO2 below the surface of an aqueous solution, which contains stabilizers and solubilizers to prevent particle growth and aid in solubilization of the nanoparticles. This form of precipitation is termed rapid expansion from supercritical into aqueous solutions (RESAS). Utilization of the RESS process has been shown to produce nanoparticles with narrow particle size distribution. RESS processing of griseofulvin has produced primary particles in the size range of 150nm in diameter with significantly faster dissolution rates compared to unprocessed drug. [20]

1.4.5 Emulsion Techniques

1.4.5.1 Microemulsions

Oil and water (oil-in-water (O/W) or water-in-oil (W/O)) emulsions are utilized for the production of nanoparticle dispersions. The colloidal emulsions are stabilized by a film of surfactants and polymers, which interact with the oil and water phases to prevent aggregation and droplet growth. These microemulsions are typically used as

templates for the production of nanoparticles and solid lipid nanoparticles (SLN). Biocompatibility of the organic phase is important and limits the types of organic solvents which can be used. One method for the biocompatible template microemulsions utilizes a W/O emulsion. The drug of interest is dissolved in the organic phase at which time the drug diffuses into the aqueous droplets where it precipitates. Using this method, Debuigne et al was able to achieve particles of nimesulide in the size range of 45 – 60Å (e.g. 4.5 – 6.0 nm)with narrow distributions which remained stable for long periods of time.[21] More recently, Trotta et al. utilized this technique to formulate griseofulvin nanoparticles from O/W microemulsions.[22] Biocompatible, water miscible solvents such as butyl lactate, benzyl alcohol and triacetin were used above their miscibility level. In this process, Trotta was able to achieve microemulsions without agitation or any other added energy. The results from their study are listed in Table 1.1. Griseofulvin nanoparticles were formed in the size range of 80 – 300nm in diameter and varied depending on the surfactant and co-surfactant used during stabilization of the microemulsion. This technique, although relatively new to the pharmaceutical industry, shows potential to form nanoparticles with narrow distributions when using biocompatible organic solvents.

1.4.6 Freezing Techniques

1.4.6.1 *Spray freezing into liquid (SFL)*

The SFL process creates micronized powders with enhanced dissolution rates of poorly water soluble drugs as well as stabilization of peptides.[23] This is a particle engineering process that utilizes the atomization of a feed solution containing an active ingredient (small molecule or macromolecule) and dissolution enhancing excipient(s) or

cryoprotectants directly into a cryogenic liquid, such as nitrogen. The resulting dried powder is composed of discrete microparticles where the active ingredient is molecularly dispersed with a polymer in a porous matrix. This molecular dispersion is achieved by rapid freezing in liquid nitrogen, which prevents phase separation During the SFL process, the drug loaded organic solvent is pressurized and atomized via a poly ether–ether ketone (PEEK) nozzle below the surface of liquid nitrogen. Because of the rapid flow rate, liquid–liquid impingement and marked temperature drop in the jet, the emitted solvent is atomized into fine, high surface area microdroplets that are frozen rapidly. The suspension of frozen microdroplets is lyophilized to remove solvent, resulting in an amorphous, micronized powder. Exemplary SEM micrographs are shown in Figure 1.9. From these micrographs, it can be seen that the SFL process creates microparticles which contain a nanoparticulate network structure within. These low density particles contain protein or drug along with stabilizing agents.

1.4.7 Nanoparticulate Drug Carrier Systems

1.4.7.1 *Polymeric nanocapsules and nanoparticles*

Nanoparticles composed of polymeric materials have been extensively investigated for their use in delivery and controlled release of drug molecules, peptides and nucleotides via oral, topical and parenteral routes.[24] Polymers such as chitosan, polyglycolic acid (PGA), polylactic acid (PLA) and polylactic-glycolic acid (PLGA) are the most common types used for the production of nanoparticulate carrier systems. Although, there is a host of other novel polymers which are being developed to improve biocompatibility, biodegradability, site specific delivery, controlled release and drug loading capabilities. There are several methods which have been employed to load active

molecules the polymeric nanoparticles. The solvent evaporation method involves the dissolution of drug and polymer into an organic solvent. This solution is then emulsified into a non-solvent to form a microemulsion. Over time, and with the help of vacuum in some cases, the organic solvent will evaporate, causing supersaturation in the nanodroplets and precipitation of the polymer and drug into nanoparticles. This method creates nanoparticles with high drug loading efficiency although it is limited to drugs which are soluble in the same solvent as the polymer. Double emulsion techniques can be employed to encapsulate water soluble drugs and macromolecules. Nanoparticles containing BSA which were formed by this technique are shown in Figure 1.10. The particle size, based on the SEM technique, is about 162 nm in diameter and the distribution was approximately monodisperse with a spherical morphology. Spherical morphology is expected in nanoparticles produced by emulsion techniques.

The solvent diffusion/spontaneous emulsification process can create much smaller droplet sizes than the solvent evaporation method. In this case, the dispersed phase is composed of a water immiscible solvent and a water miscible solvent which is emulsified into an aqueous solution. The diffusion of the water miscible solvent causes turbulence and further break-up of the droplets in the emulsion. The removal of solvent can be conducted similarly to the solvent evaporation method.

Although water immiscible solvents display low solubility in water, there is some amount of solubility. The solvent diffusion/emulsification method exploits this for the production of nanoparticles.[25] In this technique, drug and polymer are dissolved in an organic, water immiscible solvent which is emulsified into an aqueous solution containing emulsifiers and stabilizers. The emulsion is then diluted with water to increase the level of organic solvent which can be dissolved in the continuous phase. This causes a decrease in organic solvent content within the dispersed phase which leads to precipitation of the polymer and drug to form nanoparticles. Polymeric nanoparticles

16

can also be formed using the aforementioned techniques such as supercritical techniques, precipitation and freezing technologies.

Encapsulation of particles within nanoparticulate carriers allows for inclusion of surface modifying agents.[24] These agents may include charge and lipophilicity modifications to prevent uptake by immune cells or to aid in localization within specific tissues or organs. Also, the nanoparticles may be coated with ligands to improve specific cell recognition, uptake and delivery of payload within a cell or tissue. Ligands may also aid in oral uptake of polymeric nanoparticles through specialized cells within the gastrointestinal tract as well as decrease breakdown of peptides through enzymatic inhibition.

1.4.7.2 Lipid based nanoparticulate carriers

Nanoparticles composed of lipids which are solid at room and physiologic temperatures are referred to as SLN.[26] These are typically composed of stabilizing surfactants, triglycerides, glyceride mixtures and waxes. The most common method for manufacturing SLNs is high pressure homogenization and can be performed at both elevated and low temperatures. Decrease in particle size is achieved similarly to homogenization of drug crystals where cavitation and turbulences are the main mechanisms. In hot high pressure homogenization, drug and lipid are co-melted above the melting point of the lipid. This dispersion is added to a heated aqueous phase, which is at an identical temperature. A course emulsion is formed through rapid stirring, after which, the droplet size is reduced through high pressure homogenization. The emulsion is then cooled to room temperature, causing recrystallization of the lipids and formation of the SLN. This technique is not suitable for temperature labile drugs, which in order to use SLN technology, must be processed through cold high pressure homogenization, which has a shorter heating time. This method requires co-melting of the drug and lipid

and then rapid cooling and cryogenic grinding to form lipid microparticles. The microparticles are dispersed in surfactant solution and homogenized to form nanoparticles. Other methods for the production of SLNs include: microemulsion technology, solvent emulsification followed by evaporation or diffusion (similar to processes used for polymer and drug nanoparticle production), w/o/w double emulsions or through ultrasonciation. Drug loading of SLNs are typically as high as 25%. SLNs have shown good stability over extended periods of time (>1 year). This method can be used to encapsulate hydrophobic and hydrophilic drugs as well as macromolecules. Figure 1.11 displays the most common morphologies that can be produced when forming SLNs. If the drug is miscible with the lipid, a solid solution can be formed, which is completely homogeneous. For drugs which are not miscible with the lipid, the drug and lipid will orient themselves into two phases. The location of these phases would be dependent on their difference in polarity compared to the dispersion medium. That is, more polar drugs would orient to the water phase to form a drug enriched shell, where as, more hydrophobic materials would move toward the core of the nanoparticle.

A novel nanoparticulate lipid based carrier system was developed by Mumper et al at the University of Kentucky.[27] This carrier system is composed of a lipophilic emulsifying wax such as cetyl alcohol/polysorbate 60 and other surfactants such as Brij 72, Brij 78 and Tween 80. The nanoparticles were formed through a warm microemulsion technique where encapsulates have included paclitaxel and plasmid DNA. The emulsification process is spontaneous and cooling of the emulsion causes solidification of the nanoparticles containing drug. This novel carrier has shown high efficiency in drug delivery across the blood brain barrier.

1.4.7.3 Polymeric micelles

Polymer engineering has yielded several new block copolymers which have the capability to entrap drug molecules or macromolecules within micelles. Their particle size is fairly monomodal, due to thermodynamic constraints on the size of a micelle formation. Block copolymers in solution, which are amphiphilic and at concentrations above the minimum micelle concentration, will associate into a core shell morphology where the interior is hydrophobic and the exterior is hydrophilic. Hydrophobic drugs can diffuse into the micelles, aiding in their solubilization and delivery. Micelles are typically on the order of 100nm in diameter (Figure 1.12) and can improve endothelial absorption through passive diffusion. However, one drawback to micelle formation is the low drug loading that can be achieved, which limits this technique to low dose drugs or macromolecules. Ligands can be associated with the polymer or be covalently bound the hydrophilic moiety that is at the exterior of the micelle, improving localization and targeting for specific applications. Micelles containing chemotherapeutic agents, such as paclitaxel and camptothecan have shown a decrease in drug related side effects due to improved solubilization as well as improved localization to the site of action. [28]

1.4.7.4 Liposomes

Consisting of non-toxic oleaginous phospholipids and cholesterol, liposomes are a versatile delivery mechanism for drug molecules.[29] Liposomes vary in size, surface charge, phospholipids content and method of manufacture. Small unilameller vesicles (SUV) are composed of a single layer of phospholipids and are on the size range of 25-50nm in diameter. Multilamellar vesicles (MLV) are composed of multiple layers of phospholipids, where the layers are separated by aqueous solutions. Liposomes composed of phospholipids, which are saturated or unsaturated, display varying degrees of rigidity and permeability. Compositions containing mostly saturated phospholipids are more rigid and nearly impermeable, whereas unsaturated phospholipids display lower stability

and rigidity and are much more permeable. Unsaturated phospholipids can be obtained from egg and soybean phosphatidylcholine. Targeting of liposomes can be achieved through surface modification by various means. Surface charge can improve uptake by certain cells, such as macrophages, as well as repel uptake, depending on the charge. Also, ligands can be associated or covalently bound to the liposomal surface, improving localization and uptake by desired cells and organs. Stealth liposomes can be constructed by modifying the surface with polyethylene glycol (PEG) which increases its half life.[30]

1.5 STRATEGIES FOR RECOVERY OF NANOPARTICLES

Most nanoparticle production processes create dispersions of nanoparticles in either an aqueous or organic medium. For intravenous or topical applications, the final dosage form may include an aqueous component and therefore will not require recovery of the nanoparticles in a dry form. However, stability as a dispersion is limited significantly compared to nanoparticles in the dry form, due to Ostwald ripening, chemical and physical degradation, oxidation and uncontrolled aggregation. Also, drying or recovery is essential for nanoparticles that are intended for delivery through dry oral dosage forms, dry powder inhalers, oleaginous based topical formulations or through redispersion of a dry pellet or cake for parenteral, oral, topical or pulmonary delivery. For this reason, most nanoparticle dispersions produced by the aforementioned processes are further processed to a dry powder by one of several recovery techniques.

1.5.1 Spray Drying

Several research groups have utilized spray drying of nanoparticle dispersions as a method for recovery.[1, 9, 16] Typically, nanoparticle dispersions with or without stabilizing agents is sprayed through a heated nozzle (~120°C) and atomized into a chamber with flowing heated air. The droplets quickly evaporate, entrapping the nanoparticles within the dissolved excipients and stabilizers. Recovery using this method can be cumbersome, due to the electrostatic forces which bind the particles to the walls and surfaces of the spray dryer as well as loss through the air exhaust system. Pharmaceuticals which are heat labile should not be recovered using this method.

1.5.2 Lyophilization

Although time consuming, lyophilization is an effective method for removal of solvent from nanoparticle dispersion. All freezing technologies require lyophilization of the frozen particles to remove solvent and produce dry nanoparticulate powders and cakes. Also, dispersions of nanoparticles can be rapidly frozen in liquid nitrogen or another cryogen and lyophilized to remove solvent. This method will ensure that the produced powder will be similar in structure to that of the nanoparticles in dispersion as well as recovering included stabilizing agents and excipients. Rapid freezing is ideal, as slow freezing can cause precipitation of dissolved drug and phase separation. Lyophilization cycles should be optimized to prevent particle growth within the lyophilizer. Similar to other solid materials, frozen liquids possess a glass transition temperature and melting point and could be affected by dispersed or dissolved components. Since lyophilization occurs at very low pressures, there is a shift in the phase diagram to the solid phase, even well above the melting point of the frozen material. However, when the temperature reaches the glass transition temperature (Tg') of the frozen material, viscous flow and crystal reorientation can occur, causing crystallization of amorphous particles, crystal growth and phase separation.[31] Tg' is

associated with the glass transition temperature of the material at the given pressure during lyophilization and differs from Tg at standard pressure. It is ideal that the lyophilization temperature be below and near the Tg' for the given system for optimum solvent removal and stability.

1.5.3 Filtration

Particles suspended in a liquid medium can be recovered using filtration, assuming that the filter pore size is smaller than the particles. Membrane filters which are used for sterile filtration range from 100nm to 450nm in diameter and would, therefore, only be able to filter dispersions containing particles larger than that diameter. To overcome this limitation, dialysis type membranes can be used to remove fluid from the nanoparticle dispersion. Dialysis membrane pores range in size from 50kD to 300kD in diameter which corresponds with 7nm to 20nm, respectively. Filter membranes are available which selectively remove solvent, while concentrating suspended solids and dissolved molecules that are larger than the pore size (eg. polymers). Reverse osmosis and nanofiltration can concentrate particles which are as small as 1nm. Concentration of particles in the range of 10nm to 100nm can be achieved through ultrafiltration membranes. Caution should be given to a membrane pore size which does not remove unwanted dissolved components such as reaction byproducts and contaminants. Ideally, membrane pores allow passage of liquid components and dissolved molecules.

1.6 METHODS FOR CHARACTERIZATION

1.6.1 Light Scattering

Light scattering techniques have been the mainstay for the determination of particle size and particle size distributions. Several theories are employed to calculate the particle size distribution level and angle of diffracted light.[32] When light is directed at a particle, it can either be deflected or absorbed by the particle, which is dependent on the size of the particle relative to the wavelength of the light source. Particles which are large compared to the wavelength of the light source tend to diffract the light source. Smaller particles, close to the size of the wavelength or smaller tend to scatter light. Most measurements are conducted on particle dispersions, rather than single particles, where most often a dilute dispersion is required. Concentration requirements are based on particle size where larger particles must be more dilute than smaller particles. Automated light scattering techniques account for this by determining light transmittance intensity as a measure of concentration, such that the user need not be concerned with particle size before the actual measurement.

1.6.1.1 *Dynamic light scattering (DLS) or photon correlation spectroscopy*

Particle size distribution measurements using DLS requires dilute dispersions of particles which are less than 6μm in diameter.[33] It is relatively simple and inexpensive to conduct measurements and computer controlled acquisition and analysis is available. DLS is well suited for measuring nanoparticles because it takes advantage of Brownian motion, which is unique to colloidal particles. For this reason, DLS is limited to particles that are small and not affected by settling forces. As was mentioned previously during the discussion on Brownian motion, DLS measures the velocity of a particle in motion and correlates this velocity to size. A laser light is utilized as a radiation source and the frequency variation of scattered light is detected. Shift frequencies due to particle motion are directly related to particle velocity and used to calculate particle size based on the

theory of Brownian motion. A distribution of shift frequencies is used to construct a particle size distribution.

1.6.1.2 Laser light scattering

Laser light diffraction particle size analyzers use either diffracted light, diffused light or both in the calculation of particle size distributions. Accurate analysis can be conducted on particles in the range of 10nm to 1mm in diameter. This method is simple and the software package allows for many thousand measurements which are averaged together to give the final distribution. This reduces the number user runs, making this measuring technique a very efficient means for ascertaining the particle size distribution of nanoparticles. Like other diffraction techniques, dilute dispersions of the nanoparticles are required for measurement. Typically, the nanoparticle dispersion is recirculated through a flow cell where the measurement takes place. This allows for measurement of a larger portion of the dispersion, rather than a limited number of particles which may be present in non-uniform distributions in the cell, as in DLS or in the Coulter counter. Also, this prevents settling of the particle or particle aggregates. Sonication is provided on several types of measuring units to aid in aggregate breakup. For particles which are above 1μm in diameter, Fraunhofer diffraction is measured and calculated into a particle size distribution. This type of measurement assumes a spherical particle. Particles which are smaller than 1μm require that the Mei theory be employed. This calculation assumes that the particles are spherical and the refractive index of the dispersion medium and particles must be known. The refractive index is an important parameter, which, if incorrect can greatly change the calculated value. This technique can also be used to determine droplet size of emulsions and microemulsions as well as droplets formed during atomization for several of the particle engineering techniques.

1.6.1.3 Coulter counter

Dilute dispersions of nanoparticles or microparticles can be evaluated using the Coulter counter, although accuracy is limited to particles that are above 400nm in diameter. Particle size distributions are calculated through electrical resistance variations when a particle in dispersion passes between two electrodes. The resistance causes a voltage pulse which is directly proportional to the particle volume of the individual particle. When the concentration of particles is sufficiently low, each voltage pulse corresponds to an individual particle such that a particle size distribution can be established. This technique requires that the particles be spherical for accurate volume measurements. Particles which are non-spherical may rotate and create a particle envelope that is much larger than its actual size. Also, porous particles will give volumes larger than their actual volume.

1.6.2 Scanning Electron Microscopy

Because of the size limitations of optical microscopes, electron microscopy plays an important role in viewing particle size of a limited number of particles and evaluating particle shape and morphology. [34] This technique, unlike environmental SEM (ESEM), requires that the sample be dry and a contrast agent applied to the surface. The contrast agent is typically gold or palladium which is added to the surface through sputter coating under high vacuum. Addition of the contrast agent or the drying procedure may change the morphology or size of the particles during viewing, which is one of the disadvantageous of using this technique. Also, a distribution of sizes is nearly impossible to determine using this method, due to limitations on number of particles which can be viewed. Evaluation of the chemical make-up of nanoparticles as well as drug content

evaluation can be conducted during SEM using energy dispersive spectroscopy (EDS) which is available as an additional component to the microscopy unit.

1.6.3 Atomic Force Microscopy

Scanning probe microscopy encompasses several techniques that can be used to characterize surface phenomenon such as height, charge and magnetism, one of which is atomic force microscopy (AFM) which measures height and contour using a force probe.[34, 35] The AFM instrument scans the sample with a nanosized tip connected to a cantilever. In contact mode, the tip is allowed to lightly tap or drag across the surface of the sample. As the tip scans the surface, vertical deflection or repulsion occurs and is measured by the instrument to indicate the height of the local surface. In non-contact mode, measurement of attraction to the sample surface is used to determine height of the local surface. The resolution of AFM is as low as 10pm and surface measurements can be conducted in both liquid and dry states. Nanoparticles are best viewed when adsorbed to the surface of a stage composed of silicone or glass. Viewing of the particles in their native state allows for optimum characterization of nanoparticles formed within particle dispersions, since significant drying can affect particle size and morphology. AFM has been used to view nanoparticles adsorbed to the surface of glass with high resolution.[34] Figure 1.13 shows AFM pictures of adsorbed SLN particles that correspond to ~300nm diameter particles.

1.6.4 Transmission Electron Microscopy (TEM)

Similar to SEM, TEM is a method for evaluating the particle size and morphology of nanoparticles. [36]   This technique is under high vacuum and requires that the sample

be dry following sample preparation. TEM tomography gives much higher resolution images compared to SEM and can resolve at much higher magnifications. The addition of a contrast agent or coating is not required for this technique. However, staining agents can be used to improve contrast between components in a mixture. An example of this can be found in Figure 1.14, where an SFL particle has been positively stained (i.e. drug has been stained) to show the size of the drug domains within the nanoparticulate microparticle. Unlike SEM, this type of electron microscopy transmits electrons through a particle rather than reflecting them. Therefore, the sample must be relatively thin. Low angle scattering due to the diffusion of electrons is what is measured during normal TEM operation. Z-contrast TEM or STEM dark-field imaging is a novel method for high resolution viewing of API/excipient mixtures without the use of electron density staining or dispersion formation and drying. This tomography process has been used in the semiconductor industry and requires the use of a high-angle annular dark field (HAADF) detector [36]. The high-angle scattering is associated with electron interaction close to the nucleus of the atom. For this reason, the detector is very sensitive to compositional changes and thickness within the specimen. Analysis of the sample contents can also be evaluated using electron energy loss spectroscopy (EELS) and EDS.

1.6.5 Analytical Ultracentrifugation

As discussed previously, colloidal particles do not display sedimentation rates according to stokes law, but rather motion within the dispersion is determined by Brownian motion. However, during centrifugation, sedimentation can be forced and the rate of sedimentation will vary depending on the particle size or particle density. Several commercial apparatuses are available which will apply a given centrifugation level and measure the sedimentation rate of the colloidal particles.[37] This method has been used extensively for polymer and inorganic particle analysis. This method requires dilute

dispersions and can be more precise than DLS measurements of Brownian motion. Similar to other techniques, spherical particles are required and can be determined through SEM analysis for particle shape.

1.7 SUMMARY AND CONCLUSION

The utility of nanoparticles is unmistakable and will yield many novel methods for their manufacture, collection and characterization in the coming years. This chapter has listed and described several of the reported techniques for the production of nanoparticles and some examples of their use in drug delivery. Collection of the nanoparticles is important for transition into a dosage form capable of being administered and can be tedious due to limitations on filter sizes and can be time consuming using other methods. Particle characterization can be achieved by several means and must be conducted to ensure optimum and robust nanoparticle production. The field of nanotechnology is effectively in its infancy with only room to grow and with funding now coming from government agencies, the research in this field will grow exponentially.

1.8 REFERENCES

1.   Liversidge, G.G.; Cundy, K.C. Particle size reduction for improvement of oral bioavailability of hydrophobic drugs: I. Absolute oral bioavailability of nanocrystalline danazol in beagle dogs. Int. J. Pharm. **1995**, *125* (1): p. 91-97.

2.   Ibrahim, N.K.; Desai, N.; Legha, S.; Soon-Shiong, P.; Theriault, R.L.; Rivera, E.; Esmaeli, B.; Ring, S.E.; Bedikian, A.; Hortobagyi et, a. Phase I and

pharmacokinetic study of ABI-007, a Cremophor-free, protein-stabilized, nanoparticle formulation of paclitaxel. Clin. Cancer Res. **2002**, *8* (5): p. 1038-1044.

3. Muller, R.H.; Keck, C.M. Challenges and solutions for the delivery of biotech drugs - a review of drug nanocrystal technology and lipid nanoparticles. J. Biotech. **2004**, *113* (1-3): p. 151-170.

4. Yu, L. Amorphous pharmaceutical solids: preparation, characterization and stabilization. Adv. Drug. Del. Rev. **2001**, *48* (1): p. 27-42.

5. Grant, D.J.W.; Brittian, H.G., *Physical Characterization of Pharmaceutical Solids*, ed. H.G. Brittian. 1995, New York: Marcel Dekker.

6. Russel, W.R.; Saville, D.A.; Schowalter, W.R., *Colloidal Dispersions*. 1989, Cambridge: Cambridge University Press.

7. Garcia-Fuentes, M.; Torres, D.; Alonso, M.J. Design of lipid nanoparticles for the oral delivery of hydrophilic macromolecules. Colloids Surf. B Biointerfaces **2003**, *27* (2-3): p. 159-168.

8. Madras, G.; McCoy, B.J.B.J. Temperature effects on the transition from nucleation and growth to Ostwald ripening. Chem. Eng. Sci. **2004**, *59* (13): p. 2753-2765.

9. Dollo, G.; Le Corre, P.; Guerin, A.; Chevanne, F.; Burgot, J.L.; Leverge, R. Spray-dried redispersible oil-in-water emulsion to improve oral bioavailability of poorly soluble drugs. Eur. J. Pharm. Sci. **2003**, *19* (4): p. 273-280.

10.   Eerikainen, H.; Watanabe, W.; Kauppinen, E.I.; Ahonen, P.P. Aerosol flow reactor method for synthesis of drug nanoparticles. Eur. J. Pharm. Biopharm. **2003**, *55* (3): p. 357-360.

11.   Merisko-Liversidge, E.; Liversidge, G.G.; Cooper, E.R. Nanosizing: a formulation approach for poorly-water-soluble compounds. Eur. J. Pharm. Sci. **2003**, *18* (2): p. 113-120.

12.   Krause, K.P.; Muller, R.H. Production and characterisation of highly concentrated nanosuspensions by high pressure homogenisation. Int. J. Pharm. **2001**, *214* (1-2): p. 21-24.

13.   Date, A.A.; Patravale, V.B. Current strategies for engineering drug nanoparticles. Curr. Op. Colloid Interface Sci. **2004**, *9* (3-4): p. 222-235.

14.   Rogers, T.L.; Johnston, K.P.; Williams, R.O., 3rd Solution-based particle formation of pharmaceutical powders by supercritical or compressed fluid CO2 and cryogenic spray-freezing technologies. Drug Dev. Ind. Pharm. **2001**, *27* (10): p. 1003-1015.

15.   Hu, J.; Johnston, K.P.; Williams, R.O., 3rd Nanoparticle engineering processes for enhancing the dissolution rates of poorly water soluble drugs. Drug Dev. Ind. Pharm. **2004**, *30* (3): p. 233-245.

16.   Rogers, T.L.; Gillespie, I.B.; Hitt, J.E.; Fransen, K.L.; Crowl, C.A.; Tucker, C.J.; Kupperblatt, G.B.; Becker, J.N.; Wilson, D.L.; Todd et, a. Development and characterization of a scalable controlled precipitation process to enhance the

dissolution of poorly water-soluble drugs. Pharm. Res. **2004**, *21* (11): p. 2048-2057.

17.   Sarkari, M.; Brown, J.; Chen, X.; Swinnea, S.; Williams, I., Robert O.; Johnston, K.P. Enhanced drug dissolution using evaporative precipitation into aqueous solution. Int. J. Pharm. **2002**, *243* (1-2): p. 17-31.

18.   Jarmer, D.J.; Lengsfeld, C.S.; Randolph, T.W. Manipulation of particle size distribution of poly(-lactic acid) nanoparticles with a jet-swirl nozzle during precipitation with a compressed antisolvent. J. Supercrit. Fluids **2003**, *27* (3): p. 317-336.

19.   Young, T.J.; Mawson, S.; Johnston, K.P.; Henriksen, I.B.; Pace, G.W.; Mishra, A.K. Rapid expansion from supercritical to aqueous solution to produce submicron suspensions of water-insoluble drugs. Biotech. Prog., *16* (3): p. 402-407.

20.   Turk, M.; Hils, P.; Helfgen, B.; Schaber, K.; Martin, H.-J.; Wahl, M.A. Micronization of pharmaceutical substances by the Rapid Expansion of Supercritical Solutions (RESS): a promising method to improve bioavailability of poorly soluble pharmaceutical agents. J. Supercrit. Fluids **2002**, *22* (1): p. 75-84.

21.   Debuigne, F.; Cuisenaire, J.; Jeunieau, L.; Masereel, B.; Nagy, J.B. Synthesis of Nimesulide Nanoparticles in the Microemulsion Epikuron/Isopropyl Myristate/Water/n-Butanol (or Isopropanol). J. Colloid Interface Sci. **2001**, *243* (1): p. 90-101.

22. Trotta, M.; Gallarate, M.; Carlotti, M.E.; Morel, S. Preparation of griseofulvin nanoparticles from water-dilutable microemulsions. Int. J. Pharm. **2003**, *254* (2): p. 235-242.

23. Yu, Z.; Garcia, A.S.; Johnston, K.P.; Williams, I., Robert O. Spray freezing into liquid nitrogen for highly stable protein nanostructured microparticles. Eur. J. Pharm. Biopharm. **2004**, *58* (3): p. 529-537.

24. Soppimath, K.S.; Aminabhavi, T.M.; Kulkarni, A.R.; Rudzinski, W.E. Biodegradable polymeric nanoparticles as drug delivery devices. **2001**, *70* (1-2): p. 1-20.

25. Leroux, J.-C.; Allemann, E.; Doelker, E.; Gurny, R. New approach for the preparation of nanoparticles by an emulsification-diffusion method. **1995**, *41* (1): p. 14-18.

26. Muller, R.H.; Mader, K.; Gohla, S. Solid lipid nanoparticles (SLN) for controlled drug delivery - a review of the state of the art. Eur. J. Pharm. Biopharm. **2000**, *50* (1): p. 161-177.

27. Oyewumi, M.O.; Mumper, R.J. Gadolinium-loaded nanoparticles engineered from microemulsion templates. Drug Dev. Ind. Pharm. **2002**, *28* (3): p. 317-328.

28. Soga, O.; van Nostrum, C.F.; Fens, M.; Rijcken, C.J.F.; Schiffelers, R.M.; Storm, G.; Hennink, W.E. Thermosensitive and biodegradable polymeric micelles for paclitaxel delivery. J. Control. Release **2005**, *103* (2): p. 341-353.

29. Mohammed, A.R.; Weston, N.; Coombes, A.G.A.; Fitzgerald, M.; Perrie, Y. Liposome formulation of poorly water soluble drugs: optimisation of drug loading and ESEM analysis of stability. Int. J. Pharm. **2004**, *285* (1-2): p. 23-34.

30. Moghimi, S.M.; Szebeni, J. Stealth liposomes and long circulating nanoparticles: critical issues in pharmacokinetics, opsonization and protein-binding properties. Prog. Lip. Res. **2003**, *42* (6): p. 463-478.

31. Tsinontides, S.C.; Rajniak, P.; Pham, D.; Hunke, W.A.; Placek, J.; Reynolds, S.D. Freeze drying--principles and practice for successful scale-up to manufacturing. Int. J. Pharm. **2004**, *280* (1-2): p. 1-16.

32. Jones, A.R. Light scattering for particle characterization. Prog. Energ. Combust. **1999**, *25* (1): p. 1-53.

33. Freud, P.J.; Plantz, P.E. Sizing nanoparticles with dynamic light scattering. Powder and Bulk Eng. **2004**: p. 1-5.

34. Dubes, A.; Parrot-Lopez, H.; Abdelwahed, W.; Degobert, G.; Fessi, H.; Shahgaldian, P.; Coleman, A.W. Scanning electron microscopy and atomic force microscopy imaging of solid lipid nanoparticles derived from amphiphilic cyclodextrins. Eur. J. Pharm. Biopharm **2003**, *55* (3): p. 279-282.

35. Shi, H.Q.G.; Farber, L.; Michaels, J.N.; Dickey, A.; Thompson, K.C.; Shelukar, S.D.; Hurter, P.N.; Reynolds, S.D.; Kaufman, M.J. Characterization of crystalline drug nanoparticles using atomic force microscopy and complementary techniques. Pharm. Res. **2003**, *20* (3): p. 479-484.

36.   Midgley, P.A.; Weyland, M. 3D electron microscopy in the physical sciences: the development of Z-contrast and EFTEM tomography. Ultramicroscopy **2003**, *96* (3-4): p. 413-431.

37.   Bootz, A.; Vogel, V.; Schubert, D.; Kreuter, J. Comparison of scanning electron microscopy, dynamic light scattering and analytical ultracentrifugation for the sizing of poly(butyl cyanoacrylate) nanoparticles. Eur. J. Pharm. Biopharm. **2004**, *57* (2): p. 369-375.

38.   Torchilin, V.P. Fluorescence microscopy to follow the targeting of liposomes and micelles to cells and their intracellular fate. Adv. Drug Del. Rev. **2005**, *57* (1): p. 95-109.

39.   Jung, J.; Perrut, M. Particle design using supercritical fluids: Literature and patent survey. J. Supercrit. Fluids **2001**, *20* (3): p. 179-219.

40.   Song, C.X.; Labhasetwar, V.; Murphy, H.; Qu, X.; Humphrey, W.R.; Shebuski, R.J.; Levy, R.J. Formulation and characterization of biodegradable nanoparticles for intravascular local drug delivery. **1997**, *43* (2-3): p. 197-212.

41.   Rogers, T.L.; Overhoff, K.A.; Shah, P.; Santiago, P.; Yacaman, M.J.; Johnston, K.P.; Williams, I., Robert O. Micronized powders of a poorly water soluble drug produced by a spray-freezing into liquid-emulsion process. Eur. J. Pharm. Biopharm. **2003**, *55* (2): p. 161-172.

1.9 DISSERTATION OBJECTIVES AND OUTLINE

The poor aqueous solubility of a growing number of new chemical entities has created a need for technologies which can improve the dissolution performance and bioavailability of these APIs. In Chapter 1, several techniques for the formation of nanoparticles and nanoparticle delivery systems were described as well as methods for their recovery and characterization. The overall objective of this dissertation was to formulate, fully characterize and evaluate nanoparticle formulations of poorly water soluble drugs through extensive *in vitro* and *in vivo* tests. Formulations were produced and evaluated based on current needs within the pharmaceutical industry, with the aid of novel particle engineering techniques and well established animal models to evaluate the performance and safety of the delivered dose and route of administration.

To fully understand the reasons for improved performance inherent in nanoparticles and amorphous naoparticles, a battery of in vitro testing on the particle morphology, particle size, crystalline character and rate of dissolution of particles produced by SFL and EPAS was conducted in Chapter 2. The objective of this study was to evaluate and compare particle morphologies produced by the two technologies, SFL and EPAS, in order to assess how morphology impacts the enhancement of the dissolution rate of a poorly water soluble API. The particles were evaluated based on degree of crystallinity, thermal characteristics, dissolution rates and morphologies. STEM micrographs and other particle properties were analyzed in context of the particle formation mechanisms to assess the degree of miscibility of the API and polymer. It was hypothesized that the differences in the particle formation mechanisms for the EPAS and SFL processes were likely to produce differences in polymer API miscibility and subsequent API bioavailability.

The differences in morphology between particles produced by SFL and EPAS processing was evident in Chapter 2. Because of this, further testing into the ability of the formulations to supersaturate a solution and how this impacts in vivo bioavailability were evaluated. The objective of Chapter 3 was to determine the level and duration of supersaturation (apparent solubility) of a poorly water soluble API, to measure bioavailability in a mouse model and to relate the *in vitro* and *in vivo* results. The enhancement of the apparent solubility of danazol will improve the level and duration of danazol absorption *in vivo*. The bioavailability of enhanced danazol formulations was evaluated in a mouse model to determine what effect the improved solubility has on the absorption of a poorly water soluble drug. The enhanced formulations (EPAS and SFL) were compared with the physical mixture and commercial capsules (Danocrine®) as controls. The effects of the differences in the properties of these two types of particles on supersaturation and bioavailability were examined. Dissolution in Chapter 2 was conducted at sink conditions, whereas in Chapter 3 has been performed above the equilibrium solubility to evaluate supersaturation. The ability to relate bioavailability to particle properties, and *in vitro* studies of dissolution rates and supersaturation is highly useful for particle engineering of poorly water soluble drugs to achieve high bioavailability.

Much of the work up to this point had been conducted with oral delivery in mind. However, the flexibility of the particle engineering technology, SFL, allows for the production of particles which may be delivered by many routes of administration. Collaboration with The University of Texas Health Science Center in San Antonio yielded a need in the medical community to improve the treatment of invasive pulmonary fungal infections. The most convenient, therapeutic and cost effective means of treating any disease is through site directed delivery of a medication. For this reason, pulmonary delivery of an antifungal agent and its pharmacokinetics were evaluated in Chapter 4. The objective of Chapter 4 was to determine the lung and serum concentrations in mice

following pulmonary dosing of amorphous nanoparticles of itraconazole (ITZ) over a 24 hour period. The hypothesis is that sufficient serum concentrations and high lung concentrations are achieved through pulmonary dosing of amorphous ITZ nanoparticles. The serum pharmacokinetics of the inhaled ITZ nanoparticles was evaluated using a one compartment model for extravascular administration. Also, the pharmacokinetic parameters for ITZ in lung tissue over a 24 hour period were calculated using non-compartmental analysis. Lastly, the steady state partitioning of ITZ in lung tissue and serum following repeated oral and pulmonary dosing was evaluated.

The delivery of an antifungal agent directly to the lung was evaluated for and compared to other known treatments in Chapter 4. Since the ultimate goal of this project was to produce a product which will one day be used in humans to treat invasive pulmonary fungal infections, the safety of the drug and route of administration needed to be established. The objective of Chapter 5 was to evaluate the inflammatory response due to an amorphous ITZ composition and solubilizing excipients (e.g. excipient placebo) dosed directly to the lungs through histological and soluble inflammatory mediator analysis (IL-12). Uptake of itraconazole by alveolar and airway macrophages can greatly improve the treatment of invasive pulmonary fungal infections by loading of macrophages with ITZ as well as piggybacking with macrophages to sites of infection. For this reason, phagocytic uptake of ITZ by pulmonary macrophages was evaluated.

Chapter 2: Comparison of Powder Produced by Evaporative Precipitation into Aqueous Solution (EPAS) and Spray Freezing into Liquid (SFL) Technologies Using Novel Z-Contrast STEM and Complimentary Techniques

2.1 ABSTRACT

The objective of this study was to compare the properties of particles formed by nucleation and polymer stabilization (e.g. evaporative precipitation into aqueous solution (EPAS)) versus rapid freezing (e.g. spray freezing into liquid (SFL)).   Powders formed by EPAS and SFL, composed of danazol and PVP K-15 in a 1:1 ratio, were characterized using X-ray powder diffraction (XRD), modulated differential scanning calorimetry (MDSC), contact angle determination, dissolution, scanning electron microscopy (SEM), environmental scanning electron microscopy (ESEM), BET specific surface area, and Z-contrast scanning transmission electron microscopy (STEM). Large differences in particle morphologies and properties were observed and explained in terms of the particle formation mechanisms.   Both techniques produced amorphous powders with high T_g and low contact angle values.   However, STEM analysis showed highly porous bicontinuous nanostructured 30 nm particles connected by narrow bridges for SFL versus aggregated 500 nm primary particles for EPAS. The combination of STEM and other characterization techniques indicates solid solutions were formed for the SFL powders consistent with rapid freezing.   In contrast, the EPAS particle cores are enriched in hydrophobic API and the outer surface is enriched in the hydrophilic polymer, with less miscibility than in the SFL powders. Consequently, dissolution rates are faster for the SFL particles, although both techniques enhanced dissolution rates of the API.

2.2 INTRODUCTION

The influence of active pharmaceutical ingredient (API) solubilization on bioavailability has become increasingly important in the pharmaceutical industry. Many APIs are poorly water soluble with high mucosal permeability [1]. These compounds are classified as biopharmaceutical classification system II compounds for which their maximum bioavailability is limited by their rate of dissolution [2]. Improving the dissolution rate of these compounds is achieved through an increase in surface area available for dissolution by decreasing the particle size of the API and optimizing its wetting characteristics [3] or through complexation with cyclodextrins[4]. Several methods have been used to impose these characteristics on poorly soluble APIs. Milling and solution based techniques have been reviewed extensively [5-7]. Our laboratories have introduced two technologies for enhancing the dissolution rate of a poorly water soluble API by creating nanostructured particles using spray freezing into liquid (SFL) [8-17]and evaporative precipitation into aqueous solution (EPAS) techniques[18-21].

The SFL process creates micronized powders with enhanced dissolution rates. This is a particle engineering process that utilizes the atomization of a feed solution containing an API and dissolution enhancing excipient(s) directly into a cryogenic liquid, such as nitrogen. The resulting dried powder is composed of discrete microparticles where the API is molecularly dispersed with a polymer in a porous matrix. This molecular dispersion is achieved by rapid freezing in liquid nitrogen, which prevents phase separation. In previous studies, it was found that enhanced dissolution is due to the amorphous nature of the produced powder, high surface area and enhanced wettability of the SFL nanostructured particles [17]. A schematic representation of the SFL apparatus has been reported [12]. During the SFL process, the API loaded organic solvent is pressurized and atomized via a poly ether-ether ketone (PEEK) nozzle below the surface

39

of liquid nitrogen. Because of the rapid flow rate, liquid-liquid impingement and marked temperature drop in the jet, the emitted solvent is atomized into fine, high surface area microdroplets that are frozen rapidly. The suspension of frozen microdroplets is lyophilized to remove solvent, resulting in an amorphous, micronized powder.

In the EPAS process, the API precipitates due to evaporation of the organic solvent near or above the boiling point and contact with an aqueous solution. A schematic representation of the EPAS process has been reported [21]. The API loaded organic solvent is pressurized, heated and atomized through an elliptical conical stainless steel nozzle into a heated water bath containing stabilizing excipients. The large pressure drop across the small nozzle orifice creates intense atomization with rapid evaporation of the primary organic solvent due to the high temperature of the feed solution and aqueous receiving solution. The rapid evaporation of the feed solvent results in supersaturation, nucleation and precipitation of the API. The excipients within the organic feed solution and/or aqueous receiving vessel stabilize the particles by preventing particle growth and recrystallization of the API precipitates. In addition, the excipients also enhanced the API particle dissolution rate and long term storage stability [21].

The morphology and performance of a nanostructured powder is expected to be highly dependent upon the particle formation process. Solid solution formation can be achieved through co-precipitation or co-melting [3, 22]. Co-precipitation and co-melting require supersaturation of the API within the matrix to be limited in time by rapid cooling and rapid removal of solvent so as to inhibit agglomeration of API particles. Solid dispersion formation is achieved through supersaturation and precipitation of the API within the matrix similar to solid solution formation. However, solid dispersions are formed during processes where nucleation and growth of the particles occurs to varying extents or through fusion of the component particles[23].

Because of the nanoscale size of API domains achieved through EPAS and SFL processing, it is difficult to evaluate the particle size and morphology of the powders.

Techniques used to evaluate products formed by particle engineering technologies typically include dissolution, x-ray powder diffraction, particle size analysis (laser light scattering or dynamic light scattering), contact angle and surface area analysis. More recently, several authors have utilized atomic force microscopy (AFM) to evaluate nanoparticles adsorbed on to the surface of glass or a film [24-27]. This technique, although useful for assessment of particles, requires that a dispersion be formed and surrounding excipients be removed from the API. This limits the technique for assessment of colloidal dispersions and other dispersible solids. Also, transmission electron microscopy (TEM), in conjunction with staining materials, has been used to evaluate the presence and size of API domains within an excipient matrix [8, 28-30]. Z-contrast TEM or STEM dark-field imaging is a novel method for high resolution viewing of API/excipient mixtures without the use of electron density staining or dispersion formation and drying. This tomography process has been used in the semiconductor industry and requires the use of a high-angle annular dark field (HAADF) detector [31]. The high-angle scattering is associated with electron interaction close to the nucleus of the atom. For this reason, the detector is very sensitive to compositional changes and thickness within the specimen. It has not been used previously on pharmaceutical formulations and could prove to be a valuable asset to researchers investigating and characterizing nanoparticles where dispersion in a solvent or staining can remove or mask important morphological features.

The objective of this study was to evaluate and compare particle morphologies produced by the two technologies, SFL and EPAS, in order to assess how morphology impacts the enhancement of the dissolution rate of a poorly water soluble API. The particles were evaluated based on degree of crystallinity, thermal characteristics, dissolution rates and morphologies. The high magnification in Z contrast STEM provides a clearer view of the morphology at the primary particle level than SEM. STEM micrographs and other particle properties were analyzed in context of the particle

formation mechanisms to assess the degree of miscibility of the API and polymer. In the organic SFL solution, both polymer and API nucleate and grow to form amorphous domains during the rapid freezing [10]. In contrast, the presence of an organic-water interface and an aqueous external phase in EPAS provides a driving force during nucleation and growth for the core of the particles to be enriched in hydrophobic API and the outer surface to be enriched in the hydrophilic polymer [21]. Only small amounts of polymer are required at the outer surface to stabilize the particles [19], API/stabilizer ratios have been as high as 93% for particles with surface areas of 3 m^2/g. It is hypothesized that the differences in the particle formation mechanisms for the EPAS and SFL processes are likely to produce differences in polymer API miscibility and subsequent API bioavailability.

2.3 MATERIALS AND METHODS

2.3.1 Materials

Micronized danazol, sodium lauryl sulfate (SDS), polyvinylpyrrolidone (PVP) K-15 and 1.0N hydrochloric acid (HCl) solution were purchased from Spectrum Chemicals (Gardena, CA). High performance liquid chromatography (HPLC) grade acetonitrile and dichloromethane were obtained from EM Science (Gibbstown, NJ).

2.3.2 Preparation of SFL Micronized Powder

A solution of 0.2% w/v danazol and 0.2% w/v PVP K15 was prepared in acetonitrile. Aliquots of the solution were loaded into a high pressure solution cell and atomized beneath the liquid nitrogen surface at 50 ml/min constant flow through a 127

μm I.D. PEEK nozzle. The PEEK tubing acted as an insulating nozzle that prevented freezing within the nozzle orifice. The constant pressure was supplied by an ISCO syringe pump (Model 100DX; ISCO, Inc., Lincoln, NE). Because of the low viscosity of the acetonitrile API solution, a pressure of only 3000 psi was required to produce a flow rate of 50 ml/min. The frozen microparticles were collected and dried by a VirTis Advantage Tray Lyophilizer (The VirTis Company, Inc. Gardiner, NY). The final powder was protected from moisture and stored under vacuum.

2.3.3 Preparation of EPAS Micronized Powder

A solution of 2% w/v danazol and 1% w/v PVP K-15 was prepared in dichloromethane. This solution was pumped via an HPLC pump at 2 ml/min through a heat exchange coil set at 80°C. After heating, the solution was sprayed under constant pressure of 5000 psi through fine, elliptical, conical nozzle, formed by crimping 0.030 inch I.D. stainless steel tubing, at ~5000 psi constant pressure into a heated water bath (80°C) containing 1% w/v PVP K-15 of equal volume. The resultant dispersion was quenched by injecting it into liquid nitrogen via a syringe and needle and lyophilized to form powder. The final powder was protected from moisture and stored under vacuum.

2.3.4 Preparation of Co-ground Physical Mixture

A co-ground physical mixture consisting of 3.0 g danazol and 3.0 g PVP was mixed by geometric dilution and ground using a mortar and pestle.

2.3.5 X-Ray Powder Diffraction (XRD)

A Philips 1710 X-ray diffractometer with a copper target and nickel filter (Philips Electronic Instruments, Inc., Mahwah, NJ) was used to obtain the XRD patterns of the samples. Powder samples were loaded onto aluminum stages having a glass bottom and leveled to a uniform height. The XRD pattern of the leveled powder was measured from 5 to 50 2Θ degrees using a step size of 0.05 2θ degrees and a dwell time of 1 sec at each step.

2.3.6 Modulated Differential Scanning Calorimetry (MDSC)

Samples in the range of 10 – 15 mg of processed and bulk powders were added to crimp sealed aluminum pans and measured on a TA Instruments model 2820 MDSC (New Castle, DE). Samples were heated at a rate of 3°C/min from 50 – 250°C at a modulating oscillatory frequency of 1.7°C/min. Samples were purged with nitrogen gas at 150 ml/min. Glass transition temperatures were measured at the midpoint of the step transition. The MDSC was calibrated using an indium standard.

2.3.7 Surface Area Analysis

The specific surface area of the prepared powders was measured using a NOVA-2000 Version 6.11 instrument with NOVA Enhanced Data Reduction Software Version 2.13 (Quantachrome Corporation, Boynton Beach, FL). A known amount of powder (~200 mg) was loaded into a Quantachrome sample cell and degassed for at least 3 hr prior to analysis.

2.3.8 Contact Angle Measurement

A 100 mg aliquot of powder was compacted using a Model M Carver Laboratory Press (Fred S. Carver, Inc., Menomonee Falls, WI). The powder pellet was formed with a 500 kg compression force. A 0.03 ml drop of SDS/Tris dissolution media was placed on the compact, and the contact angle between the sample and media was measured using a Model 100-00-115 Goniometer (Ramè-Hart Inc., Mountain Lakes, NJ).

2.3.9 Scanning Electron Microscopy (SEM)

A Hitachi S-4500 field emission scanning electron microscope was used to obtain SEM micrographs of the powder samples which had been gold-palladium sputter coated prior to analysis for 45 sec. An accelerating voltage of 5 kV was used.

2.3.10 Environmental Scanning Electron Microscopy (ESEM)

The powder was added to a 1cm diameter aluminum sample holder and observed using an Enviroscan 2020 (FEI Company, Hillsboro, Oregon) environmental scanning electron microscope with EVEX EDS. The chamber was held constant at 2 torr with an accelerating voltage of 20 kv.

2.3.11 Transmission Electron Microscopy

Samples of the dried powders were placed on 200-mesh carbon-coated copper grids (Electron Microscopy Sciences, Fort Washington, PA) and viewed on a JEOL 2010F transmission electron microscope (JEOL USA, Inc, Peabody, Massachusetts) with a HAADF STEM detector.

2.3.12 Dissolution

Dissolution testing was performed using a United States Pharmacopeia 27 (USP) apparatus II VanKel VK6010 Dissolution Testing Station with a Vanderkamp VK650A heater/circulator (Varian, Inc., Palo Alto, CA). The inherent low aqueous solubility of danazol required that a solubilizing agent be employed to allow for sufficient wetting and to ensure sink conditions for the powders which were evaluated. Aliquots of 10-15 mg of powder were weighed and placed into 900 ml of SDS/Tris dissolution media. A volume of 5 mL was collected at 2, 5, 10, 20, 30, and 60 min (n=6) using a VK8000 autosampler (Varian Inc., Cary, NC). Paddle speed and bath temperature were set at 50 rpm and 37.0±0.2 °C, respectively. A 20L volume of dissolution media was prepared consisting of 150 g SDS and 242 g Tris that was pH adjusted to 9.0 using 1 N HCl. The collected samples were filtered and evaluated via HPLC at 288 nm using a Shimadzu LC-10 liquid chromatograph (Shimadzu Corporation, Columbia, MD) equipped with an Alltech 5 μm Inertsil ODS-2 C18 reverse-phase column (Alltech Associates, Inc., Deerfield, IL). The danazol peak eluted at 5 min when running mobile phase (70% acetonitrile/30% water, v/v) at 1 ml/min.

2.4 RESULTS

2.4.1 Glass transition and contact angles

PVP has been demonstrated to increase the stability of amorphous APIs, by increasing the glass transition temperature (Tg) [32]. Also, PVP has been shown to increase dissolution rates through rapid dispersion upon contact with aqueous media [33]. Table 2.1 shows the glass transition temperatures of the binary mixtures achieved through

each of the technologies studied. The Tg for SFL and EPAS particles were 123.1°C and 143.2°C, respectively. These are lower than both the physical mixture (154.5°C) and bulk PVP (162.1°C). MDSC analysis yielded a high, single Tg for the SFL and EPAS particles (Table 2.1), which is important for stabilization purposes[34]. Due to higher mobility of the amorphous API particles near the glass transition temperature, it is important that the Tg be 50°C above the highest storage temperature in order to prevent crystallization [35].

The Gordon-Taylor equation predicts the glass transition temperature (T_{g12}) for binary mixtures and assumes miscibility and additive free volume of the substrates where w_1 and w_2 are the weight fractions of the individual components and T_{g1} and T_{g2} are their glass transition temperatures.

$$T_{g12} = \frac{w_1 T_{g1} + K w_2 T_{g2}}{w_1 + K w_2}$$

The constant K is defined by Sihma-Boyer rule where T_{g1} and T_{g2} are the glass transition temperatures of the individual components and ρ_1 and ρ_2 are their densities.

$$K \approx \frac{T_{g1} \rho_1}{T_{g2} \rho_2}$$

The Tg for binary mixes of PVP and danazol were calculated as 122°C using the Gordon-Taylor equation. This predicted value deviated from the measured values of the binary mixes prepared using SFL and EPAS processes. It has been reported that deviation from the Gordon-Taylor equation is through non-uniform distribution of free volumes within the binary mixture[36]. Since the Tg for the mixture processed by SFL (123.1°C) is near the predicted value, the components are highly miscible in a solid solution. The Tg for the EPAS powder (143.1°C) is near the midpoint of the Tg of PVP (162.1°C) and the calculated value for an ideally mixed solution. The significantly larger Tg indicates that a larger fraction of the components is present in a non-uniform distribution of the free volumes. This difference will be shown below to be consistent with the larger primary particle size. The Tg of the physical mixture was 154.5°C, only

8°C below that of pure PVP indicating a small amount of miscibility perhaps because of heat increased surface area caused by friction due to mixing using the mortar and pestle. Both EPAS and SFL processed binary mixtures exhibited a greater depression in Tg compared to the physical binary mixtures due to a greater degree of mixing and miscibility.

Similar contact angles were observed for EPAS and SFL powders as shown in (Table 2.2). The contact angles for aqueous dissolution media on the EPAS and SFL compressed pellets were 26.6° and 28°, respectively, compared to 64.3° for bulk danazol and 37.6° for the physical mixture (data not shown). The low contact angles, or high hydrophilicities suggest significant mixing between the API and stabilizer. For example, if they were completely unmixed in the SFL powder, it is likely the more hydrophobic component, danazol, would favor the surface due to lower surface energy. Instead a highly hydrophilic surface was present suggesting that the components were mixed with a substantial amount of PVP at the surface, consistent with the Tg measurements. The high wettability of the powders is likely to aid dissolution rates as will be shown below.

2.4.2 X-ray Powder Diffraction

The degree of crystallinity in the PVP/danazol mixtures will influence the dissolution rate of the processed powders. The XRD patterns for the bulk danazol, physical mixture control and processed danazol are shown in Figure 2.1. The bulk micronized danazol, as received, displayed characteristic 2θ crystalline peaks between 13 and 22.2°. Although with less intense peaks due to dilution, the physical mixture showed a high degree of crystallinity. The XRD pattern for SFL powder lacked crystalline peaks, indicating a completely amorphous morphology as has been seen previously for SFL processed API [10, 11, 14, 17]. The EPAS powder demonstrated a slight peak at the location of the major peak for danazol, indicating a small degree of crystallinity,

significantly lower than that of the bulk danazol and physical mixture. In contrast, highly crystalline danazol was produced by EPAS when PVP was used as a stabilizer in the aqueous phase, without using a stabilizer in the organic phase [19]. It is possible that the growing particles crystallized in the aqueous media before enough of the stabilizer (PVP) reached the surface of the particles. Another difference is that the API:surfactant ratio was higher in the previous study which could have prevented the PVP from effectively inhibiting crystallization during particle formation, or after the particles were dried.

The major difference in the present study was that PVP was the only excipient stabilizer, and it was included in both the organic and aqueous phases. As the particles nucleate and grow in the shrinking organic phase droplets during evaporation, the PVP is likely to protect the particle surface more effectively and inhibit crystal growth. Rasenack et al found that by changing processing conditions or through excipient/stabilizer selection, amorphous API could be formed through precipitation processes [37].

2.4.3 Surface Morphology

The morphological characteristics of the EPAS and SFL processed powders were examined using ESEM and SEM. Figures 2.2a and 2.2b show the ESEM micrographs of the powders formed by EPAS and SFL, respectively. The ESEM of the EPAS powder showed a 7-10 μm aggregate composed of many discrete primary nanoparticles that were less than 1 μm in size. The ESEM micrograph of the SFL powder demonstrates a highly porous structure, composed of a nanostructured network of particles. This finding is similar to the SEM micrographs of the SFL powders shown in Figures 2.3a and 2.3b. From the SEM it is evident that the particles formed by the SFL process are highly porous and composed of a nanostructured lattice of polymer and API. The specific surface area shown in Table 2.2 illustrates the differences in porosity and primary particle

sizes seen in the SFL and EPAS particles, with surface areas of 52.26 m^2/g and 7.41 m^2/g, respectively.

2.4.4 Scanning Transmission Electron Microscopy

High resolution z-contrast STEM was utilized to view the internal morphology of the SFL and EPAS processed powders through mass density analysis. The contrast variation in the STEM is proportional to the mass density of the region multiplied by the atomic number squared (Z) [31]. Regions of high mass density are shown in white. Since the atomic composition and mass density are similar between danazol and PVP, the contrast in the micrographs indicates an overall mass density. These micrographs do not provide direct compositional analysis of the API and polymer mixtures at a given point.

The STEM micrographs of the SFL processed powder are shown in Figures 2.4a and 2.4b and demonstrate a diffuse grey pattern throughout the particle. Low contrast variation is seen in the mass density throughout the highly interconnected particles, which is indicative of small domain sizes or lack of any large danazol/PVP enriched areas. Bicontinuous curvature is present with regions curved about particles and, in the necks or bridges between particles, regions curved about the pores. It is possible that the bicontinuous curvature indicates spinodal decomposition, although it is very difficult to conclusively delineate the boundary between nucleation and growth and spinodal decomposition [38].   Certainly the rapid freezing rates have the potential to enter the spinodal decomposition region. The areas of high electron density represent overlapping bridges within the porous SFL particle.   The STEM micrograph of the EPAS processed powder is shown in Figure 2.4c and 2.4d. High contrast variation is evident throughout the EPAS powder due to much larger API/polymer domains. Discrete particles can be seen in the powder through the variations in mass density. These particles are much larger than those produced by SFL. They are not connected by bridges and bicontinuous

curvature is not present. The differences in these morphologies are much more apparent in STEM than SEM due to the higher magnification and resolution.

2.4.5 Dissolution

The dissolution profile shown in Figure 2.5 illustrates the enhanced dissolution rate achieved through SFL and EPAS processed powders compared to non-processed, bulk danazol. Within the first two minutes, the dissolution of the API was nearly 100% for the SFL powder, compared to 80% for the EPAS processed powder and 40% for bulk danazol, respectively. Within 10 minutes, the SFL and EPAS dissolution rates were statistically similar, and were statistically much higher than for the bulk danazol.

2.5 DISCUSSION

The mechanisms of particle formation for the SFL and EPAS technologies differ, and a direct comparison of how these differences affect the particle morphology has not been reported previously. The combination of the MDSC data, the high contrast/high resolution STEM micrographs and an analysis of the phase separation mechanisms in the processes will provide insight into the changes in composition of the particles from the core to the outer surface. The application of the three synergistic methods provides a more detailed description of particle morphology than has been available previously.

The porous morphologies seen in the SEM of SFL particles were composed of nanostructured API-polymer networks on the order of 500nm in diameter. The high porosity is achieved through the rapid freezing, liquid-liquid impingement and intense atomization. The freezing rate is sufficient such that separation of API and polymer is inhibited and pores are generated by the removal of the solvent during lyophilization.

This significantly improves wettability and allows for close proximity of the API to the dissolution media resulting in enhanced wetting and dissolution of API. There are no distinct particle domains indicated on the STEM micrograph. The lack of distinct particles illustrates a dispersion on the molecular level, which is indicative of a solid solution. This is consistent with the hypothesis that the freezing process and nucleation during co-evaporation creates much smaller particle domains than does EPAS processing. This is due to the molecular dispersion of the danazol within the PVP that extends beyond the magnification of the STEM.

EPAS particles, in contrast, were aggregates of larger nanoparticles composed of danazol and PVP according to the ESEM analysis. The smaller number of fine pores reflected the larger primary particles due to particle formation in solution rather than particle formation during freezing. High surface areas were not generated during quench freezing due to the slower freezing rate (quench freezing vs. atomization into liquid nitrogen) and higher concentration of API and stabilizer within the frozen material. Since the rate of freezing is slower with quench freezing compared to freezing of atomized droplets, segregation of particles and dissolved solids can occur, yielding lower surface areas [10]. The lack of fine pores indicates that the solvent was not located within these 8-10 μm aggregates since they were formed prior to freeze quenching. The larger primary particle size could be the reason for the smaller surface area and porosity observed in the ESEM micrograph, compared to the SFL particles. These findings were further established through BET specific surface area measurements, where the SFL particles showed significantly higher specific surface area, due to high porosity and a nanostructured network of polymer and API. Through Z-contrast STEM analysis; micrographs of the EPAS processed powders show distinct particles due to variations in the mass density which caused contrast changes throughout the powder. This further corroborates the results shown in ESEM as well as the establishment of prior particle precipitation and solid dispersion formation.

The SFL process created high surface area, porous, particles composed of submicron primary particles through rapid freezing followed by lyophilization to remove solvent. Betagari, et al. reported that the physical traits of a solid solution or solid dispersion formed by lyophilization from a solvent is dependent on the freezing process [39]. Solid solution formation requires that all components be soluble in the solvent during processing [3]. Because of the rapid freezing of a co-dissolved solution of API and stabilizer, the co-precipitation may create a solid solution of amorphous API intermingled with the polymer chain network. The solid solution may be preserved during sublimation of the solvent during lyophilization.

In contrast, the EPAS process creates particles through precipitation in an aqueous solution, where the stabilizer (PVP K-15) is soluble. However, if during EPAS, stabilizer is contained in the organic phase, co-precipitation would be possible as the organic solvent evaporates. Even though the PVP is soluble in water, the chemical potential of PVP in the water appeared to be sufficient to prevent the PVP from leaving the amorphous solid solution in the nonaqueous phase. It appeared that the precipitated particles remain amorphous during the EPAS process due to stabilization by the PVP polymer chains in the amorphous solid solution. Several authors have reported that the inhibitory effect of PVP on crystallization is due to its molecular interaction with the supersaturated API during co-precipitation from a solvent [36, 40]. Also, inhibition of crystallization is dependent on API type, API/PVP ratio and the molecular weight and viscosity of the PVP. Previous studies on EPAS have shown that crystallization inhibition does not occur for all APIs when using PVP [21]. The XRD results show that both the SFL and EPAS technologies, when using this API/PVP ratio created amorphous danazol. Also, the single Tg peaks, depressed from that of pure PVP, indicate varying degrees of mixing of danazol within the polymer. Favorable intermolecular interactions between PVP and danazol would aid solid solution formation. Taylor et al reported that a binary mixture of indomethacin and PVP formed by solvent evaporation created a

powder consistent with a glass or a non-equilibrium supercooled liquid due to interactions on the molecular level [36].

The contributions of each of the previously mentioned attributes of SFL and EPAS powders on dissolution rate were evident in this study. SFL powders had significantly higher dissolution rate compared to both EPAS powders and bulk danazol within the first 2 minutes of dissolution testing. The higher surface area and greater miscibility of API and PVP in the powders led to the more rapid dissolution of danazol. True solid solutions will dissolve at a rate comparable to the dissolution rate of the stabilizer of a binary mixture under sink conditions [3]. Since PVP is highly soluble in the dissolution media, the dissolution rates of the PVP/API solid solution are enhanced. Since EPAS produced powders have lower porosity, larger primary particle sizes, lower surface area, and less miscibility between the API and PVP, the dissolution rate is slower than that of the SFL powders. However, the surface area is still relatively large and the particles are wetted rapidly leading to significantly faster dissolution than for bulk danazol. Also, after the first two minutes, the rate of dissolution closely resembles that of crystalline bulk danazol. As was indicated through XRD, the EPAS powders were partially crystalline. API that has been rendered amorphous display significantly faster dissolution rate compared to crystalline materials [41]. Taylor and Zografi indicated that the rate of dissolution of binary mixtures of amorphous and crystalline material would show a change in rate following complete dissolution of the amorphous material [36].

2.6 CONCLUSIONS

Through the use of several characterization techniques, it was shown that the SFL and EPAS technologies form large surface area, wettable powders with rapid dissolution. The STEM revealed 30 nm primary domains in SFL particles and several 100 nm primary domains in EPAS particles, providing unparalleled contrast in mass density

across these domains. Based on STEM analysis, measurement of Tg, and the mechanisms of the processes, the SFL process forms powders consistent with a solid solution, whereas EPAS powders tend to be enriched in API towards the center and more enriched in PVP near the surface with a lower degree of miscibility between components. The ability to view contrast in mass density across primary particles on the order of 30 nm offers new insight into particle formation mechanisms that is useful for designing processes and formulations for poorly water soluble APIs with high dissolution rates.

2.7 ACKNOWLEDGMENTS

2.8 REFERENCES

[1]   J.B. Dressman and C. Reppas, In vitro-in vivo correlations for lipophilic, poorly water-soluble drugs, Eur. J. Pharm. Sci. 11 (2000) S73-S80.

[2]   D. Horter and J.B. Dressman, Influence of physicochemical properties on dissolution of drugs in the gastrointestinal tract, Adv. Drug Deliv. Rev. 46 (2001) 75-87.

[3]   C. Leuner and J. Dressman, Improving drug solubility for oral delivery using solid dispersions, Eur. J. Pharm. Biopharm. 50 (2000) 47-60.

[4]   S.I.F. Badawy, A.L. Marshall, M.M. Ghorab, and C.M. Adeyeye, A study of the complexation between danazol and hydrophilic cyclodextrin derivatives, Drug Dev. Ind. Pharm. 22 (1996) 959-966.

[5]   T.L. Rogers, K.P. Johnston, and R.O. Williams, Solution-based particle formation of pharmaceutical powders by supercritical or compressed fluid CO2 and cryogenic spray-freezing technologies, Drug Dev. Ind. Pharm. 27 (2001) 1003-1015.

[6]   E. Reverchon, Supercritical antisolvent precipitation of micro- and nano-particles, J. Supercrit. Fluids 15 (1999) 1-21.

[7]   J.H. Hu, K.P. Johnston, and R.O. Williams, Nanoparticle engineering processes for enhancing the dissolution rates of poorly water soluble drugs, Drug Dev. Ind. Pharm. 30 (2004) 233-245.

[8]   T.L. Rogers, K.A. Overhoff, P. Shah, P. Santiago, M.J. Yacaman, K.P. Johnston, and R.O. Williams, Micronized powders of a poorly water soluble drug produced by a spray-freezing into liquid-emulsion process, Eur. J. Pharm. Biopharm. 55 (2003) 161-172.

[9]   T.L. Rogers, A.C. Nelsen, M. Sarkari, T.J. Young, K.P. Johnston, and R.O. Williams, Enhanced aqueous dissolution of a poorly water soluble drug by novel particle engineering technology: Spray-freezing into liquid with atmospheric freeze-drying, Pharm. Res. 20 (2003) 485-493.

[10]   T.L. Rogers, A.C. Nelsen, J.H. Hu, J.N. Brown, M. Sarkari, T.J. Young, K.P. Johnston, and R.O. Williams, A novel particle engineering technology to enhance

dissolution of poorly water soluble drugs: spray-freezing into liquid, Eur. J. Pharm. Biopharm. 54 (2002) 271-280.

[11] T.L. Rogers, K.P. Johnston, and R.O. Williams, Physical stability of micronized powders produced by spray-freezing into liquid (SFL) to enhance the dissolution of an insoluble drug, Pharm. Dev. Technol. 8 (2003) 187-197.

[12] T.L. Rogers, J.H. Hu, Z.S. Yu, K.P. Johnston, and R.O. Williams, A novel particle engineering technology: spray-freezing into liquid, Int. J. Pharm. 242 (2002) 93-100.

[13] Z.S. Yu, T.L. Rogers, J.H. Hu, K.P. Johnston, and R.O. Williams, Preparation and characterization of microparticles containing peptide produced by a novel process: spray freezing into liquid, Eur. J. Pharm. Biopharm. 54 (2002) 221-228.

[14] J.H. Hu, T.L. Rogers, J. Brown, T. Young, K.P. Johnston, and R.O. Williams, Improvement of dissolution rates of poorly water soluble APIs using novel spray freezing into liquid technology, Pharm. Res. 19 (2002) 1278-1284.

[15] J.H. Hu, K.P. Johnston, and R.O. Williams, Rapid dissolving high potency danazol powders produced by spray freezing into liquid process, Int. J. Pharm. 271 (2004) 145-154.

[16] J.H. Hu, K.P. Johnston, and R.O. Williams, Stable amorphous danazol nanostructured powders with rapid dissolution rates produced by spray freezing into liquid, Drug Dev. Ind. Pharm. 30 (2004) 695-704.

[17]   J.H. Hu, K.P. Johnston, and R.O. Williams, Spray freezing into liquid (SFL) particle engineering technology to enhance dissolution of poorly water soluble drugs: organic solvent versus organic/aqueous co-solvent systems, Eur. J. Pharm. Sci. 20 (2003) 295-303.

[18]   X. Chen, Z. Benhayoune, R.O. Williams, and K.P. Johnston, Rapid dissolution of high potency itraconazole particles produced by evaporative precipitation into aqueous solution, J. Drug Deliv. Sci. Technol. 14 (2004) 299-304.

[19]   X.X. Chen, J.M. Vaughn, M.J. Yacaman, R.O. Williams, and K.P. Johnston, Rapid dissolution of high-potency danazol particles produced by evaporative precipitation into aqueous solution, J. Pharm. Sci. 93 (2004) 1867-1878.

[20]   X.X. Chen, T.J. Young, M. Sarkari, R.O. Williams, and K.P. Johnston, Preparation of cyclosporine A nanoparticles by evaporative precipitation into aqueous solution, Int. J. Pharm. 242 (2002) 3-14.

[21]   M. Sarkari, J. Brown, X.X. Chen, S. Swinnea, R.O. Williams, and K.P. Johnston, Enhanced drug dissolution using evaporative precipitation into aqueous solution, Int. J. Pharm. 243 (2002) 17-31.

[22]   B. Rambali, G. Verreck, L. Baert, and D.L. Massart, Itraconazole formulation studies of the melt-extrusion process with mixture design, Drug Dev. Ind. Pharm. 29 (2003) 641-652.

[23]   B.M. Tashtoush, Z.S. Al-Qashi, and N.M. Najib, In vitro and in vivo evaluation of glibenclamide in solid dispersion systems, Drug Dev. Ind. Pharm. 30 (2004) 601-607.

[24] I. Montasser, H. Fessi, and A.W. Coleman, Atomic force microscopy imaging of novel type of polymeric colloidal nanostructures, Eur. J. Pharm. Biopharm. 54 (2002) 281-284.

[25] H. Sato, T. Ohtsu, and I. Komasawa, Atomic force microscopy study of ultrafine particles prepared in reverse micelles, J. Colloid Interface Sci. 230 (2000) 200-204.

[26] N. Masaki, K. Machida, H. Kado, K. Yokoyama, and T. Tohda, Molecular-Resolution Images of Aspirin Crystals with Atomic Force Microscopy, Ultramicroscopy 42 (1992) 1148-1154.

[27] H.Q.G. Shi, L. Farber, J.N. Michaels, A. Dickey, K.C. Thompson, S.D. Shelukar, P.N. Hurter, S.D. Reynolds, and M.J. Kaufman, Characterization of crystalline drug nanoparticles using atomic force microscopy and complementary techniques, Pharm. Res. 20 (2003) 479-484.

[28] S.C. Yang and J.B. Zhu, Preparation and characterization of camptothecin solid lipid nanoparticles, Drug Dev. Ind. Pharm. 28 (2002) 265-274.

[29] T. Banerjee, S. Mitra, A.K. Singh, R.K. Sharma, and A. Maitra, Preparation, characterization and biodistribution of ultrafine chitosan nanoparticles, Int. J. Pharm. 243 (2002) 93-105.

[30] L.M. Lacava, B.M. Lacava, R.B. Azevedo, Z.G.M. Lacava, N. Buske, A.L. Tronconi, and P.C. Morais, Nanoparticle sizing: a comparative study using atomic force microscopy, transmission electron microscopy, and ferromagnetic resonance, J. Magn. Magn. Mater. 225 (2001) 79-83.

[31] P.A. Midgley and M. Weyland, 3D electron microscopy in the physical sciences: the development of Z-contrast and EFTEM tomography, Ultramicroscopy 96 (2003) 413-431.

[32] G. Van den Mooter, M. Wuyts, N. Blaton, R. Busson, P. Grobet, P. Augustijns, and R. Kinget, Physical stabilisation of amorphous ketoconazole in solid dispersions with polyvinylpyrrolidone K25, Eur. J. Pharm. Sci. 12 (2001) 261-269.

[33] A.S. Kearney, D.L. Gabriel, S.C. Mehta, and G.W. Radebaugh, Effect of Polyvinylpyrrolidone on the Crystallinity and Dissolution Rate of Solid Dispersions of the Antiinflammatory Ci-987, Int. J. Pharm. 104 (1994) 169-174.

[34] S. Corveleyn and J.P. Remon, Stability of freeze-dried tablets at different relative humidities, Drug Dev. Ind. Pharm. 25 (1999) 1005-1013.

[35] L. Yu, Amorphous pharmaceutical solids: preparation, characterization and stabilization, Adv. Drug Deliv. Rev. 48 (2001) 27-42.

[36] L.S. Taylor and G. Zografi, Spectroscopic characterization of interactions between PVP and indomethacin in amorphous molecular dispersions, Pharm. Res. 14 (1997) 1691-1698.

[37] N. Rasenack, H. Hartenhauer, and B.W. Muller, Microcrystals for dissolution rate enhancement of poorly water-soluble drugs, Int. J. Pharm. 254 (2003) 137-145.

[38] D.J. Dixon, K.P. Johnston, and R.A. Bodmeier, Polymeric Materials Formed by Precipitation with a Compressed Fluid Antisolvent, Aiche J. 39 (1993) 127-139.

[39]   G.V. Betageri and K.R. Makarla, Enhancement of dissolution of glyburide by solid dispersion and lyophilization techniques, Int. J. Pharm. 126 (1995) 155-160.

[40]   M. Yoshioka, B.C. Hancock, and G. Zografi, Inhibition of Indomethacin Crystallization in Poly(Vinylpyrrolidone) Coprecipitates, J. Pharm. Sci. 84 (1995) 983-986.

[41]   A.R. Paradkar, B. Chauhan, S. Yamamura, and A.P. Pawar, Preparation and characterization of glassy celecoxib, Drug Dev. Ind. Pharm. 29 (2003) 739-744.

Chapter 3: Supersaturation Produces High Bioavailability of Amorphous Danazol Particles Formed by Evaporative Precipitation into Aqueous Solution (EPAS) and Spray Freezing into Liquid (SFL) Technologies

3.1 ABSTRACT

The bioavailability of high surface area danazol formulations was evaluated in a mouse model to determine what effect high supersaturation, as measured in vitro, has on the absorption of a poorly water soluble drug. Danazol, a biopharmaceutics classification system II (BCS II) compound, was used as the model drug. Evaporative precipitation into aqueous solution (EPAS) and spray freezing into liquid (SFL) technologies were used to prepare powders of danazol/PVP K-15 in a 1:1 ratio. The EPAS and SFL compositions, physical mixture and commercial product were dosed by oral gavage to 28 male Swiss/ICR mice for each arm of the study. Time points were taken from 0.5 to 24 hours. Pooled mouse serum was analyzed for danazol by high performance liquid chromatography (HPLC). Powders were analyzed for their ability to form supersaturated solutions through dissolution at concentrations of 1mg/mL, which was the dose delivered to the mouse models. SFL and EPAS compositions displayed higher Cmax at 392.5 ng/mL and 430.1 ng/mL, respectively, compared to the physical mixture (204.4 ng/mL) and Danocrine ® (199.3 ng/mL). The Tmax for all compositions studied was near the 1 hour time point. The AUC (Table 3.1) for the SFL composition was 2558 ng.h/ml compared to EPAS composition at 1534 ng.h/ml. The AUC for the physical mixture and Danocrine ® were 672 ng.h/ml and 1519 ng.h/ml, respectively. The elimination rate

constants for the EPAS composition, SFL composition and physical mixture were similar at ~0.15 hrs^{-1} where as the Danocrine ® capsules displayed an elimination rate constant of 0.103 hrs^{-1}. The extent of danazol absorption in the mouse model was higher for SFL composition, compared to the less amorphous EPAS composition, physical mixture and Danocrine ® powders.   Both EPAS and SFL compositions were able to form supersaturated solutions. However, the SFL composition displayed higher supersaturation (33% above control) and was able to maintain supersaturation (90 min) longer than EPAS composition (27% above control, 60min).   Through the use of a testing method for supersaturation, it was found that EPAS and SFL compositions achieve higher apparent solubilities when compared to the physical mixture and commercial Danocrine® capsules. Because of the greater extent of dissolution of the SFL composition, the bioavailability was enhanced in a mouse model.

3.2 INTRODUCTION

Bioavailability enhancement of poorly water soluble active pharmaceutical ingredients (API) is key for improving existing therapies and allowing for formulation of certain new chemical entities. APIs described by the biopharmaceutics classification system (BCS) as class II display poor water solubility with high mucosal permeability. The rate limiting step for absorption of these APIs is dependent on the dissolution rate and the APIs apparent solubility. APIs which are poorly water soluble may be poorly absorbed due to a lack of sufficient concentrations of solubilized drug. Improved bioavailability of poorly water soluble API has been achieved by several means. Particle size reduction through milling [1] or formulation in a solubilized soft gelatin capsule [2] have shown improved bioavailability. Other methods include formulation with cyclodextrins [3-6], microemulsions [7-9], solid solution formation [10] and solid lipid nanoparticles[11]. Our laboratories have introduced two technologies, spray freezing into liquid (SFL) [12-21] and evaporative precipitation into aqueous solution (EPAS) [22-25], for improving bioavailability by creating nanostructured particles which show rapid dissolution and enhanced apparent solubilities.

The SFL process produces powders with surface areas from 12 to 83 and thus enhanced dissolution rates. In this particle engineering process, a feed solution containing an API and dissolution enhancing excipient(s) is atomized directly into a cryogenic liquid, such as nitrogen. The resulting dried powder is composed of discrete microparticles where the API is molecularly dispersed with a polymer in a porous matrix. [26] This molecular dispersion is achieved by rapid freezing in liquid nitrogen, which prevents phase separation. In previous studies, it was found that enhanced dissolution is due to the amorphous morphology, high surface area and enhanced wettability of the SFL nanostructured particles [21]. A schematic representation of the SFL apparatus has been

reported [16]. In the SFL process, the API loaded organic solvent is pressurized and atomized via a poly ether-ether ketone (PEEK) nozzle below the surface of liquid nitrogen. This type of atomization may be utilized for other cryogens, for example liquid CO_2.[27] Because of the rapid flow rate, liquid-liquid impingement and marked temperature drop in the jet, the emitted solvent is atomized into fine, high surface area microdroplets that are frozen rapidly. The suspension of frozen microdroplets is lyophilized to remove solvent, resulting in an amorphous, micronized powder.

In the EPAS process, the API precipitates due to evaporation of the organic solvent near or above the boiling point and contact with an aqueous solution. A schematic representation of the EPAS process has been reported [25]. The API loaded organic solvent is pressurized, heated and atomized through a nozzle, for example an elliptical conical stainless steel nozzle into a heated water bath containing stabilizing excipients. The large pressure drop across the small nozzle orifice creates intense atomization with rapid evaporation of the primary organic solvent due to the high temperature of the feed solution and aqueous receiving solution. The rapid evaporation of the feed solvent results in supersaturation, nucleation and precipitation of the API. The excipients within the organic feed solution and/or aqueous receiving vessel stabilize the particles by preventing particle growth and recrystallization of the API precipitates. In addition, the excipients also enhance the API particle dissolution rate and long term storage stability [25].

Amorphous API is metastable and upon dissolution in aqueous media, can form solutions with high degrees of supersaturation. Solid dispersions of amorphous APIs have been shown to form supersaturated dispersion *in vitro*[28-31] leading to significant improvements in bioavailability.[32] However, very few studies have related bioavailability of high surface area formulations of nanoparticles or nanostructured aggregates to in vitro studies of dissolution and supersaturation. Nanoparticles of API also display the ability to form supersaturated dispersions due to an increase in chemical

65

potential due to the high curvature and large fraction of surface molecules as described by the Kelvin equation [33, 34]. Because the bioavailability of a poorly soluble API is dependent on the solubility and concentration of drug available for absorption within the lumen of the gastrointestinal tract, the ability to increase the apparent solubility of the drug, above the equilibrium value for the crystalline form, for an extended time period will improve its bioavailability.

Danazol, which is a BCS class II compound, was utilized as a model drug to evaluate particle formation processes, supersaturation (apparent solubility enhancement) and bioavailability improvement from nanoparticles formed by EPAS and SFL. In vitro-in vivo correlations have been evaluated previously with danazol. [35, 36] Also, the bioavailability of nanoparticle danazol formulations[1], solubilized danazol[2] and cyclodextrin complexed danazol[37] has been evaluated. The effect of physiological conditions on the bioavailability of danazol has been studied.[38]

The objective of this study was to determine the level and duration of supersaturation (apparent solubility) of a poorly water soluble API, to measure bioavailability in a mouse model and to relate the *in vitro* and *in vivo* results. The enhancement of the apparent solubility of danazol will improve the level and duration of danazol absorption *in vivo*. The bioavailability of enhanced danazol formulations was evaluated in a mouse model to determine what effect the improved solubility has on the absorption of a poorly water soluble drug. The enhanced formulations (EPAS and SFL) were compared with the physical mixture and commercial capsules (Danocrine®) as controls. The bioavailability is described in terms of the new *in vitro* measurements of supersaturation, as well as other properties of the particles reported recently.[26] Briefly, the SFL composition displayed amorphous character, a primary danazol particle size of 30 nm and was consistent with a solid solution. The EPAS composition was mostly amorphous with slight crystallinity, a primary danazol particle size of 500 nm and was consistent with a solid dispersion. The effects of the differences in the properties of

these two types of particles on supersaturation and bioavailability is examined. Dissolution in the previous work was conducted at sink conditions, whereas in the current work has been performed above the equilibrium solubility to evaluate supersaturation. The ability to relate bioavailability to particle properties, and *in vitro* studies of dissolution rates and supersaturation is highly useful for particle engineering of poorly water soluble drugs to achieve high bioavailability.

3.3 MATERIALS AND METHODS

3.3.1 Materials

Micronized danazol, polyvinylpyrrolidone (PVP) K-15 and 1.0N hydrochloric acid (HCl) solution were purchased from Spectrum Chemicals (Gardena, CA). Hexanes, dichloromethane and high performance liquid chromatography (HPLC) grade acetonitrile were obtained from EM Science (Gibbstown, NJ). Danocrine ® Capsules (Sanofi-Synthelabo Inc., New York, NY) were purchased from University Health Services Pharmacy (Austin, TX).

3.3.2 Preparation of SFL Micronized Powder

A solution of 0.2% w/v danazol and 0.2% w/v PVP K15 was prepared in acetonitrile. Aliquots of the solution were loaded into a high pressure solution cell and atomized beneath the liquid nitrogen surface at 50 ml/min constant flow through a 127 μm I.D. PEEK nozzle. The PEEK tubing acted as an insulating nozzle that prevented freezing within the nozzle orifice. The constant pressure was supplied by an ISCO syringe pump (Model 100DX; ISCO, Inc., Lincoln, NE). Because of the low viscosity of

the acetonitrile API solution, a pressure of only 3000 psi was required to produce a flow rate of 50 ml/min. The frozen microparticles were collected and dried by a VirTis Advantage Tray Lyophilizer (The VirTis Company, Inc. Gardiner, NY). The final powder was protected from moisture and stored under vacuum.

3.3.3 Preparation of EPAS Micronized Powder

A solution of 2% w/v danazol and 1% w/v PVP K-15 was prepared in dichloromethane. This solution was pumped via an HPLC pump at 2 ml/min through a heat exchange coil set at 80°C. After heating, the solution was sprayed under constant pressure of 5000 psi through fine, elliptical, conical nozzle, formed by crimping 0.030 inch I.D. stainless steel tubing, at ~5000 psi constant pressure into a heated water bath (80°C) containing 1% w/v PVP K-15 of equal volume. The resultant dispersion (danazol:PVP K-15 1:1) was quenched by injecting it into liquid nitrogen via a syringe and needle and lyophilized to form powder. The final powder was protected from moisture and stored under vacuum.

3.3.4 Preparation of Co-ground Physical Mixture

A co-ground physical mixture consisting of 3.0 g danazol and 3.0 g PVP was mixed by geometric dilution and ground using a mortar and pestle.

3.3.5 Oral Dosing of a Murine Model

Four groups of 28 mice were dosed with 12.5mg/kg danazol by oral gavage of a 1 mg/mL dispersion. The danazol formulations included an enhanced SFL

composition, enhanced EPAS composition, physical mixture or Danocrine ® capsule powder. Mice were sacrifice by CO2 narcosis at 0.5, 1, 2, 4, 6, 12 and 24 hours following oral dosing. Blood was drawn by cardiac puncture, allowed to clot, centrifuged and serum was collected for HPLC analysis.

3.3.6 Supersaturation In Vitro Analysis

The apparatus used for supersaturation testing consisted of a VanKel VK 6010 Dissolution Tester with a Vanderkamp VK650A heater/circulator (Varian, Inc., Palo Alto, CA) USP IV paddle dissolution apparatus connected via 3mm Teflon tubing to a Cole-Parmer Masterflex peristaltic pump (Cole Parmer Instruments Company, Vernon Hills, IL) followed by a QS 10mm path length flow cell (Agilent Technologies, Palo Alto, CA) inside a Cary 3E UV-Visible spectrophotometer (Varian, Inc., Palo Alto, CA). The pump circulates a small portion of the 50 ml of medium (0.75% SDS, 1.2% Tris buffer adjusted to pH 9 with 1N HCl) from the 100 mL dissolution vessel through the flow cell and returns the fluid to the vessel at a rate of 30 ml per minute. Under these flow conditions, the time required for the transport of a fluid element from the dissolution vessel to the detector flow cell was 10 seconds. Measurement of the drug concentration in solution was done by adding 50 mg danazol equivalent drug powder to dissolution medium containing SDS surfactant and monitoring the danazol peak absorbance wavelength (264nm) to determine the concentration of danazol in solution. A 1 mg/mL dispersion was formed during measurement and the equilibrium solubility of danazol in the medium is 0.47 mg/mL (data not shown).   During measurement of the supersaturated concentration, an inline membrane filtration unit was placed between the pump and flow cell to retain suspended solids that would scatter light and introduce error into the measurement.   The filter unit was comprised of an aluminum housing inside which a

medium porosity glass frit supports a 90 mm nylon membrane with a mean pore size of 200 nm. Data sampling of the flow cell concentration was done at a rate of 3 Hz.

3.3.7 Chromatographic Method

Calibration standards and serum were analyzed using a method previously published[39]. Briefly, pooled serum from the four mice at each time point (1 mL) was analyzed for danazol by liquid-liquid extraction by reversed phase high performance liquid chromatography (RP-HPLC) To the 1mL mouse serum, 8 mL of hexanes was added and vortex mixed for 1.5 minutes, followed by centrifugation at 3000G (15 minutes). The supernatant was transferred to separate centrifuge tubes and dried under a stream of nitrogen at 60°C.

Samples were then reconstituted with 250 μL mobile phase (70% acetonitrile: 30% water) and vortex mixed (1 minute) before transferring into HPLC injection vials with low volume inserts (150 μL). Each sample was analyzed using a Shimadzu LC-10 liquid chromatograph (Shimadzu Corporation, Kyoto, Japan) equipped with a heated (37°C) C-18 base-deactivated column (5 μm, 50 x 4.6 mm) protected by a C-18 guard column (5 μm, 7.5 x 4.6 mm) (Alltech Associates, Inc., Deerfield, IL). The mobile phase eluted a danazol peak (263 nm) at 7 minutes at a flow-rate of 1.0 mL/min and an absorption wavelength of 288 nm (λ_{max}).

3.4 RESULTS

3.4.1 Danazol Supersaturation

70

The results from dissolution of a supersaturated dispersion of danazol are shown in Figure 3.1. From the figure, it can be seen that the SFL composition displayed 33% supersaturation compared to the physical mixture (crystalline microparticles and PVP K-15) and remained above supersaturation for 90 minutes. The EPAS composition dissolved to form a supersaturated dispersion which was 27% above the control physical mixture and remained supersaturated for 60 minutes. The equilibrium solubility of crystalline danazol in the dissolution medium is 0.47 mg/mL. The physical mixture displayed higher apparent solubility compared to the Danocrine ® capsule powder, within the time frame of analysis which was due to the addition of PVP within the physical mixture formulation.

3.4.2 Danazol Bioavailability

The danazol pharmacokinetic profiles are shown in Figure 3.2. SFL and EPAS compositions displayed higher Cmax at 392.5 ng/mL and 430.1 ng/mL, respectively, compared to the physical mixture (204.4 ng/mL) and Danocrine ® (199.3 ng/mL). The Tmax for each of the compositions studied was at the 1 hour time point. The AUC (Table 3.1) for the SFL composition was 2558 ng.h/ml compared to the EPAS processed composition at 1534 ng.h/ml. The AUC for the physical mixture and Danocrine ® were 672 ng.h/ml and 1519 ng.h/ml, respectively. The elimination rate constants for the EPAS composition, SFL composition and physical mixture were similar at ~0.15 hrs^{-1} whereas the Danocrine ® capsules displayed an elimination rate constant of 0.103 hrs^{-1}. The extent of danazol absorption in the mouse model was higher for the SFL composition, compared to the EPAS composition, physical mixture and Danocrine ® powders.

3.5 DISCUSSION

In the current study, danazol was used as a model drug to compare the ability of enhanced danazol formulations to form supersaturated solutions in vitro and how this affects its bioavailability in vivo. Danazol formulated with PVP K-15 and processed using both SFL and EPAS technologies were evaluated in our laboratories in a previous study.[26] The SFL powders collected displayed complete amorphous character as was evaluated through x-ray powder diffraction (XRD). Thus, the SFL composition was shown to form a solid dispersion on the molecular level through the ability of the freezing process to prevent nucleation and growth. . Also, the SFL composition displayed the highest mixing and miscibility within the PVP polymer compared to the EPAS composition and physical mixture powders as determined from the Tg measured by differential scanning calorimetry and interpreted with the Gordon-Taylor equation. This aspect improves the ability of the formulation to prevent re-crystallization and particle growth when in the solid state.

In contrast, the EPAS composition displayed partially crystalline character (XRD) and larger primary particle sizes compared to the SFL composition. The nucleation and growth of particles during the EPAS process allows for nanoparticle formation which may be crystalline or amorphous, depending on the stabilizer used and processing conditions. The particles used in this study were partially crystalline with a 500nm primary particle size. The level of mixing with the PVP was less than the SFL composition according to the Tg measured by DSC, although higher than the physical mixture.

APIs in BCS class II are poorly absorbed due to a lack of sufficient concentrations of solubilized drug. Formulations which are amorphous can overcome this by supersaturation of the dissolution medium allowing for greater absorption of the delivered dose as well as improving the dissolution rate.[40]

$$\frac{dC}{dt} = \frac{AD(Cs - C)}{h} \tag{1}$$

The dissolution rate of a particle can be described by the Noyes-Whitney equation (1) where dC/dt is the rate of dissolution, A is the surface area of the particle, D is the diffusion coefficient, Cs is the apparent solubility of the drug in the dissolution medium, C is the concentration of the drug in the dissolution medium at time t, and h is the thickness of the diffusion boundary layer. The diffusion coefficient is dependent on the drug in question and cannot be adjusted. Also, the thickness of the boundary layer can be manipulated in vitro through increased agitation; however, this proves to be difficult in vivo. The rate of dissolution can be improved (increased) by creating particles which have a high surface area, improved wettability (higher surface area in contact with dissolution medium) or by increasing the apparent solubility of the drug. Through the production of nanoparticles or aggregates of nanoparticles with high surface area, the surface area of the particle increases significantly, thereby increasing the rate of dissolution. Nanoparticles can also form supersaturated dispersions, although not to the same extent as amorphous particles. According to the Ostwald-Freundlich/Kelvin equations, small droplets of liquid dispersed in a gas-liquid medium evaporate more quickly and to a greater extent than do large droplets due to increased curvature at the droplet surface which raises the vapor pressure of the liquid.[34] This theory is also applicable to solid-liquid interfaces as well. By decreasing the size of solid particles to the nanometer scale, the high energy state which is achieved will increase the extent to which it can dissolve due to an increase in dissolution pressure. In turn, this will increase the apparent solubility of the dissolving particles. A decrease in the interfacial tension between the particle and water, due to coating by a stabilizing excipient, will decrease the supersaturation due to curvature.

The amorphous nature and small particle size of the enhanced formulations (EPAS and SFL) allows for higher apparent solubilities, thereby increasing the dissolution rate and increasing the concentration of drug available for absorption. In this study, the amorphous SFL composition was able to attain a concentration which was 33% above the apparent solubility of the physical mixture, which was made up of microparticulate crystalline danazol. The EPAS composition was able to achieve supersaturation which was 27% above the control physical mixture. The ability of the enhanced formulations to achieve higher apparent solubilities translated to higher Cmax values in the in vivo study, because more API was available for absorption. Yamashita et al formed solid dispersions of tacrolimus in various stabilizers to evaluate their ability to form supersaturated solutions.[32] In their study, solid dispersions of tacrolimus were formed by solvent evaporation and were amorphous. The dispersions formed supersaturated solutions at nearly the same initial concentration. However, the time above supersaturation varied significantly. In vivo data from this study found that the supersaturating formulations displayed significantly higher and extended absorption of the API.

Partially crystalline and nanoparticulate danazol formed by the EPAS process was also able to enhance the apparent solubility of the drug over a 60 minute time period, with a Cs-max of 27% above the physical mixture. Although not completely amorphous, the EPAS composition did display some level of amorphous character as well as being composed of nanoparticle domains of danazol. As with the SFL composition, the amorphous regions of the danazol domains would display similar abilities to supersaturate the dispersion in vitro and in vivo, although the crystalline regions can cause a premature reduction in the solubility due to seeding of the dissolved API.[41] This phenomenon was seen in the in vitro supersaturation analysis as well as the in vivo study. The time course for supersaturation was shorter for the EPAS composition and the extent of absorption was much lower than the SFL composition in vivo. Precipitation of

the drug within the GI tract could significantly reduce the extent of absorption of the EPAS composition. Both the Danocrine® capsule powder and physical mixture showed relatively low Cmax values and lower AUC values compared to the SFL processed danazol. Because these formulations are microparticulate and crystalline, the degree and extent of absorption is limited by the equilibrium solubility of the drug, rather than an enhanced apparent solubility which was achieved through the EPAS and SFL compositions.

3.6 CONCLUSION

Quantitation of degree of supersaturation, both level and time duration, correlated well with in vivo results obtained for danazol. Through the use of a testing method for supersaturation, it was found that EPAS and SFL compositions achieve higher apparent solubilities when compared to the physical mixture and commercial Danocrine® capsules. This improvement in solubility allowed for more danazol to be available for absorption in vivo. Because of the greater extent of dissolution of the SFL composition, the bioavailability was enhanced in a mouse model.

3.7 ACKNOWLEDGMENTS

3.8 REFERENCES

1. Liversidge, G.G.; Cundy, K.C. Particle size reduction for improvement of oral bioavailability of hydrophobic drugs: I. Absolute oral bioavailability of nanocrystalline danazol in beagle dogs. International Journal of Pharmaceutics 1995, *125* (1): p. 91-97.

2. Erlich, L.; Yu, D.; Pallister, D.A.; Levinson, R.S.; Gole, D.G.; Wilkinson, P.A.; Erlich, R.E.; Reeve, L.E.; Viegas, T.X. Relative bioavailability of danazol in dogs from liquid-filled hard gelatin capsules. International Journal of Pharmaceutics 1999, *179* (1): p. 49-53.

3. Muraoka, A.; Tokumura, T.; Machida, Y. Evaluation of the bioavailability of flurbiprofen and its [beta]-cyclodextrin inclusion complex in four different doses upon oral administration to rats. European Journal of Pharmaceutics and Biopharmaceutics 2004, *58* (3): p. 667-671.

4. Jambhekar, S.; Casella, R.; Maher, T. The physicochemical characteristics and bioavailability of indomethacin from [beta]-cyclodextrin, hydroxyethyl-[beta]-cyclodextrin, and hydroxypropyl-[beta]-cyclodextrin complexes. International Journal of Pharmaceutics 2004, *270* (1-2): p. 149-166.

5. Wong, J.W.; Yuen, K.H. Improved oral bioavailability of artemisinin through inclusion complexation with [beta]- and [gamma]-cyclodextrins. International Journal of Pharmaceutics 2001, *227* (1-2): p. 177-185.

6.   Savolainen, J.; Jarvinen, K.; Matilainen, L.; Jarvinen, T. Improved dissolution and bioavailability of phenytoin by sulfobutylether-[beta]-cyclodextrin ((SBE)7m-[beta]-CD) and hydroxypropyl-[beta]-cyclodextrin (HP-[beta]-CD) complexation. International Journal of Pharmaceutics 1998, *165* (1): p. 69-78.

7.   Kawakami, K.; Yoshikawa, T.; Hayashi, T.; Nishihara, Y.; Masuda, K. Microemulsion formulation for enhanced absorption of poorly soluble drugs: II. In vivo study. Journal of Controlled Release 2002, *81* (1-2): p. 75-82.

8.   Kang, B.K.; Lee, J.S.; Chon, S.K.; Jeong, S.Y.; Yuk, S.H.; Khang, G.; Lee, H.B.; Cho, S.H. Development of self-microemulsifying drug delivery systems (SMEDDS) for oral bioavailability enhancement of simvastatin in beagle dogs. International Journal of Pharmaceutics 2004, *274* (1-2): p. 65-73.

9.   Wang, X.-q.; Dai, J.-d.; Chen, Z.; Zhang, T.; Xia, G.-m.; Nagai, T.; Zhang, Q. Bioavailability and pharmacokinetics of cyclosporine A-loaded pH-sensitive nanoparticles for oral administration. Journal of Controlled Release 2004, *97* (3): p. 421-429.

10.   Kapsi, S.G.; Ayres, J.W. Processing factors in development of solid solution formulation of itraconazole for enhancement of drug dissolution and bioavailability. International Journal of Pharmaceutics 2001, *229* (1-2): p. 193-203.

11.   Sznitowska, M.; Gajewska, M.; Janicki, S.; Radwanska, A.; Lukowski, G. Bioavailability of diazepam from aqueous-organic solution, submicron emulsion

and solid lipid nanoparticles after rectal administration in rabbits. European Journal of Pharmaceutics and Biopharmaceutics 2001, *52* (2): p. 159-163.

12. Rogers, T.L.; Overhoff, K.A.; Shah, P.; Santiago, P.; Yacaman, M.J.; Johnston, K.P.; Williams, R.O. Micronized powders of a poorly water soluble drug produced by a spray-freezing into liquid-emulsion process. European Journal of Pharmaceutics and Biopharmaceutics 2003, *55* (2): p. 161-172.

13. Rogers, T.L.; Nelsen, A.C.; Sarkari, M.; Young, T.J.; Johnston, K.P.; Williams, R.O. Enhanced aqueous dissolution of a poorly water soluble drug by novel particle engineering technology: Spray-freezing into liquid with atmospheric freeze-drying. Pharmaceutical Research 2003, *20* (3): p. 485-493.

14. Rogers, T.L.; Nelsen, A.C.; Hu, J.H.; Brown, J.N.; Sarkari, M.; Young, T.J.; Johnston, K.P.; Williams, R.O. A novel particle engineering technology to enhance dissolution of poorly water soluble drugs: spray-freezing into liquid. European Journal of Pharmaceutics and Biopharmaceutics 2002, *54* (3): p. 271-280.

15. Rogers, T.L.; Johnston, K.P.; Williams, R.O. Physical stability of micronized powders produced by spray-freezing into liquid (SFL) to enhance the dissolution of an insoluble drug. Pharmaceutical Development and Technology 2003, *8* (2): p. 187-197.

16. Rogers, T.L.; Hu, J.H.; Yu, Z.S.; Johnston, K.P.; Williams, R.O. A novel particle engineering technology: spray-freezing into liquid. International Journal of Pharmaceutics 2002, *242* (1-2): p. 93-100.

17.   Yu, Z.S.; Rogers, T.L.; Hu, J.H.; Johnston, K.P.; Williams, R.O. Preparation and characterization of microparticles containing peptide produced by a novel process: spray freezing into liquid. European Journal of Pharmaceutics and Biopharmaceutics 2002, *54* (2): p. 221-228.

18.   Hu, J.H.; Rogers, T.L.; Brown, J.; Young, T.; Johnston, K.P.; Williams, R.O. Improvement of dissolution rates of poorly water soluble APIs using novel spray freezing into liquid technology. Pharmaceutical Research 2002, *19* (9): p. 1278-1284.

19.   Hu, J.H.; Johnston, K.P.; Williams, R.O. Rapid dissolving high potency danazol powders produced by spray freezing into liquid process. International Journal of Pharmaceutics 2004, *271* (1-2): p. 145-154.

20.   Hu, J.H.; Johnston, K.P.; Williams, R.O. Stable amorphous danazol nanostructured powders with rapid dissolution rates produced by spray freezing into liquid. Drug Development and Industrial Pharmacy 2004, *30* (7): p. 695-704.

21.   Hu, J.H.; Johnston, K.P.; Williams, R.O. Spray freezing into liquid (SFL) particle engineering technology to enhance dissolution of poorly water soluble drugs: organic solvent versus organic/aqueous co-solvent systems. European Journal of Pharmaceutical Sciences 2003, *20* (3): p. 295-303.

22.   Chen, X.; Benhayoune, Z.; Williams, R.O.; Johnston, K.P. Rapid dissolution of high potency itraconazole particles produced by evaporative precipitation into aqueous solution. Journal of Drug Delivery Science and Technology 2004, *14* (4): p. 299-304.

23.   Chen, X.X.; Vaughn, J.M.; Yacaman, M.J.; Williams, R.O.; Johnston, K.P. Rapid dissolution of high-potency danazol particles produced by evaporative precipitation into aqueous solution. Journal of Pharmaceutical Sciences 2004, *93* (7): p. 1867-1878.

24.   Chen, X.X.; Young, T.J.; Sarkari, M.; Williams, R.O.; Johnston, K.P. Preparation of cyclosporine A nanoparticles by evaporative precipitation into aqueous solution. International Journal of Pharmaceutics 2002, *242* (1-2): p. 3-14.

25.   Sarkari, M.; Brown, J.; Chen, X.X.; Swinnea, S.; Williams, R.O.; Johnston, K.P. Enhanced drug dissolution using evaporative precipitation into aqueous solution. International Journal of Pharmaceutics 2002, *243* (1-2): p. 17-31.

26.   Vaughn, J.M.; Gao, X.; Yacaman, M.-J.; Johnston, K.P.; Williams III, R.O. Comparison of powder produced by evaporative precipitation into aqueous solution (EPAS) and spray freezing into liquid (SFL) technologies using novel Z-contrast STEM and complimentary techniques. European Journal of Pharmaceutics and Biopharmaceutics 2005, *60* (1): p. 81-89.

27.   Young, T.J.; Johnston, K.P.; Mishima, K.; Tanaka, H. Encapsulation of lysozyme in a biodegradable polymer by precipitation with a vapor-over-liquid antisolvent. Journal Of Pharmaceutical Sciences 1999, *88* (6): p. 640-650.

28.   Yamada, T.; Saito, N.; Imai, T.; Otagiri, M. Effect of grinding with hydroxypropyl cellulose on the dissolution and particle size of a poorly water-soluble drug. Chemical & Pharmaceutical Bulletin 1999, *47* (9): p. 1311-1313.

29.   Kohri, N.; Yamayoshi, Y.; Xin, H.; Iseki, K.; Sato, N.; Todo, S.; Miyazaki, K. Improving the oral bioavailability of albendazole in rabbits by the solid dispersion technique. The Journal Of Pharmacy And Pharmacology 1999, *51* (2): p. 159-164.

30.   Suzuki, H.; Sunada, H. Influence of water-soluble polymers on the dissolution of nifedipine solid dispersions with combined carriers. Chemical & Pharmaceutical Bulletin 1998, *46* (3): p. 482-487.

31.   Suzuki, H.; Sunada, H. Comparison of nicotinamide, ethylurea and polyethylene glycol as carriers for nifedipine solid dispersion systems. Chemical & Pharmaceutical Bulletin 1997, *45* (10): p. 1688-1693.

32.   Yamashita, K.; Nakate, T.; Okimoto, K.; Ohike, A.; Tokunaga, Y.; Ibuki, R.; Higaki, K.; Kimura, T. Establishment of new preparation method for solid dispersion formulation of tacrolimus. International Journal Of Pharmaceutics 2003, *267* (1-2): p. 79-91.

33.   Muller, R.H.; Keck, C.M. Challenges and solutions for the delivery of biotech drugs - a review of drug nanocrystal technology and lipid nanoparticles. Journal of Biotechnology 2004, *113* (1-3): p. 151-170.

34.   Grant, D.J.W.; Brittian, H.G., *Physical Characterization of Pharmaceutical Solids*, ed. H.G. Brittian. 1995, New York: Marcel Dekker.

35.   Sunesen, V.H.; Pedersen, B.L.; Kristensen, H.G.; Mullertz, A. In vivo in vitro correlations for a poorly soluble drug, danazol, using the flow-through dissolution method with biorelevant dissolution media. European Journal of Pharmaceutical Sciences 2005, *24* (4): p. 305-313.

36. Dressman, J.B.; Reppas, C. In vitro-in vivo correlations for lipophilic, poorly water-soluble drugs. European Journal of Pharmaceutical Sciences 2000, *11* (Supplement 2): p. S73-S80.

37. Farag Badawy, S.I.; Ghorab, M.M.; Adeyeye, C.M. Characterization and bioavailability of danazol-hydroxypropyl [beta]-cyclodextrin coprecipitates. International Journal of Pharmaceutics 1996, *128* (1-2): p. 45-54.

38. Sunesen, V.H.; Vedelsdal, R.; Kristensen, H.G.; Christrup, L.; Mullertz, A. Effect of liquid volume and food intake on the absolute bioavailability of danazol, a poorly soluble drug. European Journal of Pharmaceutical Sciences 2005, *24* (4): p. 297-303.

39. He, H.B.; Sun, S.L.; Liu, D.L.; Zheng, H.E. Analysis of danazol and its metabolites in serum by RP-HPLC with maxplot UV detector. Yao Xue Xue Bao = Acta Pharmaceutica Sinica 1988, *23* (9): p. 698-702.

40. Yu, L. Amorphous pharmaceutical solids: preparation, characterization and stabilization. Advanced Drug Delivery Reviews 2001, *48* (1): p. 27-42.

41. Otsuka, M.; Kato, F.; Matsuda, Y. Physicochemical stability of cimetidine amorphous forms estimated by isothermal microcalorimetry. AAPS PharmSciTech 2002, *3* (4): p. E30.

Chapter 4: Single Dose and Multiple Dose studies of Aerosolized Itraconazole Nanoparticles

4.1 ABSTRACT

The objective of this study was to determine and compare the lung and serum concentrations in mice following oral and pulmonary dosing of amorphous nanoparticulate itraconazole (ITZ) compositions as well as the Sporanox ® oral solution. Secondly, the steady state partitioning of ITZ in lung tissue and circulatory compartments following repeated oral and pulmonary dosing was determined. The pulmonary formulation (ITZ-pulmonary) consisted of ITZ, polysorbate 80 and poloxamer 407 in a 1:0.75:0.75 ratio and the oral formulation (ITZ-oral) consisted of ITZ, PEG 8000, poloxamer 188, and Span 80 in a 1:1:2:1 ratio. Mice were dosed every 12 hours by nebulization with ITZ-pulmonary, or by oral gavage with ITZ-oral or Sporanox ® oral solution (n=12 per study arm). Twelve hours after the last dose on days 3, 8 and 12, four mice were sacrificed by carbon dioxide narcosis. Two deaths and symptoms of dehydration were noted in the Sporanox ® group The Sporanox ® oral solution serum concentrations were significantly greater than the other groups on all days ($p<0.05$). On day 3, the serum levels achieved by the ITZ-pulmonary and ITZ-oral groups were not statistically different, although, on days 8 and 12, the ITZ-oral serum concentrations were significantly greater than ITZ-pulmonary ($p<0.05$). ITZ-pulmonary achieved significantly greater (>10 fold) lung tissue concentrations compared to the Sporanox ® oral solution and ITZ-oral. There were no statistical differences between the two oral formulations which were dosed. ITZ-pulmonary achieved significantly greater lung levels per unit

serum concentration compared to the orally dosed ITZ compositions. High and sustained lung tissue concentrations were achieved via inhalation of an amorphous nanoparticulate ITZ pulmonary composition while maintaining serum levels which are above the minimum lethal concentration (MLC) of *Aspergillus fumigatus*.

4.2 INTRODUCTION

With an ever increasing population of patients at risk for invasive fungal infections, the incidence of these infections has increased dramatically over the past 20 years. Much of the dramatic increase is due to proliferation of diseases and procedures which render patients in an immunocompromised state. These populations include patients with acquired immunodeficiency syndrome (AIDS), patients who have undergone solid organ or hematopoietic stem cell transplants (HSCT), individuals receiving immunosuppressant therapy and patients receiving aggressive chemotherapy for malignancies. *Aspergillus* spores can be found airborne or on many hospital surfaces. It has been associated with an increasing incidence among immunocompromised patients with very high mortality rates.[1, 2] The portal of entry is typically the lungs where the fungi will present as pneumonia, cavitary infiltrates or nodules.[3] Dissemination of the *aspergillus* infection is typically through the lymph system and can involve organs such as the heart, kidney, central nervous system, gastrointestinal tract, spleen, liver, thyroid gland and pancreas.[1] Mortality rates for *aspergillus* infections are nearly always fatal in disseminated disease with up to 90% mortality rates among central nervous system (CNS) patients.[4]

The first line treatment for invasive aspergillosis is the polyene amphotericin B deoxycholate.[5] It shows extensive infusion related and liver toxicity in many patients.

For this reason, liposomal and colloidal lipid dispersions were developed and showed much lower toxicities, although not significantly improving mortality rates.[6]   It has been reported that amphotericin B and liposomal amphotericin B formulations have been administered through nebulization to treat and prevent infections in patients with high risk of infection.[7-10] Prophylaxis with amphotericin B inhalation was unsuccessful in patients with prolonged neutropenia.[11]

ITZ is a poorly water soluble active pharmaceutical ingredient (API) which displays low solubility and pH dependent dissolution which causes low and variable oral absorption. Absolute bioavailability of the oral capsule is 55% in the fed state and 40% lower in the non-fed state.[12] Following intravenous administration the volume of distribution is 10.7 L/kg and it is 99.8% protein bound. [13] Tissue distribution is high in the nails, skin, muscle and liver, where as, distribution to the cerebral spinal fluid, eye, saliva and sputum is negligible.[14] Improvement of ITZ therapy through particle engineering processes and novel delivery mechanisms have been reported. [15]   Lung concentrations of ITZ resulting from oral or intravenous administration have been reported in mice [16] and in humans[17]. In those references, lung:serum ratios for the orally administered Sporanox® oral solution differs from the levels found in this study. In mice [16], the lung:serum ratio was much lower than what was found in this study, whereas, in humans[17] the ratio was much higher. Although, lung:serum concentration ratios have not been reported for ITZ dosed via inhalation.   ITZ pulmonary administration has shown significant improvements in survival of a murine infection model compared to the Sporanox ® oral solution.[18]

Formation of amorphous ITZ nanoparticles can be achieved through SFL processing. In this particle engineering process, a feed solution containing an API and dissolution enhancing excipient(s) is atomized directly into a cryogenic liquid, such as nitrogen. The resulting dried powder is composed of discrete microparticles where the API is molecularly dispersed with a polymer in a porous matrix. [19] This molecular

dispersion is achieved by rapid freezing in liquid nitrogen, which prevents phase separation. In previous studies, it was found that enhanced dissolution is due to the amorphous morphology, high surface area and enhanced wettability of the SFL nanostructured particles [20]

The objective of this study was to determine the lung and serum concentrations in mice following pulmonary dosing of amorphous nanoparticles of ITZ over a 24 hour period. The hypothesis is that sufficient serum concentrations and high lung concentrations are achieved through pulmonary dosing of amorphous ITZ nanoparticles. The serum pharmacokinetics of the inhaled ITZ nanoparticles were evaluated using a one compartment model for extravascular administration. Also, the pharmacokinetic parameters for ITZ in lung tissue over a 24 hour period were calculated using non-compartmental analysis. Lastly, the steady state partitioning of ITZ in lung tissue and serum following repeated oral and pulmonary dosing was evaluated.

4.3 MATERIALS AND METHODS

4.3.1 Materials

The following materials were purchased: itraconazole USP (ITZ; Hawkins Chemical, Minneapolis, MN); ketoconazole USP, poloxamer 407, polysorbate 80, poloxamer 188, Span 80, polyethylene glycol (PEG) 8000, potassium phosphate monobasic, sodium hydroxide (NaOH) and sodium chloride (NaCl) (Spectrum Chemicals, Gardena, CA); high performance liquid chromatography (HPLC) grade acetonitrile and dichloromethane (EM Industries Inc., Gibbstown, NJ). Liquid nitrogen was obtained from Boc Gases (Murray Hill, NJ).

4.3.2 Production of ITZ Nanoparticles

Amorphous nanoparticulate ITZ compositions (ITZ-pulmonary and ITZ-oral) were produced using the particle engineering process spray freezing into liquid (SFL).[21] ITZ-pulmonary consisted of ITZ, polysorbate 80 and poloxamer 407 in a 1:0.75:0.75 ratio and the ITZ-oral consisted of ITZ, PEG 8000, poloxamer 188, and Span 80 in a 1:1:2:1 ratio. ITZ and excipients were dissolved in an acetonitrile/dichloromethane co-solvent system and atomized through a 63μm poly-ether-ether-ketone (PEEK) nozzle (Upchurch Scientific, Oak Harbor, WA) via an HPLC pump (Jasco PU-2086 plus, Jasco Inc., Easton, MD) at 20 mL/min below the surface of liquid nitrogen. The frozen nanostructured aggregates were then separated from the liquid nitrogen and the solvent was removed by lyophilization (VirTis Advantage, VirTis, Gardiner, NY). The dried powders were stored under vacuum until administration.

4.3.3 Pulmonary Dosing of a Murine Model

Twenty-six male Harlan-Spague-Dawley ICR mice (Hsd:ICR, Harlan Sprague Dawley, Inc., Indianapolis, IN) were dosed with ITZ-pulmonary using the dosing chamber described in [22]. Briefly, the chamber consisted of a polymethylmethacrylate (PMMA) airtight box (40.6 x 11.4 x 21.6 cm) with a hinged top, having a nominal wall thickness of 1.25 cm. The chamber was designed to hold up to 14 mice, each having a floor area of approximately 63 cm^2, in accordance with The University of Texas at Austin and the University of Texas Health Science Center at San Antonio Institutional Animal Care and Use Committees (IACUC) guidelines. A 20 mg/mL ITZ-pulmonary dispersion was formed in 4 mL of normal saline by first wetting the powder followed by sonication for 1 min prior to dosing. An Aeroneb® Pro micro pump nebulizer (Aerogen, Inc., Mountain View, CA) was situated at the inlet of the chamber and nebulization of 8 mL

dispersions was conducted over 20 minutes for each dose. For the 24 hr pharmacokinetic study, two mice were sacrificed by carbon dioxide narcosis at each time point (0.5, 1, 2, 4, 6, 10, 24 hours), and their serum was collected and lungs were extracted and both analyzed for ITZ content. Multiple dosing was conducted every 12 hours through the completion of the study. Twelve hours after the last dose (trough levels) on days 3, 8 and 12, four mice were sacrificed by carbon dioxide narcosis. Blood was collected by cardiac puncture, allowed to clot for 20 min, centrifuged and serum was collected. Surgery was performed on each mouse to extract the lung tissue which was then homogenized in 1 mL of normal saline and four 0.25 mL aliquots were analyzed for ITZ by reverse phase high performance liquid chromatography (HPLC).

4.3.4 Oral Dosing of a Murine Model

Male ICR mice were dosed with either ITZ-oral or Sporanox ® oral solution by oral gavage twice daily through the completion of the study. The ITZ-oral composition was prepared by dispersing ITZ-oral (0.96 mg ITZ/ 0.4 mL) in deionized water followed by sonication for 1 min. The Sporanox ® oral solution was diluted to 0.96 mg/ 0.4 mL) with a United States Pharmacopoeia (USP) phosphate buffer at pH 1.7. The mice were dosed with 0.4 mL of the dispersion by oral gavage. Twelve hours after the last dose on days 3, 8 and 12, four mice from each group were sacrificed by carbon dioxide narcosis. Blood was collected by cardiac puncture, allowed to clot for 20 min, centrifuged, and serum was collected. Surgery was performed on each mouse to extract the lung tissue which was then homogenized in 1mL of normal saline and separated into four 0.25mL aliquots.

4.3.5 Validated Serum and Lung Extraction and Analysis Using Chromatography

Calibration standards, serum and homogenized lung samples were analyzed using a method previously published [23]. Briefly, normal saline (1mL) was added to each harvested lung sample, this was then homogenized using tip ultrasonication. Aliquots of homogenate (250 µL) were transferred to 4 separate vials and drug was extracted similarly to the serum samples. Barium hydroxide 0.3 N (50µL) and 0.4 N zinc sulfate heptahydrate solution (50 µL) was then added to each to precipitate out water-soluble proteins. The samples were then vortex mixed (30 seconds). Acetonitrile (1 mL) containing 100 ng/mL ketoconazole as an internal standard was added before a further vortex mixing (1.5 minute), followed by centrifugation at 3000G (15 minutes). The supernatant was transferred to 1.5 mL centrifuge tubes and seated in an aluminum heating block (60°C), under a stream of nitrogen to dryness over 1 hour.

Samples were then reconstituted with 250 µL mobile phase (62% acetonitrile: 38% 0.05M potassium phosphate monobasic buffer adjusted to pH 6.7 with NaOH) and vortex mixed (1 minute) before filtering (0.45 µm) into HPLC glass injection vials with low volume inserts (150 µL). Each sample was analyzed using a Shimadzu LC-10 liquid chromatograph (Shimadzu Corporation, Columbia, Maryland) equipped with a heated (37°C) C-18 base-deactivated column (5 µm, 250 x 4.6 mm) protected by a C-18 guard column (5 µm, 7.5 x 4.6 mm) (Alltech Associates, Inc., Deerfield, IL). The mobile phase eluted an ITZ peak at 17.7 minutes and ketoconazole at 7.3 min at a flow-rate of 1.0 mL/min, an injection volume of 100 µL and an absorption wavelength of 263 nm (λ_{max}). The limit of detection for ITZ was 10 ng/mL and the limit of quantitation of 30 ng/mL.

4.3.6 Pharmacokinetic Analysis

Mice which were dosed with the ITZ-pulmonary composition were evaluated for their 24 hr lung and serum pharmacokinetics. The lung tissue concentrations vs. time were evaluated using a non-compartmental model in WinNonlin version 4.1 (Pharsight Corporation, Mountain View, CA). The serum concentrations vs. time were evaluated using a one-compartmental analysis from extravascular administration using Win-NonLin. Graphing of the serum data on a semi-log plot revealed a first order absorption phase and a first order elimination phase. For this reason, a one compartment model was constructed and estimations of the pharmacokinetic parameters were calculated. Figure 4.1 illustrates the model used and the parameters which were calculated.

4.3.7 Statistical Analysis

One-way analysis of variance (ANOVA) was used to determine statistically significant differences between results. Results with p-values < 0.05 were considered statistically significant.

4.4 RESULTS

4.4.1 Single Dose, Twenty-four Hour Pharmacokinetics

The one-compartment model which was utilized for analysis of the serum concentrations is illustrated in Figure 4.1. Concentration vs. time for the lung tissue and serum are shown in Figures 4.2 and 4.3. From the figures and Table 4.1, the lung tissue C_{max}, T_{max}, $T_{1/2}$, K_{10}, and AUC_{inf} were 13.4 µg/g, 1 hr, 5.5 hrs, 0.13 hrs^{-1} and 85.8 µg.h/mL, respectively. Based on a one compartmental analysis the predicted serum C_{max},

T_{max}, $T_{1/2\ k01}$, $T_{1/2\ k10}$, K_{01}, K_{10} and AUC_{inf} were 0.12 µg/mL, 5.35 hrs, 3.73 hrs, 3.7 hrs, 0.186 hrs^{-1}, 0.188 hrs^{-1} and 1.69 µg.h/mL.

4.4.2 Morphological Observations in Repeat Dose Groups

Over the 12 day dosing period, morphological observations of the morbidity and mortality of the mice were noted and are shown in Table 4.2. Two deaths associated with toxicity to the Sporanox ® oral solution occurred on day 7 of dosing. Poor skin turger was noted in the Sporanox ® oral solution group which is a sign of dehydration associated with diarrhea, which was also observed in that entire group. The grooming practices in the Sporanox ® oral solution group began to decline following multiple day dosing (>7 days) which was indicated by unkempt fur. Furthermore, the mice in the Sporanox ® oral solution group were highly resistant to dosing, due to the taste or low pH of the solution, or some other unmeasured property of the oral solution. None of these symptoms were noted in the amorphous ITZ groups, either pulmonary or oral. The mice in these groups appeared healthy throughout the study and no deaths occurred. Their fur was groomed and skin showed good turger upon scruffing of the neck region during oral dosing, due to adequate hydration. No diarrhea was noted in either of the SFL dosed groups.

4.4.3 Steady State Trough Serum Levels

The average trough serum levels on days 3, 8 and 12 for each of the groups studied are shown in Figure 4.4. From Figure 4.4, the average serum trough concentrations (µg/mL) for ITZ-pulmonary, Sporanox ® oral solution and ITZ-oral on day 3 were 0.12, 0.31 and 0.16; on day 8 were 0.11, 0.37 and 0.26; and on day 12 were

0.11, 0.39, and 0.29, respectively. The Sporanox ® oral solution serum concentrations were significantly greater than the other groups on all days (p<0.05). On day 3, the serum levels achieved by ITZ-oral and ITZ-pulmonary were not statistically different, although, on days 8 and 12, the ITZ-oral serum concentrations were significantly greater than ITZ-pulmonary (p<0.05).

4.4.4 Steady State Trough Lung Tissue Concentrations

The average trough lung tissue concentrations on days 3, 8 and 12 for each of the groups studied are shown in Figure 4.5. From Figure 4.5, the average lung tissue concentrations (µg/g lung tissue) for ITZ-pulmonary, Sporanox ® oral solution and ITZ-oral on day 3 were 2.16, 0.19 and 0.16; on day 8 were 2.22, 015 and 0.23; and on day 12 were 2.52, 0.18 and 0.15, respectively. ITZ-pulmonary achieved significantly greater (>10 fold) lung tissue concentrations compared to the Sporanox ® oral solution and ITZ-oral. There were no statistical differences between the two oral formulations which were dosed.

4.4.5 Lung–to-Serum Ratios

The ratio of lung-to-serum concentrations achieved through oral and pulmonary dosing was calculated from the measured values and is shown in Table 4.3. From the table, the lung:serum ratios for ITZ-pulmonary, Sporanox ® oral solution and ITZ-oral on day 3 were 18.15, 0.61 and 1.03; on day 8 were 20.18, 0.40 and 0.89; on day 12 were 22.27, 0.45 and 0.54, respectively. Pulmonary dosed amorphous nanoparticles of ITZ (ITZ-pulmonary) achieved significantly greater lung levels per unit serum concentration compared to the orally dosed ITZ compositions. The data suggests that in a murine

model, the partitioning of ITZ is greater in the circulatory system than in the lung tissue following oral absorption, except for day 3 of ITZ-oral. However, significant amounts of ITZ are retained in the lung tissue, compared to the circulatory compartment for mice which were dosed via inhalation.

4.5 DISCUSSION

The present studies indicate that pulmonary dosing of ITZ is an effective mode of delivery for antifungal therapy and is able to achieve significant and sustained levels in the lung tissue. It was found that the concentrations which must be delivered via the pulmonary route are significantly lower than what is required orally, to achieve therapeutic serum and lung levels in vivo. Absolute bioavailability of the oral capsule is 55% in the fed state and 40% lower in the non-fed state.[12] The bioavailability is further reduced (40% of absolute bioavailability) when co-administered with a histamine-2-receptor (H_2)-antagonist. Also, patients with certain disorders (eg. human immunodeficiency virus, HIV), which causes the stomach to have low gastric acidity (hypochlorhydria) showed high variability of absorption, due to poor dissolution of the drug. Co-administration of an acidic soda beverage is recommended in patients who use the capsule formulation of itraconazole.[24] The bioavailability of Sporanox ® oral solution, taken in a fasting condition, is approximately 60% higher than that of the capsules taken with a meal at . However, hypochlorhydria does decrease the oral absorption of the solution.[12] Dosing directly to the lung tissue eliminates many of the problems (ph dependence) with variability in absorption due to variability in gastric conditions, while achieving relatively high (> MLC) serum concentrations and extensive pulmonary concentrations, which remain above the MLC over a 24hr period.

In this study, the mice were exposed to 30 mg/kg through inhalation and dosed orally with 30 mg/kg by gavage. Although the Sporanox ® oral solution and ITZ-oral

displayed significantly higher serum levels than ITZ-pulmonary, the pulmonary group sustained serum levels above 100 ng/mL at the trough. This is well above the suggested MLC determined by Allendeorfer et al at 70 ng/mL.[16] The ultimate goal is enabling the ability to achieve a lower Cmax (reduced toxicity) with extended time above the MLC for the organism. Furthermore, ITZ-pulmonary achieved nearly 10-times the lung tissue concentrations of the orally dosed ITZ at the trough.

Dosing of the Sporanox ® oral solution elicited several symptoms associated with toxicity. It is well documented that toxicity due to oral administration of cyclodextrins is high and mainly due to significant gastrointestinal side effects, such as diarrhea.[25] This significantly limits the dose which can be administered for the treatment of invasive fungal infections. These side effects were noted in the group dosed with the Sporanox ® oral solution. Dehydration, secondary to diarrhea was noted in all of the animals in that group. Secondly, there were two deaths associated with toxicity, probably due to lethal diarrhea. Decreased grooming of the Sporanox ® oral solution group was also noted. This is evidence of generally very poor health observed among this group due to the dosing of the commercial cyclodextrin formulation of ITZ. It has been reported in human studies that diarrhea is associated with administration of Sporanox ® oral solution.[26] The degree and frequency of diarrhea was dose dependent and due to osmotic effects caused by the cyclodextrin component of the formulation. Local delivery of ITZ to the lung tissue should minimize systemic side effects while maintaining serum concentrations above the minimum lethal concentration (MLC) at the site of infection and eliminate the need for formulation with a cyclodextrin.

Serum and lung tissue trough levels following multiple dosing of ITZ have never been reported in a murine model. Allendoerfer et al evaluated median steady state concentrations of ITZ in a murine model.[16] Twelve hours following once daily dosing for 3 days of 100 mg/kg Sporanox ® oral solution, they measured serum levels via a bioassay as high as 9 μg/mL in the serum and a concentration of 2.5 g/g of wet lung

tissue. The ratio of lung:serum concentrations for the Allendoerfer et al study was much lower than what we found in the present study for orally dosed Sporanox ® oral solution on day 3 (0.28 compared to 0.61), although the lung concentrations were significantly higher than what was required for effective treatment, based on an MLC of 70 ng/mL. Furthermore, their study found that lung tissue levels as high as 2.5 μg/mL were not nearly sufficient to prevent death in mice infected with *A. fumigatus*.

Studies in our laboratory have found that administration of ITZ-pulmonary significantly enhanced survival of mice which were infected with *A. fumigatus*.[18] Similar to Allendoerfer et al,[16] we found that Sporanox ® oral solution did not significantly enhance the survival of the mice in this infection model. Interestingly, the lung tissue concentrations achieved by Allendoerfer et al through dosing of 100 mg/kg are similar to what was achieved in the current study through pulmonary dosing of only 30 mg/kg, although survival was significantly enhanced in the case of pulmonary administration.[18] It is evident that, although similar lung tissue concentrations can be achieved by both oral and pulmonary dosing, significantly higher doses of ITZ are required orally and survival is greater when dosed via inhalation. This would be due to better distribution into the airway and interstitial spaces of the lung tissue as well as distribution to areas which may have low blood circulation because of fungal infiltration. It is also possible that toxicity due to dosing of 100 mg/kg Sporanox ® oral solution could have impacted the survival rates achieved by Allendoerfer et al which has not been associated with pulmonary administration of ITZ-pulmonary (Chapter 5). Toxicity due to diarrhea and dehydration was noted in the current study with only 60 mg/kg given daily in two divided doses.

Infection models using mice are cost effective and repeatable for the study of aspergillus infections and their treatments. However, the distribution of ITZ may be vastly different between human and murine subjects. A study comparing lung and serum ITZ concentrations in patients which died as a result of aspergillosis was conducted by

Coronel et al.[17]   Their study found that human patients display a higher lung:serum ratio for orally dosed ITZ, than was found in our study.   The pharmacokinetic mechanisms for distribution into lung tissue from serum must be different in mice than in humans, as is evident by a lung:serum ratio of less than one in the orally dosed mice compared to lung:serum ratios of greater than 3 in the human subjects.   Coronel et al suggested that, although the lung levels were high in theses patients, their prognosis for survival did not improve. As a result, the patients died due to respiratory failure or dissemination of the aspergillus from the lungs to other organs.   Also, lung tissue ITZ concentrations were not measured in the infected areas of the lung tissue, which could be lower than other regions of the lung.   This proves advantageous for dosing of pulmonary ITZ to human subjects.   Our study has found that excellent lung tissue concentrations were achieved by nebulization, which, based on Coronel's work, would remain high in the lung tissue, due to higher partitioning compared to the mouse model.

The lung:serum ratios achieved through pulmonary dosing is a significant advantage in treating or preventing aspergillus infections in patients at risk.   The portal of entry for aspergillus is primarily through the pulmonary route.   Achieving rapid and sustained levels locally, while minimizing systemic side effects (lower Cmax) is an optimum criterion for prophylaxis.   Based on the murine model, significant ITZ levels are achieved after only 3 days of twice daily dosing of ITZ via inhalation.

4.6 CONCLUSION

Pulmonary dosing of ITZ compositions is an effective method for delivery of antifungal therapy for the treatment and prophylaxis of invasive fungal infections. High and sustained lung tissue concentrations were achieved via inhalation of an amorphous nanoparticulate ITZ pulmonary composition while maintaining serum levels which are above the MLC of *A. fumigatus*.   The lung:serum ratio was significantly greater in

pulmonary dosed ITZ and could prove to enhance treatment while reducing side effects, by decreasing the systemic Cmax and maintaining serum levels above the MLC. By enhancing the local delivery and reducing the potential for side effects of ITZ delivery, this delivery method can greatly improve morbidity and mortality for patients who are at risk of or infected with life threatening fungal infections.

4.7 ACKNOWLEDGMENTS

4.8 REFERENCES

1. Clark, T.A.; Hajjeh, R.A. Recent trends in the epidemiology of invasive mycoses. Current Opinion In Infectious Diseases 2002, *15* (6): p. 569-574.

2. Denning, D.W.; Lee, J.Y.; Hostetler, J.S.; Pappas, P.; Kauffman, C.A.; Dewsnup, D.H.; Galgiani, J.N.; Graybill, J.R.; Sugar, A.M.; Catanzaro, A. NIAID mycoses study group multicenter trial of oral itraconazole therapy for invasive aspergillosis. The American Journal of Medicine 1994, *97* (2): p. 135-144.

3. Singh, N.; Husain, S. Aspergillus infections after lung transplantation: clinical differences in type of transplant and implications for management. The Journal of Heart and Lung Transplantation 2003, *22* (3): p. 258-266.

4. Chiller, T.M.; Stevens, D.A. Treatment strategies for Aspergillus infections. Drug Resistance Updates 2000, *3* (2): p. 89-97.

5. Polak, A., *Antifungal therapy - State of the Art at the Beginning of the 21st Century*, in *Antifungal Agents: Advances and Problems*, E. Jucker, Editor. 2003, Birkhauser Verlag: Basel. p. 59-190.

6. Rapp, R.P. Changing strategies for the management of invasive fungal infections. Pharmacotherapy 2004, *24* (2, Part 2): p. 4S-28S; quiz 29S-32S.

7. Lambros, M.P.; Bourne, D.W.; Abbas, S.A.; Johnson, D.L. Disposition of aerosolized liposomal amphotericin B. Journal Of Pharmaceutical Sciences 1997, *86* (9): p. 1066-1069.

8.   Monforte, V.; Roman, A.; Gavalda, J.; Lopez, R.; Pou, L.; Simo, M.; Aguade, S.; Soriano, B.; Bravo, C.; Morell et, a. Nebulized amphotericin B concentration and distribution in the respiratory tract of lung-transplanted patients. Transplantation 2003, *75* (9): p. 1571-1574.

9.   Boots, R.J.; Paterson, D.L.; Allworth, A.M.; Faoagali, J.L. Successful treatment of post-influenza pseudomembranous necrotising bronchial aspergillosis with liposomal amphotericin, inhaled amphotericin B, gamma interferon and GM-CSF. Thorax 1999, *54* (11): p. 1047-1049.

10.   Koizumi, T.; Kubo, K.; Kaneki, T.; Hanaoka, M.; Hayano, T.; Miyahara, T.; Okada, K.; Fujimoto, K.; Yamamoto, H.; Kobayashi et, a. Pharmacokinetic evaluation of amphotericin B in lung tissue: lung lymph distribution after intravenous injection and airspace distribution after aerosolization and inhalation of amphotericin B. Antimicrobial Agents And Chemotherapy 1998, *42* (7): p. 1597-1600.

11.   Wade, J.C. Aerosolized amphotericin B inhalation is not effective prophylaxis of invasive aspergillus infections during prolonged neutropenia in patients after chemotherapy or autologous bone marrow transplantation. Evidence-based Oncology 2000, *1* (3): p. 87-88.

12.   De Beule, K. Itraconazole: pharmacology, clinical experience and future development. International Journal of Antimicrobial Agents 1996, *6* (3): p. 175-181.

13. KOKS, C.H.W.; MEENHORST, P.L.; BULT, A.; BEIJNEN, J.H. ITRACONAZOLE SOLUTION: SUMMARY OF PHARMACOKINETIC FEATURES AND REVIEW OF ACTIVITY IN THE TREATMENT OF FLUCONAZOLE-RESISTANT ORAL CANDIDOSIS IN HIV-INFECTED PERSONS. Pharmacological Research 2002, *46* (2): p. 195-201.

14. Willems, L.; van der Geest, R.; de Beule, K. Itraconazole oral solution and intravenous formulations: a review of pharmacokinetics and pharmacodynamics. Journal Of Clinical Pharmacy And Therapeutics 2001, *26* (3): p. 159-169.

15. McConville, J.T.; Overhoff, K.A.; Sinswat, P.; Frei, B.L.; Burgess, D.; Talbert, R.L.; Peters, J.I.; Johnston, K.P.; III, R.O.W. Lung Deposition and Clearance of Itraconazole in the Murine Model for Treatment of Acute Fungal Infections. Article In Press.

16. Allendoerfer, R.; Loebenberg, D.; Rinaldi, M.G.; Graybill, J.R. Evaluation of SCH51048 in an experimental model of pulmonary aspergillosis. Antimicrobial Agents And Chemotherapy 1995, *39* (6): p. 1345-1348.

17. Coronel, B.; Levron, J.C.; Dorez, D.; Van Devenne, A.; Archimbaud, E.; Mercatello, A. Itraconazole lung concentrations in haematological patients. Mycoses 2000, *43* (3-4): p. 125-127.

18. McConville, J.T.; Overhoff, K.A.; Sinswat, P.; Frei, B.L.; Burgess, D.S.; Talbert, R.L.; Peters, J.I.; Johnston, K.P.; III, R.O.W. *Novel Treatment of Pulmonary Aspergillosis Using Nebulized Itraconazole Nanoparticles in the Murine Model*.

in *Proceedings of Respiratory Drug Delivery-Europe 2005 Conference*. May 2005. Paris, France.

19. Vaughn, J.M.; Gao, X.; Yacaman, M.-J.; Johnston, K.P.; Williams III, R.O. Comparison of powder produced by evaporative precipitation into aqueous solution (EPAS) and spray freezing into liquid (SFL) technologies using novel Z-contrast STEM and complimentary techniques. European Journal of Pharmaceutics and Biopharmaceutics 2005, *60* (1): p. 81-89.

20. Hu, J.H.; Johnston, K.P.; Williams, R.O. Spray freezing into liquid (SFL) particle engineering technology to enhance dissolution of poorly water soluble drugs: organic solvent versus organic/aqueous co-solvent systems. European Journal of Pharmaceutical Sciences 2003, *20* (3): p. 295-303.

21. Rogers, T.L.; Hu, J.H.; Yu, Z.S.; Johnston, K.P.; Williams, R.O. A novel particle engineering technology: spray-freezing into liquid. International Journal of Pharmaceutics 2002, *242* (1-2): p. 93-100.

22. McConville, J.T.; Williams, R.O.; Carvalho, T.C.; Iberg, A.N.; Johnston, K.P.; Talbert, R.L.; Burgess, D.; Peters, J.I. Design and evaluation of a restraint-free small animal inhalation dosing chamber. Drug Development and Industrial Pharmacy 2005, *31* (1): p. 35-42.

23. Gubbins, P.O.; Gurley, B.J.; Bowman, J. Rapid and sensitive high performance liquid chromatographic method for the determination of itraconazole and its hydroxy-metabolite in human serum. Journal of Pharmaceutical and Biomedical Analysis 1998, *16* (6): p. 1005-1012.

24.   Lange, D.; Pavao, J.H.; Wu, J.; Klausner, M. Effect of a cola beverage on the bioavailability of itraconazole in the presence of H2 blockers. Journal Of Clinical Pharmacology 1997, *37* (6): p. 535-540.

25.   Winston, D.J.; Maziarz, R.T.; Chandrasekar, P.H.; Lazarus, H.M.; Goldman, M.; Blumer, J.L.; Leitz, G.J.; Territo, M.C. Intravenous and oral itraconazole versus intravenous and oral fluconazole for long-term antifungal prophylaxis in allogeneic hematopoietic stem-cell transplant recipients - A multicenter, randomized trial. Annals of Internal Medicine 2003, *138* (9): p. 705-713.

26.   Vandewoude, K.; Vogelaers, D.; Decruyenaere, J.; Jaqmin, P.; De Beule, K.; Van Peer, A.; Woestenborghs, R.; Groen, K.; Colardyn, F. Concentrations in plasma and safety of 7 days of intravenous itraconazole followed by 2 weeks of oral itraconazole solution in patients in intensive care units. Antimicrobial Agents And Chemotherapy 1997, *41* (12): p. 2714-2718.

Chapter 5: Murine Airway Histology and Alveolar Macrophage

Uptake of Inhaled Amorphous ITZ

5.1 ABSTRACT

The purpose of this study was to evaluate the pulmonary histology and macrophage uptake of an inhaled amorphous itraconazole (ITZ) composition. Amorphous ITZ was produced using the particle engineering process spray freezing into liquid (SFL). Mice were dosed with the inhaled nebulizer dispersions of the amorphous ITZ composition, excipient placebo or a saline control twice daily for up to 12 days. Broncho-alveolar lavage (BAL) was conducted on sacrificed mice to collect pulmonary fluid and cells.   Cellular components were separated from the fluid through centrifugation, washed and analyzed for ITZ by high performance liquid chromatography – mass spectroscopy (HPLC-MS). The supernatant was analyzed for cytokine induction by an ELISA assay. Lungs from sacrificed mice in each group were fixed with formaldehyde, sectioned and viewed under light microscopy for histological aberrations. Supernatant from BAL samples were analyzed for the presence and elevation of interleukin (IL-12) to determine if inflammation was elicited as a result of pulmonary dosing of the amorphous ITZ composition or excipient placebo alone compared to the control. The amorphous ITZ composition, excipient placebo and saline control groups were all similar to the negative control which indicated a lack of cytokine induction in any of the groups.   It was confirmed that ITZ was present within the pulmonary macrophages of the amorphous ITZ composition groups (days1, 3, 8 and 12), suggesting that amorphous ITZ particles were taken up by the pulmonary macrophages. There was no evidence of bronchiolar infiltrates, peribronchiolar infiltrates or perivascular infiltrates

in any of the treatment groups. Vascular congestion and edema were similar in all treatment groups and likely secondary to termination by CO_2 narcosis. No epithelial ulceration or evidence of repair was observed in any of the treatment groups. The Cimolai histopathological scores at day 3 for the amorphous ITZ comoposition, excipient placebo and saline control were 2.4,2.25,and 3.0; and at day 8 the scores were 3.3,2.7,and 3.6, respectively (p>0.05). Pulmonary administration of ITZ or excipients does not cause inflammation or changes in alveolar and airway histology. Uptake of ITZ by alveolar and airway macrophages occurs following inhalation of an amorphous ITZ composition. The nebulization of amorphous ITZ is a safe method to administer antifungal doses for the treatment and/or prophylaxis of invasive fungal infections.

5.2 INTRODUCTION

Incidence for infections of fungal origin has seen a steady rise in recent years due to a number of diseases that compromise the immune system.[1] The most notable culprits for these infections include members of the candida and aspergillus species. With the introduction of fluconazole, the incidence of candida infections has decreased yielding a surge in the incidence of aspergillus infections.[2] Infection due to the aspergillus sp. is primarily seen in immunocompromised patients, the mode of entry is typically through inhalation into the lungs and dissemination is almost always fatal.[3] The primary treatment for invasive aspergillosis is intravenous amphotericin B or one of it's liposomal formulations.[4] Renal toxicity and dose related reactions to amphotericin administration is relatively high and treatment efficacy for invasive aspergillosis is low, yielding an overall poor prognosis for patients afflicted with aspergillosis.[2] ITZ, a triazole antifungal, displays a broad spectrum of antifungal action with good coverage for the aspergillus species.[5] However, poor oral bioavailability, variable absorption and

toxicity due to cyclodextrin administration has limited it to a second or third line of treatment for invasive fungal infections.[6, 7]

Because the portal of entry for most aspergillus infections is through the pulmonary cavity, treatment of these infections has been focused on achieving high therapeutic lung levels through systemic administration.[8] Recently it has been proposed that treatment as well as prophylaxis of pulmonary aspergillosis can be achieved through direct administration of antifungal drugs to the lungs through inhalation.[9] It has been reported that amphotericin B and liposomal amphotericin B formulations have been administered through nebulization to treat and prevent infections in patients with high risk of infection.[10-13] Prophylaxis with amphotericin B inhalation was unsuccessful in patients with prolonged neutropenia.[14] Toxicity has been reported for inhalation of the deoxycholate formulation of amphotericin, with little data to support toxicity associated with the lipid formulations.[15] However, inhalation of foreign lipid materials may elicit exogenous lipoid pneumonia and fibrosis of the lung tissue.[16] There has also been development of an inhaled dry powder formulation containing amphotericin B in a lipid complex.[17]

Dissemination could be due to spore migration through the lymphatic and circulatory systems.[3] Inhalation of ITZ nanoparticle dispersions has been proposed to improve localization of ITZ to the site of initial infection for treatment and/or prophylaxis of invasive aspergillosis. Studies in our laboratories have shown improved survival of an infection model through the inhalation of ITZ nanoparticles compared to the Sporanox® oral solution.[18] Toxicological data and drug disposition following inhalation of ITZ has not been evaluated.

The objective of this study was to evaluate the inflammatory response due to an amorphous ITZ composition and solubilizing excipients (e.g. excipient placebo) dosed directly to the lungs through histological and soluble inflammatory mediator analysis (IL-12). Phagocytic uptake of ITZ by pulmonary macrophages was evaluated.

5.3 MATERIALS AND METHODS

5.3.1 Materials

The following materials were purchased: ITZ (ITZ; Hawkins Chemical, Minneapolis, MN); poloxamer 407, polysorbate 80 and NaCl (Spectrum Chemicals, Gardena, CA); acetonitrile and dichloromethane (EM Industries Inc., Gibbstown, NJ).

5.3.2 Production of ITZ Nanoparticles

Amorphous nanoparticles of ITZ were produced using the particle engineering process spray freezing into liquid (SFL).[19] A solution of ITZ, polysorbate 80 and poloxamer 407 was prepared at a 1:0.75:0.75 ratio in acetonitrile with 4% w/w dichloromethane as a cosolvent. This solution was atomized through a 63μm poly-ether-ether-ketone (PEEK) nozzle (Upchurch Scientific, Oak Harbor, WA) via an HPLC pump (Jasco PU-2086plus, Jasco Inc., Easton, MD) at 20 mL/min below the surface of liquid nitrogen. The frozen microparticles were then separated from the liquid nitrogen and the solvent was removed by lyophilization (VirTis Advantage, VirTis, Gardiner, NY). The dried powders were stored under vacuum until dispersion and administration.

5.3.3 Pulmonary dosing of ITZ, Excipient Placebo and Saline Control

The mice were dosed with either an amorphous ITZ composition, an excipient placebo or saline control using the dosing apparatus described recently [20].   Briefly, the chamber consisted of a polymethylmethacrylate (PMMA) airtight box (40.6 x 11.4 x 21.6

cm) with a hinged top, having a nominal wall thickness of 1.25 cm. The chamber was designed to hold up to 14 mice, each having a floor area of approximately 63 cm^2, in accordance with The University of Texas at Austin and the University of Texas Health Science Center at San Antonio Institutional Animal Care and Use Committees (IACUC) guidelines. Table 5.1 lists the number of mice used in each of the groups and the analysis which was performed within each group. The saline control consisted of a 0.85% NaCl solution which was used for dosing and dispersion of the excipient and drug formulations. The excipient placebo consisted of 15mg/mL polysorbate 80 and 15mg/mL poloxamer 407 which was dissolved in normal saline. A 20 mg/mL dispersion of the amorphous ITZ composition was formed in 4 mL of normal saline by first wetting the solution followed by sonication for 1 min prior to dosing. An Aeroneb$^®$ Pro micro pump nebulizer (Aerogen, Inc., Mountain View, CA) was situated at the inlet of the chamber and nebulization of 8 mL solutions or dispersions was conducted over 20 minutes every 12 hours.

5.3.4 Broncho-alveolar Lavage Procedure

Surgery was performed on the sacrificed mice to expose the pleural cavity and trachea at the throat. A small incision was cut into the trachea and a cannula consisting of a 23 gauge needle with a sheath of plastic tubing (0.037" outside diameter (OD) and 0.025" ID) was inserted through the incision to the base of the trachea and clamped to seal the opening. An aliquot (0.75 mL) of phosphate buffered saline was instilled through the cannula into the lungs and then removed to wash the bronchial and alveolar surfaces. This process was repeated for a total of three washes. The phosphate buffered saline containing cells was placed into centrifuge vials and centrifuged at 3000rpm (MiniSpin Plus, Eppendorf International, Hamburg, DE). The supernatant was removed leaving the collected cells in the pellet. Washing of the cells was conducted by

redispersion of the pellet in 1 mL phosphate buffered saline, vortexing for 30 sec, recentrifugation and supernatant removal for a total of three washes. Aliquots of the cells were viewed by light microscopy (Axioskop 2 plus, Carl Zeiss International, Thornwood, NY) to confirm the presence of pulmonary macrophages and analyzed by high performance liquid chromatography, fractionation and mass spectrometry (HPLC-MS) for the presence of ITZ. The supernatant from the BAL was analyzed by enzyme-linked immunosorbent assay (ELISA) for IL-12 elevation (n=2 per sample tested). The ELISA kit (murine IL-12p70) was purchased from R&D Systems (Minneapolis, MN) and conducted according to the manufacturers instructions.

5.3.5 HPLC-MS of Washed Pulmonary Cells

Cells which were recovered from the lung through BAL were subjected to drug extraction using the method initially described in [21] which has been modified and validated for serum extraction in our laboratories. Briefly, the pellets containing the cells were redispersed in 0.25 mL phosphate buffered saline (pH 7.6, 25°C) and vortexed for 30 sec. Zinc sulfate and barium hydroxide were added to each sample in 50 µL aliquots and vortexed for 30 seconds. One milliliter of acetonitrile was added and vortexed for 1.5 min, centrifuged at 3000rpm for 15 min, after which, the supernatant was transferred to a separate vial and dried at 60°C under a stream of dry nitrogen gas. After drying to evaporation, the extracted drug was redispersed in 0.25 mL of mobile which consisted of 62% acetonitrile and 38% water.

The extracted sample was then manually fractionated using HPLC on a Shimadzu LC-10vp (Shimadzu Scientific Instruments, Columbia, MD) with an Alltima 5mm 250 x 4.6mm (Alltech Associates, Deerfield, IL) column held constant at 37°C. The injection volume was 100 µL and a flow rate of 1 mL/min with an ITZ retention time of 17.7min and a peak width of 0.75 min based on standard solutions. The standard solutions

consisted of ITZ concentrations of 1.2 µg/mL and 12 ng/mL which were subjected to fractionation and MS analysis. Drug fractions were collected between 17 min and 18.5 min and then run on mass spectroscopy for qualitative confirmation of ITZ presence. The samples were analyzed by MS at the Center for Research and Environmental Disease.

5.3.6 Histological Analysis

Mice undergoing histological analysis from each group were sacrificed by CO_2 narcosis and 0.75 mL of 10% formaldehyde instilled into the lungs via the trachea using the method outlined in the BAL procedure. Lungs were then harvested and placed into 10% formaldehyde followed by processing and embedding into paraffin wax. Coronal sections of the entire lung were stained and viewed by light microscopy. The Cimolai histopathologic inflammatory score [22] of 0-26 (least to most severe histological response based on) was obtained for each lobe. Evidence of bronchiolar ulceration and tissue repair were also assessed.

5.4 RESULTS AND DISCUSSION

5.4.1 Interleukin-12 Cytokine Analysis

Supernatant from the BAL samples was analyzed for the presence and elevation of IL-12 to determine if inflammation was elicited from pulmonary dosing of the amorphous ITZ composition or the excipient placebo compared to the control. As can be seen in Figure 5.1, the positive control, which was supplied with the ELISA kit, was within the specified concentration range (32-56 pg/mL) at 56.15 pg/mL. The amorphous

ITZ composition, excipient placebo and saline control groups were all similar to the negative control which indicated a lack of cytokine induction in any of the groups.

The cytokine IL-12 is a stimulatory molecule for the innate immune system and is responsible for induction of natural killer T cells. Upon recognition of a foreign pathogenic substance, IL-12 is released by phagocytic cells and other antigen-presenting cells such as macrophages, monocytes, kupfer cells, mesangial cells and glial cells.[23] An increase in the cytokine level in treatment groups would have suggested an underlying inflammation not observed during histological analysis. However, the ELISA results suggest that there was no elicitation and induction of inflammation due to the inhalation of ITZ nanoparticles or the excipients (e.g. polysorbate 80 and poloxamer 407). Typically, pro-inflammatory cytokines are measured from serum, however local inflammation may not elicit a systemic response as was reported by Repa et al.[24] In their study, sensitization with a known allergen via the subcutaneous route elicited a systemic and airway immune response, however, aerosolization of the allergen produced only a small systemic response with a high local airway immune response. For this reason, cytokine analysis was conducted on BAL fluids from the ITZ treated and untreated mice. The utility of BAL fluid for the analysis of IL-12 was reported by Ichinose et al.[25] In their study, instillation of a known irritant to the lungs of mice caused a significant rise in IL-12 release from pro-inflammatory cells, which was observed through ELISA analysis of the BAL fluid. Within the BAL supernatants, Ichinose found IL-12 levels that ranged from 200 – 900 pg/mL, which was not seen in the current study. ITZ has been shown to elicit an elevation in IL-12 through systemic administration to healthy human volunteers. [26] In healthy human volunteers, oral itraconazole therapy shows an increase in the immunomodulator protein IL-12p40. Although, this study has shown that effect of ITZ on local pulmonary IL-12 concentrations is below measurable levels. Furthermore, polysorbate 80 and poloxamers, such as poloxamer 407, have not been associated with increased cytokine levels. [27]

After incubation of solid lipid nanoparticle formulations containing various surfactants, such as polysorbate 80 and poloxamer 407, with macrophages, Sholer et al found that there was no induction in IL-12 or other cytokine release from the macrophages.[27] In the current study, we found that inhalation of poloxamer 407 and polysorbate 80 did not induce release of the cytokine IL-12p70 from immune cells.

5.4.2 Macrophage Uptake of ITZ

Microscopic analysis of the BAL pellet was conducted to ensure the presence of pulmonary macrophages. Figure 5.2 gives some representative micrographs of the pulmonary macrophages following the BAL procedure, centrifugation and cell washing. The macrophages are readily distinguishable from other cells through visualization of the phagosomes within the cells. The remaining cells not used for microscopic analysis underwent drug extraction, chromatographic separation and mass spectroscopic analysis for the presence of ITZ within the cells. ITZ was confirmed present within the pulmonary macrophages which were collected from the mice dosed with the amorphous ITZ composition (days1, 3, 8 and 12), indicating that amorphous ITZ was taken up by the pulmonary macrophages.

Pulmonary macrophages may reside in several locations within the lungs and include airway macrophages, alveolar macrophages and interstitial macrophages. Macrophages which are located on the epithelial surfaces of the airways or alveoli would be the first to engulf inhaled particles and are the cells which would be evaluated using BAL. Particles which migrate out of the airway could be engulfed by interstitial macrophages which could increase particle residence time within the lung. It has been reported that pulmonary macrophage uptake of particles is very rapid; and at low concentrations, particle removal is typically complete within 24 hours, although the process is saturable.[28] The presence of particles has been observed within alveolar

111

macrophages at 1 hour following inhalation.[29] Recognition of foreign particles by alveolar macrophages is dependent on hydrophilicity, size and surface charge. Particles in the size range of 0.2 – 10 μm which are hydrophobic and/or negatively charged are preferentially taken up by macrophages.[30] Inhaled amorphous ITZ which is hydrophobic would, therefore, be taken up by alveolar macrophages. Upon inhalation, the colloidal amorphous ITZ particles will mix with pulmonary fluids and surfactants and migrate toward the epithelial surfaces. The particles are coated with endogenous pulmonary surfactants and proteins, which facilitate their uptake by macrophages.[28] Surfactant removal from the drug surface within the lungs, causing aggregation of the nanoparticles would enhance uptake by the macrophages, by increasing the size and hydrophobicity of the particles.

The main host defense for aspergillus conidia and hyphea is through pulmonary monocyte and macrophage phagocytosis.[31] The ability of ITZ to be taken up by macrophages presents a unique situation for augmentation of host defense with drug treatment through the presence of antifungal activity within the cells which engulf the fungal spores. In the case of azithromycin, both in vitro and in vivo models have shown that the antimicrobial is taken up by phagocytic cells (macrophages and neutrophils) and transported to the site of infection where it can be released. [32] Infection with aspergillus causes a migration of phagocytic cells to the site of infection due to cytokine and chemokine release by pulmonary macrophages.[33] Loading macrophages with ITZ and fungal induced localization of those cells at the site of infection, where it can be released, will aid in treatment of fungal infection and prevention of dissemination.

5.4.3 Airway Histology

Fixed lungs were sectioned and viewed for pulmonary damage and/or inflammation secondary to ITZ or excipient inhalation. Sections from the saline control

group, excipient placebo and amorphous ITZ composition dosed lung sections are shown in Figure 5.3 (a,b), (c,d) and (e,f), respectively As can be seen from the figure, in all groups, the alveoli are intact and do not display damage, inflammation or cell migration. Airways are clear and display a single cell layer, indicative of non-inflamed airways. There was no evidence of bronchiolar, peribronchiolar infiltrates or perivascular infiltrates in any of the groups. Vascular congestion and edema was equal in all groups and likely secondary to termination by CO_2 narcosis. No epithelial ulceration or evidence of repair was observed in any of the groups. The Cimolai[22] histopathological scores at day 3 for ITZ, excipient placebo, and saline control was 2.4,2.25,and 3.0; and at day 8 the scores were 3.3,2.7,and 3.6 respectively (p>0.05).

Histology following inhaled ITZ has not been reported in the literature to date. The histological scores were calculated based on recommendations from Cimolai et al.[22] The scoring can range from 0-26 and is based on histological findings which include the quantity and quality of peribronchiolar and peribronchial infiltrates, luminal exudates, perivascular infiltrates, and parenchymal pneumonia.   It can be seen from the figures that the bronchial and bronchiolar regions (a) are clear and lack any sign of infiltration by immune cells.   The alveolar spaces (b) are clear and undamaged. Perivasculature edema (c) can be seen in all of the samples due to pulmonary edema secondary to CO_2 narcosis.   Other features included in the histology samples include lymphatic tissue (d) and smooth muscle vasculature (e) adjacent to the airways (a). ITZ, delivered via inhalation to laboratory animals, showed a lack of inflammation, cell migration or tissue damage due to administration.   Amphotericin B administration via inhalation of the commercial products has shown excipient related and drug related toxicities. Abe et al found that aerosilization of the deoxycholate formulation of amphotericin B caused lipoid pneumonia in renal transplant patients. [34] The liposomal formulations showed fewer incidences of severe side effects. Experimental trials with inhaled amphotericin B were shown to cause side effects such as dyspnea, bronchospasm,

cough, elevated granulocytes, nausea, vomiting and even coma.[35] Lung surfactant alterations have been seen in studies with ampthotericin B formulations containing deoxycholic acid. [36] It would be expected, from the literature reviewed here, that amphotericin B deoxycholate administration via inhalation would lead to histological aberrations, although it has not be evaluated to date.

The excipients used in the inhaled composition did not elicit an immune response or cause toxicity at the levels which were dosed. Polysorbate 80 is contained within several commercial and experimental formulations and is well established as a safe surfactant for pulmonary administration.[37] However, no commercial product containing poloxamer 407 has been approved by the FDA; and poloxamer 407 has not been studied for pulmonary dosing. In this study, we have shown that pulmonary exposure to 22.5mg/kg of poloxamer 407 twice daily over 8 days did not cause any changes in histology or cytokine elevation. Based on histological analysis, the formulations dosed to the mice did not elicit an immune response or histological changes over an 8 day period. Itraconazole dosed to the lungs was demonstrated to be a safe and efficient method for dosing of the antifungal drug, ITZ, directly to the site of initial infection for patients at risk of acquiring life threatening aspergillosis.

5.5 CONCLUSION

Pulmonary administration of amorphous ITZ nanoparticles or excipient placebo does not cause inflammation or changes in alveolar and airway histology. Uptake of ITZ by alveolar and airway macrophages occurs following inhalation of an amorphous ITZ composition. Nebulization of amorphous ITZ is a safe and non-inflammatory method to administer antifungal doses for the treatment and/or prophylaxis of invasive fungal infections.

5.6 ACKNOWLEDGEMENTS

5.7 REFERENCES

1.   Kontoyiannis, D.P.; Mantadakis, E.; Samonis, G. Systemic mycoses in the immunocompromised host: an update in antifungal therapy. Journal of Hospital Infection 2003, *53* (4): p. 243-258.

2.   Wingard, J.R.; Leather, H. A new era of antifungal therapy. Biology of Blood and Marrow Transplantation 2004, *10* (2): p. 73-90.

3.   Hori, A.; Kami, M.; Kishi, Y.; Machida, U.; Matsumura, T.; Kashima, T. Clinical significance of extra-pulmonary involvement of invasive aspergillosis: a retrospective autopsy-based study of 107 patients. Journal of Hospital Infection 2002, *50* (3): p. 175-182.

4.   Wenzel, R.; Del Favero, A.; Kibbler, C.; Rogers, T.; Rotstein, C.; Mauskopf, J.; Morris, S.; Schlamm, H.; Troke, P.; Marciniak et, a. Economic evaluation of voriconazole compared with conventional amphotericin B for the primary treatment of aspergillosis in immunocompromised patients. The Journal Of Antimicrobial Chemotherapy 2005, *55* (3): p. 352-361.

5.   Chiller, T.M.; Stevens, D.A. Treatment strategies for Aspergillus infections. Drug Resistance Updates 2000, *3* (2): p. 89-97.

6.   Kapsi, S.G.; Ayres, J.W. Processing factors in development of solid solution formulation of itraconazole for enhancement of drug dissolution and bioavailability. International Journal of Pharmaceutics 2001, *229* (1-2): p. 193-203.

7.   Allendoerfer, R.; Loebenberg, D.; Rinaldi, M.G.; Graybill, J.R. Evaluation of SCH51048 in an experimental model of pulmonary aspergillosis. Antimicrobial Agents And Chemotherapy 1995, *39* (6): p. 1345-1348.

8.   Coronel, B.; Levron, J.C.; Dorez, D.; Van Devenne, A.; Archimbaud, E.; Mercatello, A. Itraconazole lung concentrations in haematological patients. Mycoses 2000, *43* (3-4): p. 125-127.

9.   O'Riordan, T.G. Inhaled antimicrobial therapy: from cystic fibrosis to the flu. Respiratory Care 2000, *45* (7): p. 836-845.

10.   Lambros, M.P.; Bourne, D.W.; Abbas, S.A.; Johnson, D.L. Disposition of aerosolized liposomal amphotericin B. Journal Of Pharmaceutical Sciences 1997, *86* (9): p. 1066-1069.

11.   Monforte, V.; Roman, A.; Gavalda, J.; Lopez, R.; Pou, L.; Simo, M.; Aguade, S.; Soriano, B.; Bravo, C.; Morell et, a. Nebulized amphotericin B concentration and distribution in the respiratory tract of lung-transplanted patients. Transplantation 2003, *75* (9): p. 1571-1574.

12.   Boots, R.J.; Paterson, D.L.; Allworth, A.M.; Faoagali, J.L. Successful treatment of post-influenza pseudomembranous necrotising bronchial aspergillosis with liposomal amphotericin, inhaled amphotericin B, gamma interferon and GM-CSF. Thorax 1999, *54* (11): p. 1047-1049.

13.   Koizumi, T.; Kubo, K.; Kaneki, T.; Hanaoka, M.; Hayano, T.; Miyahara, T.; Okada, K.; Fujimoto, K.; Yamamoto, H.; Kobayashi et, a. Pharmacokinetic evaluation of amphotericin B in lung tissue: lung lymph distribution after

intravenous injection and airspace distribution after aerosolization and inhalation of amphotericin B. Antimicrobial Agents And Chemotherapy 1998, *42* (7): p. 1597-1600.

14.   Wade, J.C. Aerosolized amphotericin B inhalation is not effective prophylaxis of invasive aspergillus infections during prolonged neutropenia in patients after chemotherapy or autologous bone marrow transplantation. Evidence-based Oncology 2000, *1* (3): p. 87-88.

15.   Ruijgrok, E.J.; Vulto, A.G.; Van Etten, E.W. Efficacy of aerosolized amphotericin B desoxycholate and liposomal amphotericin B in the treatment of invasive pulmonary aspergillosis in severely immunocompromised rats. The Journal Of Antimicrobial Chemotherapy 2001, *48* (1): p. 89-95.

16.   Spickard, A., 3rd; Hirschmann, J.V. Exogenous lipoid pneumonia. Archives Of Internal Medicine 1994, *154* (6): p. 686-692.

17.   Shah, S.P.; Misra, A. Development of liposomal amphotericin B dry powder inhaler formulation. Drug Delivery 2004, *11* (4): p. 247-253.

18.   McConville, J.T.; Overhoff, K.A.; Sinswat, P.; Frei, B.L.; Burgess, D.; Talbert, R.L.; Peters, J.I.; Johnston, K.P.; III, R.O.W. Lung Deposition and Clearance of Itraconazole in the Murine Model for Treatment of Acute Fungal Infections. Article In Press.

19.   Rogers, T.L.; Hu, J.H.; Yu, Z.S.; Johnston, K.P.; Williams, R.O. A novel particle engineering technology: spray-freezing into liquid. International Journal of Pharmaceutics 2002, *242* (1-2): p. 93-100.

20. McConville, J.T.; Williams, R.O.; Carvalho, T.C.; Iberg, A.N.; Johnston, K.P.; Talbert, R.L.; Burgess, D.; Peters, J.I. Design and evaluation of a restraint-free small animal inhalation dosing chamber. Drug Development and Industrial Pharmacy 2005, *31* (1): p. 35-42.

21. Gubbins, P.O.; Gurley, B.J.; Bowman, J. Rapid and sensitive high performance liquid chromatographic method for the determination of itraconazole and its hydroxy-metabolite in human serum. Journal of Pharmaceutical and Biomedical Analysis 1998, *16* (6): p. 1005-1012.

22. Cimolai, N.; Taylor, G.P.; Mah, D.; Morrison, B.J. Definition and Application of a Histopathological Scoring Scheme for an Animal-Model of Acute Mycoplasma-Pneumoniae Pulmonary Infection. Microbiology and Immunology 1992, *36* (5): p. 465-478.

23. Kang, B.Y.; Kim, E.; Kim, T.S. Regulatory mechanisms and their therapeutic implications of interleukin-12 production in immune cells. Cellular Signalling 2005, *17* (6): p. 665-673.

24. Repa, A.; Wild, C.; Hufnagl, K.; Winkler, B.; Bohle, B.; Pollak, A.; Wiedermann, U. Influence of the route of sensitization on local and systemic immune responses in a murine model of type I allergy. Clinical And Experimental Immunology 2004, *137* (1): p. 12-18.

25. Ichinose, T.; Nishikawa, M.; Takano, H.; Sera, N.; Sadakane, K.; Mori, I.; Yanagisawa, R.; Oda, T.; Tamura, H.; Hiyoshi, K. Pulmonary toxicity induced by

intratracheal instillation of Asian yellow dust (Kosa) in mice. Environmental Toxicology and Pharmacology 2005, *20* (1): p. 48-56.

26.   Inoue, H.; Iwasaki, H.; Abe, S.; Yamaguchi, H.; Ueda, T. Modulation of the human interleukin-12p40 response by a triazole antifungal derivative, itraconazole. Scandinavian Journal Of Infectious Diseases 2004, *36* (8): p. 607-609.

27.   Scholer, N.; Olbrich, C.; Tabatt, K.; Muller, R.H.; Hahn, H.; Liesenfeld, O. Surfactant, but not the size of solid lipid nanoparticles (SLN) influences viability and cytokine production of macrophages. International Journal Of Pharmaceutics 2001, *221* (1-2): p. 57-67.

28.   Geiser, M. Morphological aspects of particle uptake by lung phagocytes. Microscopy Research And Technique 2002, *57* (6): p. 512-522.

29.   Bosquillon, C.; Preat, V.; Vanbever, R. Pulmonary delivery of growth hormone using dry powders and visualization of its local fate in rats. Journal of Controlled Release 2004, *96* (2): p. 233-244.

30.   Makino, K.; Yamamoto, N.; Higuchi, K.; Harada, N.; Ohshima, H.; Terada, H. Phagocytic uptake of polystyrene microspheres by alveolar macrophages: effects of the size and surface properties of the microspheres. Colloids and Surfaces B: Biointerfaces 2003, *27* (1): p. 33-39.

31.   Herbrecht, R.; Natarajan-Ame, S.; Letscher-Bru, V.; Canuet, M. Invasive pulmonary aspergillosis. Seminars in Respiratory and Critical Care Medicine 2004, *25* (2): p. 191-202.

32.   Gordon, E.M.; Blumer, J.L. Rationale for single and high dose treatment regimens with azithromycin. Pediatric Infectious Disease Journal 2004, *23* (2): p. S102-S107.

33.   Pylkkanen, L.; Gullsten, H.; Majuri, M.-L.; Andersson, U.; Vanhala, E.; Maatta, J.; Meklin, T.; Hirvonen, M.-R.; Alenius, H.; Savolainen, K. Exposure to Aspergillus fumigatus spores induces chemokine expression in mouse macrophages. Toxicology 2004, *200* (2-3): p. 255-263.

34.   Abe, M.; Kondo, K.; Fujino, S.; Hirasawa, Y.; Yokoyama, A.; Kohno, N.; Hiwada, K. Lipoid pneumonia combined with pulmonary nocardiosis caused by inhalation of amphotericin-B after renal transplantation. Nihon Kyobu Shikkan Gakkai Zasshi 1996, *34* (6): p. 737-740.

35.   Dubois, J.; Bartter, T.; Gryn, J.; Pratter, M.R. The physiologic effects of inhaled amphotericin B. Chest 1995, *108* (3): p. 750-753.

36.   Ruijgrok, E.J.; Vulto, A.G.; Van Etten, E.W.M. Efficacy of aerosolized amphotericin B desoxycholate and liposomal amphotericin B in the treatment of invasive pulmonary aspergillosis in severely immunocompromised rats. Journal of Antimicrobial Chemotherapy 2001, *48* (1): p. 89-95.

37.   Williams III, R.O.; Liu, J. Formulation of a protein with propellant HFA 134a for aerosol delivery. European Journal of Pharmaceutical Sciences 1999, *7* (2): p. 137-144.

TABLES AND FIGURES

Table 1.1: Photon correlation spectroscopy diameter, polydispersity index, after and

before diaultrafiltration, and Z-potential of griseofulvin suspensions

Solvent	Surfactant mixture	Cosurfactant	Size (nm)		Z-potential (mV)
			After	Before	
Butyl lactate	Lecithin–ethanol	TDC	162 ± 15 (0.12)	240 ± 32 (0.18)	−31
Butyl lactate	Lecithin–1,2-propanediol	TDC	212 ± 24 (0.15)	286 ± 44 (0.18)	−36
Butyl lactate	Lecithin–ethanol	KG	85 ± 12 (0.09)	98 ± 15 (0.11)	−38
Butyl lactate	Lecithin–1,2-propanediol	KG	103 ± 13 (0.08)	116 ± 18 (0.09)	−32

Table 2.1 – Glass transition temperatures for the SFL and EPAS samples compared to

control and bulk excipients

Sample Type	Glass Transition Temperature (Tg °C)
SFL Danazol/PVP 1/1	123.1
EPAS Danazol/PVP 1/1	143.2
Physical Mixture	154.5
Bulk PVP	162.1

Table 2.2 - Various Characterization Results for EPAS and SFL formulations

Characterization Technique	EPAS	SFL
BET Surface Area	7.41 m^2/g	52.2 m^2/g
Contact Angle	26.6°	28.0°
LLD Aggregate Particle Size	6.50 μm	3.50 μm

Table 3.1: Pharmacokinetic parameters calculated using noncompartmental analysis in Win-Nonlin of the mice dosed with the EPAS and SFL compositions, physical mixture and Danocrine ® capsule powder.

ITZ Formulation	Cmax (ng/mL)	Tmax (hrs)	$T_{1/2}$ (hrs)	K_{el} (hrs-1)	AUC (0-24) (ng.h/mL)	AUC_{inf} (ng.h/mL)
Danocrine ® capsules	199.3	1.0	6.7	0.103	1519	1648
Physical Mixture (danazol:PVP-K15 1:1)	204.4	1.0	4.5	0.154	672	703
EPAS Composition (danazol:PVP-K15 1:1)	430.1	1.0	4.6	0.150	1534	1613
SFL Composition (danazol:PVP-K15 1:1)	392.5	1.0	4.4	0.158	2558	2626

Table 4.1: Pharmacokinetic parameters for lung and serum concentrations from mice

dosed with the amorphous ITZ pulmonary composition.

Pharmacokinetic Parameter	Lung[α]	Serum[β]
C_{max} (µg/g)	13.4	0.12
T_{max} (hrs)	1	5.35
$T_{1/2\ K01}$ (hrs)		3.73
$T_{1/2\ K10}$ (hrs)	5.5	3.70
K_{01} (hrs^{-1}) absorption		0.186
K_{10} (hrs^{-1}) elimination	0.13	0.188
AUC_{inf} (µg.h/mL)	85.8	1.69

[α]Based on non-compartmental analysis of the lung tissue concentrations vs. time.

[β]Calculated based on one-compartmental analysis of the serum concentrations vs. time

for extravascular administration.

Table 4.2: Morphological observations in mice dosed with ITZ-pulmonary, ITZ-oral and

with the Sporanox ® oral solution; (+) symptoms were observed in mice

from that group; (-) no symptoms were observed.

	ITZ-Pulmonary	Sporanox ® Oral Solution	ITZ-Oral
Dose related deaths$^\phi$	0	2	0
Evidence of dehydration$^\alpha$	-	+	-
Diarrhea$^\beta$	-	+	-
Decreased grooming$^\chi$	-	+	-
Dosing resistance$^\delta$	-	+	-

$^\phi$Indicates the total number of deaths during the study period

$^\alpha$Mice displayed poor skin turgor upon scruffing during dosing and were lethargic.

$^\beta$Diarrhea was evident by moist and watery stool.

$^\chi$Decreased grooming was noted as fur which was unkempt and soiled.

$^\delta$Immediate resistance to dosing upon insertion of the gavage tip into the oral cavity.

Table 4.3: Average lung and serum trough levels in mice dosed with ITZ-oral, ITZ-pulmonary and the Sporanox ® oral solution

      which were used to calculate the lung:serum ratios for each group and time point. Lung:serum ratios from other

      published studies are included in the table for comparison.

	Average Lung Concentrations (ug/g)			Average Serum Concentrations (ug/mL)			Lung:Serum Ratio			Reference Lung:Serum Ratios	
Day	3	8	12	3	8	12	3	8	12	Mice$^{\alpha}$ [16]	Human$^{\beta}$ [17]
Amorphous ITZ: Pulmonary	2.16	2.22	2.52	0.12	0.11	0.11	18.15	20.18	22.27		
Amorphous ITZ: Oral	0.16	0.23	0.15	0.16	0.26	0.29	1.03	0.89	0.54		
Sporanox ® Oral Liquid	0.19	0.15	0.18	0.31	0.37	0.39	0.61	0.40	0.45	0.28	3.7 - 12.2

$^{\alpha}$Mice were dosed with 100 mg/kg Sporanox ® oral solution once daily for three days. Lung and serum levels were measured 6 hours

      after the last dose.

$^{\beta}$Human subjects were dosed with 200mg of Sporanox ® oral solution or capsules twice daily until death ensued at which time the

      lung and serum ITZ was measured.

Table 5.1: Number of mice dosed with the amorphous ITZ composition, excipient

placebo composition or saline control and the procedures which were

conducted on those mice at specific time points. Sacrifice was conducted 15

minutes following the final dose of the given day.

	Amorphous ITZ Composition	Excipient Placebo	Saline Control
BAL	5 – Day 1 3 – Day 3 2 – Day 8 2 – Day 12	3 – Day 3 3 – Day 8	3 – Day 3 3 – Day 8
Histology	5 – Day 3 5 – Day 8	2 – Day 3 2 – Day 8	2 – Day 3 2 – Day 8

Table A.1: Materials which were utilized during lung and serum extractions

Compound	Composition Supplied	Manufacturer	CAS #	Product Number	Lot#
0.3 N Barium Hydroxide	Stock Solution	Sigma		B4059-500ML	073K6033
ZnSO4 + 7H2O	Powder	Sigma	7446-20-0	Z4750-100G	113K0037
Drug Free Mouse Serum	Frozen Liquid	Sigma		S-7273	023K8933
Methanol (HPLC Grade)	Liquid	EM Science	67-56-1	MX0475-1	42246236
Acetonitrile (HPLC Grade)	Liquid	EMD	75-05-8	AX0145-1	43209331
Potassium Phosphate, Monobasic	Powder	Fisher Scientific	7778-77-0	P285-500	17115
Sodium Hydroxide	Pellets	Spectrum Chemical	1310-73-2	S0170	QB1002
Itraconazole	Powder	Hawkins, Inc.	84625-61-6	007192	PH03100204
Ketoconazole	Powder	Spectrum Chemical	65277-42-1	K1149	
Alltima 5μm 250 x 4.6mm	Packed HPLC Column	Alltech Incorporated		88056	
Alltima 5μm 7.5 x 4.6mm	Guard column	Alltech Incorporated		96080	
HPLC Vials (12x32mm) 1.8mL	100 count box	Kimble Glass Inc.		60822W-1232	
HPLC Vial Tops	1000 count case	Kimble Chromatography		73826B-2	
HPLC 150μL vial inserts	100 count case	Kimble Chromatography		60843P-529	
MicroTubes Centrifuge Vials (1.5mL)	500 count bag	Sarstedt		72.690	
0.45 μm 50mm bottle top filter	1 each	Nalgene		295-4520	503752
Test Tubes (16x100mm)	250 count box	VWR Brand		47729-576	

Table A.2: Protocol used to prepare standards and stock solutions for the

chromatographic analysis of ITZ in lung and serum.

	Component	Concentration	Theoretical
0.3N Barium Hydroxide	Pre-made	Pre-made	Pre-made
0.4N ZnSO4 + 7H20	ZnSO4 + 7H2O	5.75% w/v	5.75g
	Water	QS	100mL
ITZ Standard Solution	Itraconazole	0.012% w/v	0.012g / 100mL
	Mobile Phase	QS	100mL
ITZ Dilutions	1		
	2		
	3		
	4		
	5		
	6		
	7		
	8		
	9		
	10		
ITZ Spiking Solution	Itraconazole	0.012% w/v	0.012g / 100mL
	Methanol	QS	100mL
ITZ Dilutions	1		
	2		
	3		
	4		
	5		
	6		
	7		
	8		
	9		
	10		
Ketoconazole Stock Solution	Ketoconazole	0.012% w/v	0.012g/100mL
	Acetonitrile	QS	100mL
Extraction Solution	Ketoconazole SS		0.5 mL
	Acetonitrile	QS	100mL
			Final Concentration
NaOH solution 0.2M	NaOH	0.2M	8g
	Water	QS	1000mL
Phospate Buffer 0.05M	Potassium Phosphate, monobasic	0.2M	27.22g
USP 24	Water	QS	1000mL

Take 500mL of this solution and add to 2000mL bottle and add 162.4mL of 0.2M NaOH
QS this solution to 2000mL with water, measure pH
Adjust pH with 0.2M NaOH

pH 6.7

Mobile Phase composition

1) Phosphate Buffer   100% v/v   2000mL
This composition is filtered through a 0.45μm filter and degassed under sonication for 15min

2) Acetonitrile   100% v/v   2000mL
This composition is filtered through a 0.45μm filter and degassed under sonication for 15min

These components can be premixed or run on two separate pumps to achieve the ratio listed below

Table A.3: Protocol used for the extraction of spiked serum samples and animal serum and lung samples and the chromatographic conditions utilized during their analysis

---

Protocol for Sample Preparation

Spiked Serum Extraction Procedure

1 Spike serum samples by adding 10μL of the dilutions from above made in methanol
2 Vortex for 30 seconds
3 Add 50μL of 0.3N Barium Hydroxide solution
4 Add 50μL of 0.4N ZnSO4 + 7H2O solution
5 Vortex for 30 seconds
6 Add 1mL of extraction solution
7 Vortex for 1.5 mins
8 Centrifuge at 3000rpm for 15 mins
9 Transfer supernatant to a clean vial
10 Dry under nitrogen stream
11 Redisperse with 0.25mL of mobile phase
12 vortex for 1min
13 Centrifuge at 3000rpm for 15 mins
14 Transfer supernatant to an HPLC vial with 150μL insert
15 Run on HPLC

Serum Sample Preparation and Extraction	**Lung Tissue Sample Preparation and Extraction**
1 Vortex samples for 30seconds	1 Add 1 mL of normal saline to hydrated lung
2 Transfer 0.25mL to clean vial	2 Disrupt cells through sonication for 20 sec
3 Add 50μL of 0.3N Barium Hydroxide solution	3 Transfer 0.25 mL to clean vial
4 Add 50μL of 0.4N ZnSO4 + 7H2O solution	4 Add 50μL of 0.3N Barium Hydroxide solution
5 Vortex for 30 seconds	5 Add 50μL of 0.4N ZnSO4 + 7H2O solution
6 Add 1mL of extraction solution	6 Vortex for 30 seconds
7 Vortex for 1.5 mins	7 Add 1mL of extraction solution
8 Centrifuge at 3000rpm for 15 mins	8 Vortex for 1.5 mins
9 Transfer supernatant to a clean vial	9 Centrifuge at 3000rpm for 15 mins
10 Dry under nitrogen stream	10 Transfer supernatant to a clean vial
11 Redisperse with 0.25mL of mobile phase	11 Dry under nitrogen stream
12 vortex for 1min	12 Redisperse with 0.25mL of mobile phase
13 Centrifuge at 3000rpm for 15 mins	13 vortex for 1min
14 Transfer supernatant to an HPLC vial with 150μL insert	14 Centrifuge at 3000rpm for 15 mins
15 Run on HPLC	15 Transfer supernatant to an HPLC vial with 150μL insert
	16 Run on HPLC

Chromatographic Conditions

Column	Alltima 5μm 250 x 4.6mm
Guard Column	Alltima 5μm 7.5 x 4.6mm
Column Temperature	37°C
Flow Rate	1mL/min
Mobile Phase	62% Organic/38% Aqueous
UV absorbance	263nm
Injection Volume	100μL
Retention time - Itraconazole	17.5
- Ketoconazole	7.6

Table A.4: Calculation of an average dry lung weight which was utilized for the determination of the concentration of ITZ in mice dosed with the amorphous ITZ pulmonary composition.

Sample #	Hydrated Lung Weight (g)	Dry Lung Weight (g)	% Solids
1	0.3539	0.0763	21.56
2	0.3362	0.0753	22.40
3	0.2195	0.0512	23.33
4	0.2732	0.0554	20.28
5	0.2116	0.0451	21.31
6	0.2764	0.0577	20.88
7	0.2543	0.0494	19.43
8	0.2169	0.0486	22.41
Average	0.2678	0.0574	21.45
Std Dev.	0.0541	0.0120	1.26
%RSD	20.1914	20.9655	5.8876

Table A.5: Wet weight calculations for the lungs extracted from mice dosed with the amorphous ITZ pulmonary composition.

Theses lung weights were used to calculate the level of ITZ within each extracted lung from the sacrificed mice.

Mouse ID#	Sample ID	Weight of Collection Container (g)	Weight (Container + Lung) (g)	Weight of Lung (g)
1	Dose Uniformity 1	1.9558	2.1900	0.234
2	Dose Uniformity 2	1.9985	2.2605	0.262
3	Dose Uniformity 3	1.9646	2.1947	0.230
4	Dose Uniformity 4	1.9928	2.2489	0.256
5	Dose Uniformity 5	1.9391	2.1741	0.235
6	Dose Uniformity 6	1.9400	2.1952	0.255
7	Dose Uniformity 7	1.9829	2.3066	0.324
8	Dose Uniformity 8	1.9397	2.2002	0.261
9	Dose Uniformity 9	1.9539	2.1947	0.241
10	Dose Uniformity 10	1.9538	2.1860	0.232

Table B.1: Formulation parameters and potencies for the fluid-bed processing of the

danazol EPAS dispersions.

Formulation	Volume of EPAS Dispersion	% PVP	Quantity of Substrate	Danazol Potency
AG	200mL	5	200g	2.5%
BG	200mL	5	50g	5%
CG	800mL	5	50g	10%
DG	300mL	0	50g	6%
E[1]	200mL	0	0	50%

1. Formulation quench frozen and lyophilized

Table C.1: Particle size analysis of the dispersions and powders produced by EPAS processing using the steel crimped nozzle with (u-c-1 – u-c-3) and without (c-1 – c-3) ultrsonication. The final dispersion and powder consisted of danazol/PVP K-15 in a 1/3 ratio.

| Crimped nozzle (Δp 5000psi) with ultrasonic horn | | | | | | Crimped nozzle alone (Δp 5000psi) | | | | | |
| Suspension | | | Powder | | | Suspension | | | Powder | | |
	D(v, 0.5) (μm)	Span Index		D(v, 0.5) (μm)	Span Index		D(v, 0.5) (μm)	Span Index		D(v, 0.5) (μm)	Span Index
U-C1	11.19	3.222	U-C1	11.74	1.824	C1	11.33	2.487	C1	11.06	2.337
U-C2	6.64	3.347	U-C2	4.27	2.447	C2	5.13	3.483	C2	5.63	1.529
U-C3	8.02	1.301	U-C3	6.94	2.237	C3	6.03	5.497	C3	4.54	5.337

Table C.2: Particle size analysis of the dispersions produced by EPAS processing using the steel crimped nozzle with ultrsonication at various ultrasonic outputs. The final dispersion consisted of danazol/PVP K-15 in a 1/3 ratio.

Ultrasonic Output	D(v, 0.5) μm	Span Index
30W	13.24	2.220
60W	6.55	2.654
90W	9.85	1.653

Table C.3: Particle size analysis of the dispersions produced by EPAS processing using the steel crimped nozzle with ultrsonication at various at various organic feed flow rates. The final dispersion consisted of danazol/PVP K-15 in a 1/3 ratio.

Flow rate (ml/min)	D(v, 0.5) μm	Span Index
2	5.10	1.698
5	6.55	2.654
10	9.66	2.943

Table D.1: Formulation utilized for manufacture of SFL powders containing various

acidulants at a 1:1 ratio with the model compound ITZ

Components	%w/w	Amount Weighed (g)
Itraconazole	0.3	0.21
Poloxamer 407	0.6	0.42
Acidulant	0.3	0.21
1,3-dioxolane	49.4	34.58
DI water	49.4	34.58

Table D.2: Formulations which were processed using SFL. The components were

dissolved in a 1,3-dioxolane/water 1/1 cosolvent mixture such that the

concentration of ITZ was 0.3% w/w.

Formulation	Itraconazole	PVP K-15	Poloxamer 407	Succinic Acid
1	1	2		1
2	1	3		1
3	1	1	1	1
4	1	2	0.5	1

Table D.3: Formulations which were processed using SFL. The components were dissolved in a 1,3-dioxolane/water 1/1

cosolvent mixture such that the concentration of ITZ was 0.3% w/w.

Formulation	Itraconazole	Sodium Dodecyl Sulfate	Poloxamer 407	Succinic Acid	Deoxycholic Acid	Lactose Monohydrate	Manitol
1	1	1		1			
2	1	2		1			
3	1	1	1	1			
4	1	2	0.5	1			
5	1	1					
6	1	2					
7	7	3					
8	10	1					
9	5	2			2.5		
10	5	2				2.5	
11	5	2					2.5
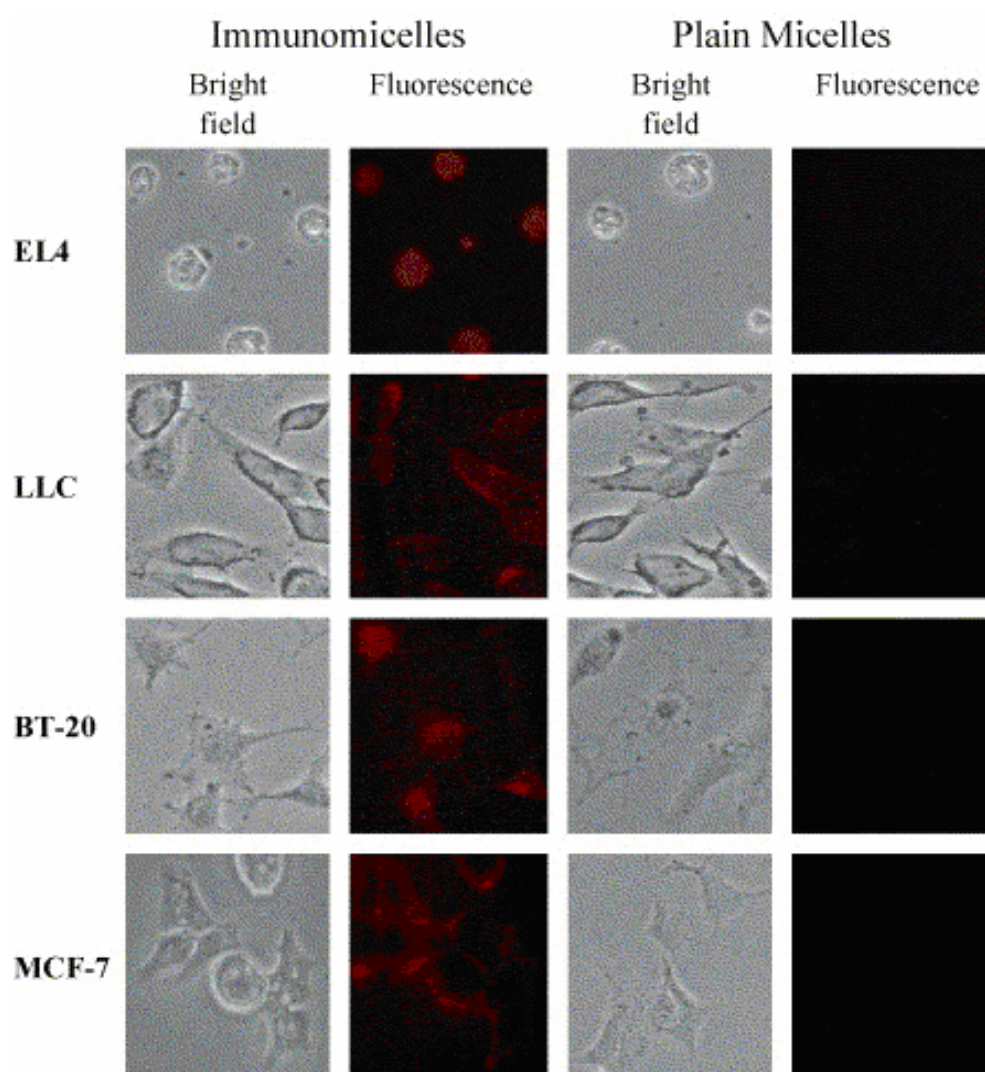
Figure 1.1: Fluorescence microscopy of the binding of Rh-PE-labeled paclitaxel-loaded

PEG-PE-based micelles to murine EL4 and LLC cells; and human BT-20

and MCF-7 cells. With permission from [38]
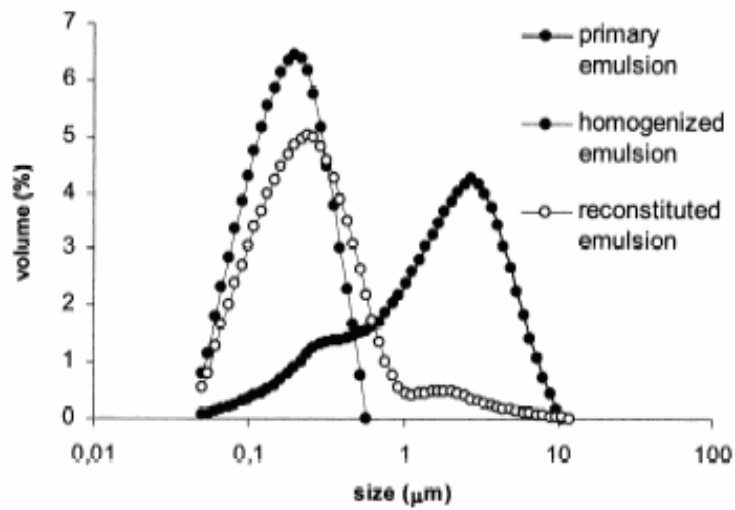
Figure 1.2: Size histograms obtained for the 5-PDTT containning emulsion before and

after reconstitution. With permission from [9]
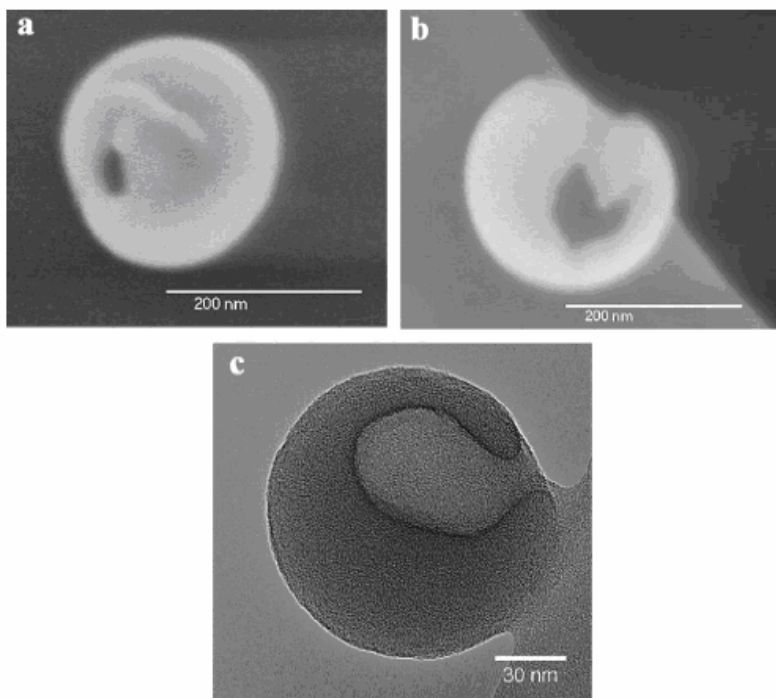
Figure 1.3: SEM (a,b) and TEM (c) images of hollow nanoparticles produced by an
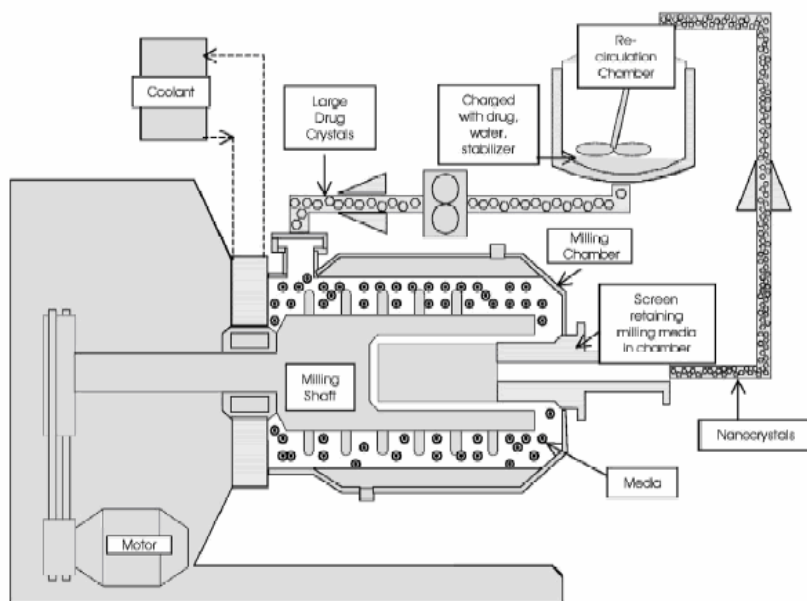
aerosol flow reactor. With permission from [10]

Figure 1.4: A schematic representation of the NanoCrystal milling apparatus. With

permission from [11]
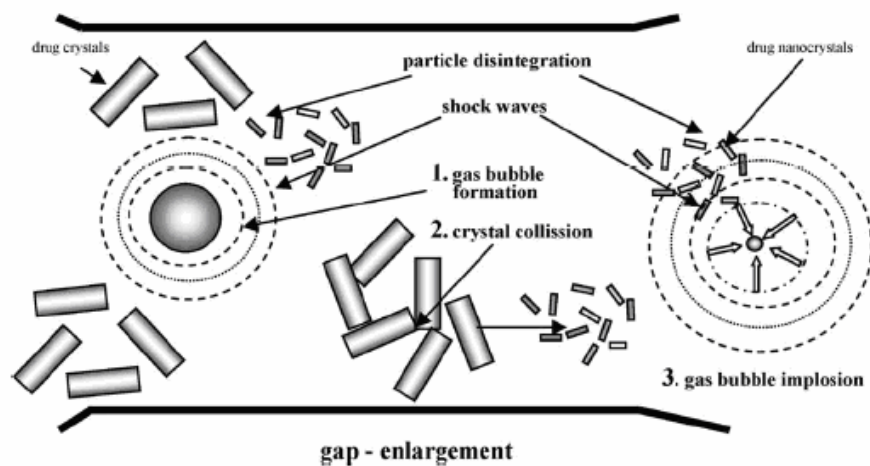
Figure 1.5: The mechanism of particle dimmunition during piston-gap homogenization.
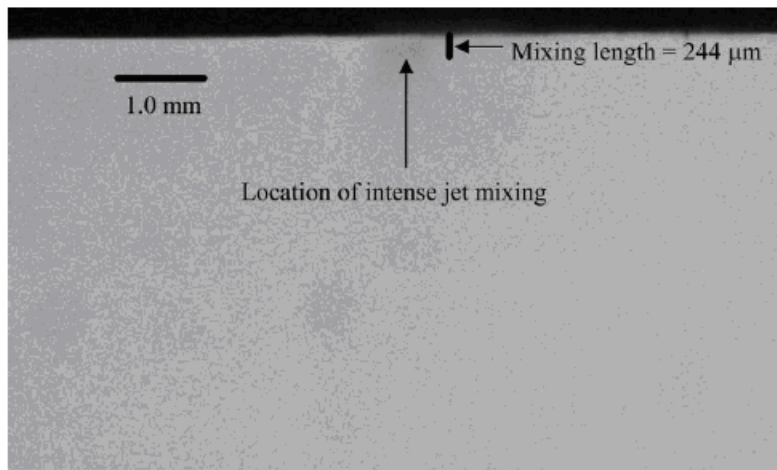
With permission from [3]
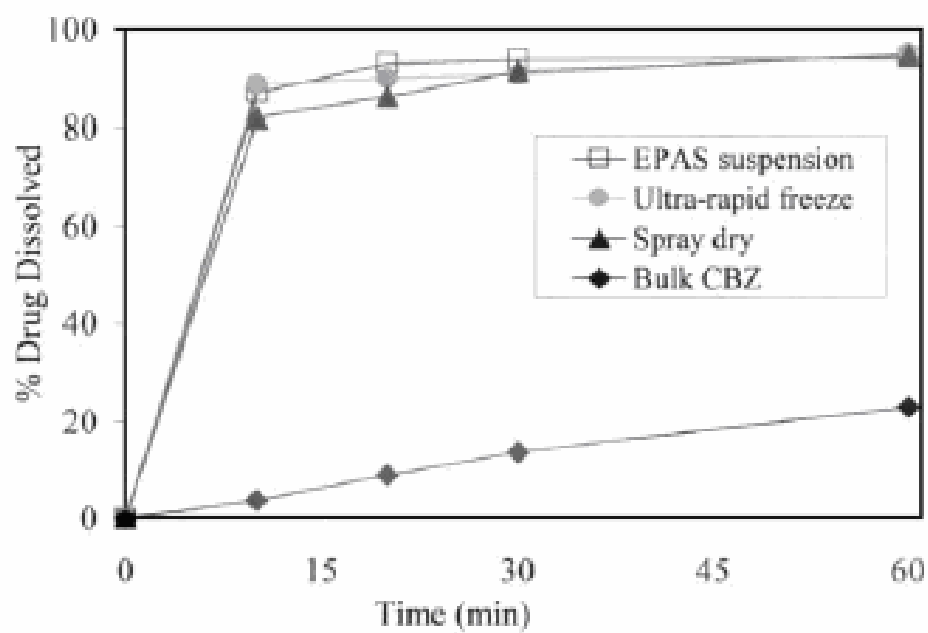
Figure 1.6: A Dissolution profile of carbamazepine produced by the EPAS process,

ultra-rapid freezing, spray drying and bulk drug. With permission from [17]

Figure 1.7: (a) Image of the PCA jet mixing between a swirling hollow-cone jet. (b) Photo of a swirling hollow-cone jet being injected into stagnant supercritical CO2. With permission from [18]
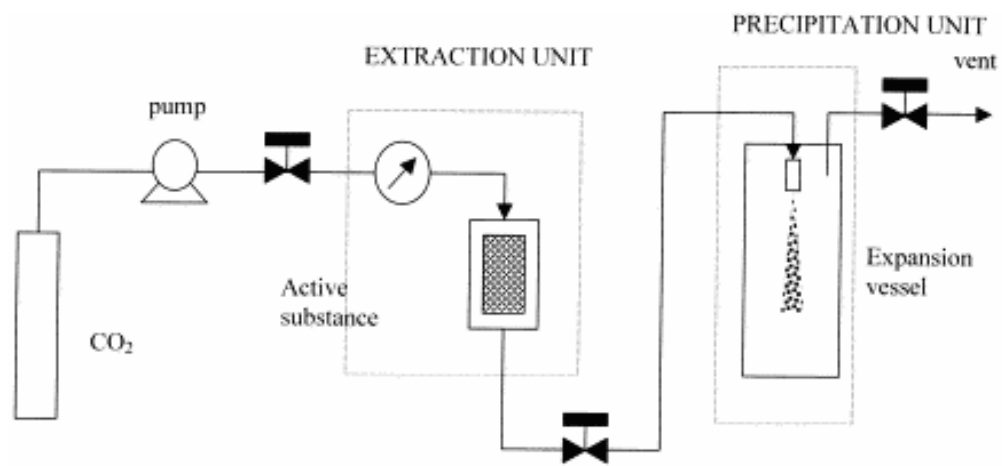
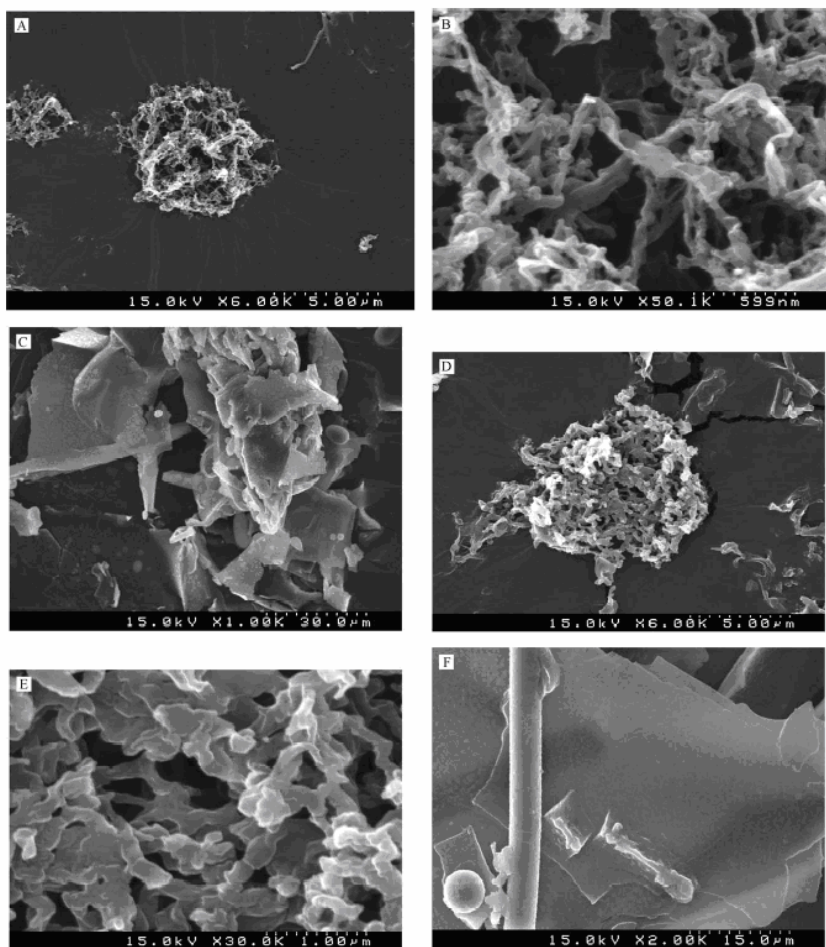Figure 1.8: A schematic representation of the RESS process. With permission from [39]

Figure 1.9: SEM micrographs of SFL BSA powders. SFL BSA (A,B); Slow Frozen

BSA (C); SFL BSA/Tyloxapol (D, E); Slow Frozen BSA/Tyloxapol (F).
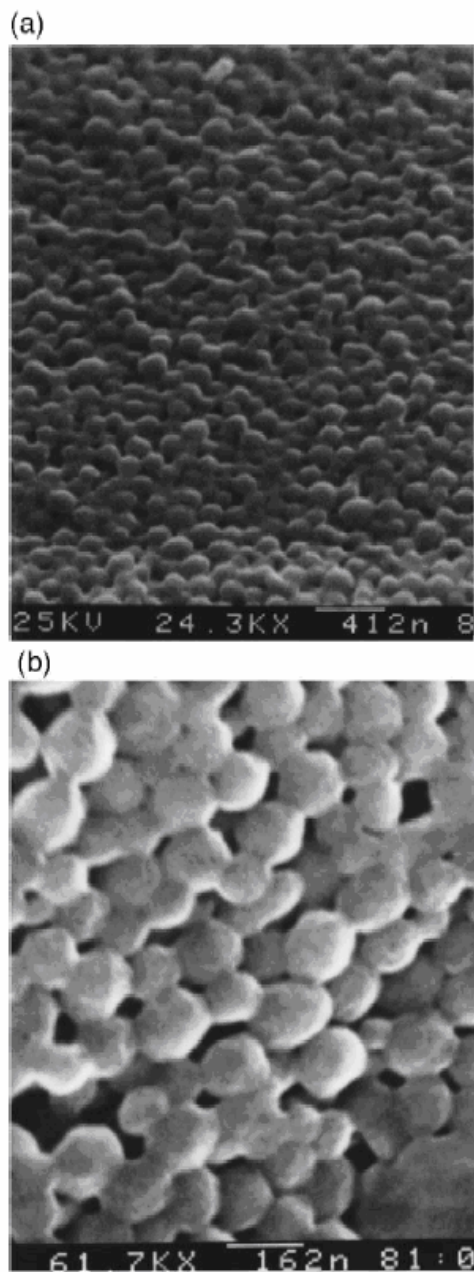
With permission from [23]

Figure 1.10: Scanning electron micrograph of BSA loaded PLGA nanoparticles. With permission from [40]

solid solution

drug-enriched shell

lipid shell

drug molecularily
dispersed
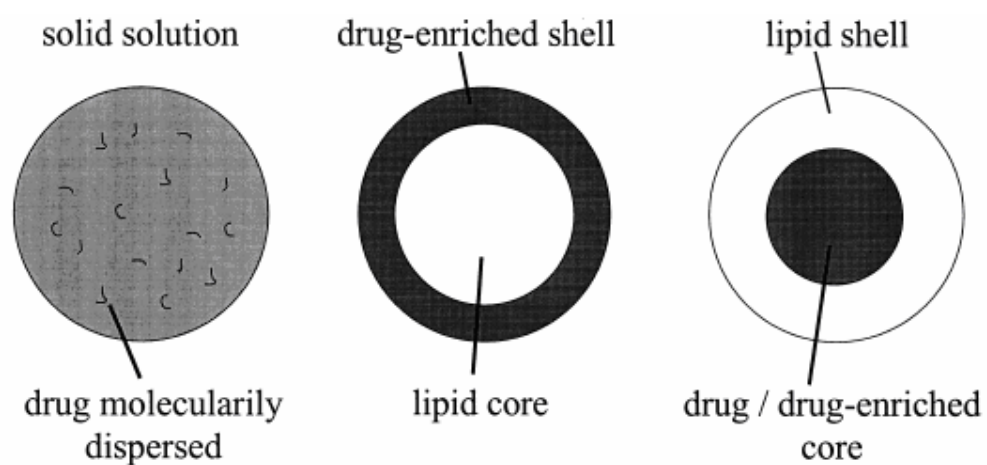
lipid core

drug / drug-enriched
core

Figure 1.11: Drug incorporation models for solid lipid nanoparticles. With permission
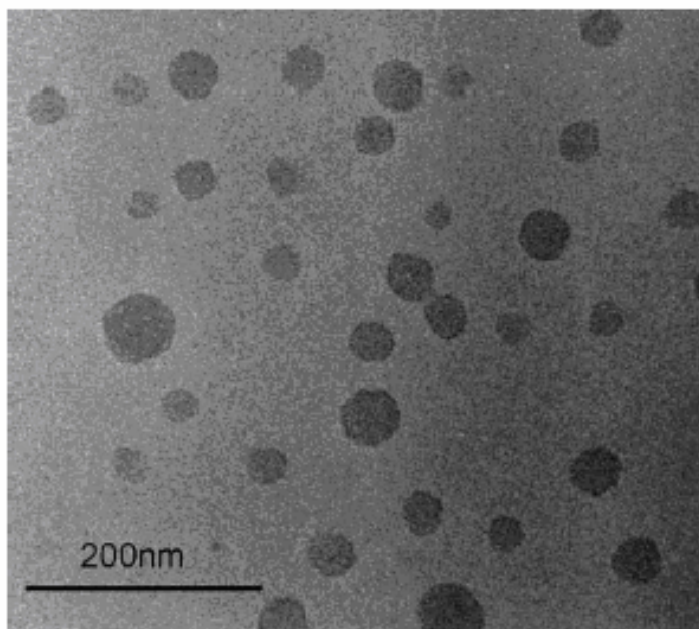
from [26]

Figure 1.12: Cryo-TEM image of PTX-loaded pHPMAmDL-b-PEG micelles. With
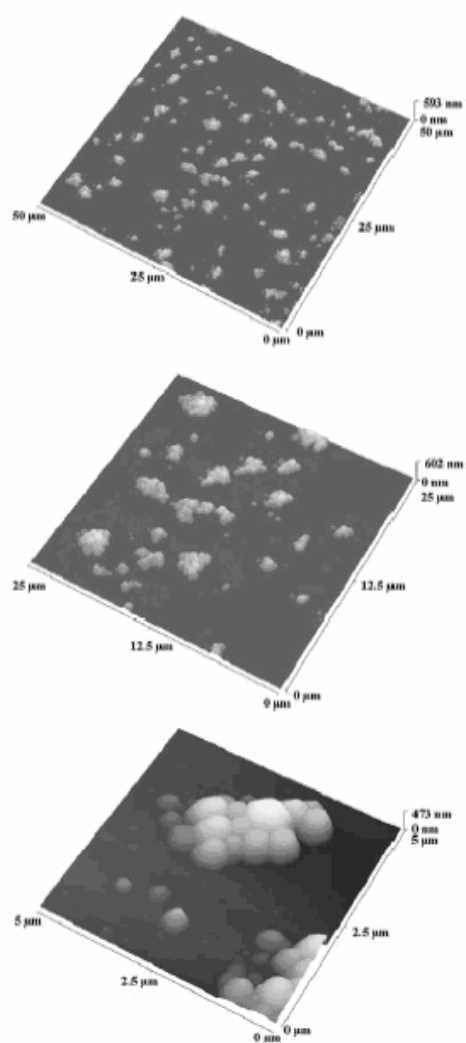
permission from [28]

Figure 1.13: Non-Contact mode AFM images of SLNs at scan ranges of: (a) 50 um (b) 25 um and (c) 5 um. With permission from [34]
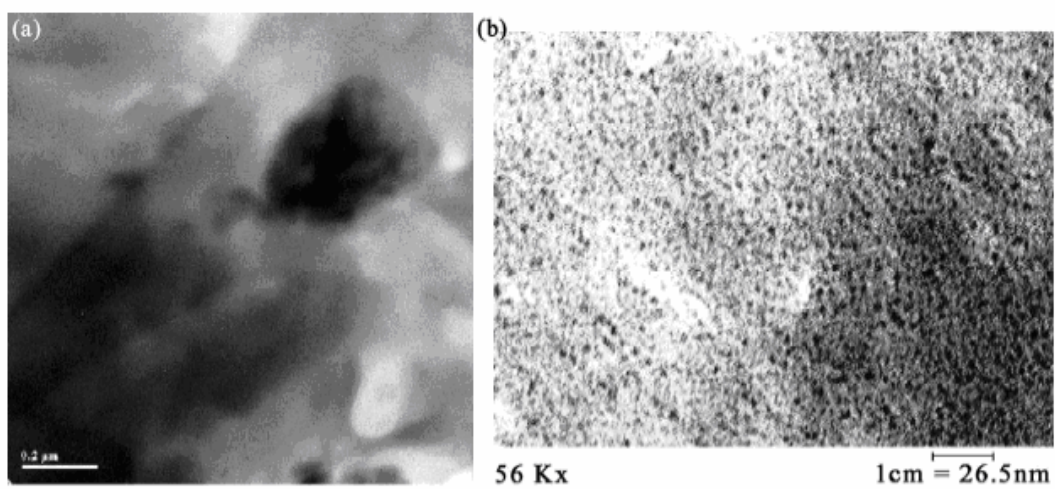
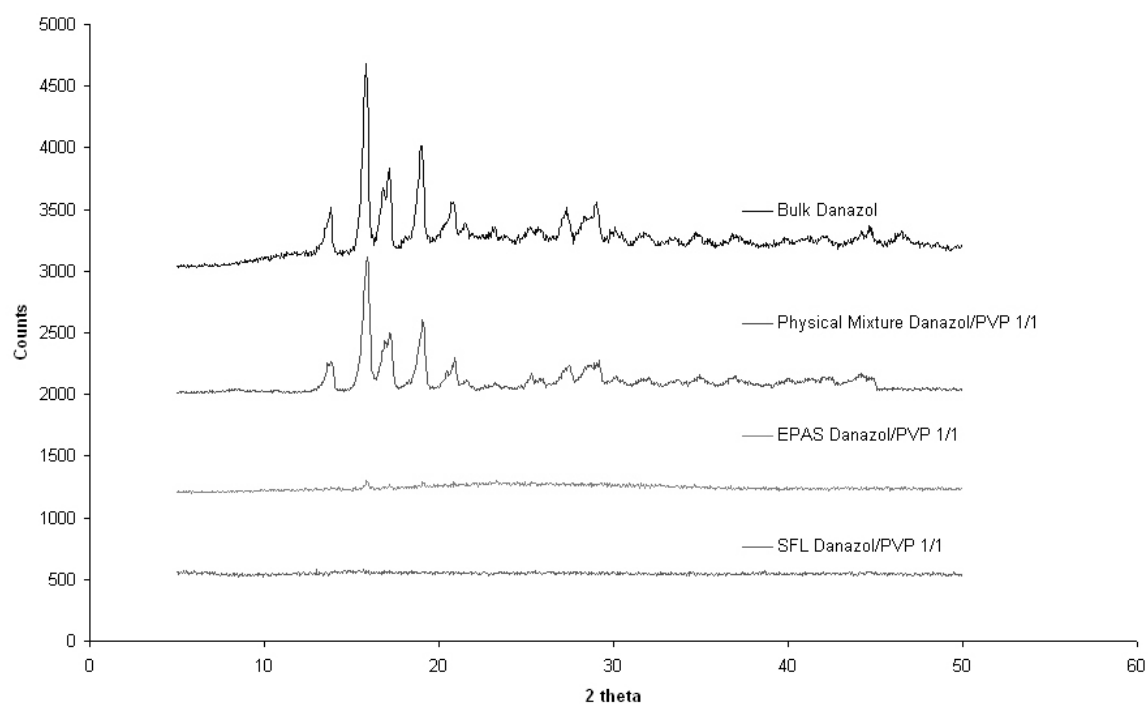Figure 1.14: TEM micrographs of SFL powders (a, b) With permission from [41]

Figure 2.1: X-Ray Diffraction patterns for the EPAS and SFL formulations compared to

bulk danazol and the physical mixture
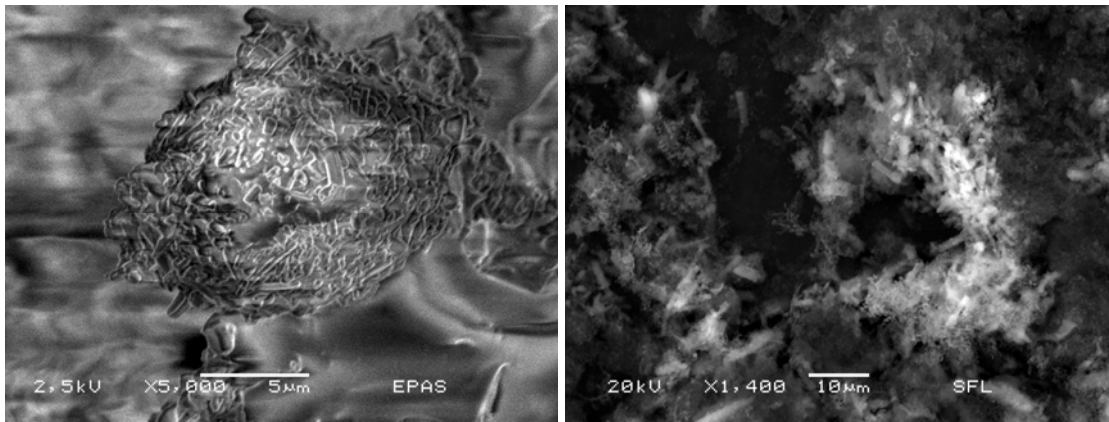
156

Figure 2.2: ESEM micrographs for the EPAS (a) and the SFL (b) powders
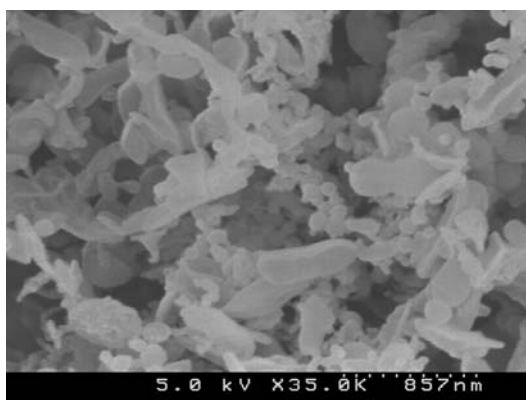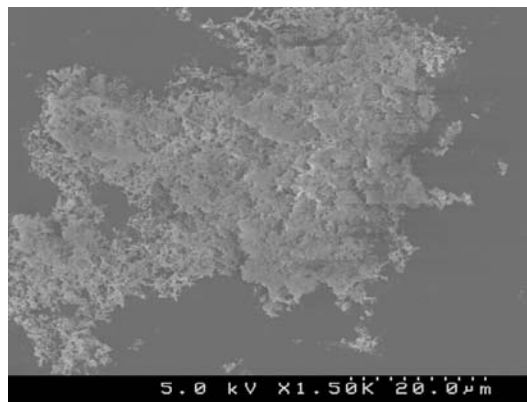
a)   b)

Figure 2.3: SEM micrographs of the SFL processed danazol
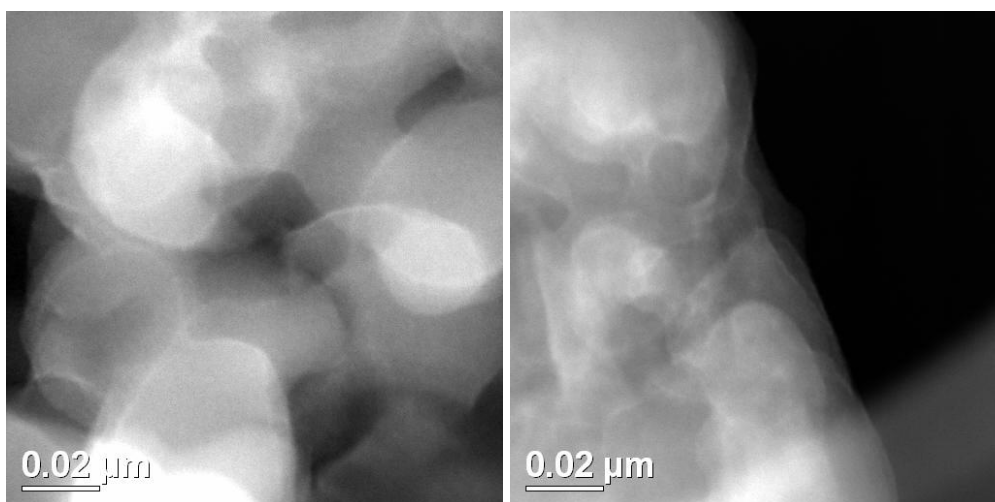
a)   b)
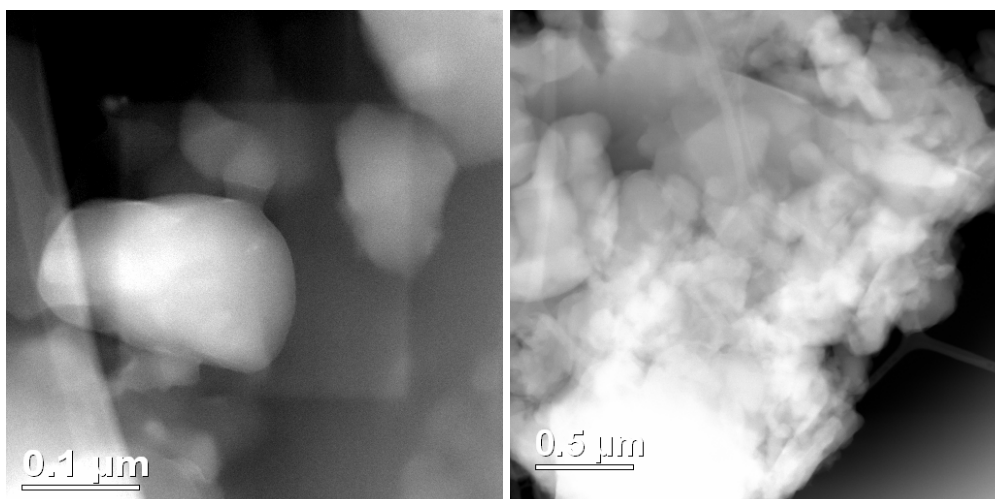
c)   d)

Figure 2.4: STEM micrographs of the SFL (a,b) processed danazol and the EPAS (c,d)

processed danazol

159
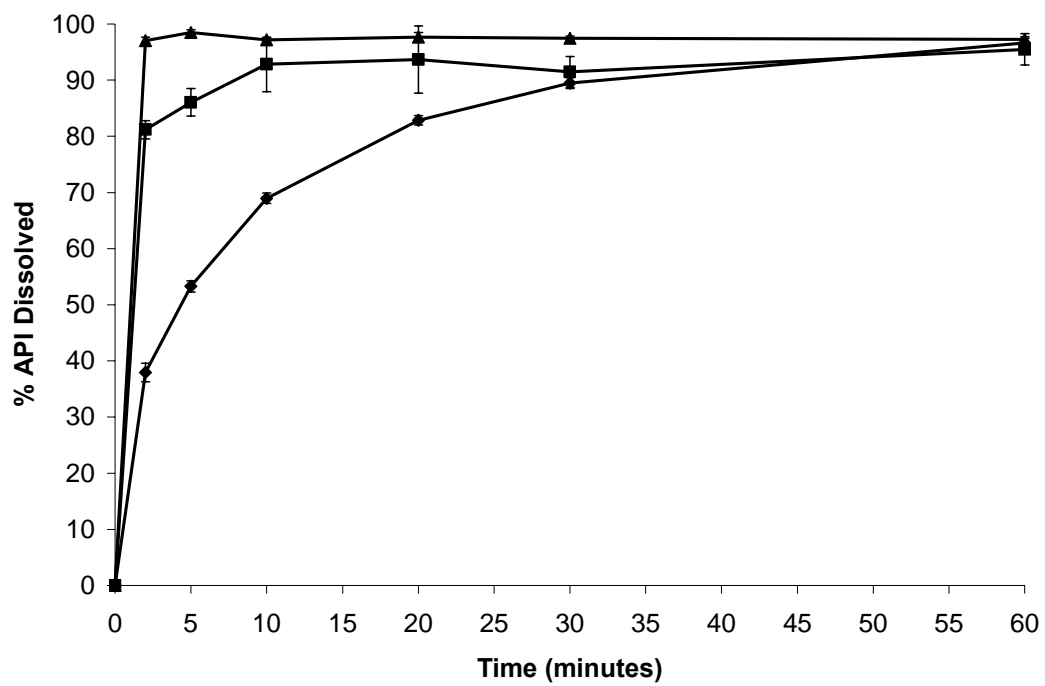
Figure 2.5: Dissolution profile for SFL (▲) and EPAS (■) processed danazol compared to the bulk danazol(♦) (USP II, 50 rpm, 0.5% SDS pH 9 Tris buffer, n = 6)
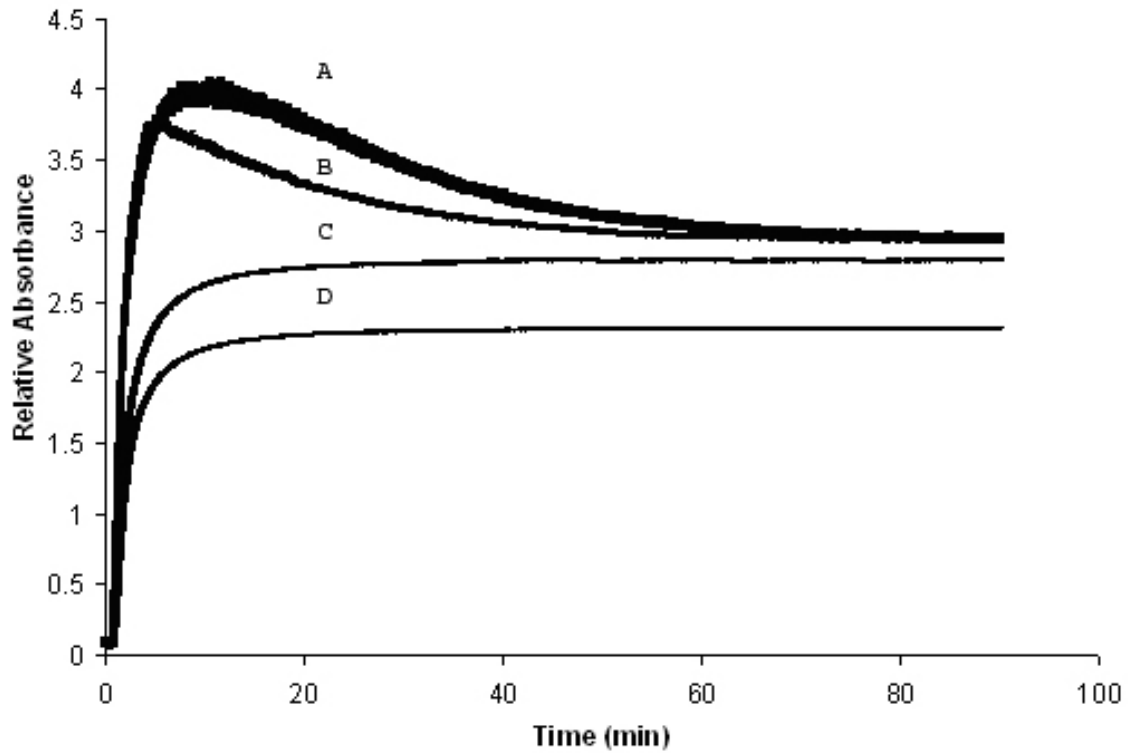
Figure 3.1: Supersaturated dissolution in 0.75% SDS, 1.21% Tris buffer at pH 9 for the

SFL composition (danazol:PVP-K15 1:1) (A), EPAS composition

(danazol:PVP-K15 1:1) (B), physical mixture (danazol:PVP-K15 1:1) (C)

and Danocrine ® capsule (D).
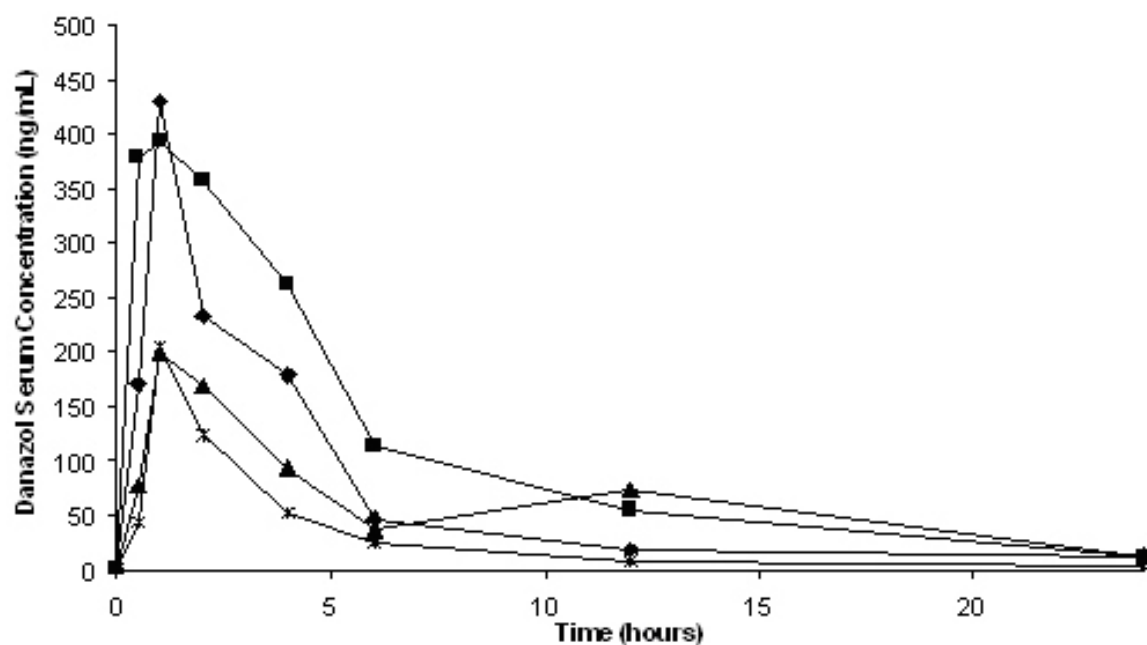
Figure 3.2: Oral bioavailability of danazol in a mouse model for the SFL composition

(danazol:PVP-K15 1:1) (■), EPAS composition (danazol:PVP-K15 1:1)

(♦), physical mixture (danazol:PVP-K15 1:1) (∗) and Danocrine ® capsule

(▲).
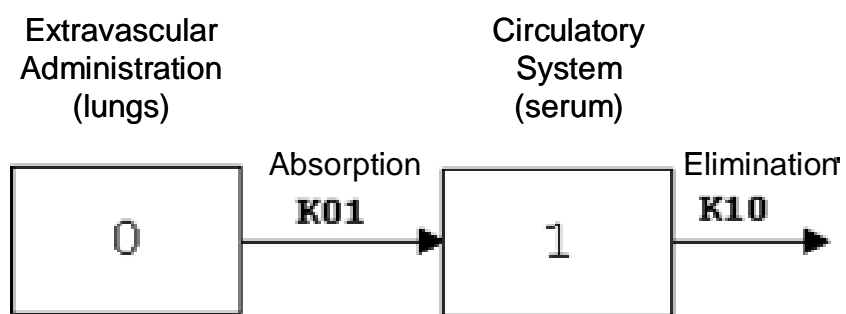
Figure 4.1: One-compartment pharmacokinetic model used to evaluate the serum

concentrations measured from mice dosed with the ITZ-pulmonary and to

estimate pharmacokinetic parameters.
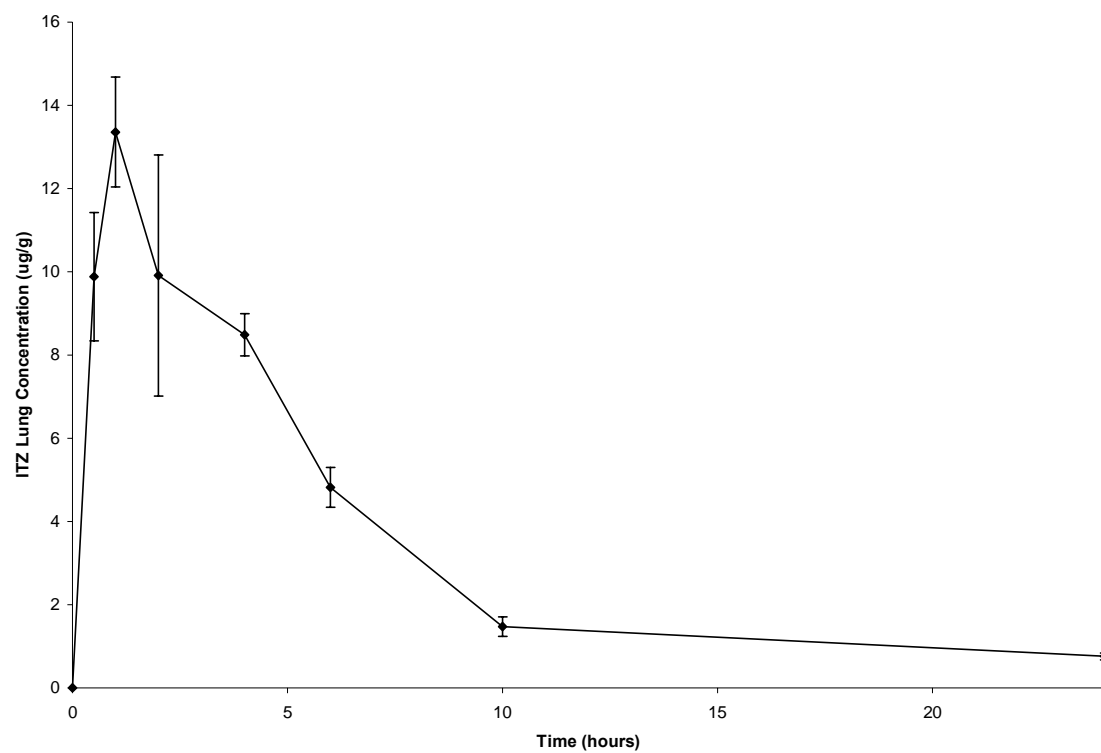
Figure 4.2: Average ITZ lung tissue concentrations in mice dosed with ITZ-pulmonary.

N=2 mice per time point with 4 individual extractions from each mouse.
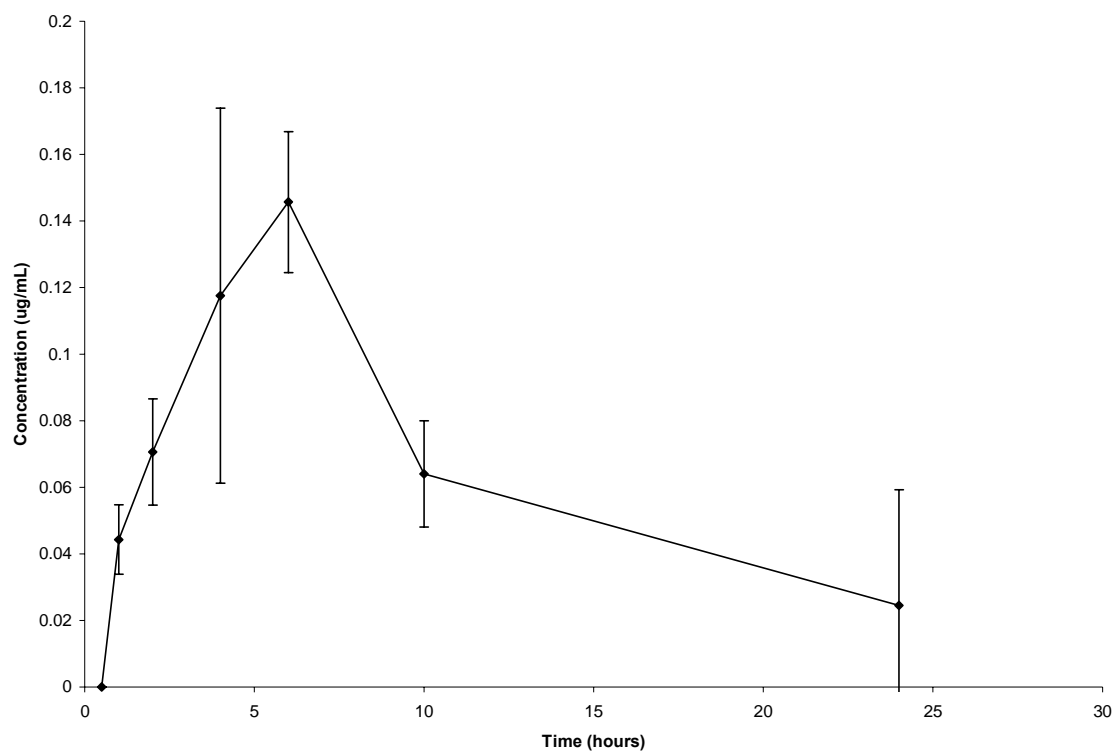
Figure 4.3: Average ITZ serum concentrations over a 24 hour period for mice dosed with

ITZ-pulmonary. N=2 mice per time point.
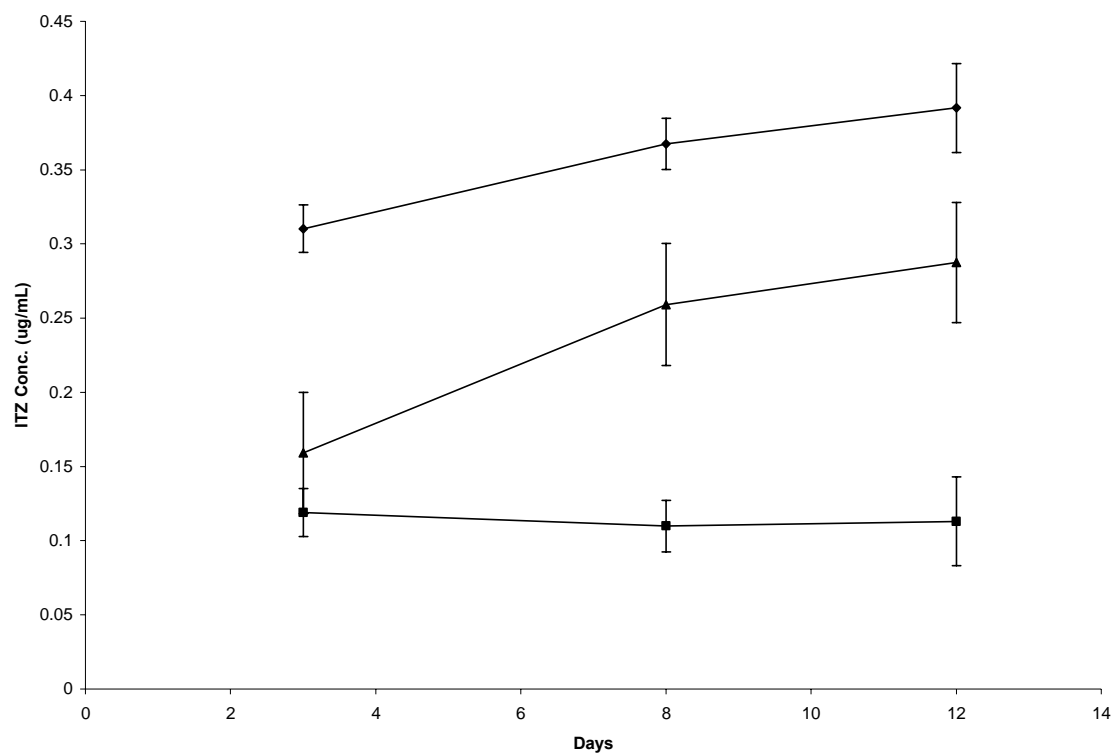
Figure 4.4: Average serum concentrations for mice dosed with ITZ-oral (▲), Sporanox

® Oral Solution (♦) or ITZ-pulmonary (■)
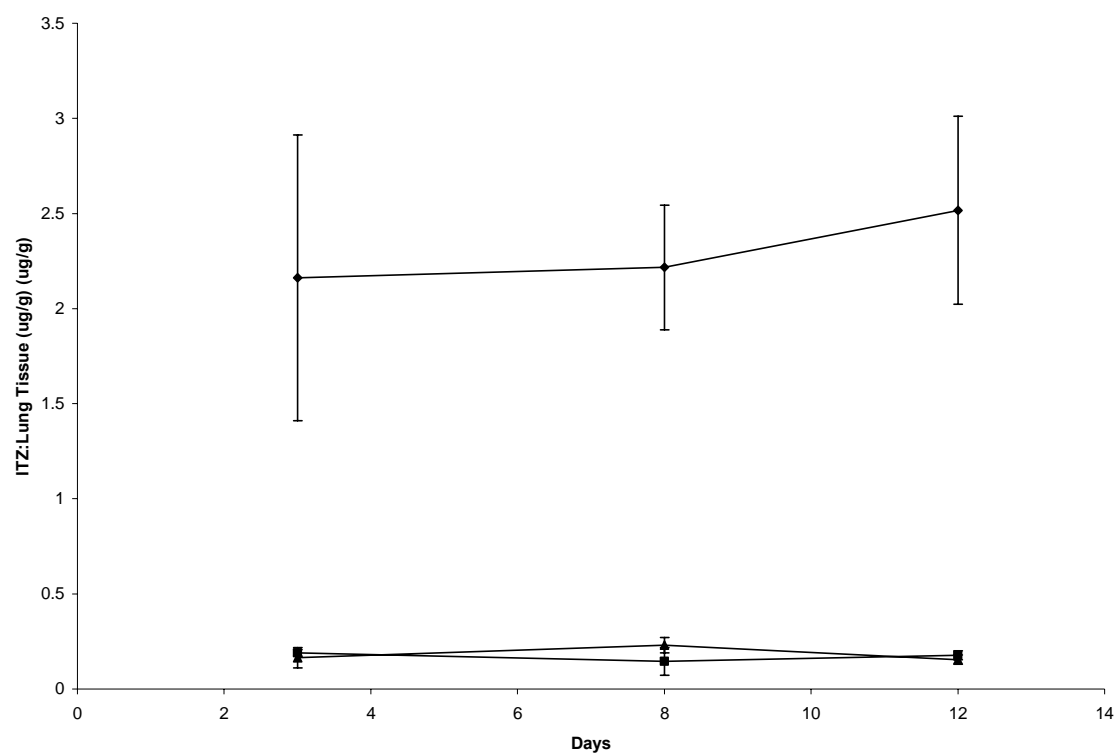
Figure 4.5: Average lung tissue ITZ concentrations in mice dosed with ITZ-oral (▲)

Sporanox ® Oral Solution (■) or ITZ-pulmonary (♦)
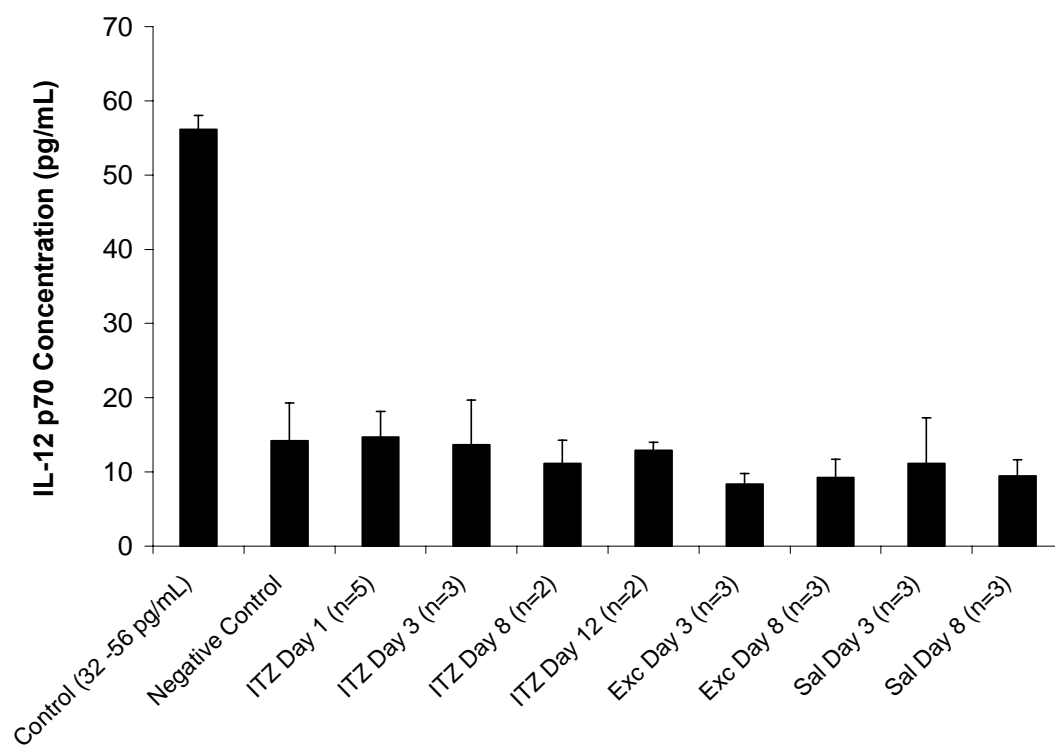
Figure 5.1: Mean IL-12p70 concentrations measured via ELISA assay of the positive control, negative control and BAL supernatants of sacrificed mice
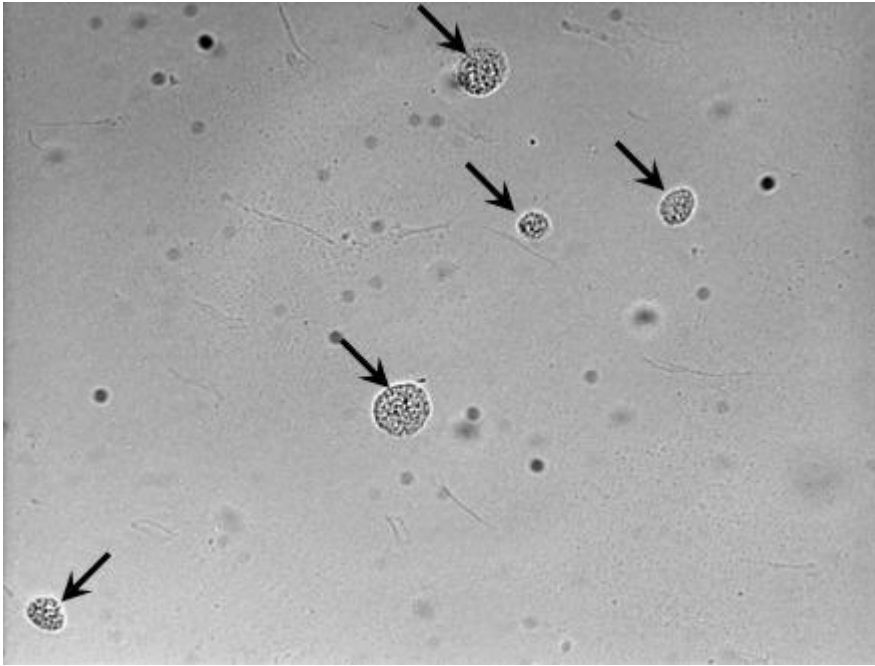
Figure 5.2: Representative micrograph showing the presence of macrophages within the

BAL pellet following centrifugation of BAL fluid and washing with

phosphate buffered saline.
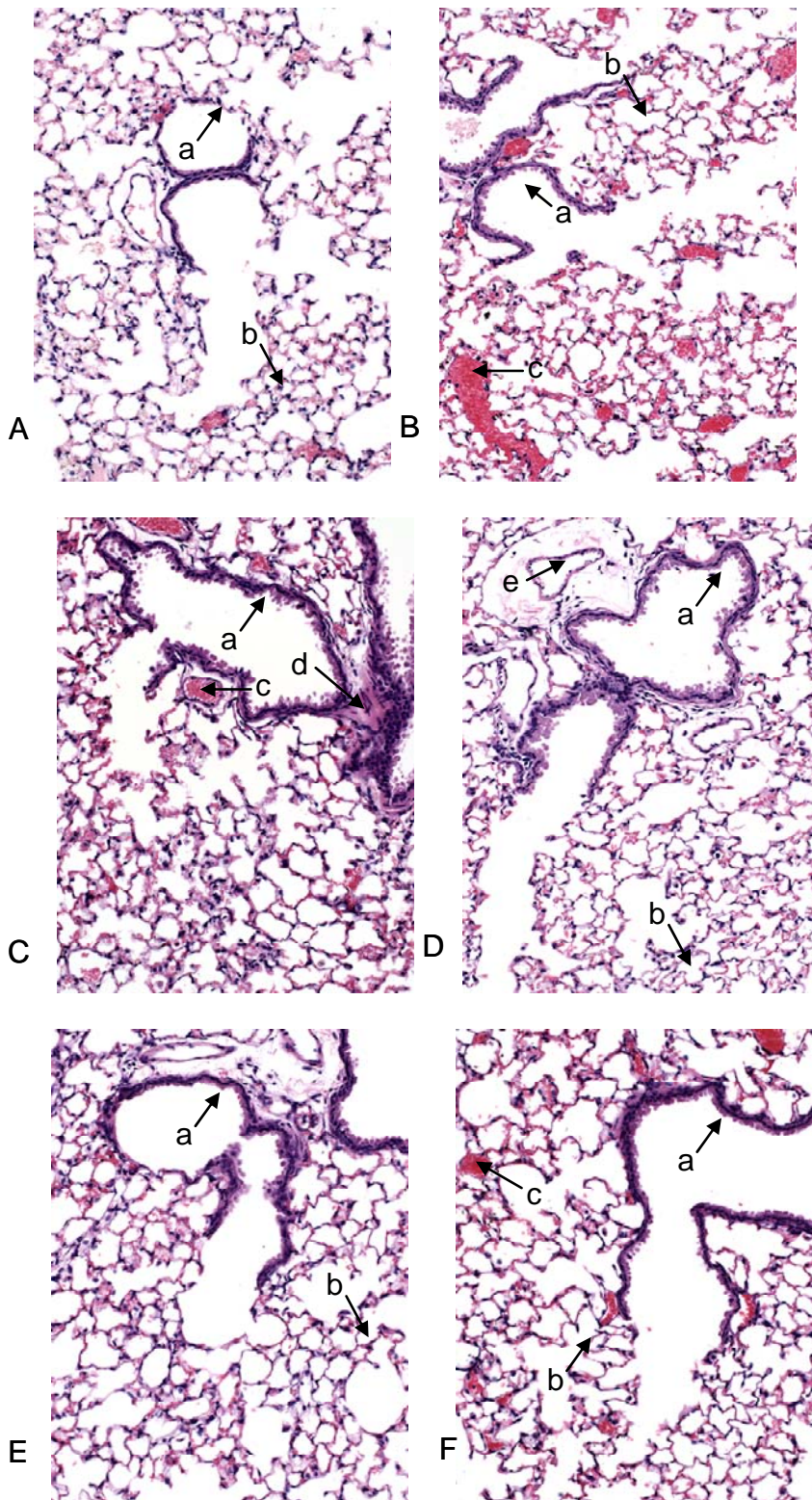
Figure 5.3: Representative histological stained samples from the saline control (A-day

3,B-day 8), excipient placebo (C-day 3,D-day 8) and amorphous ITZ

composition groups (E-day 3, F-day 8). Structures noted in the histology

samples are labeled: airways (a), alveolar spaces (b), capillaries (c), lymph

tissue (d) and arteriols (e).
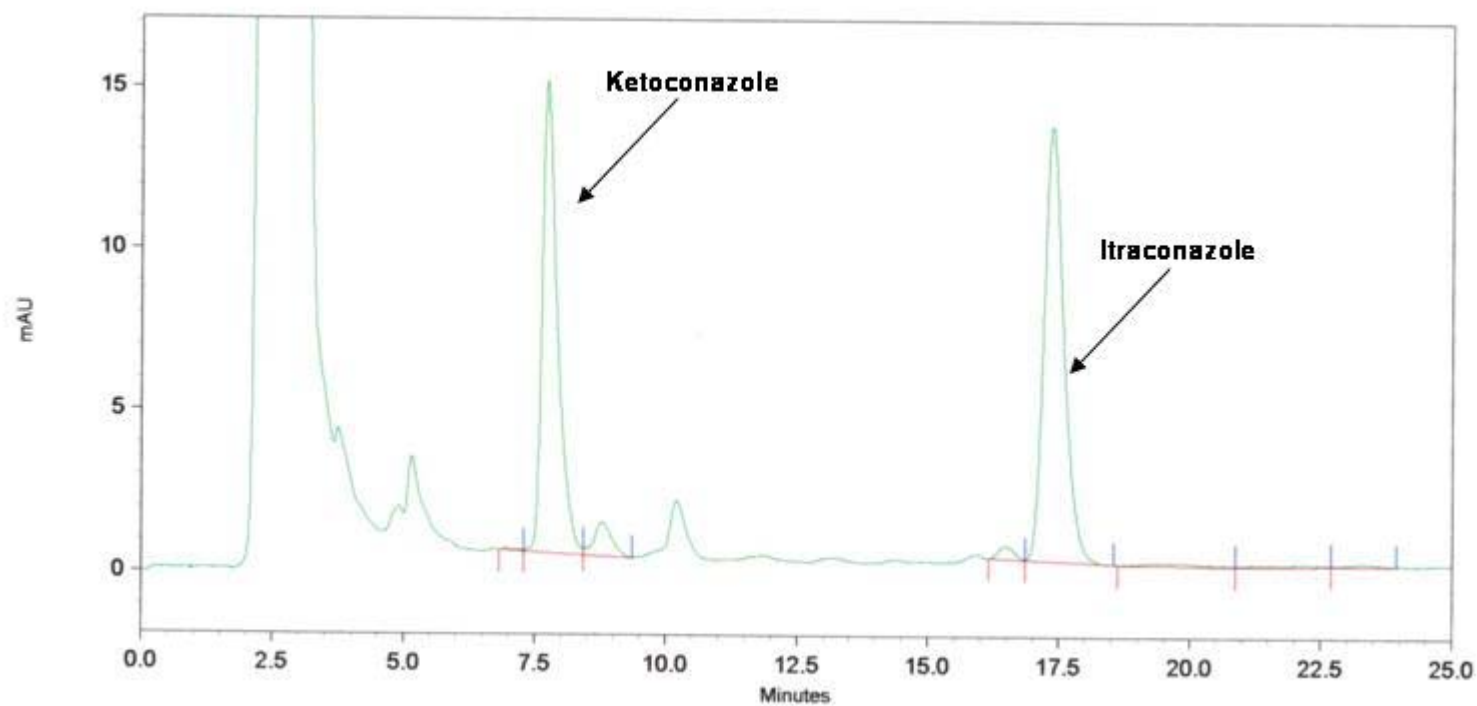
Figure A.1: Sample chromatogram for an extracted ITZ serum sample containing ketoconazole as an internal standard. The retention time for ketoconazole was 7.6 min and itraconazole was 17.5 min.
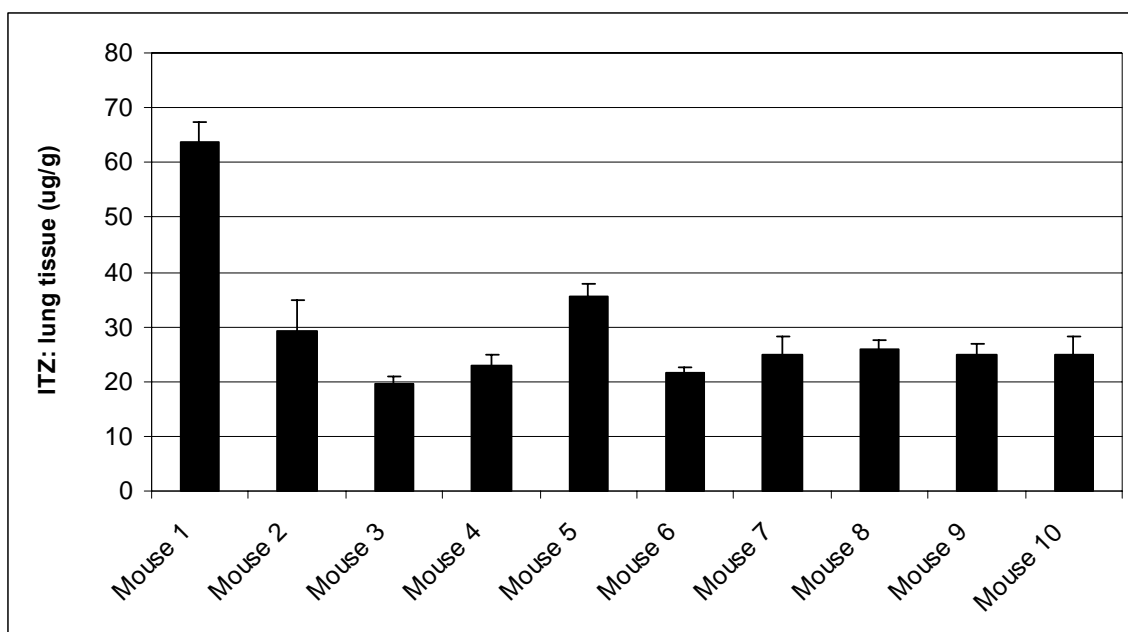
Figure A.2: Dose uniformity based on an average dry lung weight of mice dosed with an

amorphous ITZ pulmonary composition
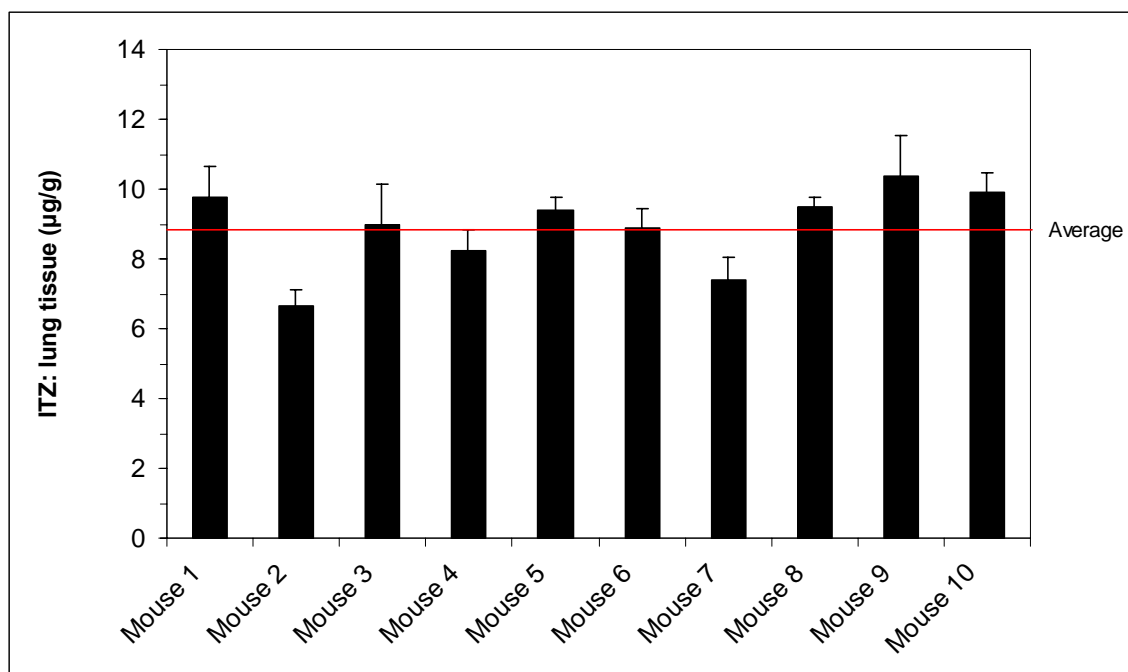
Figure A.3. Dose uniformity based on individual wet lung weights for mice dosed with

an amorphous ITZ pulmonary composition.
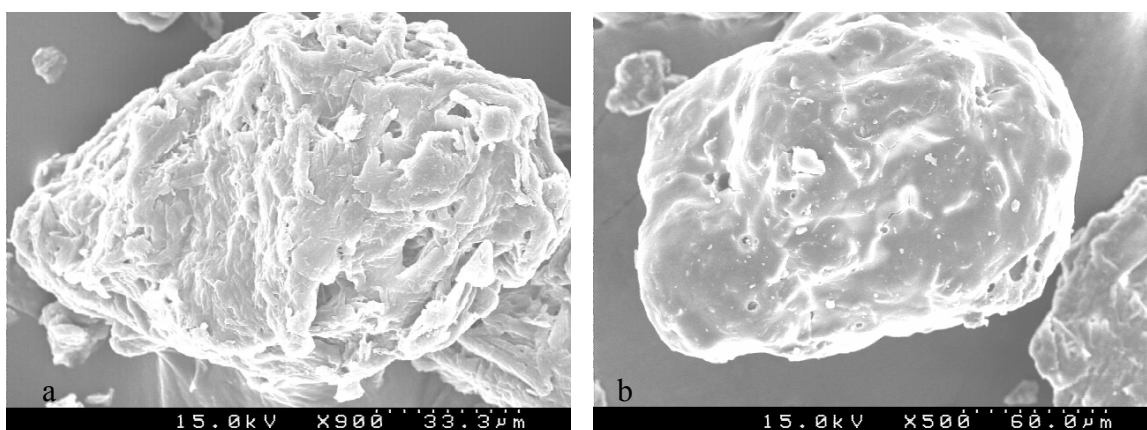
Figure B.1: Scanning electron micrographs of the bulk microcrystalline cellulose (a) and

MCC from the fluid-bed processed formulation AG (b)
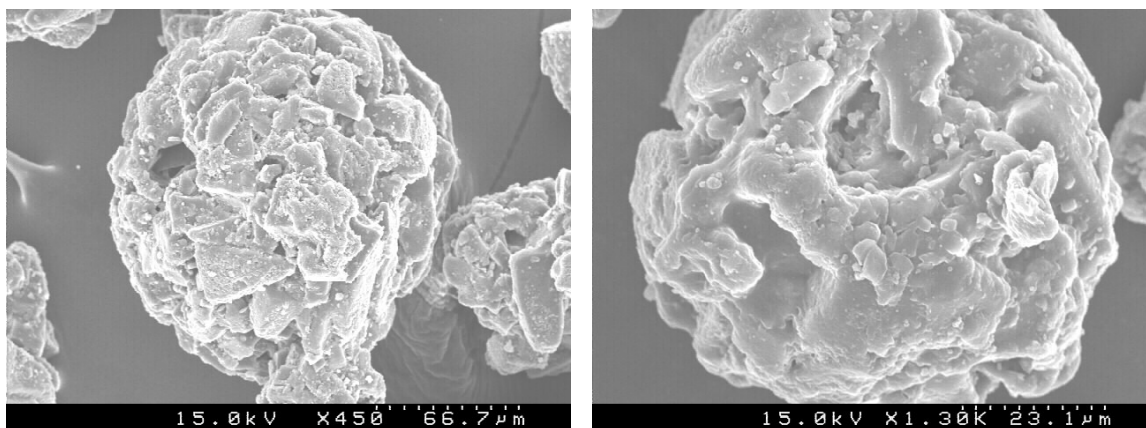
Figure B.2: Scanning electron micrographs of the bulk lactose monohydrate (a) and

lactose monohydrate from the fluid-bed processed formulation AG (b)
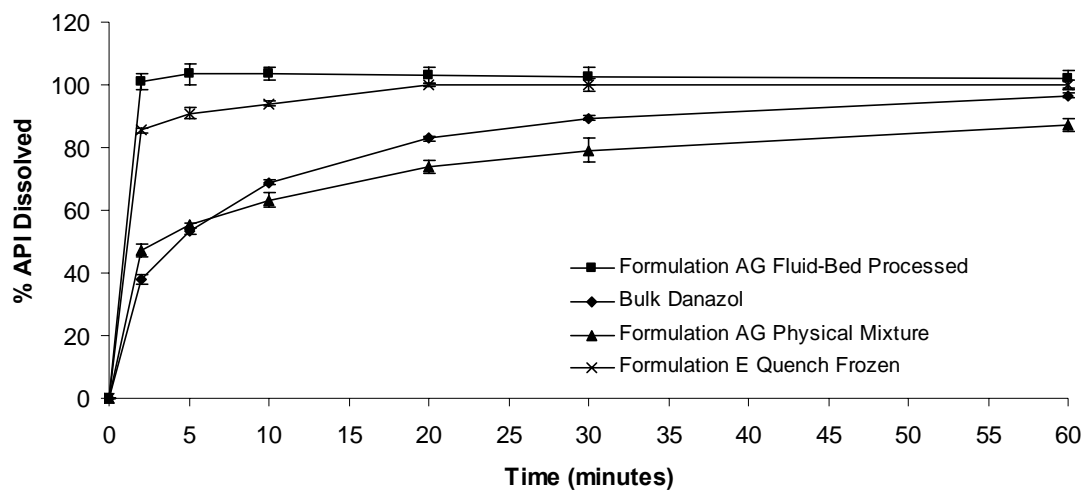
Figure B.3: Dissolution rate of fluid-bed processed EPAS danazol compared to a fluid bed processed physical mixture, quench frozen EPAS powder and bulk danazol
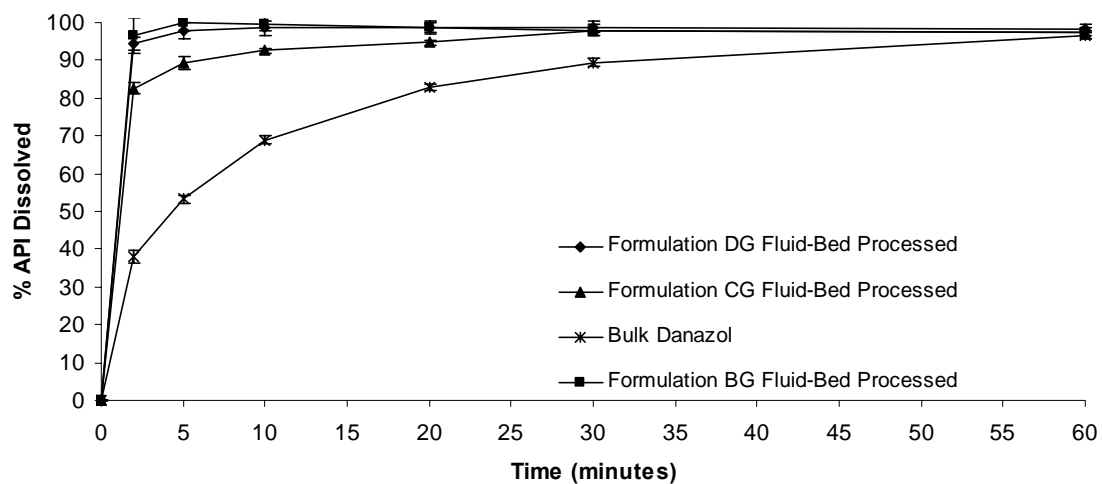
Figure B.4: Dissolution rate of higher potency fluid-bed processed EPAS formulations

compared to bulk danazol
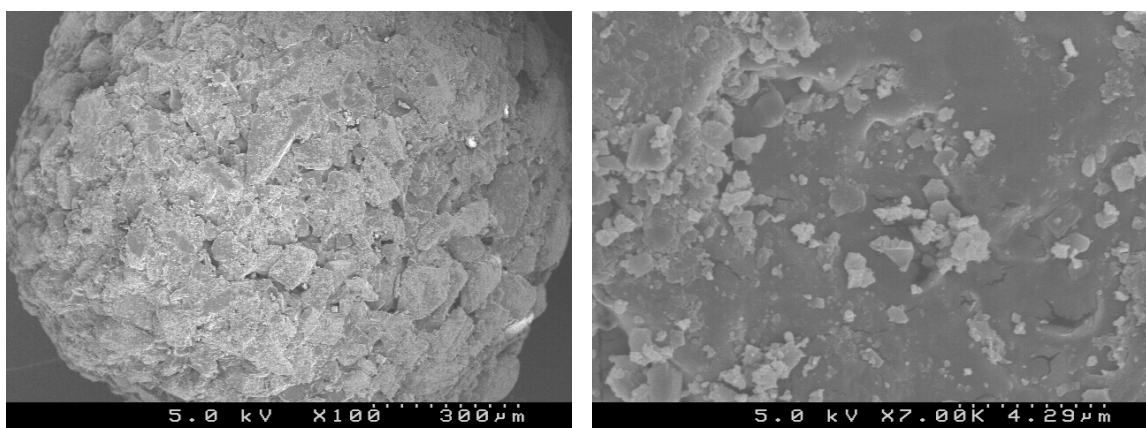
Figure B.5: SEM micrographs of the beads produced by wet-mass extrusion and

spheronization which contain EPAS processed danazol
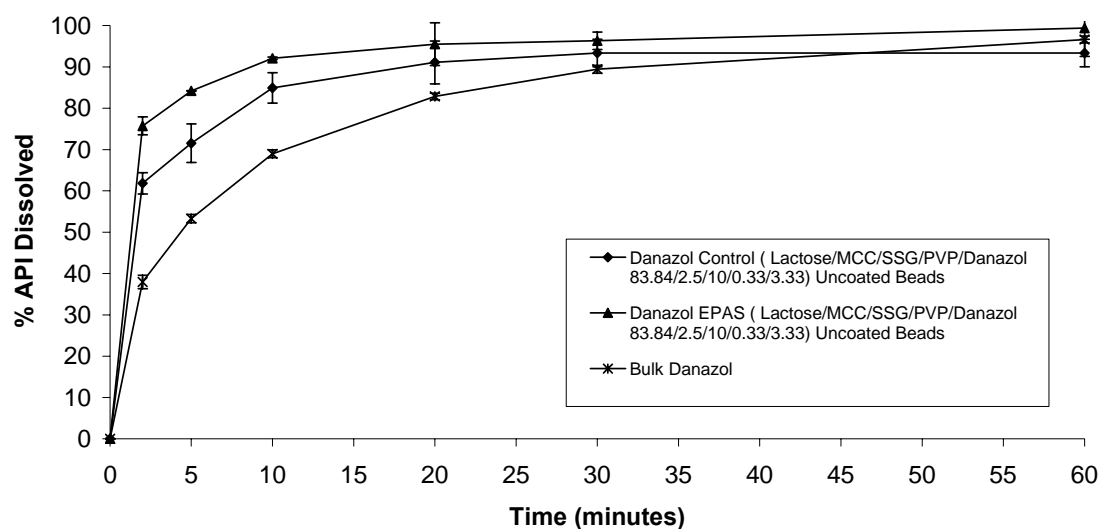
Figure B.6: Dissolution rate of beads produced by wet-mass extrusion and
spheronization containing either and EPAS dispersion or physical mixture
dispersion compared to bulk microcrystalline danazol
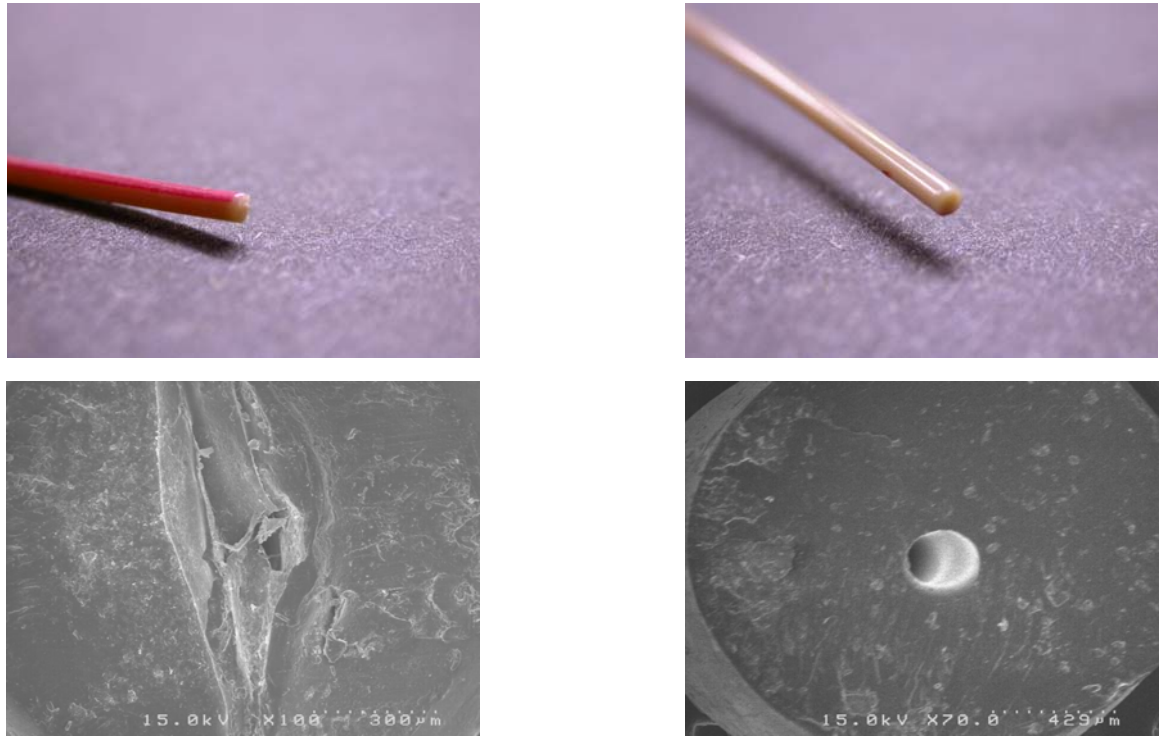
Figure C.1: Photographic images of the crimped (a) and uncrimped (b) PEEK nozzles
produced by cutting with wire cutters or a razor blade, respectively. SEM
micrographs of the crimped (c) and uncrimped (b) PEEK nozzle orifices.
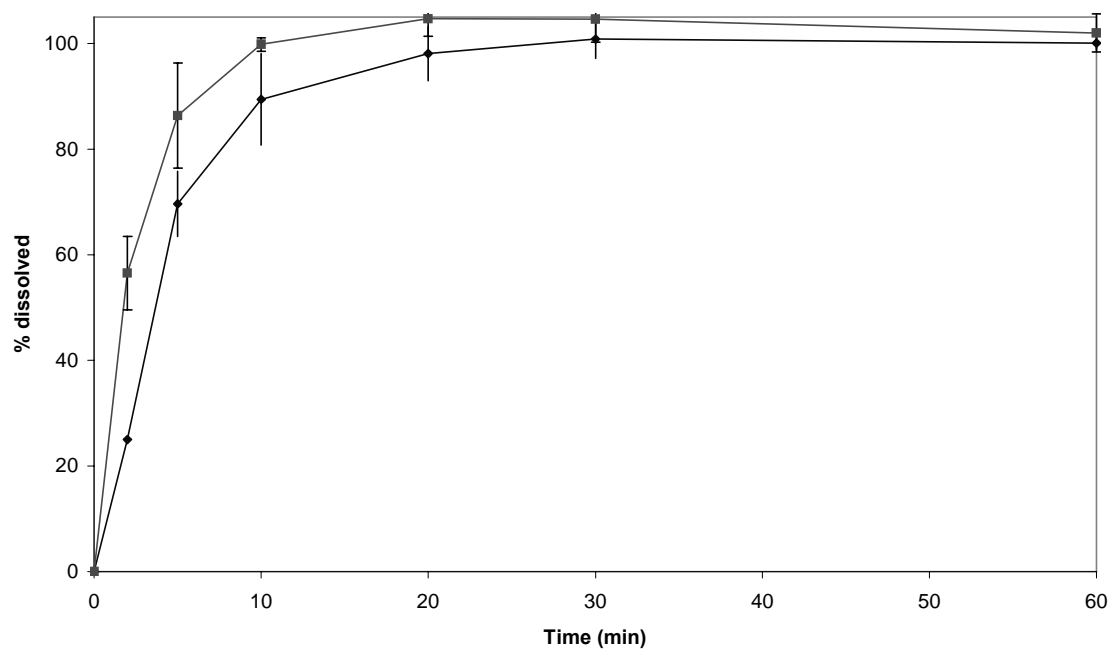
Figure C.2: Dissolution rate of powders produced by the SFL process consisting of ITZ/poloxamer 407/succinic acid in a 1/2/1 ratio using the crimped (■) and uncrimped (♦) PEEK nozzle geometry. 0.3% SDS, 0.1N HCL, 900mL 37°C USP II (paddle) 50 rpm n=3
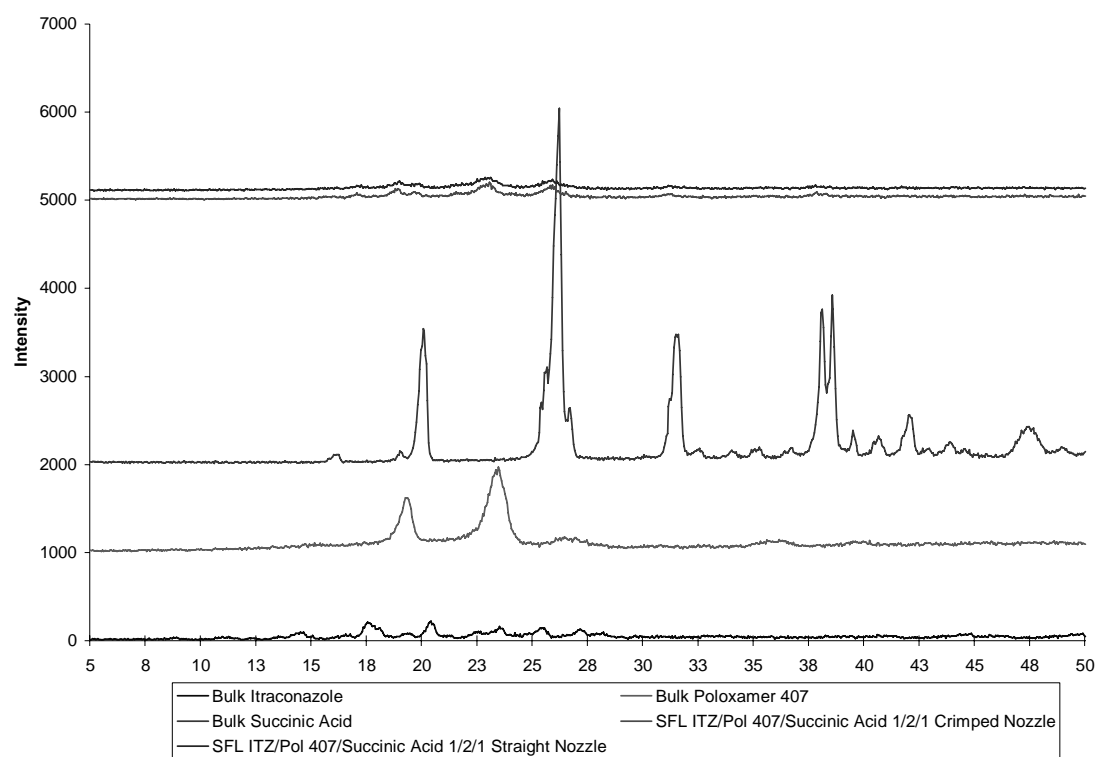
Figure C.3: X-ray powder diffraction of the bulk itraconazole, bulk succinic acid, bulk
poloxamer and SFL processed powders which were atomized via a crimped
or un-crimped PEEK nozzle.
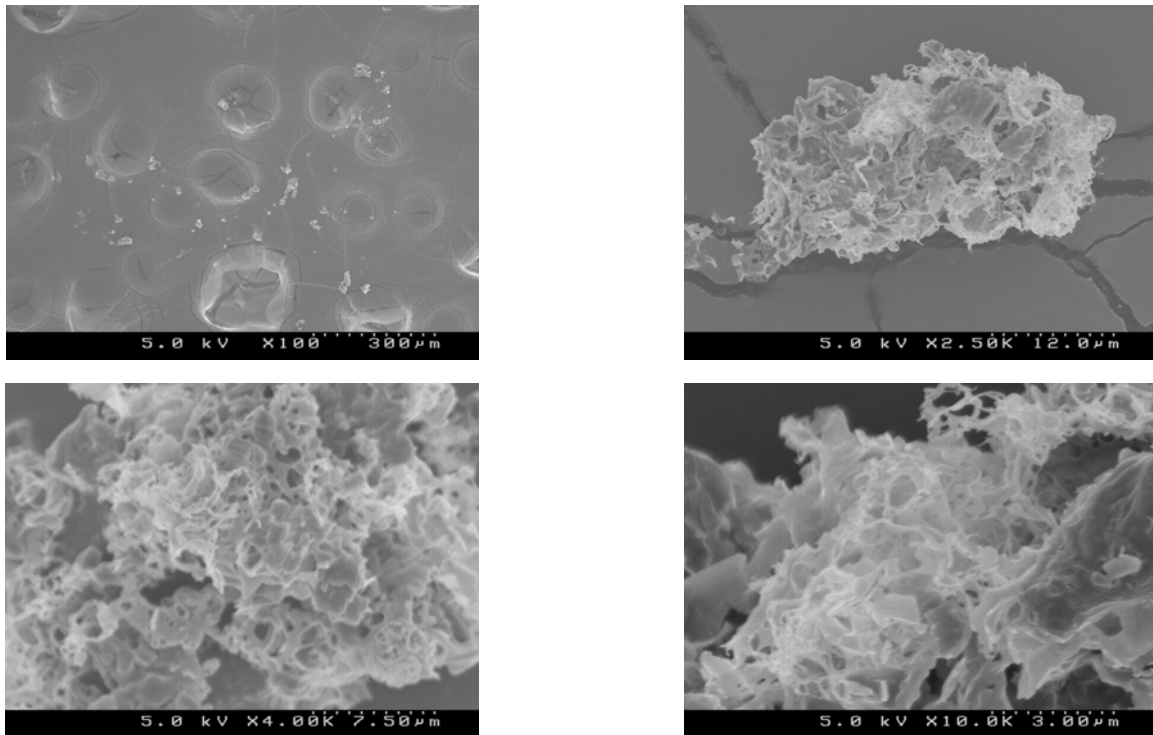
Figure C.4: SEM microphages of the SFL powder which was processed using the

crimped PEEK nozzle.
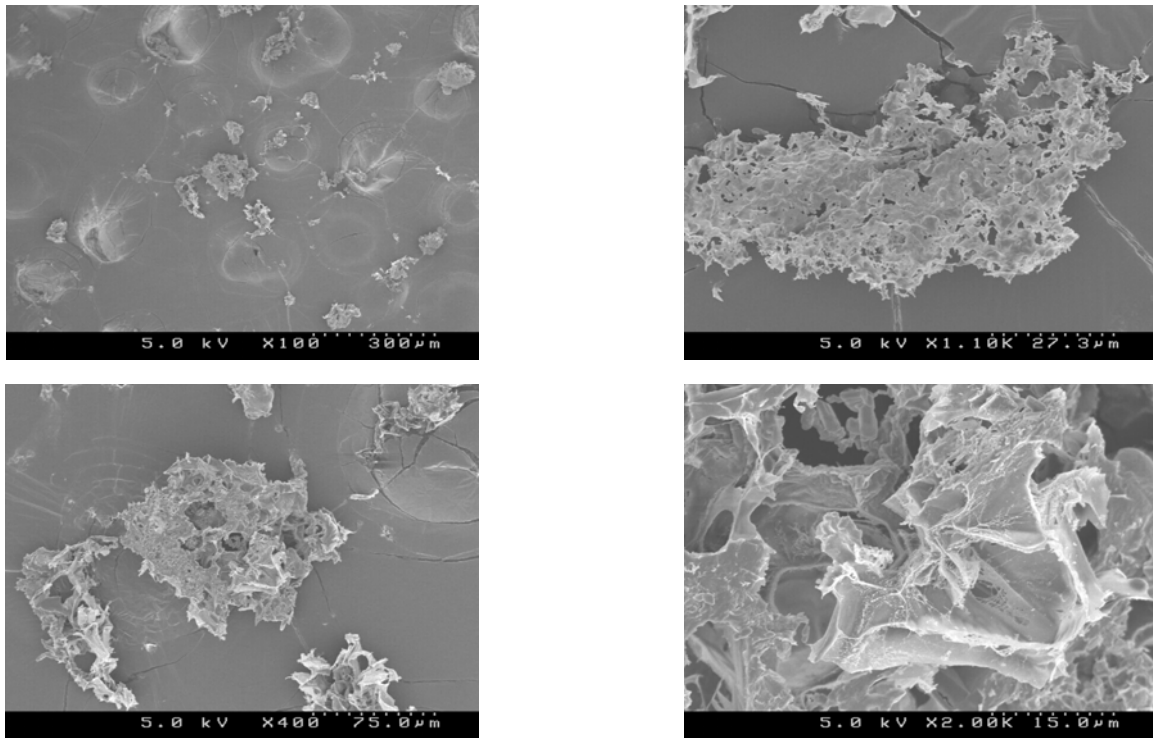
Figure C.5: SEM microphages of the SFL powder which was processed using the un-
crimped PEEK nozzle.
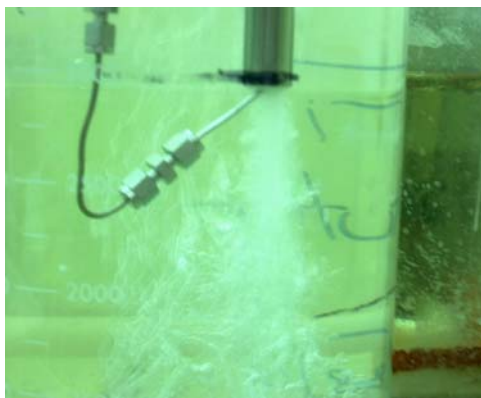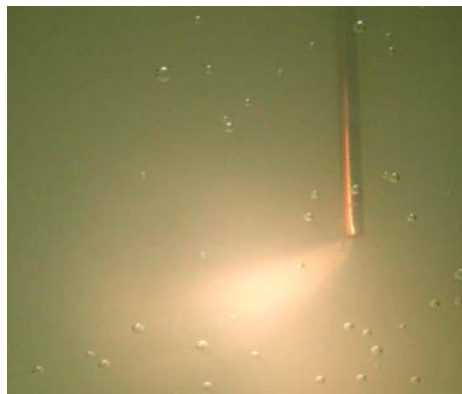
a)   b)

Figure C.6: Photographic representation of the EPAS process when using a crimped

nozzle with (a) and withough (b) an ultrasonic horn.
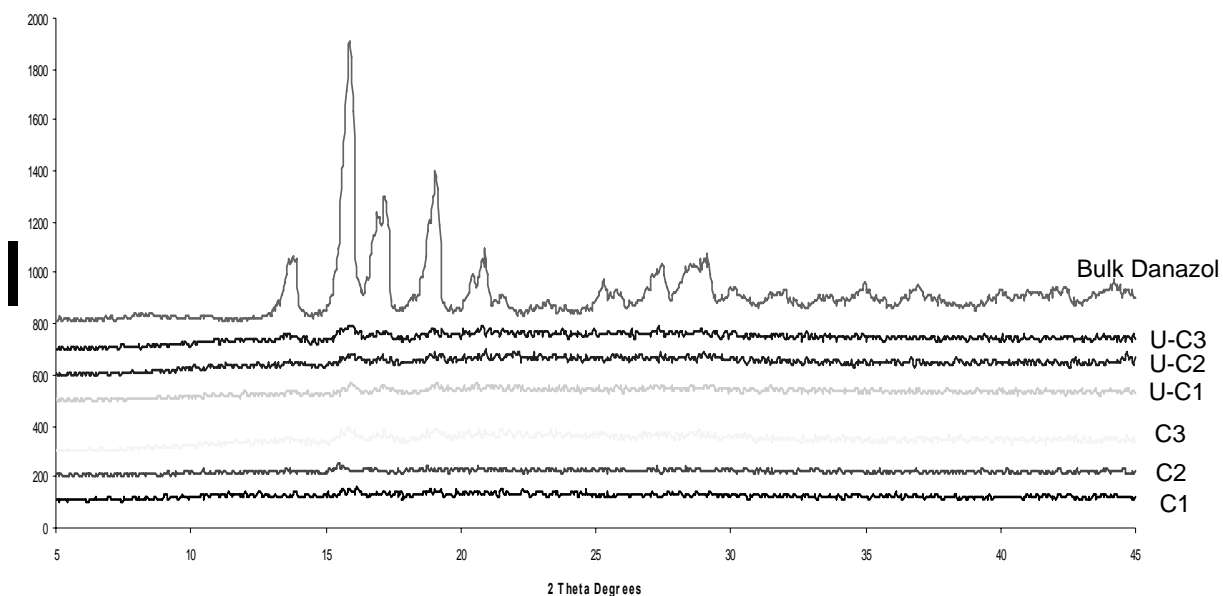
Figure C.7: X-ray diffraction patterns of the powders produced by EPAS processing

using the steel crimped nozzle with (u-c-1 – u-c-3) and without (c-1 – c-3)

ultrsonication and bulk danazol. The final powder consisted of danazol/PVP
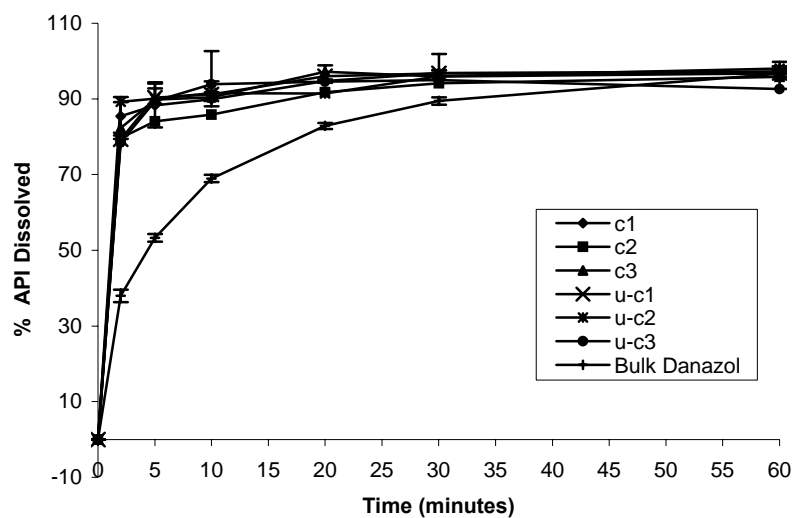
K-15 in a 1/3 ratio.

Figure C.8: Dissolution rate of the powders produced by EPAS processing using the

steel crimped nozzle with (u-c-1 – u-c-3) and without (c-1 – c-3)

ultrsonication and bulk danazol. The final powder consisted of danazol/PVP

K-15 in a 1/3 ratio.
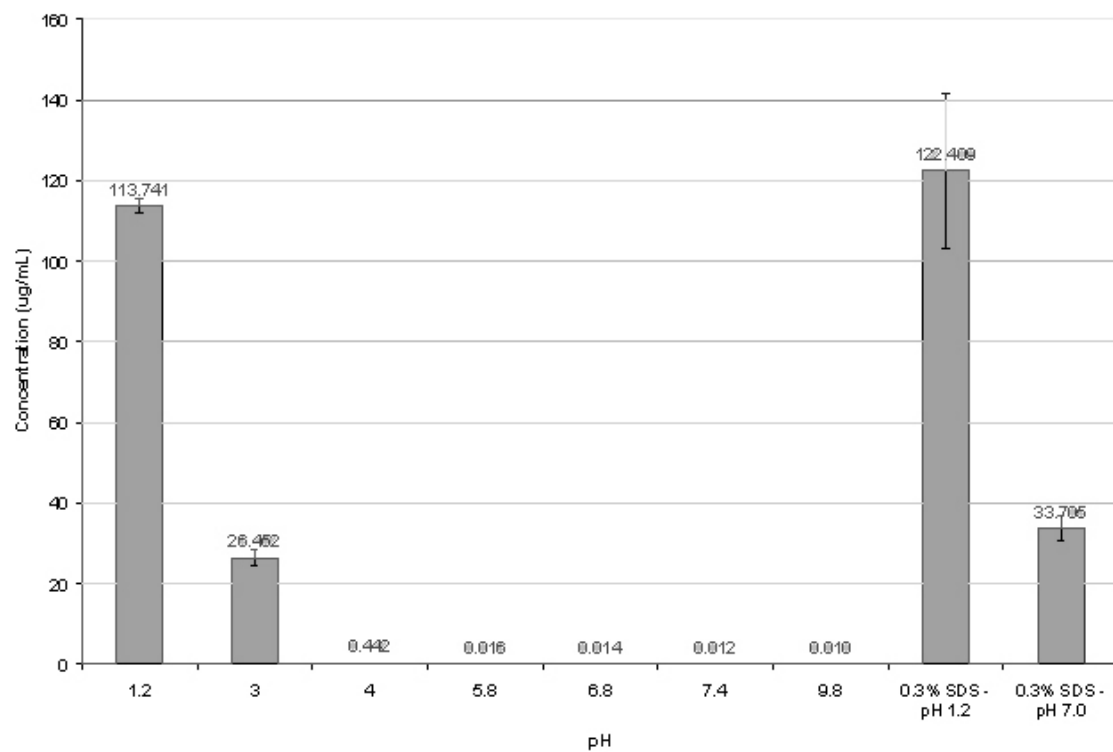
Figure D.1: pH solubility profile for ITZ at various pH conditions and in dissolution

media containing 0.3% SDS at pH 1.2 and pH 7.

189
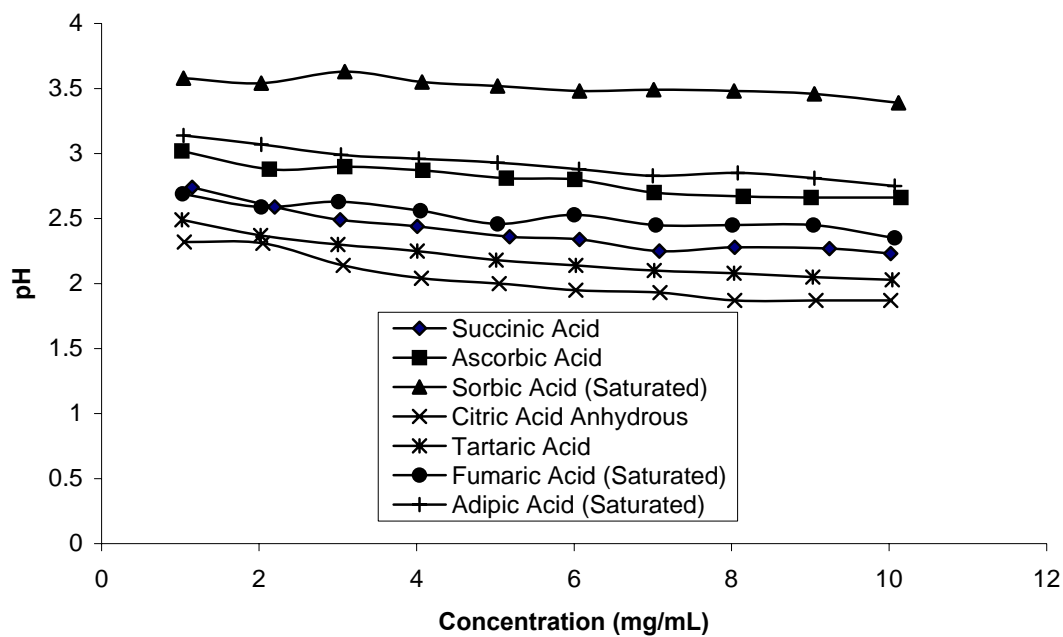
Figure D.2: pH concentration profile for various acidifying agents from 1 mg/mL to 10 mg/mL in deionized water. pH meter was calibrated between pH 1 and pH 7.

a)
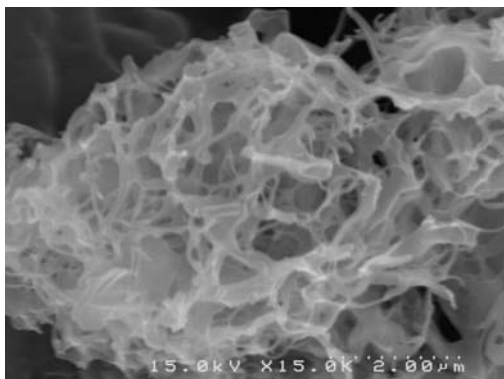
b)
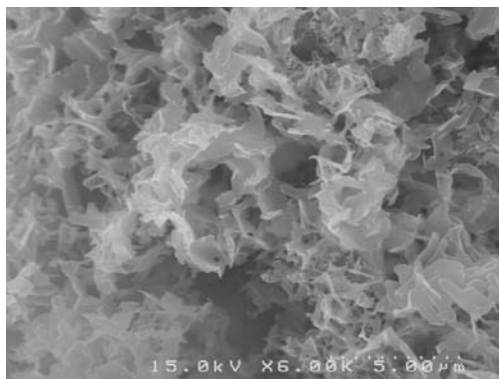
c)
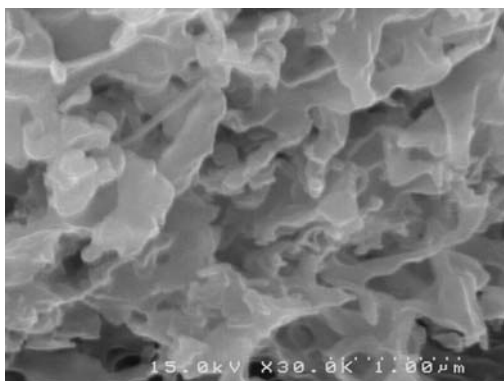
d)
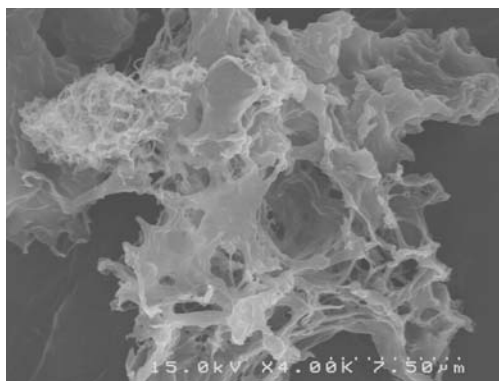
e)
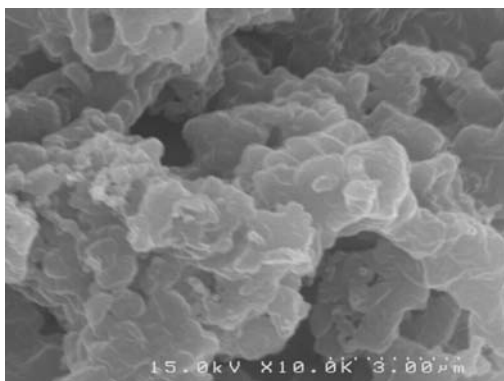
f)
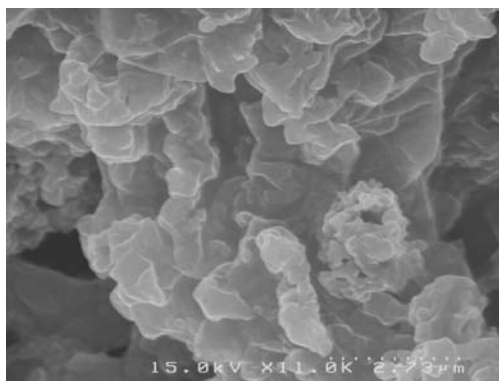
Figure D.3: SEM micrographs of the powders produced by SFL processing containing ITZ/poloxamer 407/acidulant at a 1/2/1 ratio. The acidulants used are adipic acid (a), succinic acid (b), fumaric acid (c), ascorbic acid (d), citric acid (e) and tartaric acid (f). The citric acid formulation contains PVP due to collapse during lyophilization.
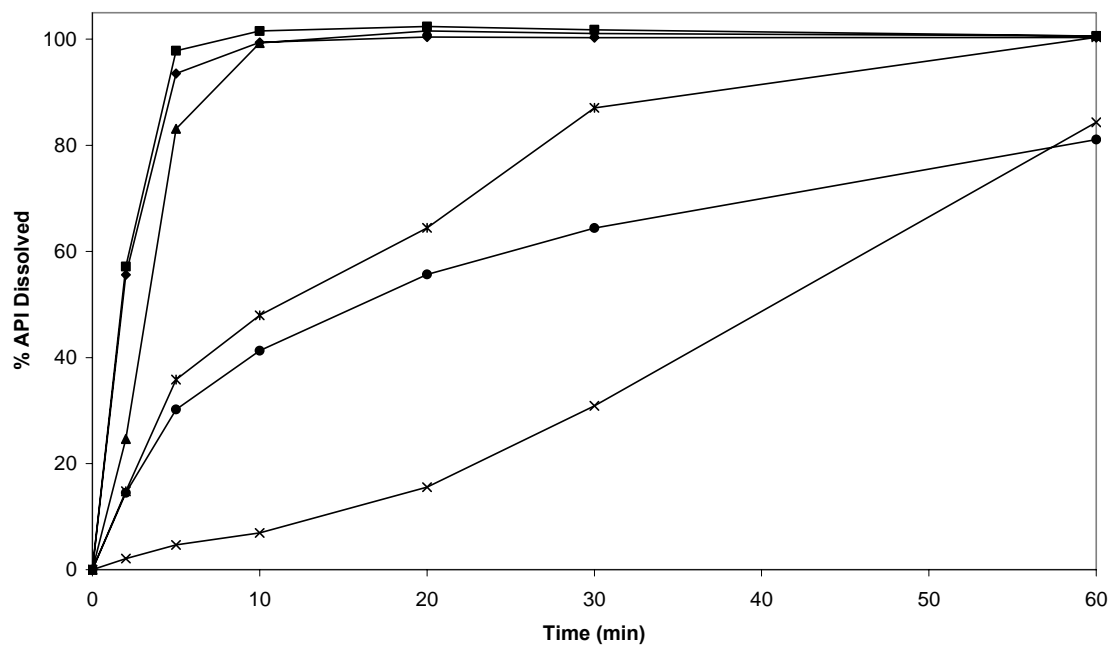
Figure D.4: Dissolution rate of the powders produced by SFL processing containing

ITZ/poloxamer 407/adipic acid 1/2/1 (♦), ITZ/poloxamer 407/succinic acid

1/2/1 (■), ITZ/poloxamer 407/fumaric acid 1/2/1 (▲), ITZ/poloxamer

407/ascorbic acid 1/2/1 (×), ITZ/poloxamer 407/citric acid/PVP K-15

1/2/1/1 (∗) and ITZ/poloxamer 407/tartaric acid 1/2/1 (●), . (0.3% SDS,

0.1N HCL, 900mL 37°C USP II (paddle) 50 rpm)
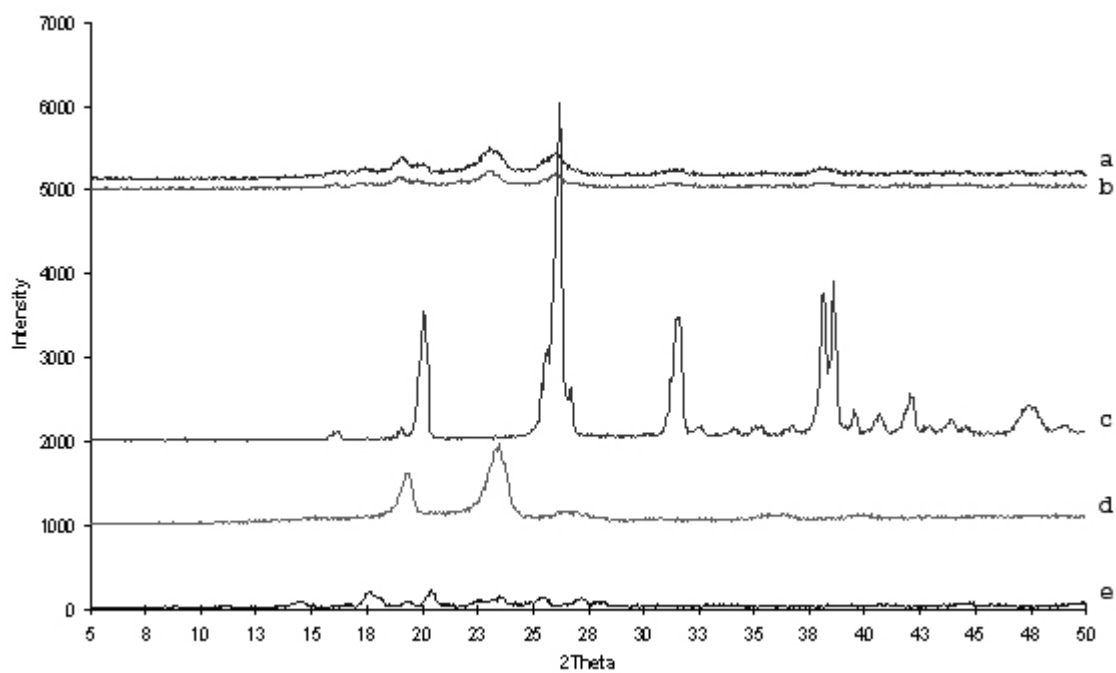
Figure D.5: X-ray powder diffraction of powders produced by SFL (a) and URF (b)

processing containing ITZ/poloxamer 407/succinic acid in a 1/2/1 ratio, bulk

succinic acid (c), bulk poloxamer 407 (d) and bulk ITZ (e).
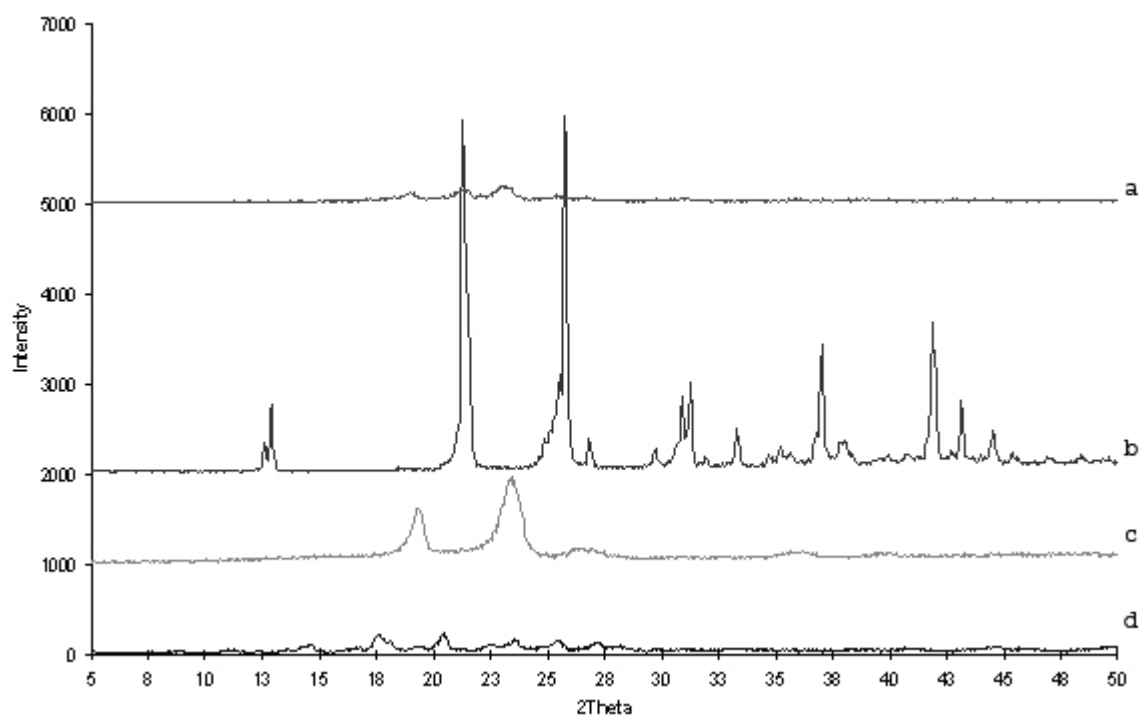
Figure D.6 X-ray powder diffraction of powders produced by SFL (a) processing

containing ITZ/poloxamer 407/adipic acid in a 1/2/1 ratio, bulk adipic acid

(b), bulk poloxamer 407 (c) and bulk ITZ (d).
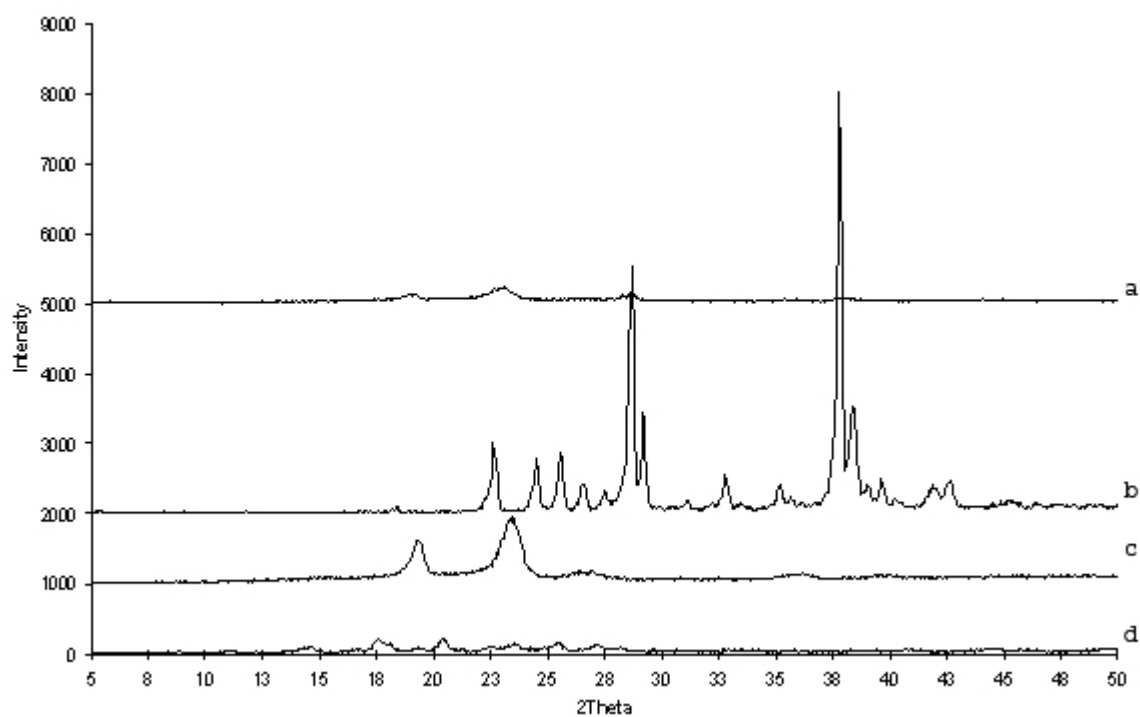
Figure D.7 X-ray powder diffraction of powders produced by SFL (a) processing

containing ITZ/poloxamer 407/fumaric acid in a 1/2/1 ratio, bulk fumaric

acid (b), bulk poloxamer 407 (c) and bulk ITZ (d).
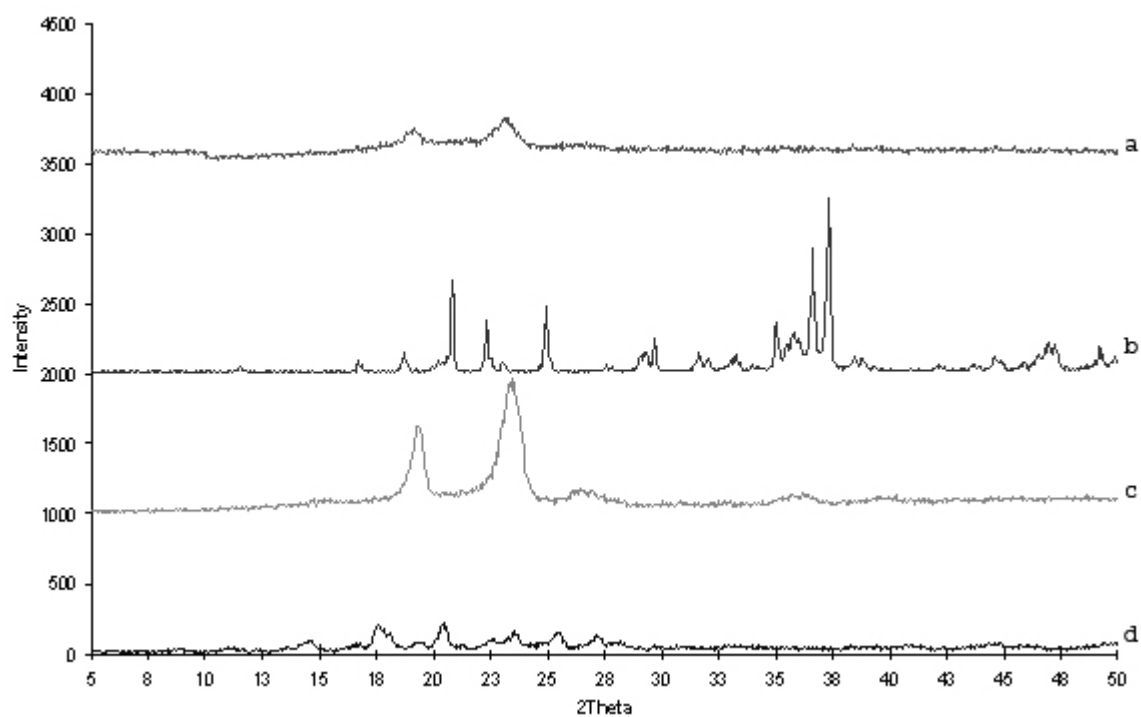
Figure D.8 X-ray powder diffraction of powders produced by SFL (a) processing

containing ITZ/poloxamer 407/tartaric acid/PVP K-15 in a 1/2/1/1 ratio,

bulk tartaric acid (b), bulk poloxamer 407 (c) and bulk ITZ (d).
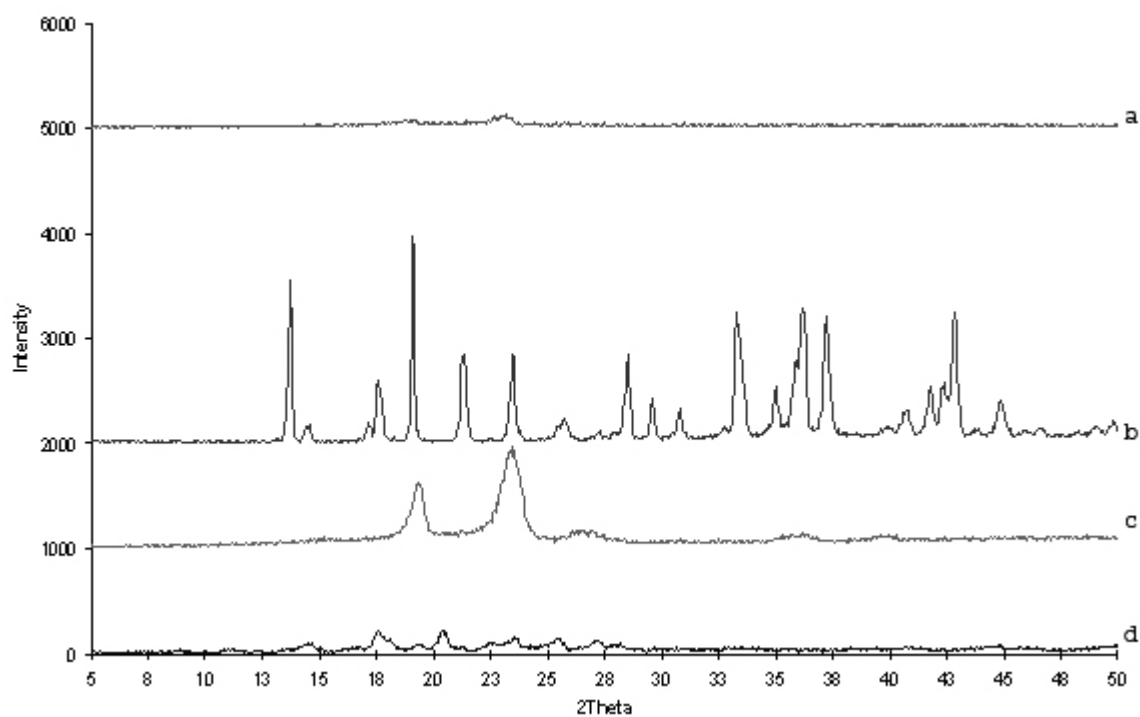
Figure D.9 X-ray powder diffraction of powders produced by SFL (a) processing

containing ITZ/poloxamer 407/citric acid/PVP K-15 in a 1/2/1/1 ratio, bulk

citric acid (b), bulk poloxamer 407 (c) and bulk ITZ (d).
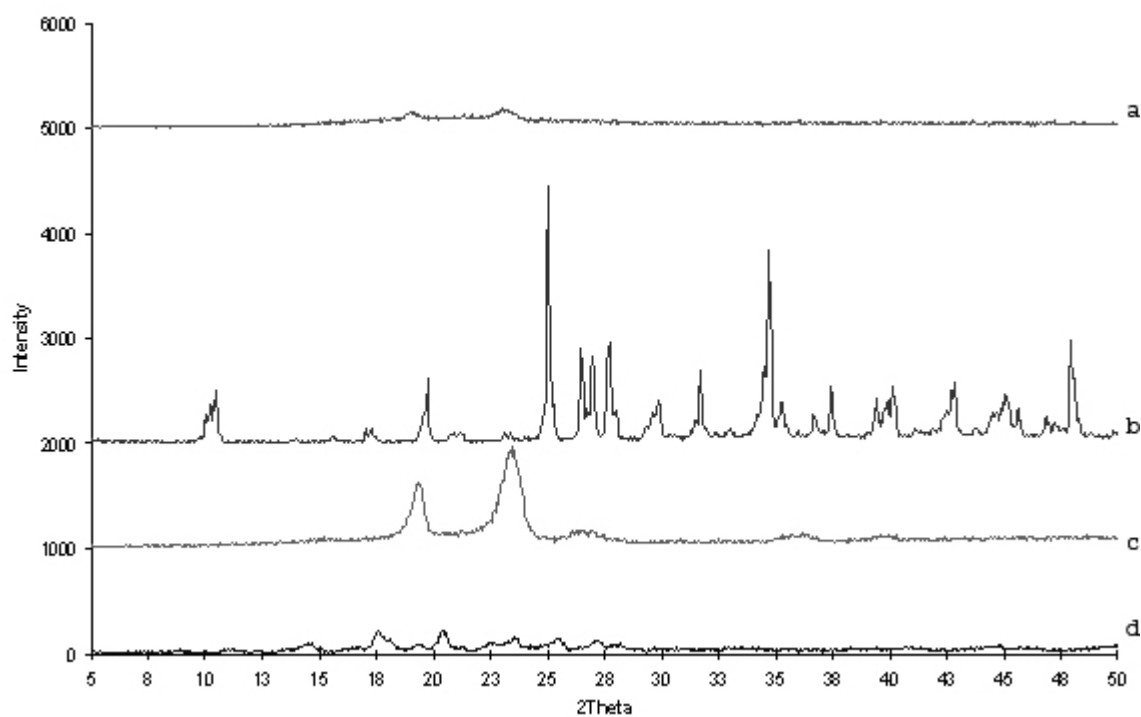
Figure D.10 X-ray powder diffraction of powders produced by SFL (a) processing

containing ITZ/poloxamer 407/ascorbic acid in a 1/2/1 ratio, bulk ascorbic

acid (b), bulk poloxamer 407 (c) and bulk ITZ (d).
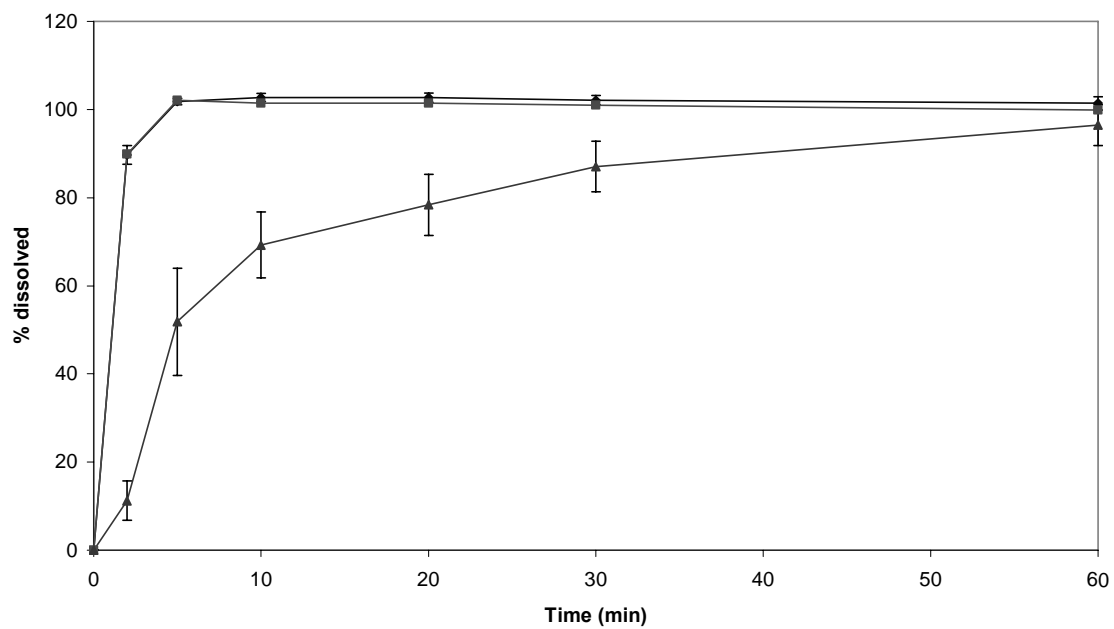
Figure D.11: Dissolution rate of SFL ITZ/poloxamer 407/succinic acid 1/2/1 (■), a tablet

powder composition containing SFL ITZ/poloxamer 407/succinic acid 1/2/1

prior to compression (♦) and that formulation following compression (▲)

(0.3% SDS, 0.1N HCL, 900mL 37°C USP II (paddle) 50 rpm)

200
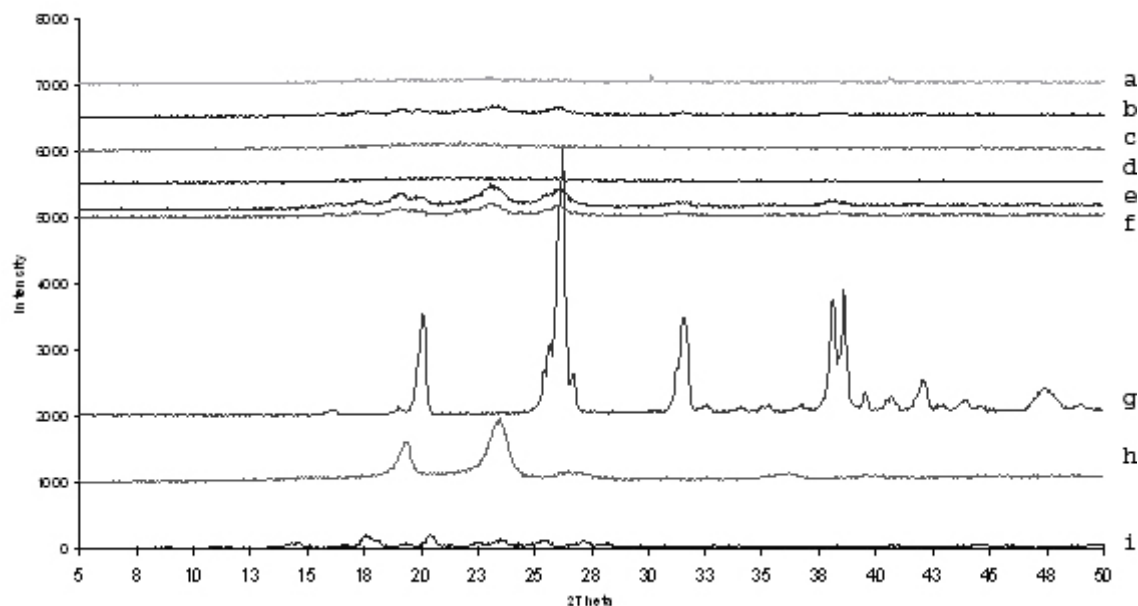
Figure D.12 X-ray powder diffraction of powders produced by SFL composed of

ITZ/poloxamer 407/PVP K-15/succinic acid 1/0.5/2/1 (a), ITZ/poloxamer

407/PVP K-15/succinic acid 1/1/1/1 (b), ITZ/PVP K-15/succinic acid 1/3/1

(c), ITZ/PVP K-15/succinic acid 1/2/1 (d), ITZ/poloxamer 407/succinic acid

1/2/1 (e), URF ITZ/poloxamer 407/succinic acid 1/2/1 (f) bulk succinic acid

(g), bulk poloxamer 407 (h) and bulk ITZ (i).
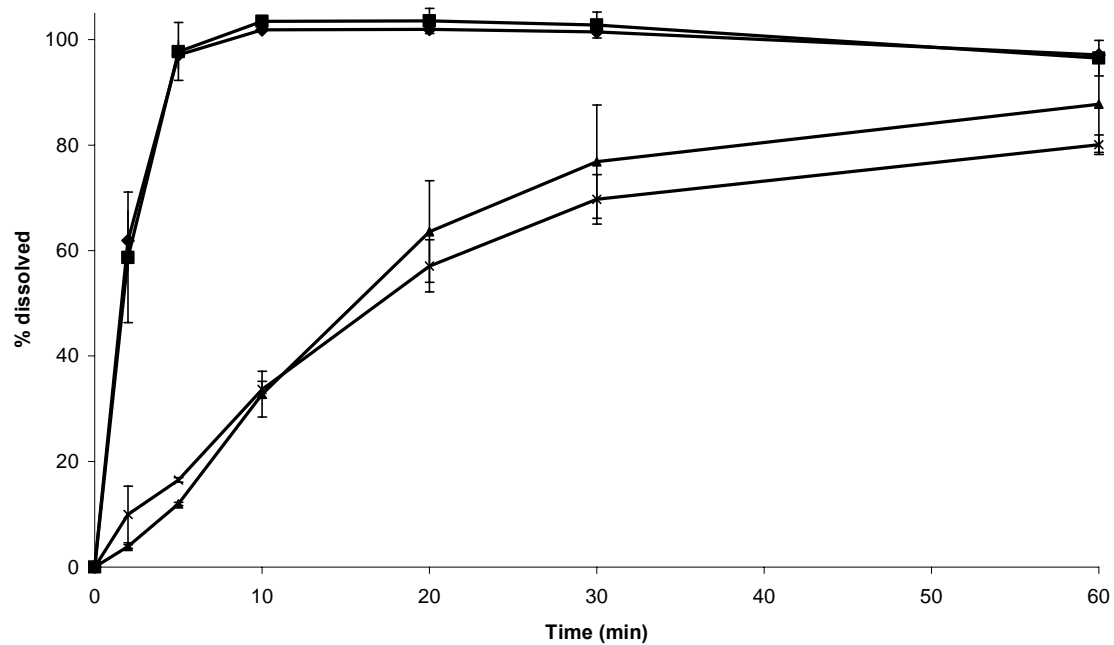
Figure D.13: Dissolution rate of powders produced by SFL composed of ITZ/poloxamer

407/PVP K-15/succinic acid 1/0.5/2/1 (■), ITZ/poloxamer 407/PVP K-

15/succinic acid 1/1/1/1(●), ITZ/PVP K-15/succinic acid 1/3/1(×), ITZ/PVP

K-15/succinic acid 1/2/1 (▲)(0.3% SDS, 0.1N HCL, 900mL 37°C USP II

(paddle) 50 rpm)
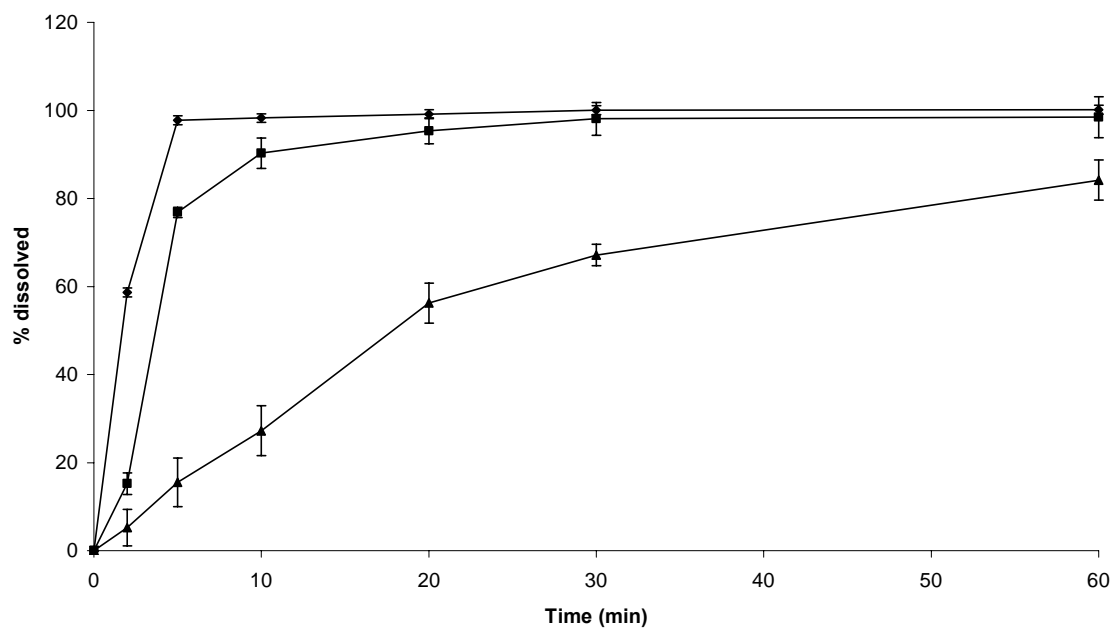
Figure D.14: Dissolution rate of SFL ITZ/PVP K-15/poloxamer 407/succinic acid

1/2/0.5/1 (♦), a tablet powder composition containing SFL ITZ/PVP K-

15/poloxamer 407/succinic acid 1/2/0.5/1 (■) in a table and a physical

mixture composed of ITZ/PVP K-15/poloxamer 407/succinic acid 1/2/0.5/1

which was formulated into a tablet (▲)(0.3% SDS, 0.1N HCL, 900mL 37°C

USP II (paddle) 50 rpm)
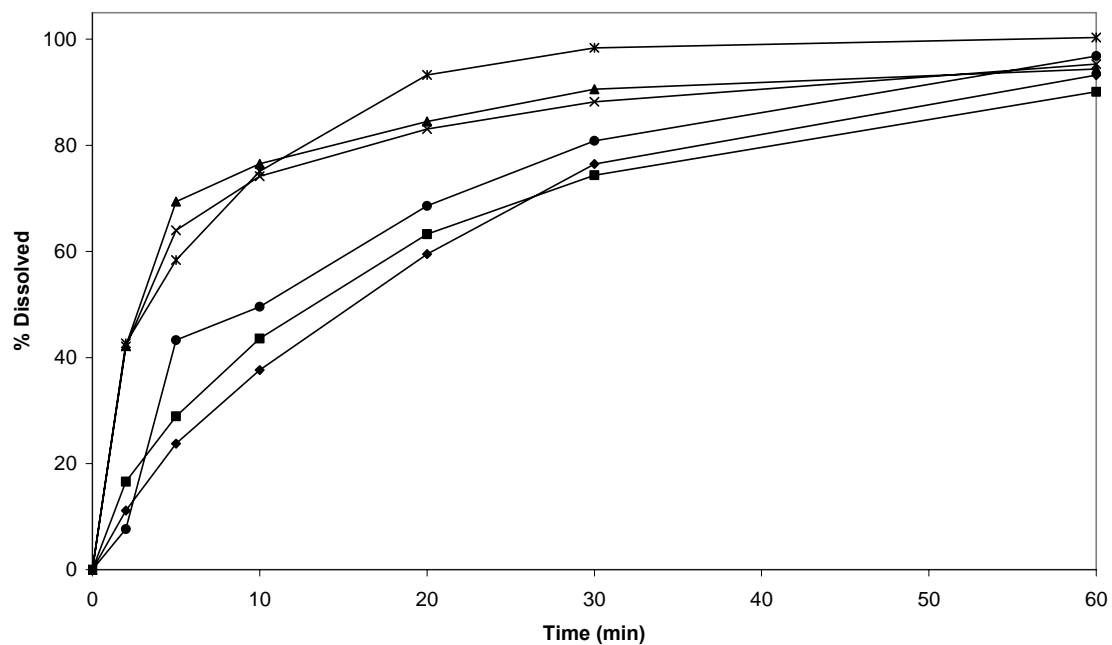
Figure D.15 Dissolution rate of powders processed by SFL and composed

ITZ/poloxamer 407/SDS/succinic acid 1/1/1/1 (♦), ITZ/poloxamer

407/SDS/succcinic acid 1/0.5/2/1 (■), ITZ/SDS 1/2 (▲), ITZ/SDS 1/1 (×),

ITZ/SDS/succinic acid 1/2/1 (∗) and ITZ/SDS/succinic acid 1/1/1 (●) (0.3%

SDS, 0.1N HCL, 900mL 37°C USP II (paddle) 50 rpm)
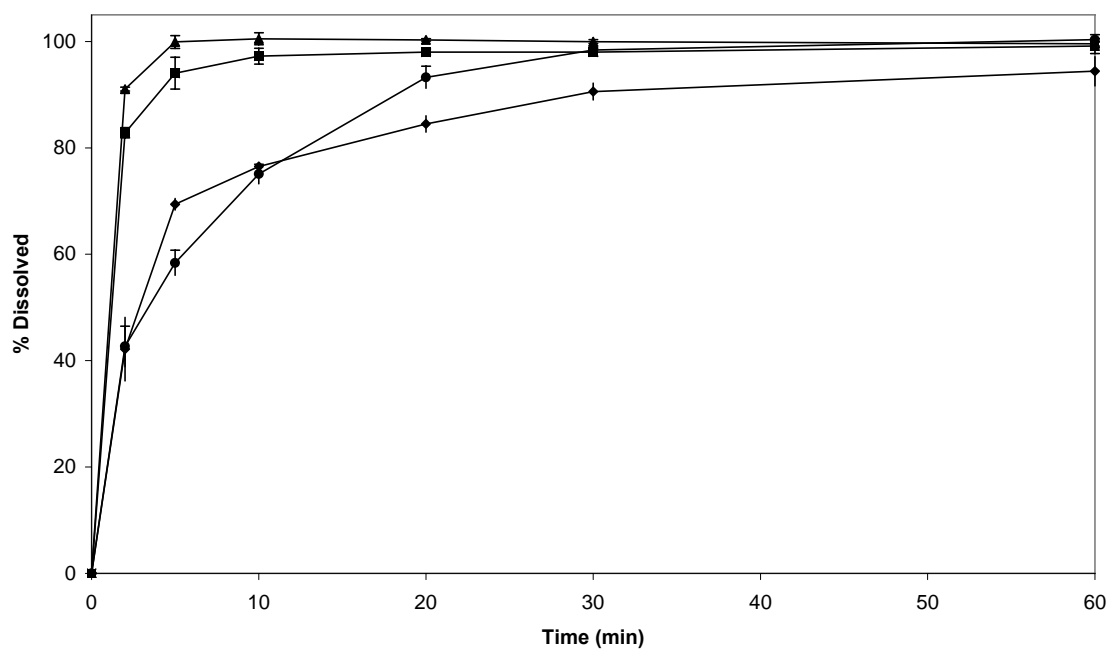
Figure D.16:   Dissolution rate of powders produced by SFL processing and composed of

ITZ/SDS 1/2 (♦) and ITZ/SDS/succinic acid1/2/1 (●) at pH 1.2 (0.3% SDS,

0.1N HCL, 900mL 37°C USP II (paddle) 50 rpm) and ITZ/SDS 1/2 (▲)

and ITZ/SDS/succinic acid1/2/1 (■) at pH 7.0 (0.05M Na2HPO4/Citric acid

buffer, 0.3% SDS, 900mL 37°C USP II (paddle) 50 rpm).

205

a)   b)
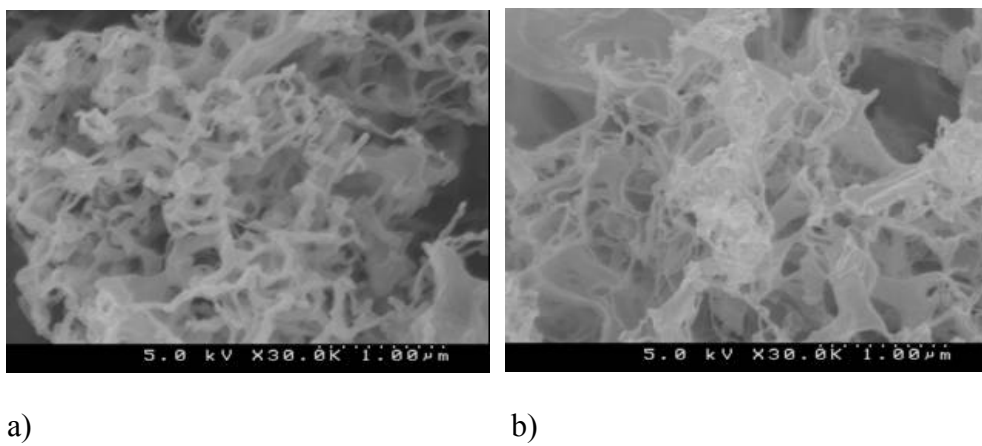
Figure D.17: SEM micrographs of SFL powders composed of ITZ/SDS 7/3 (a) and

ITZ/SDS 10/1 (b)
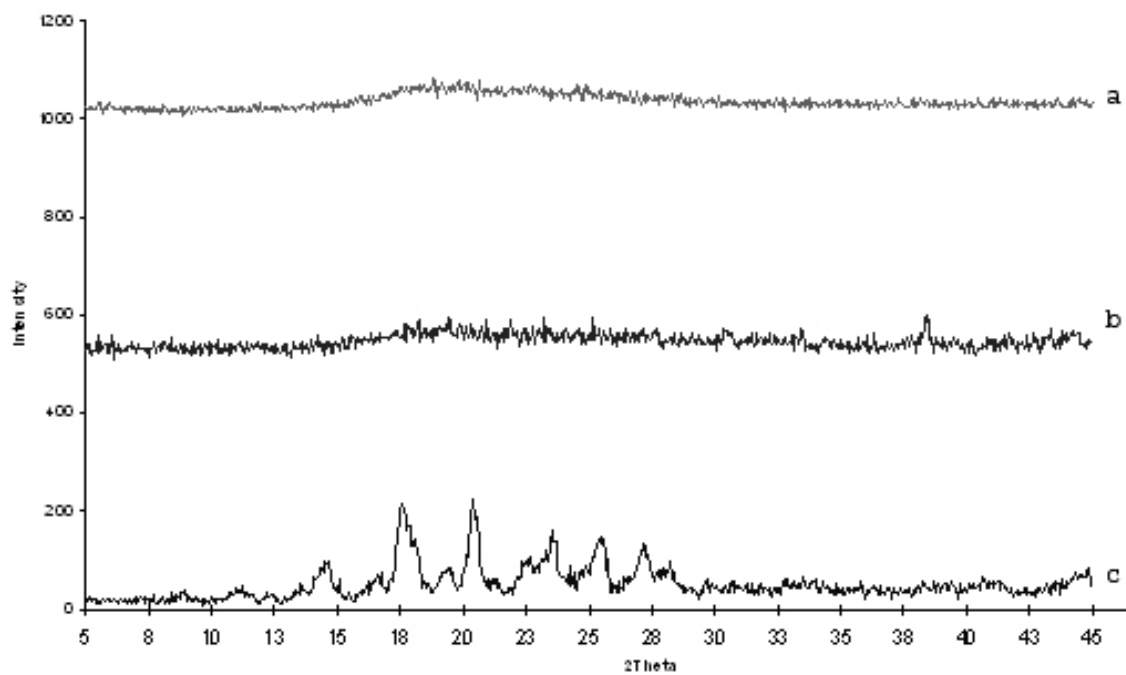
Figure D.18 X-ray powder diffraction of powders produced by SFL processing

containing ITZ/SDS 7/3 (a) or ITZ/SDS 10/1 (b) compared to bulk ITZ (c).
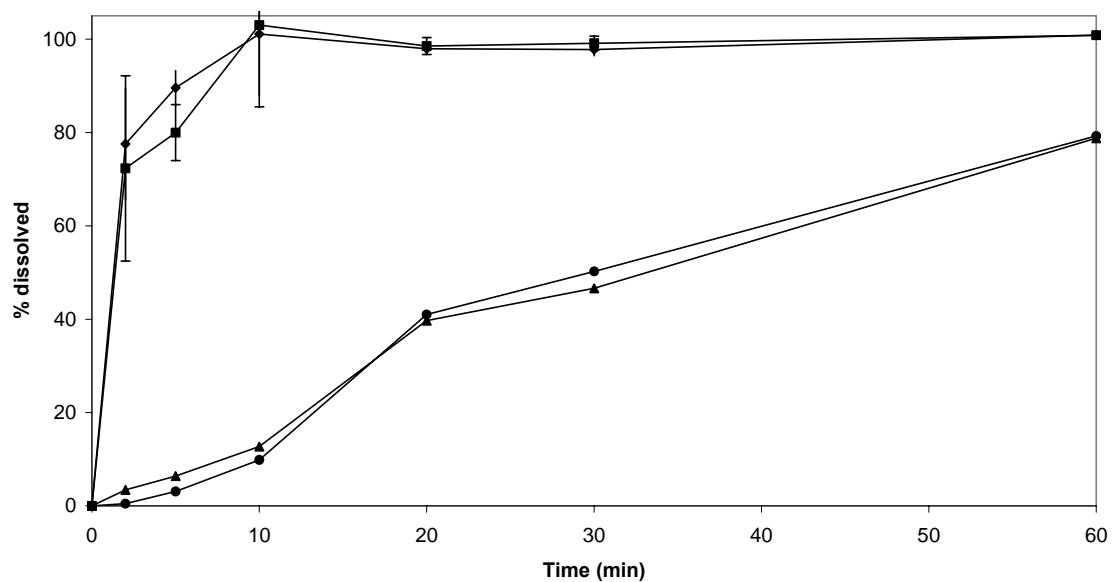
Figure D.19 Dissolution rate of powders produced by SFL processing and composed of

ITZ/SDS 7/3 (▲) and ITZ/SDS 10/1 (●) at pH 1.2 (0.3% SDS, 0.1N HCL,

900mL 37°C USP II (paddle) 50 rpm) and ITZ/SDS 7/3 (♦) and ITZ/SDS

10/1 (■) at pH 7.0 (0.05M Na2HPO4/Citric acid buffer, 0.3% SDS, 900mL

37°C USP II (paddle) 50 rpm).
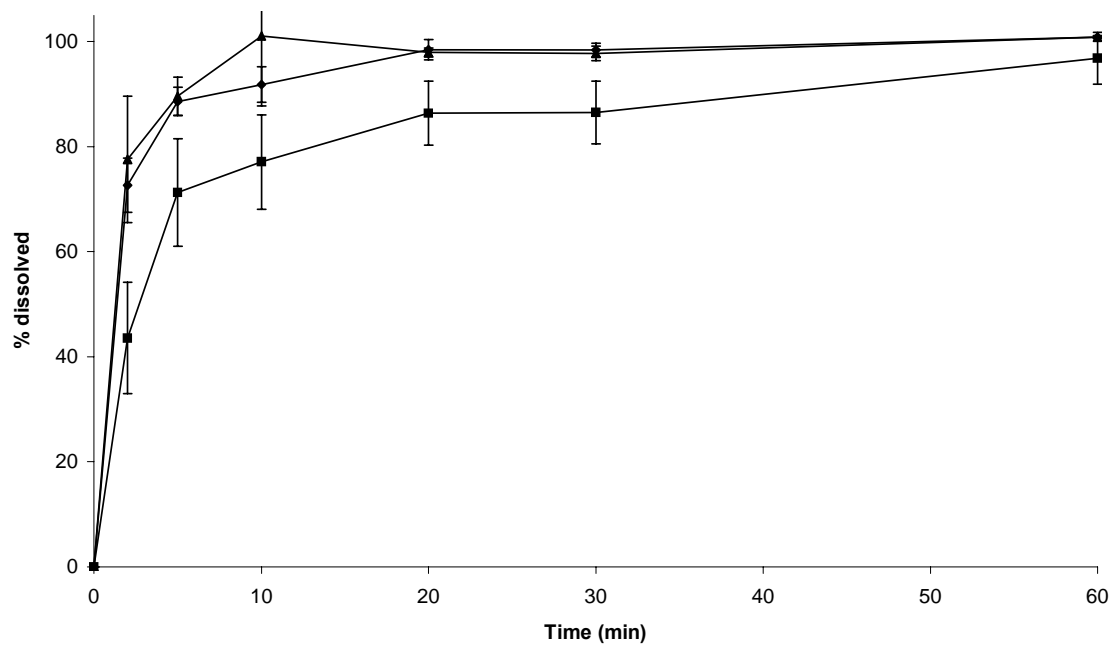
Figure D.20: Dissolution rate of powders produced by SFL and composed of
ITZ/SDS/manitol 7/3/3.5 (♦), ITZ/SDS/DCA 7/3/3.5 (■) and ITZ/SDS 7/3
(▲) in pH 7.0 media (0.05M Na2HPO4/Citric acid buffer, 0.3% SDS,
900mL 37°C USP II (paddle) 50 rpm).

Appendix A: Itraconazole Inhalation Dosing Uniformity and Average Dose Delivered in a Murine Dosing Chamber

A.1 PURPOSE

The purpose of this study was to investigate the level and uniformity of itraconazole which was delivered to a murine model using the inhalation dosing chamber described in Chapter 4. The dose delivered to the mouse model would be useful in pharmacokinetic calculations. Also, the uniformity in dosing among 10 mice dosed simultaneously was evaluated. The chamber design allows for multiple mice (up to 14) to be dosed via inhalation concurrently and the uniformity of the dosing was needed to ensure that the level of itraconazole available for absorption was similar among the subjects.

A.2 MATERIALS AND METHODS

A.2.1 Materials

The materials used for this study were described in Chapter 5.2.1 and are summarized in Table A.1.

A.2.2 Production of an Amorphous ITZ Composition

The method for manufacture of the amorphous ITZ composition was described in Chapter 5.2.3

A.2.3 Dosing of the Murine Model

Ten male ICR mice were placed in the chamber and dosed with an amorphous itraconazole formulation for 20 minutes (equivalent to a theoretical lung exposure of 30 mg/kg mouse weight) using the dosing chamber described in Chapter 5.3.3. Following dosing, the mice were removed from the chamber and allowed to equilibrate for 15 minutes. The mice were sacrificed and lungs (all lobes) were harvested from each animal.

A.2.4 Lung Weight Calculations

In the first study, 8 un-dosed male ICR mice (~32 g) were sacrificed and their lungs were harvested. The weight of the hydrated lung was determined followed by freezing of the lung in liquid nitrogen. The frozen lung was lyophilized to remove water by a VirTis Advantage Tray Lyophilizer (The VirTis Company, Inc. Gardiner, NY). The dried lungs were then weighed and averaged to determine an average dry lung weight. The lung weights and average are shown in Table A.4. The average lung weight was used to determine the concentration of ITZ per gram of lung tissue. In the second study, the hydrated lungs from each of the dosed mice were weighed individually and used in the calculation of ITZ lung concentrations. The hydrated lung weights for the individual mice are shown in Table A.5.

A.2.5 Analysis of Lung Concentrations

The level of ITZ within each lobe was analyzed using the extraction procedure and chromatographic method described in Chapter 4.3. The protocol which was utilized during the extraction of lung and serum samples are listed in Table A.2 and Table A.3. A sample chromatogram is shown in Figure A.1.

A.3 RESULTS

The variability in dosing was measured *in vivo* as a determination of treatment efficiency and precision in dosing. In the first study, the concentrations based on an average dry lung weight (Table A.4) are shown in Figure A.2. The average concentration was 29.3 μg/g (SD = 12.8). In the second study, based on lung weights (Table A.5) from each sacrificed mouse (wet lung weight) the concentration of itraconazole by inhalation had an average concentration of 8.9 μg/g (SD = 1.16) wet lung weight (Figure A.1), error bars indicate the standard deviation obtained for each individual mouse (n = 4). It was observed in the second study that mice with higher individual lungs weights had higher drug loading of itraconazole, and is consistent with an increased lung tidal volume, which was unable to determined in the first study because of the use of an average dry lung weight. Overall, the variation of the entire mouse population (n = 10) within the dosing chamber was only 13% RSD, a very acceptable variance considering physiological differences which could not be accounted for (i.e. breathing rate, mobility of each mouse and their individual location within the dosing chamber over the specified 20 minute dosing exposure period).

Appendix B: Formulation and Dosage Form Development of Poorly Water Soluble Drugs Using Particle Engineering Processes

B.1 FLUID-BED PROCESSING AND WET-MASS EXTRUSION AND SPHERONIZATION OF EPAS DISPERSIONS

B.1.1 Objectives

The objectives of these studies were to investigate pharmaceutical formulations of a poorly water-soluble drug micronized by evaporative precipitation into aqueous solution (EPAS), and to demonstrate enhanced dissolution and to investigate the use of fluidized-bed technology to formulate EPAS micronized and surfactant stabilized API. Also, wet mass extrusion/spheronization of the dispersion mixed with a substrate was studied.

B.1.2 Methods and Materials

B.1.2.1 Materials

Micronized danazol, sodium lauryl sulfate (SDS), polyvinylpyrrolidone (PVP) K-15, poloxamer 407, sodium starch glycolate (SSG), deoxycholic acid (DCA), lactose monohydrate and 1.0N hydrochloric acid (HCl) solution were purchased from Spectrum Chemicals (Gardena, CA). High performance liquid chromatography (HPLC) grade acetonitrile and dichloromethane were obtained from EM Science (Gibbstown, NJ).

Microcrystalline cellulose (MCC, Avicel PH101) was purchased from FMC (FMC Corporation, Philadelphia, PA).

B.1.2.2 EPAS Processing to Form a Danazol Dispersion for Fluid-bed Processing

The EPAS procedure utilized for this experiment is described in detail in Chapter 2.3.3. Briefly, the model drug, danazol, was dissolved in dichloromethane at 2% w/v along with poloxamer 407 at 1% w/v. This solution was heated (80°C) and atomized through a crimped conical nozzle below the surface of an aqueous solution containing 1% w/v DCA. The flow rate was set at 2 mL/min with a pressure drop of ~20MPa. The resulting dispersion was then either quench frozen and lyophilized to form powder or fluid-bed processed onto a substrate of lactose and microcrystalline cellulose at an 80/20 ratio.

B.1.2.3 Fluid-Bed Processing of the EPAS Dispersion

The dispersion formed during EPAS processing (200 – 800 mL) was sprayed using a Strea-1 fluid-bed processing unit with a Wurster insert (Niro, Aeromatic-Fielder Ltd., Columbia, MD). PVP-K15 was added as a binder in some instances at a 5% w/v level. Coating dispersion was delivered by a peristaltic pump (Watson Marlow, Concord, MA) and sprayed into the fluidized-bed via a 1.2-mm spray nozzle at the atomizing pressure of 1.5 bar. The substrate consisted of an 80/20 ratio of lactose and microcrystalline cellulose in batch sizes of 50 – 200 g. The drying temperature was set at

55 – 60°C to achieve and outlet temperature of 35 - 40°C with a spray rate of 2.5 mL/min. The spray time varied from 2 – 4 hours depending on the volume sprayed and drying of the bed was conducted for 15 minutes following the completion of the atomization. The formulations, EPAS dispersion volume, % PVP K-15 and quantity of substrate used are shown in Table B.1.

B.1.2.4 EPAS Processing to Form a Danazol Dispersion for Wet Mass Extrusion and Speronization

The EPAS procedure utilized for this experiment is described in detail in Chapter 2.3.3. Briefly, the model drug, danazol, was dissolved in 200 mL dichloromethane at 5% w/v along with PVP K-15 at 2.5% w/v. This solution was heated (80°C) and atomized through a crimped conical nozzle below the surface of an 300 mL aqueous solution containing 1% w/v PVP K-15. The flow rate was set at 3 mL/min with a pressure drop of ~20MPa. The dispersion was further processed to remove excess stabilizer by centrifugation of the dispersion at 3000 rpm for 15 minutes, decantation of the supernatant and redispersion of the pellet with 100 mL of a 1% PVP K-15 solution. The resultant dispersion was used for wet-mass extrusion and spheronization.

B.1.2.5 Wet-mass Extrusion and Spheronization of an EPAS Dispersion

The substrate which was used for the bead manufacture consisted of 290 g of 10% sodium starch glycolate (SSG), 2.5% microcrystalline cellulose (MCC) and 87.5% lactose monohydrate which was mixed via geometric dilution on a V-powder blender. Once homogeneously mixed, the powder was added to a rotary powder blender (Kitchen

Aid Model KSM 90, Kitchen Aid, Inc., St. Joseph, MI) and pre-wetted with 100 mL of deionized water. The EPAS dispersion was atomized onto the powder while blending using a coaxial nozzle with an air pressure of 1 bar. The resultant wet mass was then extruded (Benchtop Granulator, Model No. 5666, LCI Corporation, Charlotte, NC) into 1 mm diameter extrudates and spheronized (Caleva, Model 120, GEI Processing, Inc., Towaco, NJ) at 200 rpm for 2 minutes. The beads were dried in an oven for 18 hours at 40°C and sized between 16 – 20 mesh.

B.1.2.6 Scanning Electron Microscopy

The method for scanning electron microscopy is outlined in Chapter 2.3.9.

B.1.2.7 X-Ray Powder Diffraction

The method for measurement of crystallinity using X-ray powder diffraction is outlined in Chapter 2.3.5.

B.1.2.8 Dissolution

The procedure utilized for determination of dissolution rate is outlined in Chapter 2.3.2.

B.1.3 Results

B.1.3.1 Fluid-Bed Processing of the EPAS Dispersion

Scanning electron micrographs of the substrate microcrystalline cellulose and lactose are shown in Figures B.1 and B.2. It can be seen from the figures that before fluid-bed processing, the substrate material displays a rough surface, whereas, after fluid-bed processing, the substrate can be seen with a coating on the surface. This was due to coating of the EPAS nanoparticulate dispersion onto the substrate material. The dissolution rates of the fluid-bed processed powders are shown in Figures B.3 and B.4. From the figures, the rate of dissolution of the EPAS powder, with and without fluid-bed processing was rapid and 90 – 100% dissolved in the first 2 minutes. The bulk danazol and physical mixture formulations displayed slower rates of dissolution.

B.1.3.2 Wet-mass Extrusion and Spheronization of an EPAS Dispersion

Scanning electron micrographs of the wet-mass extrusion and spheronization beads containing EPAS dispersions are shown in Figure B.5. From the figure the spheronized extrudates displayed a rough surface, mainly due to the high water solubility of the components which added to it's brittleness. The dissolution rate (Figure B.6) of the beads was rapid, although not significantly more rapid than the control physical mixture which was followed by the bulk danazol.

217

Appendix C: Comparison of Powders and Dispersions Produced by Varying Nozzle Types for SFL and EPAS Processing

C.1 VARIATION IN PEEK NOZZLE TIP MORPHOLOGY IN SFL PROCESSING

C.1.1 Objective

To compare particle morphology and dissolution characteristics of powders produced by SFL using either a crimped or uncrimped PEEK nozzle. The crimped nozzle was formed by cutting the atomization end of the nozzle with wire cutters, which acted to crimp the end of the nozzle and produce a finer atomization during spray freezing. The uncrimped nozzle was formed by cutting the end of the nozzle with a razor blade, which produced a cylindrical opening at the tip, resulting in a stream spray geometry during processing.

C.1.2 Materials and methods

C.1.2.1 Materials

The following materials were purchased: ITZ (ITZ; Hawkins Chemical, Minneapolis, MN); poloxamer 407, succinic acid, sodium dodecyl sulfate (SDS), 0.1N HC, diethanolamine and polyvinylpyrrolidone (PVP) K-15 (Spectrum Chemicals, Gardena, CA); acetonitrile and dichloromethane (EM Industries Inc., Gibbstown, NJ).

C.1.2.2 Production of the SFL Powders

The methods for spray freezing of the model drug are described in Chapter 2.3.2. The formulation which was spray consisted of ITZ, poloxamer 407 and succinic acid in a 1:2:1 ratio dissolved in a 1,3-dioxolane/water cosolvent mixture at a 1:1 ratio to a concentration equal to 0.3% ITZ.

C.1.2.3 Scanning Electron Microscopy

The method for scanning electron microscopy is outlined in Chapter 2.3.9.

C.1.2.4 Dissolution

Dissolution testing was performed using a United States Pharmacopeia 27 (USP) apparatus II VanKel VK6010 Dissolution Testing Station with a Vanderkamp VK650A heater/circulator (Varian, Inc., Palo Alto, CA). Aliquots of 10-15 mg of powder were weighed and placed into 900 ml of 0.3% SDS, 0.1N HCl dissolution media. A volume of 5 mL was collected at 2, 5, 10, 20, 30, and 60 min (n=6) using a VK8000 autosampler (Varian Inc., Cary, NC). Paddle speed and bath temperature were set at 50 rpm and 37.0±0.2 °C, respectively. The collected samples were filtered and evaluated via HPLC at 263 nm using a Shimadzu LC-10 liquid chromatograph (Shimadzu Corporation, Columbia, MD) equipped with an Alltech 5 µm Inertsil ODS-2 C18 reverse-phase column (Alltech Associates, Inc., Deerfield, IL). The ITZ peak eluted at 7 min when running mobile phase (70% acetonitrile/30% water/0.5% diethanolamine v/v) at 1 ml/min.

C.1.2.5 X-Ray Powder Diffraction

The method for measurement of crystallinity using X-ray powder diffraction is outlined in Chapter 2.3.5.

C.1.2.6 BET Specific Surface Area

The method for measurement of surface area is outlined in Chapter 2.3.7

C.1.3 Results

C.1.3.1 PEEK Nozzle Morphology

Pictures and SEM micrographs of the crimped and uncrimped PEEK SFL nozzles are shown in Figure C.1. From the SEM micrographs, it can be seen that the crimping process creates a narrow elliptical opening a the tip of the PEEK nozzle at ~60 μm in diameter at its narrowest point. This leads to the production of a fine mist upon atomization of the feed solution. Alternatively, the SEM micrograph of the uncrimped nozzle shows an cylindrical orifice which is ~150 μm which is near to the specified inside diameter of 127 μm.

C.1.3.2 Dissolution

The rates of dissolution of the processed powders, comparing the crimped and uncrimped nozzles are shown in Figure C.2. From the figure, the powder produced by the crimped and uncrimped nozzle displayed 30% and 60% dissolved at 2 minutes, respectively. However, after 5 minutes, the dissolution curves are not significantly different from each other.

C.1.3.3 X-Ray Powder Diffraction

The crystallinity of the processed powders, ITZ and excipients, as measured by X-ray powder diffraction are illustrated in Figure C.3. The crystalline bulk ITZ, poloxamer 407 and succinic acid display charactistic crystalline peaks with varying degrees of intensity. The processed powders displayed similar traces and lacked any substantial ITZ peaks but retained noticeable succinic acid and poloxamer peaks.

C.1.3.4 Particle Morphology

Figures C.4 and C.5 display the SEM morphology of the processed powders. From the figure, it can be seen that both powders are composed of nanostructured aggregates. They were similar in structure and appearance and displayed BET surface area measurements of 17.25 m^2/g and 13.72 m^2/g for powders produced using SFL with the crimped and uncrimped nozzle geometry, respectively.

C.2 EFFECT OF THE ADDITION OF AN ULTRASONIC HORN TO THE TIP OF THE CRIMPED STEEL NOZZLE DURING EPAS PROCESSING

C.2.1 Objective

A method for producing a fine atomization using a steel nozzle combined with an ultrasonic horn was evaluated. The nozzle design was utilized for the production of fine atomization of solvent within the aqueous bath during EPAS processing. The API particle sizes, dissolution and x-ray diffraction of the dispersions and powders produced by the EPAS process were evaluated and compared for the nozzle types and for different processing parameters using the ultrasonic nozzle.

C.2.2 Methods and Materials

C.2.2.1 Materials

The materials purchased for this study are listed in Appendix C.1.2.1.

C.2.2.2 EPAS Processing Using the Crimped Steel Nozzle With and Without Ultrasonication

The methods utilized for the EPAS processing are described in Chapter 2.3.3. The formulation consisted of 2% w/v danazol and 1% w/v PVP K-15 dissolved in 50 mL dichloromethane as the organic phase and 1% w/v PVP K-15 dissolved in 300 mL water as the aqueous phase. The steel crimped nozzle utilized for this study is described in Chapter 2.3.3. For the enhanced atomization using an ultrasonic horn, the nozzle was placed at a 45° angle to the base of the horn (Figure C.6) and the apparatus was

positioned below the surface of the aqueous phase. Three separate crimped steel nozzles were produced and analyzed with (u-c1 – u-c3) and without (c1 - c3) ultrasonication. The effect of flow rate on the resulting dispersion particle size as evaluated at 2, 5 and 10 mL/min. The ultrasonic output was varied and and dispersion particle size compared at 30, 60 and 90 watts.

C.2.2.3 Particle Size Analysis

This method is described in Chapter 2.3.2

C.2.2.4 Dissolution

The dissolution testing procedure is outlined in Chapter 2.3.12.

C.2.2.5 X-Ray Powder Diffraction

This method is outlined in Chapter 2.3.5.

C.2.3 Results

Particle size analysis, which was conducted on the dispersions formed by EPAS processing using the crimped nozzle with and without ultrasonication are shown in Table C.1. From the table, there appeared to be internozzle variability with little change in particle size due to the inclusion of an ultrasonic nozzle. This was further evident with

similar levels of crystallinity (Figure C.7) and rates of dissolution (Figure C.8). The nozzles show similar results in particle size, dissolution and level of crystallinity. All of the nozzles tested formed EPAS powders with high dissolution rates and low crystallinity. The results of the nozzle characterization indicate that the addition of an ultrasonic horn has little to no effect on the particle size of the EPAS dispersions. However, changing the process parameters (ultrasonic output) during EPAS, using an ultrasonic nozzle, did change the particle size of the final dispersion, indicating the ultrasonic horn may play a limited role in effecting particle size during EPAS.

Appendix D: Formulation Development of ITZ for Oral Delivery

D.1 INCORPORATION OF AN ACIDULANT INTO ITZ SFL POWDERS

D.1.1 Objective

The objective of this study was the evaluation of acidulant properties and to investigate formulations composed of itraconazole and acidulants to determine optimum powder characteristics formed by SFL. The hypothesis is that incorporation of an acidifying agent will decrease the microenvironmental pH adjacent to the API. This will increase the local solubility and increase the concentration of drug available for absorption through the tissue.

D.1.2 Materials and Methods

D.1.2.1 pH solubility of ITZ

The solubility of ITZ at various pH conditions and in dissolution media containing a surfactant was evaluated. Several stock solutions at pH 1.2, 3, 4, 5.8, 6.8, 7.4 and 9.8 were made according to the United States Pharmacopoeia (USP) monograph on buffer solutions. The pH 1.2 dissolution media was mixed according to Appendix C.1.2.3. The pH 7 dissolution media was 0.05M Na_2HPO_4 with 0.3% w/v SDS adjusted to pH 7 with citric acid. The equilibrium solubility was determined by adding enough

ITZ to the buffer solutions (n=3) to form a saturated dispersion. The dispersions were mixed on an orbital shaker at 37°C for 72 hrs. The dispersions were filtered using a 0.45 µm syringe filter and the concentration was determined by HPLC (Appendix C.1.2.3).

D.1.2.2 Acidulant pH Concentration Profile

Various acidulants were evaluated for their ability lower pH of a solution. The acidulants, succinic acid, ascorbic acid, sorbic acid, citric acid anhydrous, tartaric acid, fumaric acid and adipic acid were dissolved in deionized water at concentrations from 1 mg/mL to 10 mg/mL. The pH of each solution was evaluated using a pH meter calibrated from pH 1 to pH 7.

D.1.2.3 Incorporation of an Acidulant to an SFL Formulation

SFL processing was conducted according to Chapter 2.3.2. The formulations sprayed are shown in Table D.1. Briefly, ITZ, poloxamer 407 and an acidulant (adipic acid, succinic acid, fumaric acid, ascorbic acid, citric acid or tartaric acid) were dissolved in a water/1,3-dioxolane 50/50 cosolvent mixture at 0.3%, 0.6%, 0.3 % w/v, respectively. The formulations were spray frozen in liquid nitrogen at 50 mL/min through a 127 µm PEEK nozzle. The frozen microparticles were lyophilized to form powder.

D.1.2.4 Incorporation of SFL Formulation Containing Succinic Acid into a Tablet Formulation

The SFL formulation composed of ITZ/poloxamer 407/succinic acid 1/2/1 was incorporated into a table formulation. The SFL powder was sieved through a 200 mesh screen to decrease the aggregate particle size and aid in mixing. The tablet contained Avicel PH113 10%, Prosolv 90 64%, SSG 5.0%, SDS 0.5%, magnesium stearate 0.5% and SFL Powder 20%. The powders were mixed via geometric dilution of the SFL powder with Avicel followed by SSG, SDS, Prosolv and magnesium stearate on a v-blender. The powder was then tableted on a rotary press using 0.3542" diameter die, a weight of 150 mg and to a hardness of 8 kg.

D.1.2.5 Scanning Electron Microscopy

The method for scanning electron microscopy is outlined in Chapter 2.3.9.

D.1.2.6 Dissolution

The method for dissolution is described in Appendix C.1.2.3.

D.1.2.7 X-Ray Powder Diffraction

The method for X-ray powder diffraction is outlined in Chapter 2.3.5.

D.1.3 Results

The pH solubility profile for ITZ is shown in Figure D.1. ITZ displays a pH dependent solubility with increased solubility at low pH (< pH 3). The solubility of ITZ in the dissolution media was significantly greater at pH 1.2 than at pH 7, as would be expected from the pH dependent solubility. The pH concentration profiles for selected acidifying agents are shown in Figure D.2 and were used as a guide for the selection of the optimum acidulant for SFL processing of ITZ. The SEM micrographs of the SFL processed formulations are shown in Figure D.3. From the figure, it can be seen that the SFL process created powders composed of nanoparticulate aggregates and were similar in all cases. There were, however, significant differences in the rate of dissolution between the various formulations (Figure D.4). From the figure, formulations containing adipic acid and succinic acid displayed the most rapid rate of dissolution followed by the formulation containing fumaric acid. The formulations containing ascorbic acid, citric acid or tartaric acid displayed poor dissolution rates. Figures D.5 to D.6 illustrate the crystallinity of the formulations compared to the bulk components as measured by X-ray powder diffraction. It can be seen from the figures that all of the bulk materials display characteristic crystalline peaks, whereas, the SFL processed powders display only those peaks which were associated with poloxamer and/or the acidulant, yielding amorphous ITZ. The formulation containing succinic acid as an acidulant displayed rapid dissolution and wetting, amorphous character and a low pH. For this reason, it was utilized to manufacture tablets containing an SFL formulation. From Figure D.11, the rate of dissolution of the SFL powder and SFL powder mixed with tableting excipients were rapid and similar in rate. However, the tableted dosage form displayed a significantly lower rate of dissolution. The slower rate of dissolution was attributed to the low glass transition temperature of the formulation, since the major component is poloxamer, which is waxy at room temperature. Upon compression, the plastic deformation of the

228

exipients (namely MCC) causes viscous flow within the SFL formulation, allowing for particle growth and segregation. For this reason, a high Tg stabilizer was included into the formulation and is discussed in the next subsection.

D.2   INCREASED GLASS TRANSITION TEMPERATURE OF THE SFL POWDER THROUGH THE INCORPORATION OF A HIGH MELTING POINT GLASSY POLYMER: PVP K-15

D.2.1 Objective

The objective of this study was the evaluation of morphology and performance of powders composed of an acidulant and a high glass transition temperature glassy polymer.   The hypothesis is that incorporation of PVP K-15 will increase the glass transition temperature and prevent viscous flow during plastic deformation of excipients during the manufacture of tablets.

D.2.2 Methods

D.2.2.1 Incorporation of PVP K-15 to an SFL Formulation

SFL processing was conducted according to Chapter 2.3.2. The formulations sprayed are shown in Table D.2. Briefly, ITZ, poloxamer 407, PVP K-15 and succinic acid were dissolved in a water/1,3-dioxolane 50/50 cosolvent mixture at the ratios

specified in table D.2 such that the concentration of ITZ was 0.3% w/w. The formulations were spray frozen in liquid nitrogen at 50 mL/min through a 127 μm PEEK nozzle. The frozen microparticles were lyophilized to form powder.

D.2.2.2 Incorporation of SFL Formulation Containing PVPK-15 into a Tablet Formulation

The SFL formulation composed of ITZ/PVP K-15/poloxamer 407/succinic acid 1/2//0.5/1 was incorporated into a table formulation. The SFL powder was sieved through a 200 mesh screen to decrease the aggregate particle size and aid in mixing. The tablet contained Avicel PH113 10%, Prosolv 90 64%, SSG 5.0%, SDS 0.5%, magnesium stearate 0.5% and SFL Powder 20%. The powders were mixed via geometric dilution of the SFL powder with Avicel followed by SSG, SDS, Prosolv and magnesium stearate on a v-blender. The powder was then tableted on a rotary press using 0.3542" diameter die, a weight of 150 mg and to a hardness of 8 kg.

D.2.2.3 Scanning Electron Microscopy

The method for scanning electron microscopy is outlined in Chapter 2.3.9.

D.2.2.4 Dissolution

The method for dissolution is described in Appendix C.1.2.3.

D.2.2.5 X-Ray Powder Diffraction

The method for X-ray powder diffraction is outlined in Chapter 2.3.5.

D.2.3 Results

The crystallinity of the formulations containing PVP-K15 is shown in Figure D.12. From the figure, the formulations lacking poloxamer as a solubilizing agent displayed no crystalline peaks and were completely amorphous, whereas, those formulations containing poloxamer showed peaks associated with succinic acid and/or poloxamer. The rates of dissolution for the formulations containing PVP K-15 are illustrated in Figure D.13. Formulations not containing poloxamer displayed poor dissolution due to the lack PVP K-15 to aid in wetting and solubilization of the formulation. However, formulations containing poloxamer displayed rapid dissolution. From this figure, it is evident that a solubilizing agent is required in PVP K-15 formulations to improve wetting and dissolution. Manufacture of tablets containing an SFL formulation was conducted and the rate of dissolution compared to the SFL powder alone and a tablet containing a physical mixture is shown in Figure D.14. From the figure, the rate of dissolution of the tablet containing SFL processed ITZ is significantly faster than the rate of dissolution of the tablet containing a physical mixture, but slower than the SFL powder alone. Although, the rate of dissolution of the tablet containing SFL processed ITZ and PVP K-15 was greater than that of the tablet containing SFL processed ITZ and poloxamer without PVP K-15 (Figure D.11).

D.3   INCREASED GLASS TRANSITION TEMPERATURE OF THE SFL POWDER THROUGH THE INCORPORATION OF A HIGH MELTING POINT SURFACTANT: SDS

D.3.1 Objective

The objective of this study was the evaluation of morphology and performance of powders composed of an acidulant and a high melting point surfactant.   The hypothesis is that incorporation of SDS will improve dissolution rate, while decreasing the need for both a stabilizer and surfactant as separate components in the formulation.

D.3.2 Methods

D.3.2.1 Incorporation of SDS to an SFL Formulation

SFL processing was conducted according to Chapter 2.3.2. The formulations sprayed are shown in Table D.3. Briefly, ITZ and excipients were dissolved in a water/1,3-dioxolane 50/50 cosolvent mixture at the ratios specified in table D.2 such that the concentration of ITZ was 0.3% w/w. The formulations were spray frozen in liquid nitrogen at 50 mL/min through a 127 μm PEEK nozzle. The frozen microparticles were lyophilized to form powder.

D.3.2.2 Scanning Electron Microscopy

The method for scanning electron microscopy is outlined in Chapter 2.3.9.

D.3.2.3 Dissolution

The method for dissolution at pH 1.2 is described in Appendix C.1.2.3. Dissolution at pH 7.0 was conducted similarly to that described in Appendix C.1.2.3, however, the dissolution media was composed of 0.05M Na_2HPO_4, 0.3% SDS and was adjusted to pH 7.0 with citric acid.

D.3.2.4 X-Ray Powder Diffraction

The method for X-ray powder diffraction is outlined in Chapter 2.3.5.

D.3.3 Results

The rates of dissolution in pH 1.2 media of formulations containing SDS are shown in Figure D.15. From the figure, it can be seen that the formulations containing SDS relatively slow, when compared to formulations composed of PVP K-15 and poloxamer (Figure D.13). The fastest rates of dissolution were observed in the formulations containing ITZ and SDS without poloxamer. When dissolution was conducted in pH 7 media, the dissolution rate was significantly faster than in pH 1.2 media (Figure D.16 Figure D.19). This finding was counter intuitive, especially since the solubility is much greater at pH 1.2 than at pH 7.0 (Figure D.1). SEM micrographs of the formulations containing ITZ/SDS 7/3 and ITZ/SDS 10/1 are shown in Figure D.17. From the figure, it can be seen that the powders are similar and display a nanoparticulate

aggregated network morphology, which is similar to other SFL formulations. The powders were amorphous (Figure D.18) and displayed rapid dissolution at pH 7 (Figure D.19) and slow dissolution at pH 1.2. The rate of dissolution of formulations composed of ITZ/SDS/mannitol and ITZ/SDS/DCA at a 7:3:3.5 ratio are shown in Figure D.20. From the graph, it can be seen that the rate of dissolution of the formulation containing mannitol is similar to that of the formulation composed of only ITZ and SDS in a 7:3 ratio. The formulation containing DCA displayed slower dissolution.

References

Liversidge, G.G.; Cundy, K.C. Particle size reduction for improvement of oral bioavailability of hydrophobic drugs: I. Absolute oral bioavailability of nanocrystalline danazol in beagle dogs. Int. J. Pharm. 1995, 125 (1): p. 91-97.

Ibrahim, N.K.; Desai, N.; Legha, S.; Soon-Shiong, P.; Theriault, R.L.; Rivera, E.; Esmaeli, B.; Ring, S.E.; Bedikian, A.; Hortobagyi et, a. Phase I and pharmacokinetic study of ABI-007, a Cremophor-free, protein-stabilized, nanoparticle formulation of paclitaxel. Clin. Cancer Res. 2002, 8 (5): p. 1038-1044.

Muller, R.H.; Keck, C.M. Challenges and solutions for the delivery of biotech drugs - a review of drug nanocrystal technology and lipid nanoparticles. J. Biotech. 2004, 113 (1-3): p. 151-170.

Yu, L. Amorphous pharmaceutical solids: preparation, characterization and stabilization. Adv. Drug. Del. Rev. 2001, 48 (1): p. 27-42.

Grant, D.J.W.; Brittian, H.G., Physical Characterization of Pharmaceutical Solids, ed. H.G. Brittian. 1995, New York: Marcel Dekker.

Russel, W.R.; Saville, D.A.; Schowalter, W.R., Colloidal Dispersions. 1989, Cambridge: Cambridge University Press.

Garcia-Fuentes, M.; Torres, D.; Alonso, M.J. Design of lipid nanoparticles for the oral delivery of hydrophilic macromolecules. Colloids Surf. B Biointerfaces 2003, 27 (2-3): p. 159-168.

Madras, G.; McCoy, B.J.B.J. Temperature effects on the transition from nucleation and growth to Ostwald ripening. Chem. Eng. Sci. 2004, 59 (13): p. 2753-2765.

Dollo, G.; Le Corre, P.; Guerin, A.; Chevanne, F.; Burgot, J.L.; Leverge, R. Spray-dried redispersible oil-in-water emulsion to improve oral bioavailability of poorly soluble drugs. Eur. J. Pharm. Sci. 2003, 19 (4): p. 273-280.

Eerikainen, H.; Watanabe, W.; Kauppinen, E.I.; Ahonen, P.P. Aerosol flow reactor method for synthesis of drug nanoparticles. Eur. J. Pharm. Biopharm. 2003, 55 (3): p. 357-360.

Merisko-Liversidge, E.; Liversidge, G.G.; Cooper, E.R. Nanosizing: a formulation approach for poorly-water-soluble compounds. Eur. J. Pharm. Sci. 2003, 18 (2): p. 113-120.

Krause, K.P.; Muller, R.H. Production and characterisation of highly concentrated nanosuspensions by high pressure homogenisation. Int. J. Pharm. 2001, 214 (1-2): p. 21-24.

Date, A.A.; Patravale, V.B. Current strategies for engineering drug nanoparticles. Curr. Op. Colloid Interface Sci. 2004, 9 (3-4): p. 222-235.

Rogers, T.L.; Johnston, K.P.; Williams, R.O., 3rd Solution-based particle formation of pharmaceutical powders by supercritical or compressed fluid CO_2 and cryogenic spray-freezing technologies. Drug Dev. Ind. Pharm. 2001, 27 (10): p. 1003-1015.

Hu, J.; Johnston, K.P.; Williams, R.O., 3rd Nanoparticle engineering processes for enhancing the dissolution rates of poorly water soluble drugs. Drug Dev. Ind. Pharm. 2004, 30 (3): p. 233-245.

Rogers, T.L.; Gillespie, I.B.; Hitt, J.E.; Fransen, K.L.; Crowl, C.A.; Tucker, C.J.; Kupperblatt, G.B.; Becker, J.N.; Wilson, D.L.; Todd et, a. Development and characterization of a scalable controlled precipitation process to enhance the dissolution of poorly water-soluble drugs. Pharm. Res. 2004, 21 (11): p. 2048-2057.

Sarkari, M.; Brown, J.; Chen, X.; Swinnea, S.; Williams, I., Robert O.; Johnston, K.P. Enhanced drug dissolution using evaporative precipitation into aqueous solution. Int. J. Pharm. 2002, 243 (1-2): p. 17-31.

Jarmer, D.J.; Lengsfeld, C.S.; Randolph, T.W. Manipulation of particle size distribution of poly(-lactic acid) nanoparticles with a jet-swirl nozzle during precipitation with a compressed antisolvent. J. Supercrit. Fluids 2003, 27 (3): p. 317-336.

Young, T.J.; Mawson, S.; Johnston, K.P.; Henriksen, I.B.; Pace, G.W.; Mishra, A.K. Rapid expansion from supercritical to aqueous solution to produce submicron suspensions of water-insoluble drugs. Biotech. Prog., 16 (3): p. 402-407.

Turk, M.; Hils, P.; Helfgen, B.; Schaber, K.; Martin, H.-J.; Wahl, M.A. Micronization of pharmaceutical substances by the Rapid Expansion of Supercritical Solutions (RESS): a promising method to improve bioavailability of poorly soluble pharmaceutical agents. J. Supercrit. Fluids 2002, 22 (1): p. 75-84.

Debuigne, F.; Cuisenaire, J.; Jeunieau, L.; Masereel, B.; Nagy, J.B. Synthesis of Nimesulide Nanoparticles in the Microemulsion Epikuron/Isopropyl Myristate/Water/n-Butanol (or Isopropanol). J. Colloid Interface Sci. 2001, 243 (1): p. 90-101.

Trotta, M.; Gallarate, M.; Carlotti, M.E.; Morel, S. Preparation of griseofulvin nanoparticles from water-dilutable microemulsions. Int. J. Pharm. 2003, 254 (2): p. 235-242.

Yu, Z.; Garcia, A.S.; Johnston, K.P.; Williams, I., Robert O. Spray freezing into liquid nitrogen for highly stable protein nanostructured microparticles. Eur. J. Pharm. Biopharm. 2004, 58 (3): p. 529-537.

Soppimath, K.S.; Aminabhavi, T.M.; Kulkarni, A.R.; Rudzinski, W.E. Biodegradable polymeric nanoparticles as drug delivery devices. 2001, 70 (1-2): p. 1-20.

Leroux, J.-C.; Allemann, E.; Doelker, E.; Gurny, R. New approach for the preparation of nanoparticles by an emulsification-diffusion method. 1995, 41 (1): p. 14-18.

Muller, R.H.; Mader, K.; Gohla, S. Solid lipid nanoparticles (SLN) for controlled drug delivery - a review of the state of the art. Eur. J. Pharm. Biopharm. 2000, 50 (1): p. 161-177.

Oyewumi, M.O.; Mumper, R.J. Gadolinium-loaded nanoparticles engineered from microemulsion templates. Drug Dev. Ind. Pharm. 2002, 28 (3): p. 317-328.

Soga, O.; van Nostrum, C.F.; Fens, M.; Rijcken, C.J.F.; Schiffelers, R.M.; Storm, G.; Hennink, W.E. Thermosensitive and biodegradable polymeric micelles for paclitaxel delivery. J. Control. Release 2005, 103 (2): p. 341-353.

Mohammed, A.R.; Weston, N.; Coombes, A.G.A.; Fitzgerald, M.; Perrie, Y. Liposome formulation of poorly water soluble drugs: optimisation of drug loading and ESEM analysis of stability. Int. J. Pharm. 2004, 285 (1-2): p. 23-34.

Moghimi, S.M.; Szebeni, J. Stealth liposomes and long circulating nanoparticles: critical issues in pharmacokinetics, opsonization and protein-binding properties. Prog. Lip. Res. 2003, 42 (6): p. 463-478.

Tsinontides, S.C.; Rajniak, P.; Pham, D.; Hunke, W.A.; Placek, J.; Reynolds, S.D. Freeze drying--principles and practice for successful scale-up to manufacturing. Int. J. Pharm. 2004, 280 (1-2): p. 1-16.

Jones, A.R. Light scattering for particle characterization. Prog. Energ. Combust. 1999, 25 (1): p. 1-53.

Freud, P.J.; Plantz, P.E. Sizing nanoparticles with dynamic light scattering. Powder and Bulk Eng. 2004: p. 1-5.

Dubes, A.; Parrot-Lopez, H.; Abdelwahed, W.; Degobert, G.; Fessi, H.; Shahgaldian, P.; Coleman, A.W. Scanning electron microscopy and atomic force microscopy imaging of solid lipid nanoparticles derived from amphiphilic cyclodextrins. Eur. J. Pharm. Biopharm 2003, 55 (3): p. 279-282.

Shi, H.Q.G.; Farber, L.; Michaels, J.N.; Dickey, A.; Thompson, K.C.; Shelukar, S.D.; Hurter, P.N.; Reynolds, S.D.; Kaufman, M.J. Characterization of crystalline drug nanoparticles using atomic force microscopy and complementary techniques. Pharm. Res. 2003, 20 (3): p. 479-484.

Midgley, P.A.; Weyland, M. 3D electron microscopy in the physical sciences: the development of Z-contrast and EFTEM tomography. Ultramicroscopy 2003, 96 (3-4): p. 413-431.

Bootz, A.; Vogel, V.; Schubert, D.; Kreuter, J. Comparison of scanning electron microscopy, dynamic light scattering and analytical ultracentrifugation for the sizing of poly(butyl cyanoacrylate) nanoparticles. Eur. J. Pharm. Biopharm. 2004, 57 (2): p. 369-375.

Torchilin, V.P. Fluorescence microscopy to follow the targeting of liposomes and micelles to cells and their intracellular fate. Adv. Drug Del. Rev. 2005, 57 (1): p. 95-109.

240

Jung, J.; Perrut, M. Particle design using supercritical fluids: Literature and patent survey. J. Supercrit. Fluids 2001, 20 (3): p. 179-219.

Song, C.X.; Labhasetwar, V.; Murphy, H.; Qu, X.; Humphrey, W.R.; Shebuski, R.J.; Levy, R.J. Formulation and characterization of biodegradable nanoparticles for intravascular local drug delivery. 1997, 43 (2-3): p. 197-212.

Rogers, T.L.; Overhoff, K.A.; Shah, P.; Santiago, P.; Yacaman, M.J.; Johnston, K.P.; Williams, I., Robert O. Micronized powders of a poorly water soluble drug produced by a spray-freezing into liquid-emulsion process. Eur. J. Pharm. Biopharm. 2003, 55 (2): p. 161-172.

J.B. Dressman and C. Reppas, In vitro-in vivo correlations for lipophilic, poorly water-soluble drugs, Eur. J. Pharm. Sci. 11 (2000) S73-S80.

D. Horter and J.B. Dressman, Influence of physicochemical properties on dissolution of drugs in the gastrointestinal tract, Adv. Drug Deliv. Rev. 46 (2001) 75-87.

C. Leuner and J. Dressman, Improving drug solubility for oral delivery using solid dispersions, Eur. J. Pharm. Biopharm. 50 (2000) 47-60.

S.I.F. Badawy, A.L. Marshall, M.M. Ghorab, and C.M. Adeyeye, A study of the complexation between danazol and hydrophilic cyclodextrin derivatives, Drug Dev. Ind. Pharm. 22 (1996) 959-966.

T.L. Rogers, K.P. Johnston, and R.O. Williams, Solution-based particle formation of pharmaceutical powders by supercritical or compressed fluid CO2 and cryogenic spray-freezing technologies, Drug Dev. Ind. Pharm. 27 (2001) 1003-1015.

E. Reverchon, Supercritical antisolvent precipitation of micro- and nano-particles, J. Supercrit. Fluids 15 (1999) 1-21.

J.H. Hu, K.P. Johnston, and R.O. Williams, Nanoparticle engineering processes for enhancing the dissolution rates of poorly water soluble drugs, Drug Dev. Ind. Pharm. 30 (2004) 233-245.

T.L. Rogers, K.A. Overhoff, P. Shah, P. Santiago, M.J. Yacaman, K.P. Johnston, and R.O. Williams, Micronized powders of a poorly water soluble drug produced by a spray-freezing into liquid-emulsion process, Eur. J. Pharm. Biopharm. 55 (2003) 161-172.

T.L. Rogers, A.C. Nelsen, M. Sarkari, T.J. Young, K.P. Johnston, and R.O. Williams, Enhanced aqueous dissolution of a poorly water soluble drug by novel particle engineering technology: Spray-freezing into liquid with atmospheric freeze-drying, Pharm. Res. 20 (2003) 485-493.

T.L. Rogers, A.C. Nelsen, J.H. Hu, J.N. Brown, M. Sarkari, T.J. Young, K.P. Johnston, and R.O. Williams, A novel particle engineering technology to enhance dissolution of poorly water soluble drugs: spray-freezing into liquid, Eur. J. Pharm. Biopharm. 54 (2002) 271-280.

242

T.L. Rogers, K.P. Johnston, and R.O. Williams, Physical stability of micronized powders produced by spray-freezing into liquid (SFL) to enhance the dissolution of an insoluble drug, Pharm. Dev. Technol. 8 (2003) 187-197.

T.L. Rogers, J.H. Hu, Z.S. Yu, K.P. Johnston, and R.O. Williams, A novel particle engineering technology: spray-freezing into liquid, Int. J. Pharm. 242 (2002) 93-100.

Z.S. Yu, T.L. Rogers, J.H. Hu, K.P. Johnston, and R.O. Williams, Preparation and characterization of microparticles containing peptide produced by a novel process: spray freezing into liquid, Eur. J. Pharm. Biopharm. 54 (2002) 221-228.

J.H. Hu, T.L. Rogers, J. Brown, T. Young, K.P. Johnston, and R.O. Williams, Improvement of dissolution rates of poorly water soluble APIs using novel spray freezing into liquid technology, Pharm. Res. 19 (2002) 1278-1284.

J.H. Hu, K.P. Johnston, and R.O. Williams, Rapid dissolving high potency danazol powders produced by spray freezing into liquid process, Int. J. Pharm. 271 (2004) 145-154.

J.H. Hu, K.P. Johnston, and R.O. Williams, Stable amorphous danazol nanostructured powders with rapid dissolution rates produced by spray freezing into liquid, Drug Dev. Ind. Pharm. 30 (2004) 695-704.

J.H. Hu, K.P. Johnston, and R.O. Williams, Spray freezing into liquid (SFL) particle engineering technology to enhance dissolution of poorly water soluble drugs:

organic solvent versus organic/aqueous co-solvent systems, Eur. J. Pharm. Sci. 20 (2003) 295-303.

X. Chen, Z. Benhayoune, R.O. Williams, and K.P. Johnston, Rapid dissolution of high potency itraconazole particles produced by evaporative precipitation into aqueous solution, J. Drug Deliv. Sci. Technol. 14 (2004) 299-304.

X.X. Chen, J.M. Vaughn, M.J. Yacaman, R.O. Williams, and K.P. Johnston, Rapid dissolution of high-potency danazol particles produced by evaporative precipitation into aqueous solution, J. Pharm. Sci. 93 (2004) 1867-1878.

X.X. Chen, T.J. Young, M. Sarkari, R.O. Williams, and K.P. Johnston, Preparation of cyclosporine A nanoparticles by evaporative precipitation into aqueous solution, Int. J. Pharm. 242 (2002) 3-14.

M. Sarkari, J. Brown, X.X. Chen, S. Swinnea, R.O. Williams, and K.P. Johnston, Enhanced drug dissolution using evaporative precipitation into aqueous solution, Int. J. Pharm. 243 (2002) 17-31.

B. Rambali, G. Verreck, L. Baert, and D.L. Massart, Itraconazole formulation studies of the melt-extrusion process with mixture design, Drug Dev. Ind. Pharm. 29 (2003) 641-652.

B.M. Tashtoush, Z.S. Al-Qashi, and N.M. Najib, In vitro and in vivo evaluation of glibenclamide in solid dispersion systems, Drug Dev. Ind. Pharm. 30 (2004) 601-607.

244

I. Montasser, H. Fessi, and A.W. Coleman, Atomic force microscopy imaging of novel type of polymeric colloidal nanostructures, Eur. J. Pharm. Biopharm. 54 (2002) 281-284.

H. Sato, T. Ohtsu, and I. Komasawa, Atomic force microscopy study of ultrafine particles prepared in reverse micelles, J. Colloid Interface Sci. 230 (2000) 200-204.

N. Masaki, K. Machida, H. Kado, K. Yokoyama, and T. Tohda, Molecular-Resolution Images of Aspirin Crystals with Atomic Force Microscopy, Ultramicroscopy 42 (1992) 1148-1154.

H.Q.G. Shi, L. Farber, J.N. Michaels, A. Dickey, K.C. Thompson, S.D. Shelukar, P.N. Hurter, S.D. Reynolds, and M.J. Kaufman, Characterization of crystalline drug nanoparticles using atomic force microscopy and complementary techniques, Pharm. Res. 20 (2003) 479-484.

S.C. Yang and J.B. Zhu, Preparation and characterization of camptothecin solid lipid nanoparticles, Drug Dev. Ind. Pharm. 28 (2002) 265-274.

T. Banerjee, S. Mitra, A.K. Singh, R.K. Sharma, and A. Maitra, Preparation, characterization and biodistribution of ultrafine chitosan nanoparticles, Int. J. Pharm. 243 (2002) 93-105.

L.M. Lacava, B.M. Lacava, R.B. Azevedo, Z.G.M. Lacava, N. Buske, A.L. Tronconi, and P.C. Morais, Nanoparticle sizing: a comparative study using atomic force

microscopy, transmission electron microscopy, and ferromagnetic resonance, J. Magn. Magn. Mater. 225 (2001) 79-83.

P.A. Midgley and M. Weyland, 3D electron microscopy in the physical sciences: the development of Z-contrast and EFTEM tomography, Ultramicroscopy 96 (2003) 413-431.

G. Van den Mooter, M. Wuyts, N. Blaton, R. Busson, P. Grobet, P. Augustijns, and R. Kinget, Physical stabilisation of amorphous ketoconazole in solid dispersions with polyvinylpyrrolidone K25, Eur. J. Pharm. Sci. 12 (2001) 261-269.

A.S. Kearney, D.L. Gabriel, S.C. Mehta, and G.W. Radebaugh, Effect of Polyvinylpyrrolidone on the Crystallinity and Dissolution Rate of Solid Dispersions of the Antiinflammatory Ci-987, Int. J. Pharm. 104 (1994) 169-174.

S. Corveleyn and J.P. Remon, Stability of freeze-dried tablets at different relative humidities, Drug Dev. Ind. Pharm. 25 (1999) 1005-1013.

L. Yu, Amorphous pharmaceutical solids: preparation, characterization and stabilization, Adv. Drug Deliv. Rev. 48 (2001) 27-42.

L.S. Taylor and G. Zografi, Spectroscopic characterization of interactions between PVP and indomethacin in amorphous molecular dispersions, Pharm. Res. 14 (1997) 1691-1698.

N. Rasenack, H. Hartenhauer, and B.W. Muller, Microcrystals for dissolution rate enhancement of poorly water-soluble drugs, Int. J. Pharm. 254 (2003) 137-145.

D.J. Dixon, K.P. Johnston, and R.A. Bodmeier, Polymeric Materials Formed by Precipitation with a Compressed Fluid Antisolvent, Aiche J. 39 (1993) 127-139.

G.V. Betageri and K.R. Makarla, Enhancement of dissolution of glyburide by solid dispersion and lyophilization techniques, Int. J. Pharm. 126 (1995) 155-160.

M. Yoshioka, B.C. Hancock, and G. Zografi, Inhibition of Indomethacin Crystallization in Poly(Vinylpyrrolidone) Coprecipitates, J. Pharm. Sci. 84 (1995) 983-986.

A.R. Paradkar, B. Chauhan, S. Yamamura, and A.P. Pawar, Preparation and characterization of glassy celecoxib, Drug Dev. Ind. Pharm. 29 (2003) 739-744.

Liversidge, G.G.; Cundy, K.C. Particle size reduction for improvement of oral bioavailability of hydrophobic drugs: I. Absolute oral bioavailability of nanocrystalline danazol in beagle dogs. International Journal of Pharmaceutics 1995, 125 (1): p. 91-97.

Erlich, L.; Yu, D.; Pallister, D.A.; Levinson, R.S.; Gole, D.G.; Wilkinson, P.A.; Erlich, R.E.; Reeve, L.E.; Viegas, T.X. Relative bioavailability of danazol in dogs from liquid-filled hard gelatin capsules. International Journal of Pharmaceutics 1999, 179 (1): p. 49-53.

Muraoka, A.; Tokumura, T.; Machida, Y. Evaluation of the bioavailability of flurbiprofen and its [beta]-cyclodextrin inclusion complex in four different doses upon oral administration to rats. European Journal of Pharmaceutics and Biopharmaceutics 2004, 58 (3): p. 667-671.

247

Jambhekar, S.; Casella, R.; Maher, T. The physicochemical characteristics and bioavailability of indomethacin from [beta]-cyclodextrin, hydroxyethyl-[beta]-cyclodextrin, and hydroxypropyl-[beta]-cyclodextrin complexes. International Journal of Pharmaceutics 2004, 270 (1-2): p. 149-166.

Wong, J.W.; Yuen, K.H. Improved oral bioavailability of artemisinin through inclusion complexation with [beta]- and [gamma]-cyclodextrins. International Journal of Pharmaceutics 2001, 227 (1-2): p. 177-185.

Savolainen, J.; Jarvinen, K.; Matilainen, L.; Jarvinen, T. Improved dissolution and bioavailability of phenytoin by sulfobutylether-[beta]-cyclodextrin ((SBE)7m-[beta]-CD) and hydroxypropyl-[beta]-cyclodextrin (HP-[beta]-CD) complexation. International Journal of Pharmaceutics 1998, 165 (1): p. 69-78.

Kawakami, K.; Yoshikawa, T.; Hayashi, T.; Nishihara, Y.; Masuda, K. Microemulsion formulation for enhanced absorption of poorly soluble drugs: II. In vivo study. Journal of Controlled Release 2002, 81 (1-2): p. 75-82.

Kang, B.K.; Lee, J.S.; Chon, S.K.; Jeong, S.Y.; Yuk, S.H.; Khang, G.; Lee, H.B.; Cho, S.H. Development of self-microemulsifying drug delivery systems (SMEDDS) for oral bioavailability enhancement of simvastatin in beagle dogs. International Journal of Pharmaceutics 2004, 274 (1-2): p. 65-73.

Wang, X.-q.; Dai, J.-d.; Chen, Z.; Zhang, T.; Xia, G.-m.; Nagai, T.; Zhang, Q. Bioavailability and pharmacokinetics of cyclosporine A-loaded pH-sensitive

nanoparticles for oral administration. Journal of Controlled Release 2004, 97 (3): p. 421-429.

Kapsi, S.G.; Ayres, J.W. Processing factors in development of solid solution formulation of itraconazole for enhancement of drug dissolution and bioavailability. International Journal of Pharmaceutics 2001, 229 (1-2): p. 193-203.

Sznitowska, M.; Gajewska, M.; Janicki, S.; Radwanska, A.; Lukowski, G. Bioavailability of diazepam from aqueous-organic solution, submicron emulsion and solid lipid nanoparticles after rectal administration in rabbits. European Journal of Pharmaceutics and Biopharmaceutics 2001, 52 (2): p. 159-163.

Rogers, T.L.; Overhoff, K.A.; Shah, P.; Santiago, P.; Yacaman, M.J.; Johnston, K.P.; Williams, R.O. Micronized powders of a poorly water soluble drug produced by a spray-freezing into liquid-emulsion process. European Journal of Pharmaceutics and Biopharmaceutics 2003, 55 (2): p. 161-172.

Rogers, T.L.; Nelsen, A.C.; Sarkari, M.; Young, T.J.; Johnston, K.P.; Williams, R.O. Enhanced aqueous dissolution of a poorly water soluble drug by novel particle engineering technology: Spray-freezing into liquid with atmospheric freeze-drying. Pharmaceutical Research 2003, 20 (3): p. 485-493.

Rogers, T.L.; Nelsen, A.C.; Hu, J.H.; Brown, J.N.; Sarkari, M.; Young, T.J.; Johnston, K.P.; Williams, R.O. A novel particle engineering technology to enhance

dissolution of poorly water soluble drugs: spray-freezing into liquid. European Journal of Pharmaceutics and Biopharmaceutics 2002, 54 (3): p. 271-280.

Rogers, T.L.; Johnston, K.P.; Williams, R.O. Physical stability of micronized powders produced by spray-freezing into liquid (SFL) to enhance the dissolution of an insoluble drug. Pharmaceutical Development and Technology 2003, 8 (2): p. 187-197.

Rogers, T.L.; Hu, J.H.; Yu, Z.S.; Johnston, K.P.; Williams, R.O. A novel particle engineering technology: spray-freezing into liquid. International Journal of Pharmaceutics 2002, 242 (1-2): p. 93-100.

Yu, Z.S.; Rogers, T.L.; Hu, J.H.; Johnston, K.P.; Williams, R.O. Preparation and characterization of microparticles containing peptide produced by a novel process: spray freezing into liquid. European Journal of Pharmaceutics and Biopharmaceutics 2002, 54 (2): p. 221-228.

Hu, J.H.; Rogers, T.L.; Brown, J.; Young, T.; Johnston, K.P.; Williams, R.O. Improvement of dissolution rates of poorly water soluble APIs using novel spray freezing into liquid technology. Pharmaceutical Research 2002, 19 (9): p. 1278-1284.

Hu, J.H.; Johnston, K.P.; Williams, R.O. Rapid dissolving high potency danazol powders produced by spray freezing into liquid process. International Journal of Pharmaceutics 2004, 271 (1-2): p. 145-154.

Hu, J.H.; Johnston, K.P.; Williams, R.O. Stable amorphous danazol nanostructured powders with rapid dissolution rates produced by spray freezing into liquid. Drug Development and Industrial Pharmacy 2004, 30 (7): p. 695-704.

Hu, J.H.; Johnston, K.P.; Williams, R.O. Spray freezing into liquid (SFL) particle engineering technology to enhance dissolution of poorly water soluble drugs: organic solvent versus organic/aqueous co-solvent systems. European Journal of Pharmaceutical Sciences 2003, 20 (3): p. 295-303.

Chen, X.; Benhayoune, Z.; Williams, R.O.; Johnston, K.P. Rapid dissolution of high potency itraconazole particles produced by evaporative precipitation into aqueous solution. Journal of Drug Delivery Science and Technology 2004, 14 (4): p. 299-304.

Chen, X.X.; Vaughn, J.M.; Yacaman, M.J.; Williams, R.O.; Johnston, K.P. Rapid dissolution of high-potency danazol particles produced by evaporative precipitation into aqueous solution. Journal of Pharmaceutical Sciences 2004, 93 (7): p. 1867-1878.

Chen, X.X.; Young, T.J.; Sarkari, M.; Williams, R.O.; Johnston, K.P. Preparation of cyclosporine A nanoparticles by evaporative precipitation into aqueous solution. International Journal of Pharmaceutics 2002, 242 (1-2): p. 3-14.

Sarkari, M.; Brown, J.; Chen, X.X.; Swinnea, S.; Williams, R.O.; Johnston, K.P. Enhanced drug dissolution using evaporative precipitation into aqueous solution. International Journal of Pharmaceutics 2002, 243 (1-2): p. 17-31.

Vaughn, J.M.; Gao, X.; Yacaman, M.-J.; Johnston, K.P.; Williams III, R.O. Comparison of powder produced by evaporative precipitation into aqueous solution (EPAS) and spray freezing into liquid (SFL) technologies using novel Z-contrast STEM and complimentary techniques. European Journal of Pharmaceutics and Biopharmaceutics 2005, 60 (1): p. 81-89.

Young, T.J.; Johnston, K.P.; Mishima, K.; Tanaka, H. Encapsulation of lysozyme in a biodegradable polymer by precipitation with a vapor-over-liquid antisolvent. Journal Of Pharmaceutical Sciences 1999, 88 (6): p. 640-650.

Yamada, T.; Saito, N.; Imai, T.; Otagiri, M. Effect of grinding with hydroxypropyl cellulose on the dissolution and particle size of a poorly water-soluble drug. Chemical & Pharmaceutical Bulletin 1999, 47 (9): p. 1311-1313.

Kohri, N.; Yamayoshi, Y.; Xin, H.; Iseki, K.; Sato, N.; Todo, S.; Miyazaki, K. Improving the oral bioavailability of albendazole in rabbits by the solid dispersion technique. The Journal Of Pharmacy And Pharmacology 1999, 51 (2): p. 159-164.

Suzuki, H.; Sunada, H. Influence of water-soluble polymers on the dissolution of nifedipine solid dispersions with combined carriers. Chemical & Pharmaceutical Bulletin 1998, 46 (3): p. 482-487.

252

Suzuki, H.; Sunada, H. Comparison of nicotinamide, ethylurea and polyethylene glycol as carriers for nifedipine solid dispersion systems. Chemical & Pharmaceutical Bulletin 1997, 45 (10): p. 1688-1693.

Yamashita, K.; Nakate, T.; Okimoto, K.; Ohike, A.; Tokunaga, Y.; Ibuki, R.; Higaki, K.; Kimura, T. Establishment of new preparation method for solid dispersion formulation of tacrolimus. International Journal Of Pharmaceutics 2003, 267 (1-2): p. 79-91.

Muller, R.H.; Keck, C.M. Challenges and solutions for the delivery of biotech drugs - a review of drug nanocrystal technology and lipid nanoparticles. Journal of Biotechnology 2004, 113 (1-3): p. 151-170.

Grant, D.J.W.; Brittian, H.G., Physical Characterization of Pharmaceutical Solids, ed. H.G. Brittian. 1995, New York: Marcel Dekker.

Sunesen, V.H.; Pedersen, B.L.; Kristensen, H.G.; Mullertz, A. In vivo in vitro correlations for a poorly soluble drug, danazol, using the flow-through dissolution method with biorelevant dissolution media. European Journal of Pharmaceutical Sciences 2005, 24 (4): p. 305-313.

Dressman, J.B.; Reppas, C. In vitro-in vivo correlations for lipophilic, poorly water-soluble drugs. European Journal of Pharmaceutical Sciences 2000, 11 (Supplement 2): p. S73-S80.

Farag Badawy, S.I.; Ghorab, M.M.; Adeyeye, C.M. Characterization and bioavailability of danazol-hydroxypropyl [beta]-cyclodextrin coprecipitates. International Journal of Pharmaceutics 1996, 128 (1-2): p. 45-54.

Sunesen, V.H.; Vedelsdal, R.; Kristensen, H.G.; Christrup, L.; Mullertz, A. Effect of liquid volume and food intake on the absolute bioavailability of danazol, a poorly soluble drug. European Journal of Pharmaceutical Sciences 2005, 24 (4): p. 297-303.

He, H.B.; Sun, S.L.; Liu, D.L.; Zheng, H.E. Analysis of danazol and its metabolites in serum by RP-HPLC with maxplot UV detector. Yao Xue Xue Bao = Acta Pharmaceutica Sinica 1988, 23 (9): p. 698-702.

Yu, L. Amorphous pharmaceutical solids: preparation, characterization and stabilization. Advanced Drug Delivery Reviews 2001, 48 (1): p. 27-42.

Otsuka, M.; Kato, F.; Matsuda, Y. Physicochemical stability of cimetidine amorphous forms estimated by isothermal microcalorimetry. AAPS PharmSciTech 2002, 3 (4): p. E30.

Clark, T.A.; Hajjeh, R.A. Recent trends in the epidemiology of invasive mycoses. Current Opinion In Infectious Diseases 2002, 15 (6): p. 569-574.

Denning, D.W.; Lee, J.Y.; Hostetler, J.S.; Pappas, P.; Kauffman, C.A.; Dewsnup, D.H.; Galgiani, J.N.; Graybill, J.R.; Sugar, A.M.; Catanzaro, A. NIAID mycoses study

group multicenter trial of oral itraconazole therapy for invasive aspergillosis. The American Journal of Medicine 1994, 97 (2): p. 135-144.

Singh, N.; Husain, S. Aspergillus infections after lung transplantation: clinical differences in type of transplant and implications for management. The Journal of Heart and Lung Transplantation 2003, 22 (3): p. 258-266.

Chiller, T.M.; Stevens, D.A. Treatment strategies for Aspergillus infections. Drug Resistance Updates 2000, 3 (2): p. 89-97.

Polak, A., Antifungal therapy - State of the Art at the Beginning of the 21st Century, in Antifungal Agents: Advances and Problems, E. Jucker, Editor. 2003, Birkhauser Verlag: Basel. p. 59-190.

Rapp, R.P. Changing strategies for the management of invasive fungal infections. Pharmacotherapy 2004, 24 (2, Part 2): p. 4S-28S; quiz 29S-32S.

Lambros, M.P.; Bourne, D.W.; Abbas, S.A.; Johnson, D.L. Disposition of aerosolized liposomal amphotericin B. Journal Of Pharmaceutical Sciences 1997, 86 (9): p. 1066-1069.

Monforte, V.; Roman, A.; Gavalda, J.; Lopez, R.; Pou, L.; Simo, M.; Aguade, S.; Soriano, B.; Bravo, C.; Morell et, a. Nebulized amphotericin B concentration and distribution in the respiratory tract of lung-transplanted patients. Transplantation 2003, 75 (9): p. 1571-1574.

Boots, R.J.; Paterson, D.L.; Allworth, A.M.; Faoagali, J.L. Successful treatment of post-influenza pseudomembranous necrotising bronchial aspergillosis with liposomal amphotericin, inhaled amphotericin B, gamma interferon and GM-CSF. Thorax 1999, 54 (11): p. 1047-1049.

Koizumi, T.; Kubo, K.; Kaneki, T.; Hanaoka, M.; Hayano, T.; Miyahara, T.; Okada, K.; Fujimoto, K.; Yamamoto, H.; Kobayashi et, a. Pharmacokinetic evaluation of amphotericin B in lung tissue: lung lymph distribution after intravenous injection and airspace distribution after aerosolization and inhalation of amphotericin B. Antimicrobial Agents And Chemotherapy 1998, 42 (7): p. 1597-1600.

Wade, J.C. Aerosolized amphotericin B inhalation is not effective prophylaxis of invasive aspergillus infections during prolonged neutropenia in patients after chemotherapy or autologous bone marrow transplantation. Evidence-based Oncology 2000, 1 (3): p. 87-88.

De Beule, K. Itraconazole: pharmacology, clinical experience and future development. International Journal of Antimicrobial Agents 1996, 6 (3): p. 175-181.

KOKS, C.H.W.; MEENHORST, P.L.; BULT, A.; BEIJNEN, J.H. ITRACONAZOLE SOLUTION: SUMMARY OF PHARMACOKINETIC FEATURES AND REVIEW OF ACTIVITY IN THE TREATMENT OF FLUCONAZOLE-RESISTANT ORAL CANDIDOSIS IN HIV-INFECTED PERSONS. Pharmacological Research 2002, 46 (2): p. 195-201.

Willems, L.; van der Geest, R.; de Beule, K. Itraconazole oral solution and intravenous formulations: a review of pharmacokinetics and pharmacodynamics. Journal Of Clinical Pharmacy And Therapeutics 2001, 26 (3): p. 159-169.

McConville, J.T.; Overhoff, K.A.; Sinswat, P.; Frei, B.L.; Burgess, D.; Talbert, R.L.; Peters, J.I.; Johnston, K.P.; III, R.O.W. Lung Deposition and Clearance of Itraconazole in the Murine Model for Treatment of Acute Fungal Infections. Article In Press.

Allendoerfer, R.; Loebenberg, D.; Rinaldi, M.G.; Graybill, J.R. Evaluation of SCH51048 in an experimental model of pulmonary aspergillosis. Antimicrobial Agents And Chemotherapy 1995, 39 (6): p. 1345-1348.

Coronel, B.; Levron, J.C.; Dorez, D.; Van Devenne, A.; Archimbaud, E.; Mercatello, A. Itraconazole lung concentrations in haematological patients. Mycoses 2000, 43 (3-4): p. 125-127.

McConville, J.T.; Overhoff, K.A.; Sinswat, P.; Frei, B.L.; Burgess, D.S.; Talbert, R.L.; Peters, J.I.; Johnston, K.P.; III, R.O.W. Novel Treatment of Pulmonary Aspergillosis Using Nebulized Itraconazole Nanoparticles in the Murine Model. in Proceedings of Respiratory Drug Delivery-Europe 2005 Conference. May 2005. Paris, France.

Vaughn, J.M.; Gao, X.; Yacaman, M.-J.; Johnston, K.P.; Williams III, R.O. Comparison of powder produced by evaporative precipitation into aqueous solution (EPAS)

257

and spray freezing into liquid (SFL) technologies using novel Z-contrast STEM and complimentary techniques. European Journal of Pharmaceutics and Biopharmaceutics 2005, 60 (1): p. 81-89.

Hu, J.H.; Johnston, K.P.; Williams, R.O. Spray freezing into liquid (SFL) particle engineering technology to enhance dissolution of poorly water soluble drugs: organic solvent versus organic/aqueous co-solvent systems. European Journal of Pharmaceutical Sciences 2003, 20 (3): p. 295-303.

Rogers, T.L.; Hu, J.H.; Yu, Z.S.; Johnston, K.P.; Williams, R.O. A novel particle engineering technology: spray-freezing into liquid. International Journal of Pharmaceutics 2002, 242 (1-2): p. 93-100.

McConville, J.T.; Williams, R.O.; Carvalho, T.C.; Iberg, A.N.; Johnston, K.P.; Talbert, R.L.; Burgess, D.; Peters, J.I. Design and evaluation of a restraint-free small animal inhalation dosing chamber. Drug Development and Industrial Pharmacy 2005, 31 (1): p. 35-42.

Gubbins, P.O.; Gurley, B.J.; Bowman, J. Rapid and sensitive high performance liquid chromatographic method for the determination of itraconazole and its hydroxy-metabolite in human serum. Journal of Pharmaceutical and Biomedical Analysis 1998, 16 (6): p. 1005-1012.

258

Lange, D.; Pavao, J.H.; Wu, J.; Klausner, M. Effect of a cola beverage on the bioavailability of itraconazole in the presence of H2 blockers. Journal Of Clinical Pharmacology 1997, 37 (6): p. 535-540.

Winston, D.J.; Maziarz, R.T.; Chandrasekar, P.H.; Lazarus, H.M.; Goldman, M.; Blumer, J.L.; Leitz, G.J.; Territo, M.C. Intravenous and oral itraconazole versus intravenous and oral fluconazole for long-term antifungal prophylaxis in allogeneic hematopoietic stem-cell transplant recipients - A multicenter, randomized trial. Annals of Internal Medicine 2003, 138 (9): p. 705-713.

Vandewoude, K.; Vogelaers, D.; Decruyenaere, J.; Jaqmin, P.; De Beule, K.; Van Peer, A.; Woestenborghs, R.; Groen, K.; Colardyn, F. Concentrations in plasma and safety of 7 days of intravenous itraconazole followed by 2 weeks of oral itraconazole solution in patients in intensive care units. Antimicrobial Agents And Chemotherapy 1997, 41 (12): p. 2714-2718.

Kontoyiannis, D.P.; Mantadakis, E.; Samonis, G. Systemic mycoses in the immunocompromised host: an update in antifungal therapy. Journal of Hospital Infection 2003, 53 (4): p. 243-258.

Wingard, J.R.; Leather, H. A new era of antifungal therapy. Biology of Blood and Marrow Transplantation 2004, 10 (2): p. 73-90.

Hori, A.; Kami, M.; Kishi, Y.; Machida, U.; Matsumura, T.; Kashima, T. Clinical significance of extra-pulmonary involvement of invasive aspergillosis: a

retrospective autopsy-based study of 107 patients. Journal of Hospital Infection 2002, 50 (3): p. 175-182.

Wenzel, R.; Del Favero, A.; Kibbler, C.; Rogers, T.; Rotstein, C.; Mauskopf, J.; Morris, S.; Schlamm, H.; Troke, P.; Marciniak et, a. Economic evaluation of voriconazole compared with conventional amphotericin B for the primary treatment of aspergillosis in immunocompromised patients. The Journal Of Antimicrobial Chemotherapy 2005, 55 (3): p. 352-361.

Chiller, T.M.; Stevens, D.A. Treatment strategies for Aspergillus infections. Drug Resistance Updates 2000, 3 (2): p. 89-97.

Kapsi, S.G.; Ayres, J.W. Processing factors in development of solid solution formulation of itraconazole for enhancement of drug dissolution and bioavailability. International Journal of Pharmaceutics 2001, 229 (1-2): p. 193-203.

Allendoerfer, R.; Loebenberg, D.; Rinaldi, M.G.; Graybill, J.R. Evaluation of SCH51048 in an experimental model of pulmonary aspergillosis. Antimicrobial Agents And Chemotherapy 1995, 39 (6): p. 1345-1348.

Coronel, B.; Levron, J.C.; Dorez, D.; Van Devenne, A.; Archimbaud, E.; Mercatello, A. Itraconazole lung concentrations in haematological patients. Mycoses 2000, 43 (3-4): p. 125-127.

O'Riordan, T.G. Inhaled antimicrobial therapy: from cystic fibrosis to the flu. Respiratory Care 2000, 45 (7): p. 836-845.

Lambros, M.P.; Bourne, D.W.; Abbas, S.A.; Johnson, D.L. Disposition of aerosolized liposomal amphotericin B. Journal Of Pharmaceutical Sciences 1997, 86 (9): p. 1066-1069.

Monforte, V.; Roman, A.; Gavalda, J.; Lopez, R.; Pou, L.; Simo, M.; Aguade, S.; Soriano, B.; Bravo, C.; Morell et, a. Nebulized amphotericin B concentration and distribution in the respiratory tract of lung-transplanted patients. Transplantation 2003, 75 (9): p. 1571-1574.

Boots, R.J.; Paterson, D.L.; Allworth, A.M.; Faoagali, J.L. Successful treatment of post-influenza pseudomembranous necrotising bronchial aspergillosis with liposomal amphotericin, inhaled amphotericin B, gamma interferon and GM-CSF. Thorax 1999, 54 (11): p. 1047-1049.

Koizumi, T.; Kubo, K.; Kaneki, T.; Hanaoka, M.; Hayano, T.; Miyahara, T.; Okada, K.; Fujimoto, K.; Yamamoto, H.; Kobayashi et, a. Pharmacokinetic evaluation of amphotericin B in lung tissue: lung lymph distribution after intravenous injection and airspace distribution after aerosolization and inhalation of amphotericin B. Antimicrobial Agents And Chemotherapy 1998, 42 (7): p. 1597-1600.

Wade, J.C. Aerosolized amphotericin B inhalation is not effective prophylaxis of invasive aspergillus infections during prolonged neutropenia in patients after chemotherapy or autologous bone marrow transplantation. Evidence-based Oncology 2000, 1 (3): p. 87-88.

Ruijgrok, E.J.; Vulto, A.G.; Van Etten, E.W. Efficacy of aerosolized amphotericin B desoxycholate and liposomal amphotericin B in the treatment of invasive pulmonary aspergillosis in severely immunocompromised rats. The Journal Of Antimicrobial Chemotherapy 2001, 48 (1): p. 89-95.

Spickard, A., 3rd; Hirschmann, J.V. Exogenous lipoid pneumonia. Archives Of Internal Medicine 1994, 154 (6): p. 686-692.

Shah, S.P.; Misra, A. Development of liposomal amphotericin B dry powder inhaler formulation. Drug Delivery 2004, 11 (4): p. 247-253.

McConville, J.T.; Overhoff, K.A.; Sinswat, P.; Frei, B.L.; Burgess, D.; Talbert, R.L.; Peters, J.I.; Johnston, K.P.; III, R.O.W. Lung Deposition and Clearance of Itraconazole in the Murine Model for Treatment of Acute Fungal Infections. Article In Press.

Rogers, T.L.; Hu, J.H.; Yu, Z.S.; Johnston, K.P.; Williams, R.O. A novel particle engineering technology: spray-freezing into liquid. International Journal of Pharmaceutics 2002, 242 (1-2): p. 93-100.

McConville, J.T.; Williams, R.O.; Carvalho, T.C.; Iberg, A.N.; Johnston, K.P.; Talbert, R.L.; Burgess, D.; Peters, J.I. Design and evaluation of a restraint-free small animal inhalation dosing chamber. Drug Development and Industrial Pharmacy 2005, 31 (1): p. 35-42.

Gubbins, P.O.; Gurley, B.J.; Bowman, J. Rapid and sensitive high performance liquid chromatographic method for the determination of itraconazole and its hydroxy-metabolite in human serum. Journal of Pharmaceutical and Biomedical Analysis 1998, 16 (6): p. 1005-1012.

Cimolai, N.; Taylor, G.P.; Mah, D.; Morrison, B.J. Definition and Application of a Histopathological Scoring Scheme for an Animal-Model of Acute Mycoplasma-Pneumoniae Pulmonary Infection. Microbiology and Immunology 1992, 36 (5): p. 465-478.

Kang, B.Y.; Kim, E.; Kim, T.S. Regulatory mechanisms and their therapeutic implications of interleukin-12 production in immune cells. Cellular Signalling 2005, 17 (6): p. 665-673.

Repa, A.; Wild, C.; Hufnagl, K.; Winkler, B.; Bohle, B.; Pollak, A.; Wiedermann, U. Influence of the route of sensitization on local and systemic immune responses in a murine model of type I allergy. Clinical And Experimental Immunology 2004, 137 (1): p. 12-18.

Ichinose, T.; Nishikawa, M.; Takano, H.; Sera, N.; Sadakane, K.; Mori, I.; Yanagisawa, R.; Oda, T.; Tamura, H.; Hiyoshi, K. Pulmonary toxicity induced by intratracheal instillation of Asian yellow dust (Kosa) in mice. Environmental Toxicology and Pharmacology 2005, 20 (1): p. 48-56.

Inoue, H.; Iwasaki, H.; Abe, S.; Yamaguchi, H.; Ueda, T. Modulation of the human interleukin-12p40 response by a triazole antifungal derivative, itraconazole. Scandinavian Journal Of Infectious Diseases 2004, 36 (8): p. 607-609.

Scholer, N.; Olbrich, C.; Tabatt, K.; Muller, R.H.; Hahn, H.; Liesenfeld, O. Surfactant, but not the size of solid lipid nanoparticles (SLN) influences viability and cytokine production of macrophages. International Journal Of Pharmaceutics 2001, 221 (1-2): p. 57-67.

Geiser, M. Morphological aspects of particle uptake by lung phagocytes. Microscopy Research And Technique 2002, 57 (6): p. 512-522.

Bosquillon, C.; Preat, V.; Vanbever, R. Pulmonary delivery of growth hormone using dry powders and visualization of its local fate in rats. Journal of Controlled Release 2004, 96 (2): p. 233-244.

Makino, K.; Yamamoto, N.; Higuchi, K.; Harada, N.; Ohshima, H.; Terada, H. Phagocytic uptake of polystyrene microspheres by alveolar macrophages: effects of the size and surface properties of the microspheres. Colloids and Surfaces B: Biointerfaces 2003, 27 (1): p. 33-39.

Herbrecht, R.; Natarajan-Ame, S.; Letscher-Bru, V.; Canuet, M. Invasive pulmonary aspergillosis. Seminars in Respiratory and Critical Care Medicine 2004, 25 (2): p. 191-202.

Gordon, E.M.; Blumer, J.L. Rationale for single and high dose treatment regimens with azithromycin. Pediatric Infectious Disease Journal 2004, 23 (2): p. S102-S107.

Pylkkanen, L.; Gullsten, H.; Majuri, M.-L.; Andersson, U.; Vanhala, E.; Maatta, J.; Meklin, T.; Hirvonen, M.-R.; Alenius, H.; Savolainen, K. Exposure to Aspergillus fumigatus spores induces chemokine expression in mouse macrophages. Toxicology 2004, 200 (2-3): p. 255-263.

Abe, M.; Kondo, K.; Fujino, S.; Hirasawa, Y.; Yokoyama, A.; Kohno, N.; Hiwada, K. Lipoid pneumonia combined with pulmonary nocardiosis caused by inhalation of amphotericin-B after renal transplantation. Nihon Kyobu Shikkan Gakkai Zasshi 1996, 34 (6): p. 737-740.

Dubois, J.; Bartter, T.; Gryn, J.; Pratter, M.R. The physiologic effects of inhaled amphotericin B. Chest 1995, 108 (3): p. 750-753.

Ruijgrok, E.J.; Vulto, A.G.; Van Etten, E.W.M. Efficacy of aerosolized amphotericin B desoxycholate and liposomal amphotericin B in the treatment of invasive pulmonary aspergillosis in severely immunocompromised rats. Journal of Antimicrobial Chemotherapy 2001, 48 (1): p. 89-95.

Williams III, R.O.; Liu, J. Formulation of a protein with propellant HFA 134a for aerosol delivery. European Journal of Pharmaceutical Sciences 1999, 7 (2): p. 137-144.

Vita

Jason Michael Vaughn was born in Austin, TX on January 29, 1976 to Terry and Sharon Vaughn. He graduated from Lanier High School in Austin, TX in 1994 and began his college career at Austin Community College. He transferred to the University of Texas, College of Natural Sciences in 1996 seeking a major in Biochemistry. He applied and was accepted to the College of Pharmacy in 1998 and received his Bachelor of Science in Pharmacy with academic and special honors in 2000. During his undergraduate pharmacy education, he worked in the laboratories of Dr. Robert O. Williams III, completed the College of Pharmacy Honors Program and presented his work at several national and international meetings. Upon graduation, he began graduate school under the direction of Dr. Williams and has since published a manuscript in The European Journal of Pharmaceutics and Biopharmaceutics, written a chapter on compounding and calculations for the American Society of Health System Pharmacists' (ASHP) PharmPrep board review text book and has submitted a chapter on Nanoparticle Engineering to the Encyclopedia of Pharmaceutical Technology. During his graduate education, Jason has been a teaching assistant and head teaching assistant for the Pharmaceutical Compounding and Calculations Laboratory and has taught a course on compounding and calculations at the ASHP annual meeting. In 2002, he was awarded the University of Texas Continuing Fellowship and was selected for an outstanding graduate paper by the Controlled Release Society in 2005. Parts of his dissertation will be submitted for publication in several high impact pharmaceutical and medical journals.

Permanent address: 16800 Tortoise St.

Round Rock, TX 78757

This dissertation was typed by the author: Jason Michael Vaughn.